



**Design and Optimization of a Separation Process for Butanediol
Dehydration for Use as a Biofuel**

Shivan Mavalal
BSc. (Eng.)

Submitted in fulfilment of the academic requirements for the degree of Master of Science in
Engineering in the School of Engineering, University of KwaZulu-Natal

December 2020

Supervisor: Dr K. Moodley

ABSTRACT

Ongoing research in incorporating renewable biofuels into the transport sector are fuels that can be used interchangeably with petroleum derived fuels. These fuels are termed “drop-in” fuels and can be used in the pure state or as a blending component. Diols such as butane-1,4-diol and butane-2,3-diol have been identified as appropriate drop-in fuels in various transport applications as they can improve octane numbers and heating values of the fuel blend. The butanediols are generally produced by the energy intensive process of chlorohydrination of butene with a subsequent hydrolysis step or hydrogenation and hydrolysis on the industrial scale. A potentially lower energy-impact process for the production of these diols is the biochemical process route which involves the fermentation of biomass (a renewable feed) by certain classes of bacteria. A low concentration aqueous mixture of the butanediols is produced, that must be dehydrated before use. Conventional distillation can be used for the dehydration and subsequent purification step, but the process is energy intensive as high-pressure steam must often be used as the heating medium, due to low concentrations of the butanediols and their high boiling points relative to water. Hence, there is merit in exploring lower-energy alternate separation schemes. The most promising options presented in the literature are hybrid techniques involving solvent extraction using butan-1-ol and recovery by distillation to first remove excess water and subsequently concentrate the butanediol product composition. However, those processes were designed based on model parameters extrapolated mostly from liquid-liquid equilibrium data only, and a limited set of vapour-liquid equilibrium (VLE) data. This yielded broadly qualitative designs in the literature.

To improve this, in this work, novel isothermal VLE experimental data were measured for the binary systems of water/butan-1-ol in combination with the butanediol component species; butane-1,4-diol and butane-2,3-diol, utilizing a dynamic-analytical apparatus at sub-atmospheric conditions. For the binary systems of water (1) + butane-1,4-diol (2)/butane-2,3-diol (2), measurements were performed at temperatures ranging from 353 – 373 K. For the binary system of butan-1-ol (1) + butane-1,4-diol (2)/butane-2,3-diol (2), measurements were performed at temperatures ranging from 353 – 388 K. Temperature ranges were selected to maintain conditions up to atmospheric pressure which are commonly used in industry for these applications. For both sets of binary measurements, the P - T - x - y data was modelled using the γ - Φ approach. To account for the liquid-phase non-ideality, the Non-Random Two-Liquid and Universal Quasi-Chemical activity coefficient models were used while the Hayden and O’Connell correlation in the virial equation of state was used to account for the non-ideality in the vapour-phase. For all binary systems considered in this study, the experimental P - T - x - y data was concluded to be of good quality as thermodynamic consistency tests such as the area test and point test

were passed with tolerances of below 10 % and 0.01, respectively, and the root mean square deviations in pressure and the absolute average deviation values in the vapour-phase mole fraction was found to be within the experimental uncertainty in these measurements.

The binary parameters regressed from the experimental VLE data were used to improve the simulated separation design to purify butane-1,4-diol and butane-2,3-diol from the aqueous mixtures that result from the biological process pathways proposed in the literature. This was executed by exploring the design potential of a hybrid extraction-assisted distillation separation process in comparison to conventional distillation. Separation techniques such as conventional distillation, heterogeneous azeotropic distillation and liquid-liquid extraction are utilized in the novel proposed separation process. To achieve the dehydration of the butanediol constituents, butan-1-ol was used as the solvent in the liquid-liquid extraction step. The design of the separation process was performed using Aspen Plus® and optimized using standard procedures to reduce duties and costs. The simulation was used to investigate the technical and economic feasibility of the process with further optimization of the design by considering heat-integration. Conventional distillation was found to be the most economically feasible process alternative for the butane-1,4-diol purification, with an estimated total annual cost in the range of \$4,532,846.67 and \$4,635,070.52 for a payback period of 3 years, while extraction assisted distillation with heat integration was found to be the economically viable option for butane-2,3-diol purification with total annual costs in the range of \$2,997,204.58 and \$3,988,868.70 for a payback period of 3 years.

DECLARATION ONE: Statement of original work

The work presented in this dissertation was carried out in the Thermodynamic Research Unit in the School of Engineering at the University of KwaZulu-Natal, Durban, from January 2019 to December 2020 under the supervision of Doctor K. Moodley.

This dissertation is submitted as the full requirement for the degree M.Sc. (Eng.) in Chemical Engineering.

I, Shivan Mavalal, therefore declare that:

- (i) The research reported in this dissertation, except where otherwise indicated, is my original work.
- (ii) This dissertation has not been submitted for any degree or examination at any other university.
- (iii) This dissertation does not contain other persons' data, pictures, graphs or other information, unless specifically acknowledged as being sourced from other persons.
- (iv) This dissertation does not contain other persons' writing, unless specifically acknowledged as being sourced from other researchers. Where other written sources have been quoted, then:
 - a) Their words have been re-written but the general information attributed to them has been referenced;
 - b) Where their exact words have been used, their writing has been placed inside quotation marks, and referenced.
- (v) This dissertation does not contain text, graphics or tables copied and pasted from the Internet, unless specifically acknowledged, and the source being detailed in the dissertation and in the References sections.
- (vi) As this thesis is submitted in the journal manuscript format, under Rule DR9 c) and d) of the University of KwaZulu-Natal, manuscript versions of published or unpublished work are presented.

Shivan Mavalal

As the candidate's supervisor, I, Dr. K Moodley, approved this dissertation for submission.

Dr K. Moodley

DECLARATION TWO: Contribution to publications

Details of contribution to publications and manuscripts

1. Mavalal, S. and Moodley, K., 2020. Isothermal vapour-liquid equilibrium measurements for the water+ butane-1, 4-diol/butane-2, 3-diol system within 353.1–373.2 K. *Fluid Phase Equilibria*, 512, p.112518.

Contribution: I conceptualized the study, developed the experimental methodology, validated the procedure, measured modelled and analysed the data, prepared the manuscript with support from Dr K Moodley.

2. Mavalal, S. and Moodley, K., 2021. Isothermal Vapour-Liquid Equilibrium Measurements for the butan-1-ol+ butane-1, 4-diol/butane-2, 3-diol system within 353.2–388.2 K. *Fluid Phase Equilibria*, 527, p.112827.

Contribution: I conceptualized the study, developed the experimental methodology, validated the procedure, measured modelled and analysed the data, prepared the manuscript with support from Dr K Moodley.

3. Mavalal, S. and Moodley, K., 2021. Techno-economic analysis of alternate process pathways for butane-1,4-diol and butane-2,3-diol purification from aqueous mixtures for use as a biofuel. Manuscript in preparation.

Contribution: I conceptualized the study, developed the experimental methodology, validated the procedure, measured modelled and analysed the data, prepared the manuscript with support from Dr K Moodley.

ACKNOWLEDGEMENTS

I would like to acknowledge the following people:

- My supervisor, Doctor K. Moodley for his invaluable expertise, guidance and patience during the completion of this research. His deep understanding of phase equilibrium thermodynamics and process separation has greatly inspired me.
- The Thermodynamics Research Unit colleagues and staff and the University of KwaZulu-Natal JW Nelson Fund for financial assistance provided for the completion of this project.
- My parents, Devanand Mavalal and Saraswathie Mavalal; my siblings Sharona Mavalal, Shikara Noothai and Neil Noothai; and my niece, Jordan Milan Noothai, for a lifetime of support, love and encouragement.

TABLE OF CONTENTS

ABSTRACT	i
DECLARATION ONE: Statement of original work.....	iii
DECLARATION TWO: Contribution to publications.....	iv
ACKNOWLEDGEMENTS.....	v
TABLE OF CONTENTS	vi
LIST OF FIGURES	xi
LIST OF TABLES.....	xvi
NOMENCLATURE	xviii
1. CHAPTER ONE	1
Introduction	1
2. CHAPTER TWO.....	4
Theoretical background.....	4
2.1. Review of Thermodynamic Principles.....	4
2.1.1. Phase Equilibrium and Chemical Potential.....	4
2.1.2. Fugacity, Fugacity Coefficient and Activity Coefficient	4
2.1.3. Fugacity and Vapour-Liquid Equilibrium.....	7
2.2. Models for VLE Data.....	7
2.2.1. Virial Equation of State.....	7
2.2.2. Correlations for the Second Virial Coefficient	8
2.2.2.1. The Hayden-O'Connell Correlation.....	8
2.2.3. Liquid-Phase Activity Coefficient Models	12
2.2.3.1. Non-Random Two-Liquid (NRTL) Activity Coefficient Model	13
2.2.3.2. Universal Quasi-Chemical Activity Coefficient (UNIQUAC) Model.....	14
2.3. The Gamma-Phi (γ - Φ) Formulation for Vapour-Liquid Equilibrium.....	16
2.4. Thermodynamic Consistency Tests	18
2.4.1. The Area Test	18
2.4.2. The Point Test	19

2.5. Calculation of Infinite Dilution Activity Coefficients	19
3. CHAPTER THREE.....	21
Equipment, Experimental, and Simulation.....	21
3.1. Dynamic Still Review	21
3.2. Equipment Layout and Item List	23
3.3. Cleaning and leak testing of the apparatus.....	24
3.4. Calibrations	25
3.4.1. Temperature Calibration	25
3.4.2. Pressure Calibration	25
3.4.3. Gas chromatograph calibrations.....	25
3.3. Simulation Work	29
4. CHAPTER FOUR.....	30
Isothermal Vapour-Liquid Equilibrium Measurements for the water + butane-1,4-diol/butane-2,3-diol system within 353.1 to 373.2 K.....	30
4.1. Abstract	30
4.2. Introduction.....	30
4.3. Theory	32
4.3.1. Modelling Approach	32
4.3.2. Model Selection	33
4.4. Experimental	33
4.4.1. Materials	33
4.4.2. Equipment and Uncertainties.....	33
4.5. Results and Discussion.....	34
4.6. Conclusion	38
5. CHAPTER FIVE	57
Isothermal Vapour-Liquid Equilibrium Measurements for the butan-1-ol + butane-1,4-diol/butane-2,3-diol system within 353.2 – 388.2 K.....	57
5.1. Abstract	57
5.2. Introduction.....	57

5.3. Theory	59
5.3.1. Modelling Approach	59
5.3.2. Model Selection	60
5.4. Experimental	60
5.4.1. Materials	60
5.4.2. Equipment and Uncertainties	60
5.5. Results and Discussion.....	61
5.6. Conclusion	65
CHAPTER SIX.....	85
Techno-economic analysis of alternate process pathways for butane-1,4-diol and butane-2,3-diol purification from aqueous mixtures for use as a biofuel	85
Abstract	85
6.1. Introduction	85
6.2. Methods and Procedure	90
6.2.1. Design Approach.....	90
6.2.2. Simulation Methodology	95
6.2.3. Aspen Plus® Model Library	95
6.2.3.1. Separation Blocks.....	96
6.2.3.2. Heat Exchanger Blocks	98
6.2.4. Convergence.....	99
6.2.4.1. Block Convergence	99
6.2.5. Recycle Streams	99
6.2.6. Solvent Selection.....	100
6.2.7. Thermodynamic Models	100
6.3. Cost Analysis.....	102
6.4. Results and discussion.....	104
6.4.1. Butane-1,4-diol production	104
6.4.1.1. Conventional Distillation – Simulation Methodology	104
6.4.1.2. Extraction-Assisted Distillation – Simulation Methodology	107

6.4.1.3. Heat Integration – Simulation Methodology	110
6.4.1.4. Cost Analysis.....	112
<i>Conventional Distillation</i>	112
<i>Extraction-Assisted Distillation without Heat Integration</i>	114
<i>Extraction-Assisted Distillation with Heat Integration</i>	116
6.4.2. Butane-2,3-diol production	118
6.4.2.1. Conventional Distillation – Simulation Methodology	118
6.4.2.2. Extraction-Assisted Distillation – Simulation Methodology	121
6.4.2.3. Heat Integration – Simulation Methodology.....	124
6.4.2.4. Cost Analysis.....	126
<i>Conventional Distillation</i>	126
<i>Extraction-Assisted Distillation without Heat Integration</i>	128
<i>Extraction-Assisted Distillation with Heat Integration</i>	130
6.5. Conclusions.....	133
CHAPTER SEVEN	134
Culminating Discussion.....	134
7.1. Chemicals and uncertainties	134
7.2. VLE measurements and modelling.	135
7.2.1. Confirmation of equipment and procedure	135
7.2.2. Novel binary VLE data	135
7.2. Separation scheme design	135
CHAPTER EIGHT	140
Conclusions	140
CHAPTER NINE	142
Recommendations	142
References	143
Appendices	152
Appendix A: Calibrations	152
Appendix B: Uncertainty estimates	164

Appendix C: Test system data	165
Appendix D: Consistency tests	166
Appendix E: Extrapolated infinite dilution activity coefficients	170

LIST OF FIGURES

Figure 2.1. Algorithm used for the regression of isothermal VLE data using the γ - Φ method Walas, (2013).....	17
Figure 3.1. Schematic of the apparatus of Joseph <i>et al.</i> , (2001) used in this work as shown in Ndlovu, (2005).....	23
Figure 3.2. Layout of the apparatus of Joseph <i>et al.</i> (2001) used in this work (as shown in Mavalal <i>et al.</i> (2019)).	24
Figure 4.1. Layout of the apparatus of Joseph <i>et al.</i> , (2001) used in this work (as shown in Mavalal <i>et al.</i> , (2019)).	44
Figure 4.2. Vapour-liquid equilibrium data for the water (1) + butane-1,4-diol system, with comparison to available literature data. P-x at 353.2 K, ●-This work, ●- Huang and Zhang, (1987), P-x at 363.2 K, ■-This work, ■- Huang and Zhang, (1987), P-x at 373.2 K, ▲-This work, P-y at 373.2 K, Δ-This work, P-x at 373.32 K, ▲- Jelinek <i>et al.</i> , (1976), P-y at 373.32 K, Δ- Jelinek <i>et al.</i> , (1976).	45
Figure 4.3. P-x-y data for the water (1) + butane-1,4-diol system. Experimental (P-x, P-y): at 353.2 K, (●, ○), 363.2 K, (■, □), 373.2 K, (▲, Δ). Model (P-x, P-y): at 353.2 K, (- - -, - - -), 363.2 K, (···, - - -), 373.2 K, (-, - -). Black lines represent the NRTL-HOC model, red lines represent the UNIQUAC-HOC model.	46
Figure 4.4. P-x-y data for the water (1) + butane-2,3-diol system. Experimental (P-x, P-y): at 353.1 K, (●, ○), 363.2 K, (■, □), 373.2 K, (▲, Δ). Model (P-x, P-y): at 353.2 K, (- - -, - - -), 363.2 K, (···, - - -), 373.2 K, (-, - -). Black lines represent the NRTL-HOC model, red lines represent the UNIQUAC-HOC model.	47
Figure 4.5. y_1 vs. x_1 for the water (1) + butane-1,4-diol system. Experimental: ●-353.2 K, ■-363.2 K, ▲-373.2 K. Model: (- - -)-353.2 K, (···)- 363.2 K, (-)-373.2 K. Black lines represent the NRTL-HOC model, red lines represent the UNIQUAC-HOC model.	48
Figure 4.6. y_1 vs. x_1 for the water (1) + butane-2,3-diol system. Experimental: ●-353.2 K, ■-363.2 K, ▲-373.2 K. Model: (- - -)-353.2 K, (···)- 363.2 K, (-)-373.2 K. Black lines represent the NRTL-HOC model, red lines represent the UNIQUAC-HOC model.	49
Figure 4.7. γ_i - x_i data for the water (1) + butane-1,4-diol system. Experimental (γ_1, γ_2): at 353.2 K, (●, ○), 363.2 K, (■, □), 373.2 K, (▲, Δ). Model (γ_1, γ_2): at 353.2 K, (- - -, - - -), 363.2 K, (- - -, ···), 373.2 K, (- - -, -). Black lines represent the NRTL-HOC model, red lines represent the UNIQUAC-HOC model.	50
Figure 4.8. γ_i - x_i data for the water (1) + butane-2,3-diol system. Experimental (γ_1, γ_2): at 353.1 K, (●, ○), 363.2 K, (■, □), 373.2 K, (▲, Δ). Model (γ_1, γ_2): at 353.2 K, (- - -, - - -), 363.2 K, (- - -, ···), 373.2 K, (- - -, -). Black lines represent the NRTL-HOC model, red lines represent the UNIQUAC-HOC model.	51

Figure 4.9. α_{12} vs. x_1 for the water (1) + butane-1,4-diol system. Experimental: ●-353.2 K, ■-363.2 K, ▲-373.2 K. Model: (- - -)-353.2 K, (···)- 363.2 K, (—)-373.2 K. Black lines represent the NRTL-HOC model, red lines represent the UNIQUAC-HOC model. 52

Figure 4.10. α_{12} vs. x_1 for the water (1) + butane-2,3-diol system. Experimental: ●-353.2 K, ■-363.2 K, ▲-373.2 K. Model: (- - -)-353.2 K, (···)- 363.2 K, (—)-373.2 K. Black lines represent the NRTL-HOC model, red lines represent the UNIQUAC-HOC model. 53

Figure 4.11. G^E/RT vs. x_1 for the water (1) + butane-1,4-diol system. Experimental: ●-353.2 K, ■-363.2 K, ▲-373.2 K. Model: (- - -)-353.2 K, (···)- 363.2 K, (—)-373.2 K. Black lines represent the NRTL-HOC model, red lines represent the UNIQUAC-HOC model. 54

Figure 4.12. G^E/RT vs. x_1 for the water (1) + butane-2,3-diol system. Experimental: ●-353.2 K, ■-363.2 K, ▲-373.2 K. Model: (- - -)-353.2 K, (···)- 363.2 K, (—)-373.2 K. Black lines represent the NRTL-HOC model, red lines represent the UNIQUAC-HOC model. 55

Figure 4.13. H^E vs. x_1 for the water (1) + butane-1,4-diol system. Literature: ■-298.136 K Amaya and Fujishiro, (1956), □-298.15 K, ◇-323.15, △-343.15 K Nagamachi and Francesconi, (2006) . Model: (—)298.15 K, (-·-·-)- 323.15 K, (— — —)-343.15 K, (- - -)-353.15 K, (···)-363.15 K, (—)-373.15 K. Black lines represent the NRTL-HOC model prediction, red lines represent the UNIQUAC-HOC model prediction. 56

Figure 5.1. Layout of the apparatus of Joseph *et al.*, (2001) used in this work (as shown in Mavalal *et al.*, (2019)). 72

Figure 5.2. P - x - y data for the butan-1-ol (1) + butane-1,4-diol system. Experimental (P - x , P - y): at 353.2 K, (●, ○), 363.2 K, (▲, △), 373.2 K, (◆, ◇), 388.2 K, (■, □). Model (P - x , P - y): at 353.2 K, (— — —, — — —), 363.2 K, (---, ---), 373.2 K, (···, — — —), 388.2 K, (—, -·-). Black lines represent the NRTL-HOC model, red lines represent the UNIQUAC-HOC model. 73

Figure 5.3. P - x - y data for the butan-1-ol (1) + butane-2,3-diol system. Experimental (P - x , P - y): at 353.2 K, (●, ○), 363.2 K, (▲, △), 373.2 K, (◆, ◇), 388.2 K, (■, □). Model (P - x , P - y): at 353.2 K, (— — —, — — —), 363.2 K, (---, ---), 373.2 K, (···, — — —), 388.2 K, (—, -·-). Black lines represent the NRTL-HOC model, red lines represent the UNIQUAC-HOC model. 74

Figure 5.4. y_1 vs. x_1 for the butan-1-ol (1) + butane-1,4-diol system. Experimental: ●-353.2 K, ▲-363.2 K, ◆-373.2 K, ■-388.2 K. Model: (— — —)-353.2 K, (- - -)- 363.2 K, (···)-373.2 K, (—)-388.2 K. Black lines represent the NRTL-HOC model, red lines represent the UNIQUAC-HOC model. 75

Figure 5.5. y_1 vs. x_1 for the butan-1-ol (1) + butane-2,3-diol system. Experimental: ●-353.2 K, ▲-363.2 K, ◆-373.2 K, ■-388.2 K. Model: (— — —)-353.2 K, (- - -)- 363.2 K, (···)-373.2 K, (—)-388.2 K. Black lines represent the NRTL-HOC model, red lines represent the UNIQUAC-HOC model. 76

Figure 5.6. γ_i - x_1 data for the butan-1-ol (1) + butane-1,4-diol system. Experimental (γ_1 , γ_2): at 353.2 K, (●, ○), 363.2 K, (▲, △), 373.2 K, (◆, ◇), 388.2 K, (■, □). Model (γ_1 , γ_2): at 353.2 K, (— — —, — — —), 363.2

K, (- - -, - · -), 373.2 K, (···, ---), 388.2 K, (-, - · -). Black lines represent the NRTL-HOC model, red lines represent the UNIQUAC-HOC model. 77

Figure 5.7. γ_i - x_i data for the butan-1-ol (1) + butane-2,3-diol system. Experimental (γ_1, γ_2): at 353.2 K, (●, ○), 363.2 K, (▲, Δ), 373.2 K, (◆, ◇), 388.2 K, (■, □). Model (γ_1, γ_2): at 353.2 K, (- - -, - · -), 363.2 K, (- - -, - · -), 373.2 K, (···, ---), 388.2 K, (-, - · -). Black lines represent the NRTL-HOC model, red lines represent the UNIQUAC-HOC model. 78

Figure 5.8. α_{12} vs. x_1 for the butan-1-ol (1) + butane-1,4-diol system. Experimental: ●-353.2 K, ▲-363.2 K, ◆-373.2 K, ■-388.2 K. Model: (- - -)-353.2 K, (- - -)- 363.2 K, (···)-373.2 K, (-)-388.2 K. Black lines represent the NRTL-HOC model, red lines represent the UNIQUAC-HOC model. 79

Figure 5.9. α_{21} vs. x_1 for the butan-1-ol (1) + butane-1,4-diol system. Experimental: ●-353.2 K, ▲-363.2 K, ◆-373.2 K, ■-388.2 K. Model: (- - -)-353.2 K, (- - -)- 363.2 K, (···)-373.2 K, (-)-388.2 K. Black lines represent the NRTL-HOC model, red lines represent the UNIQUAC-HOC model. 80

Figure 5.10. α_{12} vs. x_1 for the butan-1-ol (1) + butane-2,3-diol system. Experimental: ●-353.2 K, ▲-363.2 K, ◆-373.2 K, ■-388.2 K. Model: (- - -)-353.2 K, (- - -)- 363.2 K, (···)-373.2 K, (-)-388.2 K. Black lines represent the NRTL-HOC model, red lines represent the UNIQUAC-HOC model. 81

Figure 5.11. α_{21} vs. x_1 for the butan-1-ol (1) + butane-2,3-diol system. Experimental: ●-353.2 K, ▲-363.2 K, ◆-373.2 K, ■-388.2 K. Model: (- - -)-353.2 K, (- - -)- 363.2 K, (···)-373.2 K, (-)-388.2 K. Black lines represent the NRTL-HOC model, red lines represent the UNIQUAC-HOC model. 82

Figure 5.12. G^E/RT vs. x_1 for the butan-1-ol (1) + butane-1,4-diol system. Experimental: ●-353.2 K, ▲-363.2 K, ◆-373.2 K, ■-388.2 K. Model: (- - -)-353.2 K, (- - -)- 363.2 K, (···)-373.2 K, (-)-388.2 K. Black lines represent the NRTL-HOC model, red lines represent the UNIQUAC-HOC model. 83

Figure 5.13. G^E/RT vs. x_1 for the butan-1-ol (1) + butane-2,3-diol system. Experimental: ●-353.2 K, ▲-363.2 K, ◆-373.2 K, ■-388.2 K. Model: (- - -)-353.2 K, (- - -)- 363.2 K, (···)-373.2 K, (-)-388.2 K. Black lines represent the NRTL-HOC model, red lines represent the UNIQUAC-HOC model. 84

Figure 6.1. Flow diagram of the butane-1,4-diol production process redrawn from Satam *et al.*, (2019). 87

Figure 6.2. Flow diagram of the butane-2,3-diol production process redrawn from Haider *et al.*, (2018). 89

Figure 6.3. Conventional distillation separation route. 91

Figure 6.4. Extraction-assisted distillation separation route. 93

Figure 6.5. Extraction-assisted distillation with heat integration. 94

Figure 6.6a. Residue curve map for the ternary system of water (1) + butan-1-ol (2) + butane-1,4-diol (3). 101

Figure 6.6b. Residue curve map for the ternary system of water (1) + butan-1-ol (2) + butane-2,3-diol (3). 101

Figure 6.7. Results of the conventional distillation separation route for butane-1,4-diol. 106

Figure 6.8. Results of the extraction-assisted distillation separation route for butane-1,4-diol.....	109
Figure 6.9. Results of the extraction-assisted distillation separation route with heat integration for butane-1,4-diol.....	111
Figure 6.10. Cost analysis of the separation routes for 1,4-BDO calculated by the manual method..	114
Figure 6.11. Cost analysis of the separation routes for 1,4-BDO calculated by Aspen Process Economic Analysis.	118
Figure 6.12. Results of the conventional distillation separation route for butane-2,3-diol.....	120
Figure 6.13. Results of the extraction-assisted distillation separation route for butane-2,3-diol.....	123
Figure 6.14. Results of the extraction-assisted distillation separation route with heat integration for butane-2,3-diol.....	125
Figure 6.15. Cost analysis of the separation routes for 2,3-BDO calculated by the manual method..	127
Figure 6.16. Cost analysis of the separation routes for 2,3-BDO calculated by Aspen Process Economic Analyser.	128
Figure 7.1. Flow diagram used for the sequential optimization approach for solvent selection and simulation design. Adapted from Haider <i>et al.</i> , (2018).....	137
Figure 7.2. Comparison of the manual method and Aspen Process Economic Analysis for the 1,4-BDO separation routes. Red bars are the manual method, black bars Aspen Process Economic Analysis.	139
Figure 7.3. Comparison of the manual method and Aspen Process Economic Analysis for the 2,3-BDO separation routes. Red bars are the manual method, black bars Aspen Process Economic Analysis.	139
Figure A1. (a) Temperature calibration for Standard temperature vs. Pt-100 sensor with linear trendline. (b) Deviation plot for temperature.	152
Figure A2. (a) Pressure calibration for Standard pressure vs. WIKA P-10 transducer with linear trendline. (b) Deviation plot for pressure.....	153
Figure A3. (a) GC area ratio calibration plot for water (1) + propan-1-ol (2) (water rich region) with best fit line. (b) Composition deviation plot for water (1) + propan-1-ol (2) (water rich region).....	154
Figure A4. (a) GC area ratio calibration plot for water (1) + propan-1-ol (2) (propan-1-ol rich region) with best fit line. (b) Composition deviation plot for water (1) + propan-1-ol (2) (propan-1-ol rich region).....	155
Figure A5. (a) GC area ratio calibration plot for water (1) + butane-1,4-diol (2) (water rich region) with best fit line. (b) Composition deviation plot for water (1) + butane-1,4-diol (2) (water rich region).	156
Figure A6. (a) GC area ratio calibration plot for water (1) + butane-1,4-diol (2) (butane-1,4-diol rich region) with best fit line. (b) Composition deviation plot for water (1) + butane-1,4-diol (2) (butane-1,4-diol rich region).	157
Figure A7. (a) GC area ratio calibration plot for water (1) + butane-2,3-diol (2) (water rich region) with best fit line. (b) Composition deviation plot for water (1) + butane-2,3-diol (2) (water rich region).	158

Figure A8. (a) GC area ratio calibration plot for water (1) + butane-2,3-diol (2) (butane-2,3-diol rich region) with best fit line. (b) Composition deviation plot for water (1) + butane-2,3-diol (2) (butane-2,3-diol rich region).	159
Figure A9. (a) GC area ratio calibration plot for butan-1-ol (1) + butane-1,4-diol (2) (butan-1-ol rich region) with best fit line. (b) Composition deviation plot for butan-1-ol (1) + butane-1,4-diol (2) (butan-1-ol rich region).	160
Figure A10. (a) GC area ratio calibration plot for butan-1-ol (1) + butane-1,4-diol (2) (butane-1,4-diol rich region) with best fit line. (b) Composition deviation plot for butan-1-ol (1) + butane-1,4-diol (2) (butane-1,4-diol rich region).	161
Figure A11. (a) GC area ratio calibration plot for butan-1-ol (1) + butane-2,3-diol (2) (butan-1-ol rich region) with best fit line. (b) Composition deviation plot for butan-1-ol (1) + butane-2,3,4-diol (2) (butan-1-ol rich region).	162
Figure A12. (a) GC area ratio calibration plot for butan-1-ol (1) + butane-2,3-diol (2) (butane-2,3-diol rich region) with best fit line. (b) Composition deviation plot for butan-1-ol (1) + butane-2,3-diol (2) (butane-2,3-diol rich region).	163
Figure D1. Plot for the point test for water (1) + butane-1,4-diol (2). (a) Pressure deviation plot. (b) Vapour composition deviation plot.	166
Figure D2. Plot for the point test for water (1) + butane-2,3-diol (2). (a) Pressure deviation plot. (b) Vapour composition deviation plot.	167
Figure D3. Plot for the point test for butan-1-ol (1) + butane-1,4-diol (2). (a) Pressure deviation plot. (b) Vapour composition deviation plot.	168
Figure D4. Plot for the point test for butan-1-ol (1) + butane-2,3-diol (2). (a) Pressure deviation plot. (b) Vapour composition deviation plot.	169

LIST OF TABLES

Table 4.1. Chemical purities and suppliers. ^a	39
Table 4.2. Experimental vapour pressures and comparison to literature correlation. ^a	39
Table 4.3. Vapour-liquid equilibrium data for the water (1) + butane-1,4-diol. ^a	40
Table 4.4. Vapour-liquid equilibrium data for the water (1) + butane-2,3-diol. ^a	41
Table 4.5. Results of thermodynamic consistency tests using the NRTL-HOC model.....	42
Table 4.6. Regressed Model Parameters.....	42
Table 4.7. Infinite dilution activity coefficients from each model.....	43
Table 4.8. Regressed Model Parameters for H^E calculation.....	43
Table 5.1. Chemical purities and suppliers. ^a	66
Table 5.2. Experimental vapour pressures and comparison to literature correlation. ^a	67
Table 5.3. Vapour-liquid equilibrium data for the butan-1-ol (1) + butane-1,4-diol ^a	68
Table 5.4. Vapour-liquid equilibrium data for the butan-1-ol (1) + butane-2,3-diol. ^a	69
Table 5.5. Results of thermodynamic consistency tests using the NRTL-HOC model.....	70
Table 5.6. Regressed model parameters.....	70
Table 5.7. Infinite dilution activity coefficients from each model.....	71
Table 6.1 Feed compositions for the 1,4-BDO separation design Satam <i>et al.</i> , (2019).....	88
Table 6.2 Feed compositions for the 2,3-BDO separation design Haider <i>et al.</i> , (2018).....	89
Table 6.3 Design equations to determine the capital cost of columns and heat exchangers Hussain <i>et al.</i> , (2018).....	103
Table 6.4 Cost of the considered utilities Douglas, (1988), Turton <i>et al.</i> , (2008).	103
Table 6.5 Cost of the considered utilities as per Aspen Process Economic Analyser.	103
Table 6.6 Results of the conventional distillation separation route for butane-1,4-diol.	106
Table 6.7 Results of the extraction-assisted distillation separation route for butane-1,4-diol.	110
Table 6.8 Results of the extraction-assisted distillation separation route with heat integration for butane-1,4-diol.....	112
Table 6.9 Cost analysis of the conventional distillation separation route for butane-1,4-diol.....	113
Table 6.10 Cost analysis of the extracted-assisted distillation separation route for butane-1,4-diol without heat integration.	115
Table 6.11 Cost analysis of the extracted-assisted distillation with heat integration separation route for butane-1,4-diol.....	117
Table 6.12 Results of the conventional distillation separation route for the butane-2,3-diol.	120
Table 6.13 Results of the extraction-assisted distillation separation route for butane-2,3-diol.	124
Table 6.14 Results of the extraction-assisted distillation separation route with heat integration for butane-2,3-diol.....	126

Table 6.15 Cost analysis of the conventional distillation separation route for butane-2,3-diol.....	127
Table 6.16 Cost analysis of the extracted-assisted distillation separation route for butane-2,3-diol without heat integration.	130
Table 6.17 Cost analysis of the extracted-assisted distillation with heat integration separation route for butane-2,3-diol.....	132
Table B1. Uncertainty estimates for each contributing factor	164
Table C1. <i>P</i> - <i>x</i> - <i>y</i> plot for the water (1) + propan-1-ol (2) system at 313.15 K.	165
Table C2. Regressed model parameters for the water (1) + propan-1-ol (2) system at 313.15 K.	165
Table E1. Extrapolated infinite dilution activity coefficients by the method of Maher and Smith, (1979).	170

NOMENCLATURE

Symbols

a_i	Activity of component i
a_{ij}	NRTL/UNIQUAC model fit parameter
	Second virial coefficient ($\text{m}^3 \cdot \text{mol}^{-1}$)/parameters in Hayden-O'Connell correlation
B	O'Connell correlation
b_{ij}	NRTL/UNIQUAC model fit parameter (K)
f	Fugacity of component (kPa)
\hat{f}_i	Fugacity of species i in solution (kPa)
G	Molar Gibbs free energy ($\text{J} \cdot \text{mol}^{-1}$)
G_{ij}	NRTL model parameter
H	Molar enthalpy ($\text{J} \cdot \text{mol}^{-1}$)
n	Number of moles of component (moles)
P	Pressure (kPa)
P_D	Deviation pressure defined by Maher and Smith (1979b) (kPa)
P_i^{sat}	Saturation pressure of component i (kPa)
p_i	Partial pressure of component i (kPa)
R	Universal gas constant ($8.314 \text{ J} \cdot \text{mol}^{-1} \cdot \text{K}^{-1}$)
R_D	Radius of gyration (Angstroms)
S	Molar entropy ($\text{J} \cdot \text{mol}^{-1} \cdot \text{K}^{-1}$)
T	Temperature (K)
$u_{ij} - u_{ii}$	UNIQUAC model fit parameter ($\text{J} \cdot \text{mol}^{-1}$)
V	Total volume of vapour (m^3)/ Volts
V_i	Molar Volume of component i ($\text{m}^3 \cdot \text{mol}^{-1}$)
V_i^l	Saturated liquid molar volume of component i ($\text{m}^3 \cdot \text{mol}^{-1}$)
x	Liquid phase mole fraction
y	Vapour phase mole fraction
z	Overall composition
Z	Compressibility factor

Greek letters

α	Alpha phase/ Mixture parameter for PSRV (1986) EOS
α_{12}	Non-randomness parameter for the NRTL model/ Relative volatility
β	Beta phase

γ_i	Activity coefficient of species i
δ/Δ	Change in
δ_{ij}	Cross coefficient for virial equation of state ($\text{m}^3.\text{mol}^{-1}$)
ε	Tolerance
$\frac{\varepsilon_{ij}}{\kappa}$	Characteristic energy for the i - j interaction (K)
η_{ij}	Association parameter
κ_0	Pure component parameter for the PSRV (1986) EOS
κ_1	Pure component parameter for the PSRV (1986) EOS
$\lambda_{ij}-\lambda_{ii}$	T-K Wilson model fit parameter ($\text{J}.\text{mol}^{-1}$)
Λ	T-K Wilson model parameter
μ	Chemical potential ($\text{J}.\text{mol}^{-1}$)/ Dipole moment (C.m)
π	Pi phase
ρ	Density ($\text{kg}.\text{m}^{-3}$)
σ_{ij}	Molecular size (Angstroms)
τ_{ij}	NRTL model parameter
φ_i	Fugacity coefficient
Φ_i	Vapour correction factor
ω	Acentric factor
∞	Property at infinite dilution

Subscripts

1	Denotes component 1
2	Denotes component 2
AVG	Average quantity
c	Critical property
i	Component i
j	Component j
i,j	Mixture parameter
r	Reduced property
T	Total property

Superscripts

0	Standard state superscript
C	Combinatorial property
$calc$	Calculated property
exp	Experimentally determined property
E	Excess property

<i>ideal</i>	A property of an ideal solution
<i>lit</i>	A property obtained from the literature
<i>l</i>	Liquid phase
<i>R</i>	Residual property
<i>sat</i>	Property at saturation
<i>V</i>	Vapour phase

Abbreviations

<i>EOS</i>	Equation of state
<i>LLE</i>	Liquid-liquid equilibrium
<i>NRTL</i>	Non-random-two -liquid
<i>UNIQUAC</i>	Universal quasi-chemical activity coefficient model
<i>VLE</i>	Vapour-liquid equilibrium

Accents

\bar{M}	Partial property
\hat{M}	Mixture property

CHAPTER ONE

Introduction

Biochemical processes contribute significantly to the development of renewable chemicals through the conversion of biomass into complex constituents such as biofuels, solvents, polymers and pharmaceuticals. In the enzymatic class of bioconversion, processes can be tailored to maximize the yields of specific components by the selection of suitable unique microbe inoculum that has a propensity to produce the desired product Menon and Rao, (2012), Tahri *et al.*, (2013), Karnaouri *et al.*, (2016), Patel *et al.*, (2017), Haider *et al.*, (2018), Satam *et al.*, (2019). This work focuses on the biochemical production of butanediols, a di-alcohol with a market value estimated to be as high as \$43 billion Köpke *et al.*, (2011). Butanediols, specifically butane-1,4-diol and butane-2,3-diol have been identified as suitable drop-in fuels in certain transport applications due to their high octane-numbers and heating values. Drop-in fuels are biofuels that can be used interchangeably with petroleum derived fuels either in the pure state or as a blending component. Furthermore, these butanediols are used in the production of various polymers and are used as an industrial solvent Burgard *et al.*, (2016), Harvey *et al.*, (2016), Haider *et al.*, (2018), Satam *et al.*, (2019).

The conventional industrial procedure for butanediol production is by chlorohydrination of butene with a subsequent hydrolysis step or hydrogenation and hydrolysis. This is a highly energy intensive process. Alternatively, a biochemical process can also be used which involves the fermentation of biomass by certain classes of microbes. This second process can use renewable feedstock and has a lower energy consumption. The feasibility of the reaction section of the process has been discussed in the literature Haider *et al.*, (2018), Satam *et al.*, (2019) and will not be considered further in this work. As with many biochemical reaction processes, a low concentration aqueous mixture of the butanediols is produced, that must be dehydrated before it can be used in most applications. Conventional distillation is a technically sound process for this dehydration and subsequent purification but is highly energy intensive as high-pressure steam must often be used as the heating medium, due to low concentrations of the butanediols and their high boiling points relative to water Burgard *et al.*, (2016), Haider *et al.*, (2018). Alternate dehydration processes include pervaporation, reactive extraction, liquid-liquid extraction and salting-out extraction Haider *et al.*, (2018). Each separation technology possesses its own benefits, drawbacks and limitations with respect to its applicability in industrial operation and commercial-scale production, with the most promising options presented in the literature being hybrid techniques involving solvent extraction or evaporation and recovery by distillation to first remove excess water and subsequently concentrate the butanediol product composition Haider *et al.*, (2018), Satam *et al.*, (2019). However, those processes in the literature were designed based on model parameters derived

from insufficient vapour-liquid equilibrium (VLE) data for the relevant systems within a small temperature and pressure range, yielding broadly qualitative designs.

The aim of this project was to perform the necessary novel VLE measurements to inform a technically sound separation design of the biochemical process route for the purification of butane-1,4-diol and butane-2,3-diol to 99 wt% purity, and to optimize and economically evaluate this process using simulation software.

The objectives were to:

1. Calibrate and test a low-pressure VLE apparatus and confirm the methodology
2. Measure and model the VLE data for the water (1)/butan-1-ol (1) + butane-1,4-diol (2)/butane-2,3-diol (2), measurements were performed at temperatures ranging from 353 – 373 K
3. Perform rigorous simulations on Aspen Plus to determine the technical and economic feasibility of the purification of butane-1,4-diol and butane-2,3-diol produced by the biochemical route

A theoretical review to address the project aims and objectives is presented in Chapter 2. The VLE measurements were conducted using a dynamic-analytical apparatus (a replica of the design of Joseph *et al.*, (2001)), operated at sub-atmospheric conditions, reviewed in Chapter 3. The apparatus was calibrated and tested by performing VLE measurements for the well-studied water (1) + propan-1-ol system at 313.2 K, to confirm the functioning of the apparatus, estimate the measurement uncertainties, and confirm the experimental procedure.

Subsequently, novel isothermal VLE experimental data were measured for the binary systems of water and butan-1-ol in combination with the butanediol species; butane-1,4-diol and butane-2,3-diol to determine temperature dependent model parameters for an improved process analysis. For the novel binary systems of water (1) + butane-1,4-diol (2)/butane-2,3-diol (2), measurements were performed at temperatures ranging from 353 – 373 K. While for the binary system of butan-1-ol (1) + butane-1,4-diol (2)/butane-2,3-diol (2), measurements were performed at temperatures ranging from 353 – 388 K. These conditions were suitable for operation up to atmospheric pressure. For both sets of binary measurements, the P - T - x - y data was modelled using the γ - Φ approach to account for the mixture non-idealities, by employing the Non-Random Two-Liquid Renon and Prausnitz, (1968) and Universal Quasi-Chemical Abrams and Prausnitz, (1975) activity coefficient models with the Hayden and O'Connell correlation Hayden and O'Connell, (1975) for the virial equation of state. Thermodynamic consistency tests such as the area test and point test were also conducted. These results are presented as a series of two publications in Chapters 4 and 5.

The binary parameters regressed from the experimental VLE data were used to improve the rigour of the simulated separation design to produce butane-1,4-diol and butane-2,3-diol by exploring the designs of a hybrid extraction-assisted distillation (HED) process in comparison with a conventional distillation operation. Separation techniques such as conventional distillation, heterogeneous azeotropic distillation and liquid-liquid extraction are utilized in the HED process. To achieve the dehydration of the butanediol constituents, butan-1-ol was used as the entrainer in the liquid-liquid extraction step, which was shown in the literature to be a suitable solvent. The design of the separation process was performed using Aspen Plus® V10. The simulation was used to investigate the techno-economic feasibility of the process with further optimization of the design by considering heat integration. In Chapter 7, a culminating discussion is presented, followed by the conclusions and recommendations of the study. Since chapters 4-6 are presented in the manuscript format, there is a degree of repetition among the manuscripts and other chapters, which is unavoidable for these sections to stand alone.

CHAPTER TWO

Theoretical background

A brief description of the thermodynamic principles governing low pressure vapour-liquid equilibrium (VLE) is discussed in this chapter. This includes the criteria for phase equilibria, models for representing VLE data, the regression algorithm for bubble point pressures and thermodynamic consistency tests. Detailed revisions are given by Raal and Mühlbauer, (1998), Smith *et al.*, (2005). Walas, (2013).

2.1. Review of Thermodynamic Principles

2.1.1. Phase Equilibrium and Chemical Potential

When thermal, mechanical and chemical equilibrium are achieved in a closed system of multiple phases (at constant temperature, pressure and chemical potential), the system will reach phase equilibrium. For a closed system, at phase equilibrium, the total Gibbs free energy ($\Delta G = 0$) is constant. The chemical potential in each phase must hence be equal.

The chemical potential (μ) of a component (i) is defined as the partial differential of Gibbs energy with respect to component (i) at constant temperature, pressure and the number of moles (n) of all other components (j) within the system (Smith *et al.*, 2005):

$$\mu_i = \left[\frac{\partial(nG)}{\partial n_i} \right]_{P,T,n_{j \neq i}} \quad (2.1)$$

Considering the generalization of π different phases:

$$\mu_i^\alpha = \mu_i^\beta = \dots = \mu_i^\pi \quad (i = 1, 2, \dots, N) \quad (2.2)$$

Where α and β identify the phases and N is the number of species present in the system. At equilibrium, the system temperature, T , and pressure, P , are uniform throughout the system.

2.1.2. Fugacity, Fugacity Coefficient and Activity Coefficient

For a given temperature, the fugacity f is given by the pressure of an ideal gas that has the equivalent Gibbs free energy to a real gas. For its formal definition, consider first the reference chemical potential

of a pure species μ^0 , which is defined as the chemical potential at the reference pressure, P^0 . The difference between the chemical potential at the state of the system pressure for an ideal gas (P^{ideal}) and the chemical potential at the reference state yields:

$$\mu - \mu^0 = RT \ln \left[\frac{P^{ideal}}{P^0} \right] \quad (2.3)$$

Where R is the universal gas constant and T is the system temperature. For a real gas, the ideal gas pressure is replaced with the fugacity:

$$\mu - \mu^0 = RT \ln \left[\frac{f}{P^0} \right] \quad (2.4)$$

Rearrangement yields the formal definition of fugacity:

$$f = P^0 \exp \left[\frac{\mu - \mu^0}{RT} \right] \quad (2.5)$$

For non-ideal gas mixtures, component specific chemical potentials, μ_i , replaces pure component chemical potentials, the reference pressure is replaced with the fugacity of component i at the system temperature and pressure, f_i^0 , and fugacity in solution, \hat{f}_i is used instead of fugacity:

$$\mu_i - \mu_i^0 = RT \ln \left[\frac{\hat{f}_i}{f_i^0} \right] \quad (2.6)$$

The fugacity coefficient in solution ($\hat{\phi}_i$) is a dimensionless parameter that is used to quantify the departure from ideality of a mixture. It compares the fugacity of a species to the ideal gas partial pressure of the same species. For the vapour phase (V) it is defined by:

$$\hat{\phi}_i^V \equiv \frac{\hat{f}_i^V}{p_i} = \frac{\hat{f}_i^V}{y_i P_i} \quad (2.7)$$

Where p_i is the partial pressure and y_i the vapour mole fraction.

The fugacity coefficient is often also used and is calculated by taking the zero-pressure limit for the equivalent ideal solution version of equation 2.6:

$$G_i - G_i^0 = RT \ln \left[\frac{f_i}{f_i^0} \right] \quad (2.8)$$

Where G_i is the Gibbs energy of component i . Taking the zero-pressure limit yields:

$$\lim_{P \rightarrow 0} \left(\frac{f_i}{P} \right) = 1 \quad (2.9)$$

$$\varphi_i = \frac{f_i}{P} \quad (2.10)$$

The activity coefficient, γ_i , is a dimensionless parameter that expresses the fugacity in solution of the liquid-phase, and is defined as the ratio of the value of the fugacity in solution in the actual mixture to the fugacity in solution that the ideal solution (\hat{f}_i^{ideal}) would have at the composition of the mixture:

$$\gamma_i = \frac{\hat{f}_i}{\hat{f}_i^{ideal}} = \frac{\hat{f}_i}{x_i f_i^0} \quad (2.11)$$

Where x_i is the liquid phase mole fraction of component i . The magnitude of the activity coefficient depends on the chosen reference state. Often the reference state for component i is taken at the saturation condition, Hence, $f_i^0 = P_i^{sat}$. A general expression for the fugacity of a liquid species is then given by:

$$f_i^l = \varphi_i^{sat} P_i^{sat} \exp \left[\frac{V_i^l}{RT} (P - P_i^{sat}) \right] \quad (2.12)$$

The exponential term on the right is termed the Poynting correction. Where “ l ” refers to the liquid phase, V_i is the molar volume of a particular component i in the liquid phase and P_i^{sat} refers to the saturated pressure of a particular species.

By use of the Antoine equation or some other vapour pressure model, saturated pressure values can be obtained for different species, at different temperatures. From equation (2.11), the activity coefficient can then be expressed as:

$$\gamma_i = \frac{\hat{f}_i}{x_i P_i^{sat}} \quad (2.13)$$

2.1.3. Fugacity and Vapour-Liquid Equilibrium

Equation (2.13) is the fundamental criterion for phase equilibrium. Since all the phases that are being considered are at the same temperature and pressure, the following general criterion follows:

$$\hat{f}_i^\alpha = \hat{f}_i^\beta = \dots = \hat{f}_i^\pi \quad (i = 1, 2, \dots, N) \quad (2.14)$$

Smith *et al.*, (2005) states that multiple phases at the same temperature and pressure are in equilibrium when the fugacity in solution of each species in the system is the same for all considered phases. For the case of vapour-liquid equilibrium:

$$\hat{f}_i^v = \hat{f}_i^l \quad (i = 1, 2, \dots, N) \quad (2.15)$$

Accounting for the vapour-phase nonideality using the fugacity coefficient defined in equation (2.7) and the liquid-phase nonideality using the activity coefficient defined in equation (2.14), the modified Raoult's law with vapour correction factor is defined:

$$y_i \hat{\phi}_i P = x_i \gamma_i f_i^l \quad (2.16)$$

Or equivalently:

$$y_i \Phi_i P = x_i \gamma_i P_i^{sat} \quad (2.17)$$

Where Φ_i is the vapour correction factor, defined by:

$$\Phi_i = \frac{\hat{\phi}_i}{\phi_i^{sat}} \exp \left[\frac{-V_i^l}{RT} (P - P_i^{sat}) \right] \quad (2.18)$$

2.2. Models for VLE Data

2.2.1. Virial Equation of State

The virial equation of state (VEOS) is a power series expansion for the compressibility factor (Z) that is used to estimate fugacity coefficients of the vapour phase to account for real behaviour in low to moderate pressure systems. According to Prausnitz *et al.*, (1998), the VEOS truncated after the second virial coefficient (B) provides an accurate representation of the volumetric properties of vapour

component mixtures at low to moderate pressures. The VEOS that is truncated to two terms is defined as:

$$Z = 1 + \frac{BP}{RT} \quad (2.19)$$

In the case of ideal gas behaviour, Z will equal 1. The second virial coefficient, B , is a function of pure component temperatures. In the case of mixtures, B is calculated by a mixing rule. The second virial coefficient for mixtures can be determined by:

$$B_{mixture} = \sum_{i=1}^m \sum_{j=1}^m y_i y_j B_{ij} \quad (2.20)$$

2.2.2. Correlations for the Second Virial Coefficient

There are numerous correlations that have been proposed for the calculation of the second virial coefficient. These include the work of Pitzer and Curl, (1957), Tsonopoulos, (1974) and Hayden and O'Connell, (1975). The Hayden and O'Connell (HOC) correlation has been shown to account for vapour-phase association and is especially suited to systems of alcohols and water. Hence the correlation was selected for use in this work.

2.2.2.1. The Hayden-O'Connell Correlation

The Hayden and O'Connell correlation Hayden and O'Connell, (1975), uses chemical theory formulations to account for association and solvation in organic systems. The model incorporates several molecular structural parameters such as dipole moment, μ_d , and radius of gyration, R_d . The details of the model can be found in the original work.

In the model, the second virial coefficient between component i and j (B_{ij}) is divided into two contributions i.e., the physical force contribution (B_{ij}^F) and chemical force contribution (B_{ij}^D):

$$B_{ij} = B_{ij}^F + B_{ij}^D \quad (2.21)$$

Where

$$B_{ij}^F = (B_{nonpolar}^F)_{ij} + (B_{polar}^F)_{ij} \quad (2.22)$$

$$B_{ij}^D = (B_{metastable})_{ij} + (B_{bond})_{ij} + (B_{chemical})_{ij} \quad (2.23)$$

$(B_{nonpolar}^F)_{ij}$ and $(B_{polar}^F)_{ij}$ are the non-polar and polar contributions to the physical force contribution. $(B_{metastable})_{ij}$, $(B_{bond})_{ij}$ and $(B_{chemical})_{ij}$ are the dimerization metastable bound contribution, hydrogen bond and partial chemical association contribution. Empirical correlations with temperature dependence are used to calculate each term in the equations above and are given by:

$$(B_{nonpolar}^F)_{ij} = b_{0ij} \left(0.94 - \frac{1.47}{T_{ij}^{*T}} - \frac{0.85}{T_{ij}^{*T^2}} - \frac{1.015}{T_{ij}^{*T^3}} \right) \quad (2.24)$$

$$(B_{polar}^F)_{ij} = b_{0ij} \mu_{ij}^{*'} \left(0.74 - \frac{3.0}{T_{ij}^{*T}} - \frac{2.1}{T_{ij}^{*T^2}} - \frac{2.1}{T_{ij}^{*T^3}} \right) \quad (2.25)$$

$$(B_{metastable})_{ij} + (B_{bond})_{ij} = b_{0ij} A_{ij} \exp\left(\frac{\Delta h_{ij}}{T_{ij}^*}\right) \quad (2.26)$$

$$(B_{chemical})_{ij} = b_{0ij} E_{ij} \left[1 - \exp\left(\frac{1500 \eta_{ij}}{T}\right) \right] \quad (2.27)$$

Where

$$\frac{1}{T_{ij}^{*T}} = \frac{1}{T_{ij}^*} - 1.6\omega_{ij} \quad (2.28)$$

$$T_{ij}^* = \frac{T}{\left(\frac{\varepsilon_{ij}}{\kappa}\right)} \quad (2.29)$$

And

$$b_{0ij} = 1.26184 \sigma_{ij}^3 \quad (2.30)$$

$$\begin{aligned}
\mu_{ij}^{*'} &= \mu_{ij}^* && \text{if } \mu_{ij}^* < 0.04 \\
&= 0 && \text{if } 0.04 \leq \mu_{ij}^* < 0.25 \\
&= \mu_{ij}^* - 0.25 && \text{if } 0.25 \leq \mu_{ij}^*
\end{aligned} \tag{2.31}$$

$$A_{ij} = -0.3 - 0.05 \mu_{ij}^* \tag{2.32}$$

$$\Delta h_{ij} = 1.99 + 0.2 \mu_{ij}^{*2} \tag{2.33}$$

$$\mu_{ij}^* = \frac{7243.8 \mu_i \mu_j}{\left(\frac{\varepsilon_{ij}}{\kappa}\right) \sigma^3} \tag{2.34}$$

$$E_{ij} = \exp \left\{ \eta_{ij} \left(\frac{650}{\left(\frac{\varepsilon_{ij}}{\kappa}\right) + 300} - 4.27 \right) \right\} \text{ for } \eta_{ij} < 4.5 \tag{2.35}$$

Or

$$E_{ij} = \exp \left\{ \eta_{ij} \left(\frac{42800}{\left(\frac{\varepsilon_{ij}}{\kappa}\right) + 22400} - 4.27 \right) \right\} \text{ for } \eta_{ij} > 4.5 \tag{2.36}$$

$\frac{\varepsilon_{ij}}{\kappa}$ is defined as the characteristic energy for the i - j interaction (K), σ_{ij} is the molecular size (Ångströms), μ_{ij} is the dipole moment of component i (Debye), η_{ij} is the association parameter when $i = j$ or the solvation parameter when $i \neq j$ and ω_{ij} is the nonpolar acentric factor

For i - j , parameters $\left(\frac{\varepsilon_{ii}}{\kappa}\right)$, σ_{ii} and ω_{ii} are determined from pure component properties:

$$\omega_{ii} = 0.006026 R_{D_i} + 0.02096 R_{D_i}^2 - 0.001366 R_{D_i}^3 \tag{2.37}$$

$$\left(\frac{\varepsilon_{ii}}{\kappa}\right) = \left(\frac{\varepsilon_{ii}}{\kappa}\right)' \left\{ 1 - \xi c_1 \left[1 - \frac{\xi(1+c_1)}{2} \right] \right\} \tag{2.38}$$

$$\sigma_{ii} = \sigma_{ii}' (1 + \xi c_2)^{1/3} \tag{2.39}$$

$$\left(\frac{\varepsilon_{ii}}{\kappa}\right)' = T_{ci} \left[0.748 + 0.91\omega_{ii} - \frac{0.4\eta_{ii}}{2+20\omega_{ii}}\right] \quad (2.40)$$

$$\sigma_{ii} = (2.44 - \omega_{ii}) \left(1.0133 \frac{T_{ci}}{P_{ci}}\right)^{1/3} \quad (2.41)$$

$$\xi = 0 \quad \text{for } \mu_i < 1.45 \quad (2.42)$$

$$\xi = \frac{1.7941 \times 10^7 \mu_i^4}{\left[\left(2.882 - \frac{1.882 \omega_{ii}}{0.03 + \omega_{ii}}\right) T_{ci} \sigma_{ii}' \left(\frac{\varepsilon_{ii}}{\kappa}\right)\right]} \quad \text{for } \mu_i \geq 1.45 \quad (2.43)$$

$$c_1 = \frac{16+400\omega_{ii}}{10+400\omega_{ii}} \quad (2.44)$$

$$c_2 = \frac{3}{10+400\omega_{ii}} \quad (2.45)$$

Where, R_{D_i} , is the mean radius of gyration of component i (Angstroms), T_{ci} , is the critical temperature of component i (K), P_{ci} , is the critical pressure of component i (bar), and the cross parameters $\left(\frac{\varepsilon_{ij}}{\kappa}\right)$, σ_{ij} and ω_{ij} ($i \neq j$) are calculated from mixing rules and pure component parameters given by:

$$\omega_{ii} = \frac{1}{2} (\omega_{ii} + \omega_{jj}) \quad (2.46)$$

$$\left(\frac{\varepsilon_{ij}}{\kappa}\right) = \left(\frac{\varepsilon_{ij}}{\kappa}\right)' (1 + \xi' c_1') \quad (2.47)$$

$$\sigma_{ij} = \sigma_{ij}' (1 - \xi' c_1') \quad (2.48)$$

Where

$$\left(\frac{\varepsilon_{ij}}{\kappa}\right)' 0.7 \left[\left(\frac{\varepsilon_{ii}}{i}\right) \left(\frac{\varepsilon_{ij}}{\kappa}\right) \right]^{1/2} + \frac{0.6}{\left[\frac{1}{\left(\frac{\varepsilon_{ii}}{\kappa}\right)} + \frac{1}{\left(\frac{\varepsilon_{jj}}{\kappa}\right)}\right]} \quad (2.49)$$

$$\sigma_{ij}' = (\sigma_{ii}\sigma_{jj})^{1/2} \quad (2.50)$$

$$\xi' = \frac{\mu_i^2 \left(\frac{\varepsilon_{jj}}{\kappa}\right)^{\frac{2}{3}} \sigma_{ij}^4}{\left(\frac{\varepsilon_{ii}}{\kappa}\right) \sigma_{ij}'^6} \quad \text{for } \mu_i \geq 2 \text{ and } \mu_j = 0 \quad (2.51)$$

Or

$$\xi' = \frac{\mu_j^2 \left(\frac{\varepsilon_{kk}}{\kappa}\right)^{\frac{2}{3}} \sigma_{ij}^4}{\left(\frac{\varepsilon_{ii}}{\kappa}\right) \sigma_{ij}'^6} \quad \text{for } \mu_j \geq 2 \text{ and } \mu_i = 0 \quad (2.52)$$

Or

$$\xi' = 0 \quad \text{for all values of } \mu_i \text{ and } \mu_j \quad (2.53)$$

$$c_1' = \frac{16+400\omega_{ij}}{10+400\omega_{ij}} \quad (2.54)$$

$$c_2' = \frac{3}{10+400\omega_{ij}} \quad (2.55)$$

2.2.3. Liquid-Phase Activity Coefficient Models

From equation 2.13, it is clear that the activity coefficient is a measure of the departure of a real solution behaviour from ideal solution behaviour. It can be formally defined by considering the fundamental excess property relation as given by Smith *et al.*, (2005):

$$d\left(\frac{nG^E}{RT}\right) = \frac{nV^E}{RT} dP - \frac{nH^E}{RT^2} dT + \sum_i \ln\gamma_i dn_i \quad (2.56)$$

G^E is the molar excess Gibbs energy, V^E is the molar excess volume, and H^E is the molar excess enthalpy. By taking the partial derivative with respect to number of moles of component i , n_i the activity coefficient is defined:

$$\ln \gamma_i = \left[\frac{\partial \left[n \left(\frac{G^E}{RT} \right) \right]}{\partial n_i} \right]_{T,P,n_{j \neq i}} \quad (2.57)$$

Further from equation 2.56, the change of the Gibbs Excess energy, G^E , with temperature is given by the Gibbs-Helmholtz relation and can be used to define the excess enthalpy, H^E :

$$H^E = -RT^2 \left[\frac{\partial \left[\left(\frac{G^E}{RT} \right) \right]}{\partial T} \right]_{P,x_i} \quad (2.58)$$

This implies that the activity coefficient and the excess enthalpy can be calculated from a model of the excess Gibbs energy. Prausnitz *et al.*, (1998) states that many equations have been proposed for the excess Gibbs energy. The models used in this work to correlate the phase equilibrium data of the liquid phase were the NRTL model Renon and Prausnitz, (1968) and UNIQUAC model (Abrams and Prausnitz, 1975).

2.2.3.1. Non-Random Two-Liquid (NRTL) Activity Coefficient Model

The NRTL model was proposed by Renon and Prausnitz, (1968) as an improvement to the Wilson activity coefficient model (Wilson, (1964)) which fails to model the LLE behaviour of systems exhibiting partial immiscibility. For this work, the NRTL model is preferred due to its ability to address the issue of partial miscibility, which arises in mixtures of butan-1-ol and water, explored in the simulation component of this work. The NRTL model can describe VLE and LLE of strongly nonideal solutions. The model employs binary interaction parameters of the constituents within the system of interest and can handle combinations of polar and non-polar compounds. The Gibbs excess energy equation for the NRTL model is given by:

$$\frac{G^E}{RT} = - \sum_{i=1}^n x_i \frac{\sum_{j=1}^m \tau_{ji} G_{ji} x_j}{\sum_{l=1}^m G_{li} x_l} \quad (2.59)$$

Expressions for the activity coefficient are given by:

$$\ln \gamma_i = \frac{\sum_{j=1}^m \tau_{ji} G_{ji} x_j}{\sum_{l=1}^m G_{li} x_l} + \sum_{j=1}^m \frac{x_j G_{ij}}{\sum_{l=1}^m G_{lj} x_l} \left(\tau_{ij} - \frac{\sum_{r=1}^m x_r \tau_{rj} G_{rj}}{\sum_{l=1}^m G_{lj} x_l} \right) \quad (2.60)$$

Where:

$$G_{ij} = \exp(-\alpha_{ij} \tau_{ij}) \quad (2.61)$$

$$\tau_{ij} = \left(a_{ij} + \frac{b_{ij}}{T} \right) \quad (2.62)$$

The non-randomness parameters α_{ij} , is commonly set to a fixed value. Walas, (2013) recommended a value of:

- 0.3 for nonpolar substances, nonpolar with polar non-associated liquids and small deviations from ideality
- 0.4 for saturated hydrocarbons with polar non-associated liquids and systems that exhibit liquid-liquid immiscibility (LLE)
- 0.47 for strongly self-associated substances with nonpolar substances
- Regress the parameter if it provides a superior fit of the experimental data

τ_{ij} is the temperature dependent version of the binary interaction parameter, where a_{ij} and b_{ij} are the binary interaction parameters for the model that must be determined from the regression of phase equilibrium data.

2.2.3.2. Universal Quasi-Chemical Activity Coefficient (UNIQUAC) Model

The UNIQUAC activity coefficient model was originally derived by Abrams and Prausnitz, (1975) as an extension to the Wilson equation. The model is recommended for highly non-ideal chemical systems and can be used for VLE and LLE applications Bondi, (1964). It only has two adjustable parameters if temperature dependence is not considered and can readily be extended to multicomponent mixtures. The Gibbs excess energy expression is divided into a combinatorial part (due to entropy/size and shape) and a residual part (due to energy interactions):

$$G^E = G^{E,C} + G^{E,R} \quad (2.63)$$

The $G^{E,C}$ term is determined by the shapes and sizes of the molecules and only requires pure species data such as surface area parameters (q_i) and volume parameters (r_i). The $G^{E,R}$ term is determined by intermolecular forces. The Gibbs excess energy equation for the UNIQUAC model is given by:

$$\frac{G^E}{RT} = \sum_{i=1}^c x_i \ln \frac{\psi_i}{x_i} + \frac{\bar{Z}}{2} \sum_{i=1}^c q_i x_i \ln \frac{\theta_i}{\psi_i} - \sum_{i=1}^c q_i x_i \ln \left(\sum_{j=1}^c \theta_i \tau_{ji} \right) \quad (2.64)$$

Expressions for the activity coefficient are given by:

$$\begin{aligned} \ln \gamma_i = \ln \gamma_i^C + \ln \gamma_i^R = \ln \frac{\psi_i}{x_i} + \frac{\bar{Z}}{2} q_i \ln \frac{\theta_i}{\psi_i} + l_i - \frac{\psi_i}{x_i} \sum_{j=i}^c x_j l_j \\ + q_i \left[1 - \ln \left(\sum_{j=1}^c \theta_i \tau_{ji} \right) - \sum_{j=1}^c \left(\frac{\theta_i \tau_{ij}}{\sum_{k=1}^c \theta_k \tau_{kj}} \right) \right] \end{aligned} \quad (2.65)$$

Where:

$$\psi_i = \frac{x_i r_i}{\sum_{i=1}^c x_i r_i} \quad (2.66)$$

$$\theta = \frac{x_i q_i}{\sum_{i=1}^c x_i q_i} \quad (2.67)$$

$$\tau_{ij} = \left(a_{ij} + \frac{b_{ij}}{T} \right) \quad (2.68)$$

$$l_j = \frac{\bar{Z}}{2} (r_j - q_j) - (r_j - 1) \quad (2.69)$$

$$z = 10 \quad (2.70)$$

2.3. The Gamma-Phi (γ - Φ) Formulation for Vapour-Liquid Equilibrium

The combination of the activity coefficient and vapour correction factor allows for the modelling of real VLE behaviour for sub-atmospheric to moderate pressures. This approach is usually termed the gamma-phi (γ - Φ) formulation and requires a fitting procedure to satisfy the isofugacity condition given by equation (2.15). Note that the φ - φ formulation was not considered in this work, as the system pressures were low enough to not expect any significant improvement over the γ - Φ formulation Walas, (2013).

In the γ - Φ formulation, the fitting procedure used for bubble point calculations is attributed to Barker, (1953) (Barker's method), and uses the summability relation to first eliminate the vapour composition from equation (2.17). Activity coefficient binary interactions are fitted using an optimization algorithm and pressures are calculated. Vapour compositions are then calculated. The fitting procedure for the γ - Φ approach for a bubble point calculation is shown in Figure 2.1. In this work Aspen Plus V10 software was used for the VLE data modelling. The ordinary least squares objective function was used to minimize the pressure residual:

$$OF = \delta P = \sum (P^{exp} - P^{calc})^2 \quad (2.71)$$

Where the objective function (OF) is given by the pressure difference (δP) between the experimental (P^{exp}) and model calculated pressures (P^{calc}).

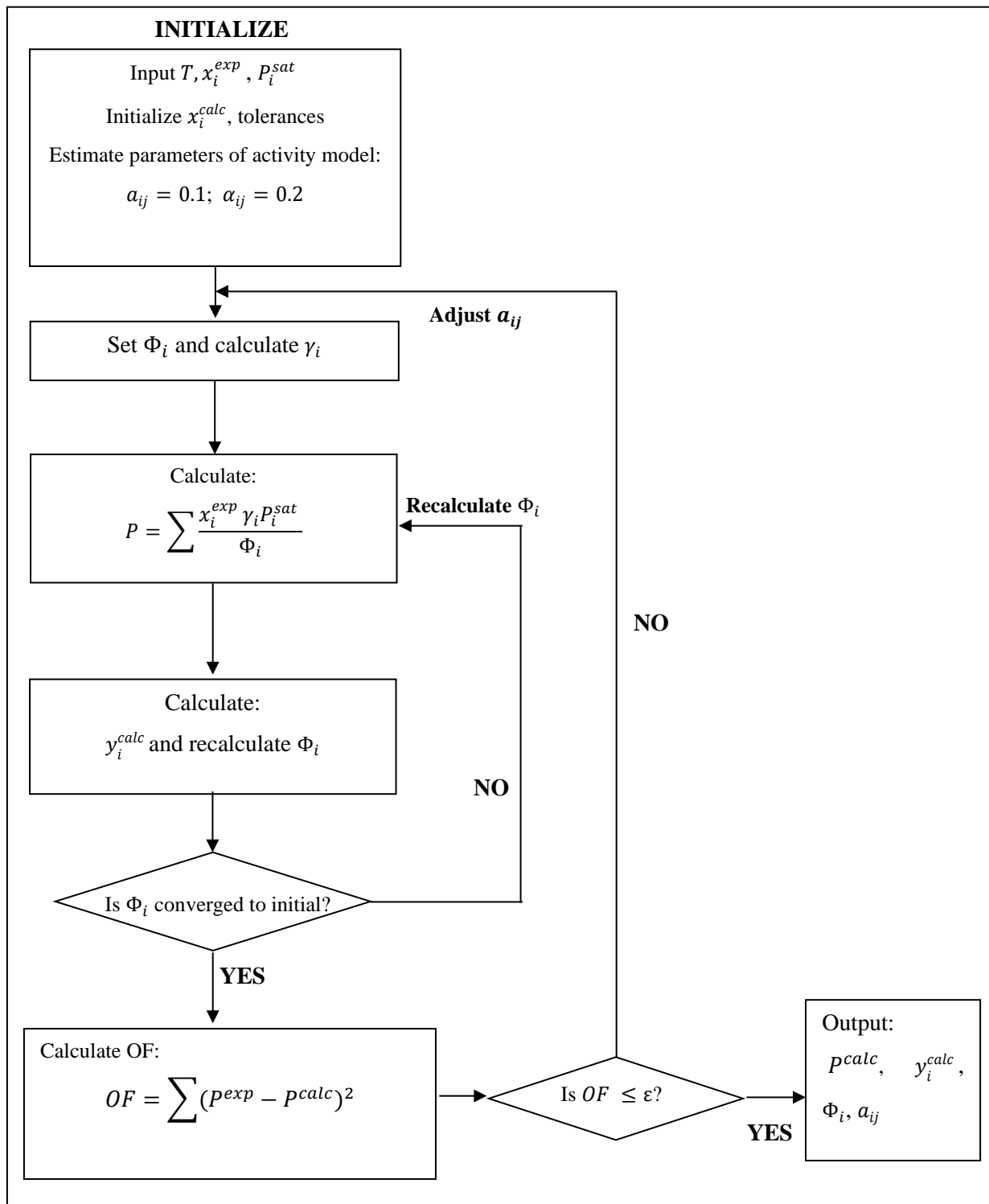


Figure 2.1. Algorithm used for the regression of isothermal VLE data using the γ - Φ method
 Walas, (2013).

2.4. Thermodynamic Consistency Tests

In the procedure used in this work for VLE measurements, pressure, temperature, liquid composition and vapour composition are measured for binary systems. Consequently, according to the phase rule, the system is over-specified. Therefore, the VLE data can be subjected to thermodynamic consistency testing, which establishes if the calculated values of any one of the four measured parameters (calculated from the three other measured parameters), corresponds to the experimental data of that parameter.

Mathematically, consistency is generally assessed by coherence with the Gibbs-Duhem relation Smith *et al.*, (2005):

$$\sum x_i d \ln \gamma_i = -\frac{V^E}{RT} dP + \frac{H^E}{RT^2} dT \quad (2.72)$$

The experimental VLE data must agree with the condition of the Gibbs-Duhem relation. For low to moderate pressure isothermal VLE, the area and point test are usually applied Raal and Mühlbauer, (1998). In an extensive study, Wisniak *et al.* (2017) have recommended the point test of Fredenslund *et al.* (1977) for isothermal VLE data, in combination with an additional test, such as the area test of Redlich and Kister (1948).

2.4.1. The Area Test

The area test of Redlich and Kister Redlich and Kister, (1948) compares the areas under the experimental $\ln \gamma_i$ curves for each species for the entire composition range. This is determined by considering the special case of constant temperature and pressure in equation 2.72.

$$\int_0^1 \ln \left(\frac{\gamma_1}{\gamma_2} \right) dx_1 = 0 \quad (2.73)$$

In a plot of $\ln \left(\frac{\gamma_1}{\gamma_2} \right)$ vs. x_1 , the ratio of the areas above and below the x-axis must be within a tolerance of at least 10% for the data to be considered consistent by the area test. More stringent tolerances are also often recommended to ensure the test has truly been passed (Van Ness, 1995). This tolerance is necessary, since in isothermal VLE measurements over the composition range, the system pressure varies. Hence, in actuality,

$$\int_0^1 \ln \left(\frac{\gamma_1}{\gamma_2} \right) dx_1 = -\int_{P_2^{sat}}^{P_1^{sat}} \frac{V^E}{RT} dP \quad (2.74)$$

The right-hand side of equation 2.74 is usually small in relation to the left and is therefore considered negligible.

2.4.2. The Point Test

The point test of Fredenslund et al. (1977) is based on the test proposed by Van Ness *et al.*, (1973). Since the vapour composition measurement is often the most unreliable measurement taken in VLE measurements Smith *et al.*, (2005), the experimental value is compared to the calculated vapour compositions from the (P, T, x_i) measurements. This difference is termed the absolute average deviation for the point test (AAD_{point}) and must usually be below 0.01. The AAD_{point} is given by:

$$AAD_{point} = \frac{1}{N} \sum_{i=1}^N |\Delta y - \Delta \bar{y}| \quad (2.75)$$

Where N is number of data points, Δy is the difference between experimental and calculated data and $\Delta \bar{y}$ is the average of Δy Narasigadu, (2011). For the point test of Fredenslund et al. (1977) a Legendre polynomial is used to fit the experimental VLE data, and to calculate Δy and ΔP . In order for the data to pass the test, the tolerance for Δy of 0.01 must be met, and the deviations, Δy and ΔP must randomly scatter as both positive and negative deviations as recommended by Wisniak et al. (2017).

2.5. Calculation of Infinite Dilution Activity Coefficients

Infinite dilution activity coefficients are necessary for the design of high purity separation units. They are generally measured directly by specialist methods such as ebulliometry, gas stripping, or differential static methods Raal and Mühlbauer, (1998). They can also be estimated from VLE data using extrapolative methods such as through an activity coefficient model, or by the model independent approach of Maher and Smith, (1979). In the Maher and Smith method, a deviation pressure is defined, P_D , is defined as:

$$P_D = P - [P_2^{sat} + (P_1^{sat} - P_2^{sat})x_1] \quad (2.76)$$

Where P is the total pressure and P_i^{sat} , the saturated vapour pressures of components 1 and 2

Taking the derivative of (2.76) with respect to x_1 yields:

$$\frac{dP_D}{dx_1} = \frac{dP}{dx_1} - (P_1^{sat} - P_2^{sat}) \quad (2.77)$$

And using L'Hôpital's rule gives the dilution points:

$$\left(\frac{P_D}{x_1 x_2}\right)_{x_1=0}^{\infty} = \left(\frac{dP_D}{dx_1}\right)_{x_1=0}^{\infty} \quad (2.78)$$

$$\left(\frac{P_D}{x_1 x_2}\right)_{x_1=1}^{\infty} = -\left(\frac{dP_D}{dx_1}\right)_{x_1=1}^{\infty} \quad (2.79)$$

If a plot of $\frac{P_D}{x_1 x_2}$ vs. x_1 is linear, the extrapolation to the end points is possible. Alternatively, the inverses can be plotted ($\frac{x_1 x_2}{P_D}$ vs. x_1) if a better linearity can be achieved:

$$\left(\frac{x_1 x_2}{P_D}\right)_{x_1=0}^{\infty} = \left[\left(\frac{dP_D}{dx_1}\right)_{x_1=0}^{\infty}\right]^{-1} \quad (2.80)$$

$$\left(\frac{x_1 x_2}{P_D}\right)_{x_1=1}^{\infty} = -\left[\left(\frac{dP_D}{dx_1}\right)_{x_1=1}^{\infty}\right]^{-1} \quad (2.81)$$

The method cannot be applied if a reasonable linear relationship between the parameters above cannot be determined.

However, if a linear plot can be extrapolated to the end points, $\left(\frac{\partial P}{\partial x_1}\right)_{x_1=0}^{\infty}$ can be calculated at a specific end point ($x_1 = 0, x_1 = 1$). $\frac{dP}{dx_1}$ can then be used to calculate the activity coefficient at infinite dilution using parameters from the virial equation of state as shown by Pividal *et al.*, (1992):

$$\gamma_i^{\infty} = \varepsilon_i^{\infty} \frac{P_j^{sat}}{P_i^{sat}} \left[1 + \beta_j \frac{1}{P_j^{sat}} \left(\frac{dP}{dx_i}\right)_{T}^{x_1 \rightarrow 0} \right] \quad (2.82)$$

Where

$$\varepsilon_i^{\infty} = \exp \left[\frac{(B_{ii} - V_i^L)(P_j^{sat} - P_i^{sat}) + \delta_{ij} P_j^{sat}}{RT} \right] \quad (2.83)$$

$$\beta_j = 1 + P_j^{sat} \left[\frac{(B_{jj} - V_j^L)}{RT} \right] \quad (2.84)$$

And

$$\delta_{ij} = 2B_{ij} - B_{ii} - B_{jj} \quad (2.85)$$

CHAPTER THREE

Equipment, Experimental, and Simulation

Low pressure vapour-liquid equilibrium measurements can be performed by the static or dynamic method. Raal and Mühlbauer, (1998) provide an excellent review of these methods. Commonly, the dynamic method is suitable for systems where online sampling is not required (systems with low toxicity and mixture vapour pressures above 1 kPa). Due to equipment availability and known functionality Moodley *et al.*, (2013), (2018), Moodley and Dorsamy, (2018), Benecke *et al.*, (2019) the dynamic method was used to measure the VLE data in this work, hence static methods will not be discussed further. In this chapter a brief review of dynamic stills is provided, with focus on circulation of both the liquid and vapour phases. The device components used in this work are also discussed, along with the calibration procedures. The experimental layout and procedure are discussed in more detail in the subsequent chapters as part of the manuscripts.

3.1. Dynamic Still Review

The dynamic or circulation method for low to moderate pressure VLE measurement is well studied in the literature. For a detailed review, the reader is referred to the text of Raal and Mühlbauer, (1998). The apparatus operates analogously to a packed distillation column operating at total reflux. A liquid mixture of the system under consideration is loaded into the boiling chamber of the device. Separation occurs in a packed equilibrium chamber. The vapour generated is condensed, collected and then siphoned back into the boiling chamber, and the liquid phase is also circulated through the chamber. Sampling of the condensed vapour and liquid phases allows for the analysis of the phases at equilibrium. The temperature and pressure at equilibrium is measured and controlled using a heat and over pressure/vacuum source. In this work, a modified version of the still of Raal and Mühlbauer, (1998), commissioned initially by Joseph *et al.*, (2001) was used for VLE measurements, which is based on earlier designs of Othmer, (1928), Gillespie, (1946) and Yerazunis *et al.*, (1964). Details of these apparatuses can be found in the original publications.

One of the earliest designs for recirculation stills was the Othmer still (Othmer, (1928)) which employed vapour-recirculation only. Temperature measurement was in the liquid chamber yielding unreliable results. The condensation of the vapour-phase occurring on the wall of the boiling chamber, poor mixing in the reboiler, vapour backflow and flashing out prompted further improvements by the researchers. Gillespie, (1946) incorporated a Cottrell-type pump (Cottrell, (1919)), which improved one-directional vapour flow, and allowed for temperature measurement of the true saturated vapour-yielding more precise

equilibrium temperature measurements Coulson *et al.*, (1948). The design of Rose and Williams, (1955) used the vapour phase as a thermal barrier which allowed the vapour to flow up through the equilibrium chamber. Heertjies, (1960) proposed using a packing material after the Cottrell tube to improve mass transfer efficiency.

The issues of long equilibrium time, heat losses to the atmosphere, poor mixing and disturbances during sampling were addressed in the work of Yerazunis *et al.* (1964). Yerazunis *et al.* (1964) proposed a packed equilibrium chamber, which improved equilibration times. Additionally, a vacuum jacketed Cottrell pump and equilibrium chamber, and lagged vessel prevented heat losses to the atmosphere. Thermodynamically consistent data have been reported in the literature when using this apparatus, Raal and Ramjugernath, (2005).

The design of Joseph *et al.*, (2001) shown in Figure 3.1 follows on from the studies of Heertjies, (1960) and Yerazunis *et al.* (1964). A lagged, vacuum-jacketed stainless-steel mesh-packed equilibrium chamber and Cottrell pump are employed. These allow for rapid attainment of equilibrium. The mesh packing structure reduces pressure losses across the bed; hence pressure fluctuations are minimized. The Cottrell pump reduces concentration and temperature gradients in the equilibrium chamber. Two heater sources (external and internal) are incorporated, which in addition to the vacuum jacket, also reduce heat losses to the environment and prevent disturbances caused by ambient conditions. These heat sources ensure quick, smooth boiling. The internal heat source is controlled manually to establish the plateau region between heat input and temperature when operating just above the two-phase region. Sufficient heat input is necessary to slightly superheat the vapour through the Cottrell pump, to overcome the energy loss due to hydrostatic head Kneisl *et al.*, (1989). When sufficient heat is supplied, a slight increase in the heat input will not cause the temperature of the vapour exiting the Cottrell pump to change in the true plateau region. For the systems containing alcohols and di-alcohols considered in this work, special consideration was given to maintain the true plateau region, as these can generally be quite difficult to establish for such components with complex intermolecular interactions. Multiple pseudo-plateau regions can occur, hence trial and error is used to establish the true region.

The configuration is designed with the aim of achieving equilibrium in a single pass. Thorough mixing in the boiling chamber and vapour collector is achieved with external magnetic stirring. Additional details of similar designs can be found in the thesis of Joseph, (2001).

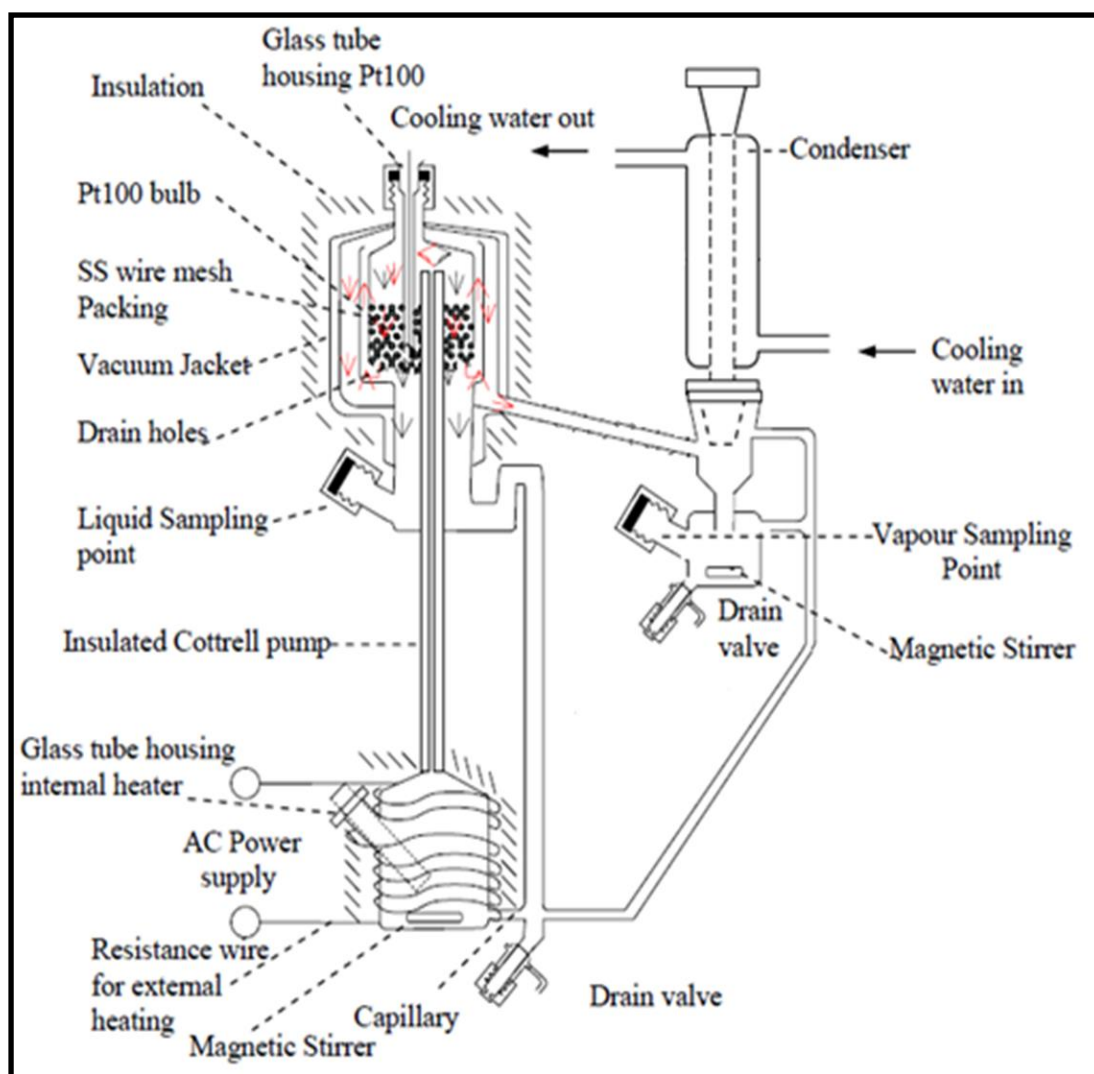


Figure 3.1. Schematic of the apparatus of Joseph *et al.*, (2001) used in this work as shown in Ndlovu, (2005).

3.2. Equipment Layout and Item List

Figure 3.2. shows the layout of the apparatus used in this work along with auxiliary components and the equipment list with relevant suppliers. Details of the layout are provided in the work of Joseph, (2001).

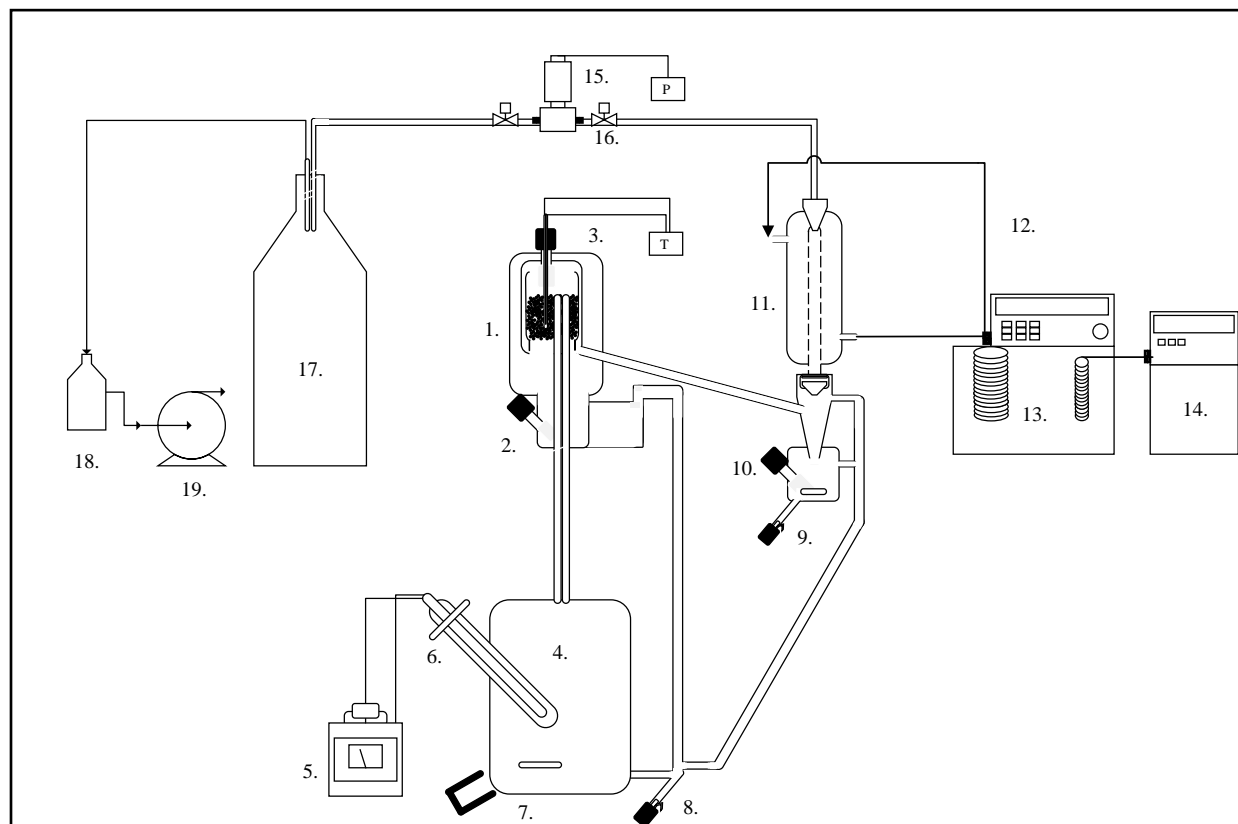


Figure 3.2. Layout of the apparatus of Joseph et al. (2001) used in this work (as shown in Mavalal et al. (2019)).

1-Equilibrium chamber. 2-Liquid sampling port. 3-Temperature measurement (Pt-100). 4-Lagged oiling chamber. 5- Variable heat supply to boiler. 6- Heater cartridge and sleeve. 7- Magnetic stirrer and bead. 8- Boiler drain valve. 9- Condensate drain valve. 10- Vapour condensate sampling point. 11- Condenser. 12- Coolant line to condenser. 13. Coolant bath (Thermo Scientific) and controller (PolyScience 7306A11B). 14- Chiller (Polyscience FT25). 15- Pressure measurement (WIKA P-10 transducer) and controller (ABB F080). 16. Isolation valves. 17- Ballast tank. 18. Cold trap. 19. Vacuum pump (Edwards).

3.3. Cleaning and leak testing of the apparatus

The VLE still and auxiliary lines must be cleaned thoroughly before use. Pure acetone is used to clean the still, by filling the boiling chamber and running the still as though a vapour pressure measurement were being performed. Circulation is allowed for 30 minutes and then the acetone is drained out. The process is

repeated, and finally the still and lines are dried under vacuum. The still is then leak tested by inducing a vacuum and isolating the still and lines. The pressure within the still is observed. If the pressure climbs toward atmospheric pressure, a leak is present and is detected by carefully dripping acetone onto all joints. A leaking joint will cause a sudden jump in the still pressure, as the acetone would exert a vapour pressure on the pressure device. The seal at the joint is improved depending on the material (tightening steel joints, vacuum grease, thread tape, etc.).

3.4. Calibrations

3.4.1. Temperature Calibration

The Pt-100 temperature sensor used in this work was calibrated against a WIKA CTH 6500 standard temperature sensor. Both probes were inserted into a WIKA CTB 9100 oil bath. The setpoint temperature of the bath was increased from 303 K to 390 K in increments of 10 K. An increase run was first performed, followed by a decrease run and a second increase run, following the same temperature increments with thermal equilibration achieved at each increment. The experimental temperature was plotted against the standard temperature to obtain the temperature calibration curve and the deviation plot was also plotted. The maximum deviation was estimated to be within 0.1 K from calibration. The temperature calibration and deviation plots are presented in Figure A1 in Appendix A.

3.4.2. Pressure Calibration

A WIKA P-10 transducer (0-1 bar, 0.05 kPa supplier uncertainty) was used for pressure measurements. The pressure transducer was calibrated using a WIKA CPH 6000 standard. The actual pressure was then plotted against the set pressure of the still and the deviation was plotted. The maximum pressure deviation from calibration was estimated to be within 0.1 kPa. The pressure calibration and deviation plots are presented in Figure A2 in the appendices.

3.4.3. Gas chromatograph calibrations

A Shimadzu GC 2014 with a thermal conductivity detector was used to determine the compositions of the liquid- and vapour-phase samples using a POROPAK-Q column (2 m x 2.2 mm). The carrier gas selected for the GC was helium. Suitable operating conditions for the GC were selected for optimal and accurate sampling; a temperature of 513.15 K for the injector, column and sample detector with a carrier gas flow of 30 ml/min. The GC was calibrated using the area ratio method. Standard gravimetrically prepared samples using a Mettler-Toledo mass balance (model AB204-S) with an uncertainty of 0.00010 g, were

used for the calibration. The composition range was divided into two regions, rich and dilute in each component. Peak repeatability for calibration was well within 1% and was conducted in triplicate. The deviation in composition from GC calibration did not exceed 0.002 mole fraction. The composition calibration and deviation plots are presented in Appendix A (Figure A3 to Figure A12) respectively in the appendices.

3.5. Uncertainties

Standard combined uncertainties ($u_c(\theta)$) for the measured variables (θ) i.e., temperature, pressure and composition were determined by the propagation of error using the procedures outlined by JCGM ISO, (2008):

$$u_c(\theta) = \sqrt{\sum u_i(\theta)^2} \quad (3.1)$$

Where $u_i(\theta)$ is the standard uncertainty for a particular variable (θ) from source i . Sources can include calibration uncertainty, precision of correlation, repeatability, accuracy, reported precision of device, stability, chemical purity etc.

For temperature and pressure, the combined uncertainties were calculated from:

$$u_c(T) = \sqrt{u_{calib}(T)^2 + u_{prec}(T)^2 + u_{stab}(T)^2} \quad (3.2)$$

$$u_c(P) = \sqrt{u_{calib}(P)^2 + u_{prec}(P)^2 + u_{stab}(P)^2} \quad (3.3)$$

Where u_{calib} , u_{prec} , u_{stab} are the calibration, device precision and stability during experiments for each parameter, respectively. Note that the uncertainty from the in-house calibration (u_{calib}), includes the uncertainty due to the accuracy and repeatability of each device.

The standard combined uncertainty for composition is calculated by:

$$u_c(x_i) = \sqrt{u_{calib}(x_i)^2 + u_{bal}(x_i)^2 + u_{pur}(x_i)^2 + u_{rep}(x_i)^2} \quad (3.4)$$

Where u_{bal} , u_{pur} , u_{rep} are the standard uncertainties due to the mass balance used for calibration sample preparations, due to the chemical purity and the repeatability during phase sampling respectively. The uncertainty breakdown can be found in Table B1 in Appendix B.

3.6. Confirmation of procedure

In order to confirm the functioning of the experimental equipment and procedure, the measurable vapour pressures of the chemicals used for the novel systems were measured and compared to correlations from the literature. This comparison is presented in Figure 3.3(a). A deviation plot between the measurements from this work and the literature is presented in Figure 3.3(b). These deviations are attributed to the uncertainties in temperature and pressure in this study, and the uncertainties of the correlations themselves. For the confirmation of the procedure for mixture measurements, the vapour-liquid equilibrium data were measured for the water (1) + propan-1-ol (2) mixture at 313.2 K and compared to literature in Figure 3.4. This system has been well studied in the research group. A good comparison with literature, within experimental uncertainty was observed. Deviations in pressure and composition did not exceed 5% with all literature data. Note that the calibration curves and tabulated data for this system can be found in Appendix A (Figures A3-A4) and Appendix C (Tables C1-C2).

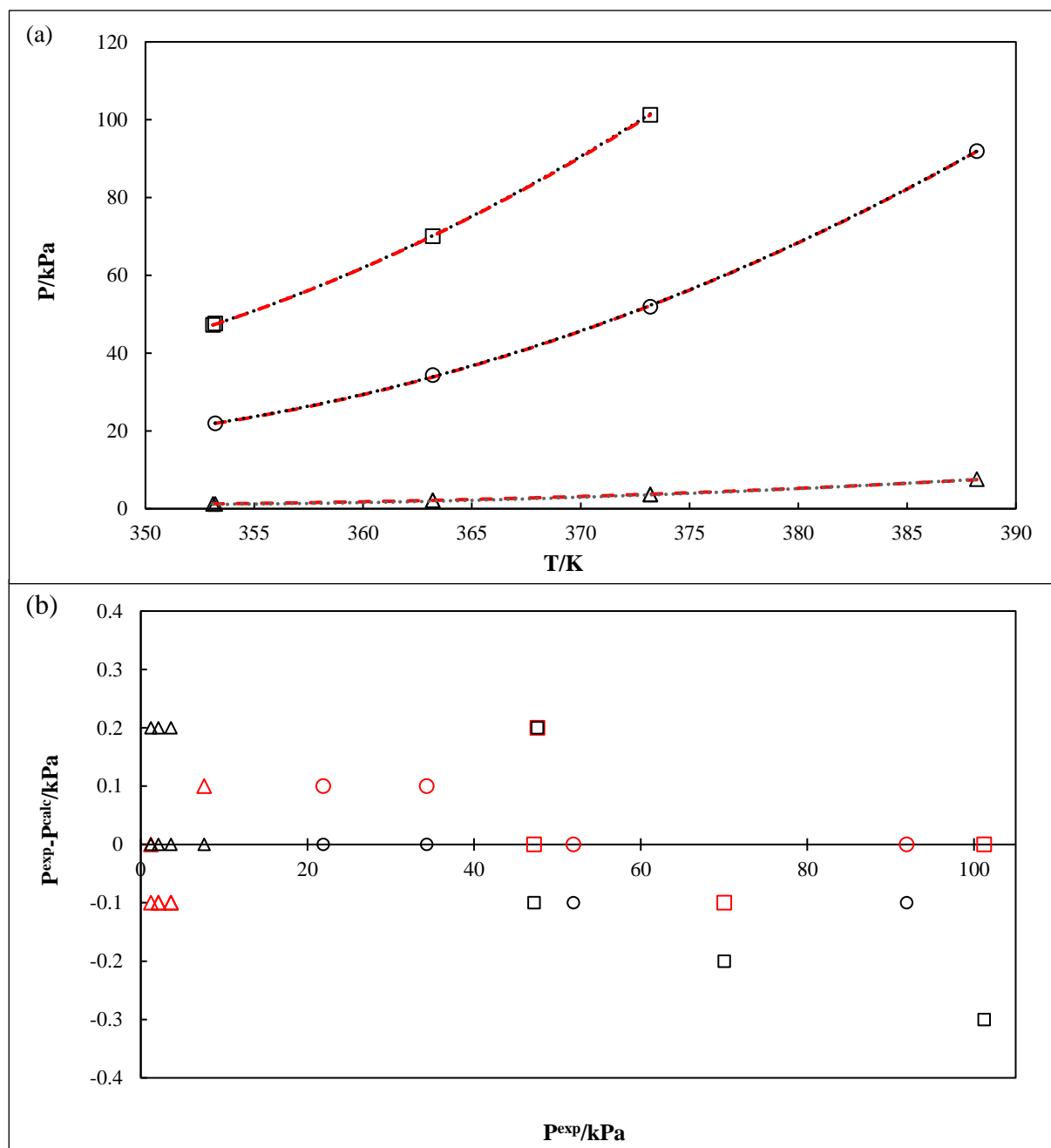


Figure 3.3. (a) Experimental vapour pressures (kPa) vs temperature (K) for water (□), butan-1-ol (○) and butane-2,3-diol (Δ). Red lines are predictions by the Antoine equation Poling *et al.*, (2001) and black lines are predictions by the Wagner equation NIST, (2019). (b) Deviations of experimental data from each predictive model with deviations for water (□), butan-1-ol (○) and butane-2,3-diol (Δ) given by red symbols for the Antoine equation and black symbols for the Wagner equation.

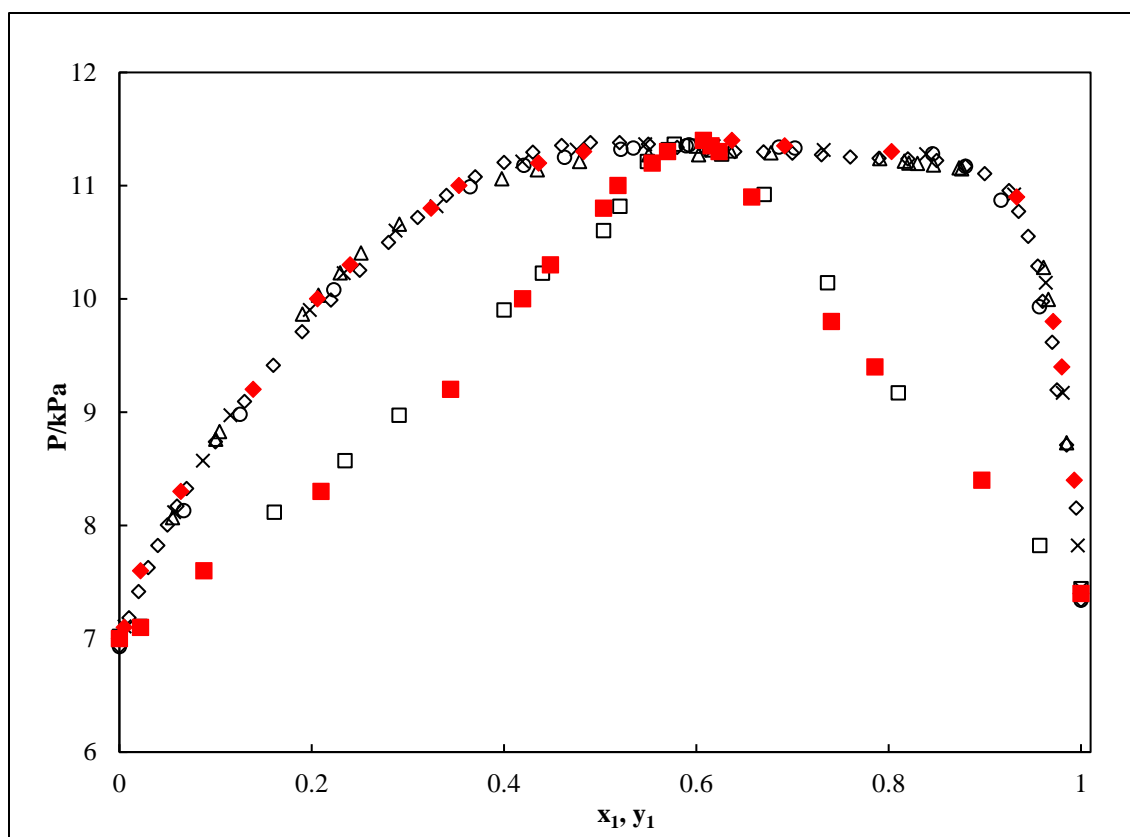


Figure 3.4. P - x - y plot for the water (1) + propan-1-ol (2) system at 313.2 K. ◆, P - x data (This work); ■, P - y data (This work); Δ, P - x data (Zielkiewicz and Konitz, (1991)); ○, P - x data (Moodley *et al.*, (2013)); ◇, P - x data Moodley *et al.*, (2019); ×, P - x data Moodley *et al.*, (2019); □, P - y data Moodley *et al.*, (2019).

3.3. Simulation Work

The steady-state design of the test and experimental system were performed on Aspen Plus®. The cost and economic feasibility of the systems were determined using Aspen Process Economics Analyser. Details of these procedures are outlined in Chapter 6.

CHAPTER FOUR

Isothermal Vapour-Liquid Equilibrium Measurements for the water + butane-1,4-diol/butane-2,3-diol system within 353.1 to 373.2 K

4.1. Abstract

The purpose of this study was to measure and model isothermal binary vapour-liquid equilibrium (VLE) data for the water + butane-1,4-diol/butane-2,3-diol system to aid in the design of separation processes. P - T - x - y phase equilibrium measurements were determined at three temperatures from approximately 353 to 373 K, utilizing a dynamic-analytic apparatus. The vapour-liquid phase equilibrium data were modelled using the $\gamma - \Phi$ approach with the Non-Random Two-Liquid and UNIQUAC activity coefficient models and the virial equation of state with the Hayden O'Connell correlation for the vapour correction. Thermodynamic consistency testing was performed using the point and area tests for the measured experimental VLE data. The experimental data sets passed both tests where the point and area tests employed a tolerance of 0.01 and 10%, respectively.

4.2. Introduction

An emerging area of research is the development of renewable biofuels which can be used interchangeably with fuels derived from petroleum sources. These alternative biofuels are termed “drop-in” fuels and can be used in their pure state or used as a blending constituent with other fuels Waldron, (2010), Harvey *et al.*, (2016), Zhang *et al.*, (2017), Haider *et al.*, (2018), van Dyk *et al.*, (2019). Components such as butane-1,4-diol and butane-2,3-diol have been identified as suitable drop-in fuels for use in certain transport applications due to their high octane-numbers and heating values (Harvey *et al.*, (2016), Satam *et al.*, (2019), van Dyk *et al.*, (2019)).

Butane-1,4-diol can be produced conventionally by the Reppe process which involves the reaction of formaldehyde with acetylene to produce butynediol, which is then hydrogenated to produce butane-1,4-diol Hort and Taylor, (2003), Haas *et al.*, (2005), Satam *et al.*, (2019). Alternatively, there have been several attempts to produce butane-1,4-diol from biological processes by the direct bioconversion of biomass and plant sugars using microorganisms, such as *Escherichia coli*, which are genetically engineered to achieve this conversion in a single step Waldron, (2010), Burgard *et al.*, (2016), Satam *et al.*, (2019).

Butane-2,3-diol can be produced following two chemical process routes. The chemical route (non-renewable process) involves the chlorohydration of butene with a subsequent hydrolysis step Haider *et al.*, (2018). The chemical route is a highly energy intensive process. An alternative route is a biochemical process (potentially renewable process) and has a lower energy consumption. This process step involves the fermentation of biomass by certain classes of microorganisms that includes *Bacillus licheniformis* Waldron, (2010), Penner *et al.*, (2017), Harvianto *et al.*, (2018).

In these processes, an aqueous solution with low to intermediate concentrations of butane-1,4-diol and butane-2,3-diol are produced. These process streams of butanediol/water mixtures require dehydration before they can be used in fuel blending, which is generally an energy intensive step.

Although conventional distillation is a technically viable separation technique to attain the dehydration and subsequent purification, the separation for these systems has a high energy demand, as high-pressure steam is often employed as the heating medium due to the low concentrations of the butanediol constituents, and because the normal boiling points of the butanediols exceed 450 K. Alternative separation processes requiring less energy have been proposed in the literature. These processes include pervaporation Shao and Kumar, (2009a), (2009b), reactive extraction Li *et al.*, (2012), liquid-liquid extraction Wu *et al.*, (2012) and salting-out extraction Wu *et al.*, (2014). Each separation technique possesses its own associated benefits, drawbacks and limitations with respect to its applicability in industrial operation and commercial-scale production. The most promising options which have been identified in the literature are hybrid techniques employing solvent extraction and recovery by distillation to first remove excess water and subsequently concentrate the required butanediol by removing the remaining water Haas *et al.*, (2005), Penner *et al.*, (2017), Haider *et al.*, (2018), Harvianto *et al.*, (2018), Satam *et al.*, (2019).

These processes are modelled and designed in the literature based on binary parameters derived from limited sources of incomplete isothermal vapour-liquid phase equilibrium for the water + butane-1,4-diol system, which has not been measured comprehensively in the region approaching the normal boiling point of water (a common operating region in the process industries). Isothermal P-x data for the water + butane-1,4-diol system is available in the literature in the range of 333 – 368 K Huang and Zhang, (1987), with the vapour phase poorly studied at isothermal conditions, while no isothermal phase equilibrium data exists for the system of water + butane-2,3-diol in the literature at these important conditions. Isothermal vapour-liquid equilibrium phase data is preferred for the modelling and design of high purity separation processes as they account for tray-to-tray energy balance calculations via the heat of mixing. To develop

thermodynamics models required to achieve the desired separation design and to improve the literature of these systems. Novel isothermal P - x - y phase equilibria data have been measured for the water + butane-1,4-diol system at 353.2, 363.2 and 373.2 K and for the water + butane-2,3-diol system at 353.1, 363.2 and 373.2 K using a dynamic apparatus for low pressure measurements designed by Raal and Mühlbauer, (1998). The VLE data was processed using the combined $(\gamma$ - $\Phi)$ approach. Thermodynamic consistency testing was performed on the measured VLE data using both the area and point tests.

4.3. Theory

4.3.1. Modelling Approach

The γ - Φ method is used extensively for the modelling of low-pressure VLE data. This method has been reviewed by several authors including Raal and Mühlbauer, (1998), Walas, (2013) and Gmehling *et al.*, (2012). To account for the liquid-phase non-ideality, an activity coefficient model is used since, at low pressures, an ideal solution reference state can be assumed for the liquid-phase. The vapour-phase non-ideality is corrected by the fugacity coefficient in solution with an equation of state such as the virial equation of state. The modified Raoult's law with vapour correction factor describes this relationship and is given by:

$$y_i \Phi_i P = x_i \gamma_i P_i^{sat} \quad (4.1)$$

Where for component i , x_i and y_i are the liquid- and vapour-phase compositions respectively, P is the total pressure, P_i^{sat} is the saturation pressure, γ_i is the activity coefficient and Φ_i is the vapour-phase correction factor given by:

$$\Phi_i = \frac{\hat{\phi}_i}{\hat{\phi}_i^{sat}} \exp \left[\frac{-V_i^L (P - P_i^{sat})}{RT} \right] \quad (4.2)$$

Where for component i , $\hat{\phi}_i$ and $\hat{\phi}_i^{sat}$ are the fugacity coefficient in solution and fugacity coefficient in solution at saturation, respectively, V_i^L is the molar volume of the liquid, R is the universal gas constant and T is the temperature.

Generally, the virial equation of state is employed to determine $\hat{\phi}_i$ and $\hat{\phi}_i^{sat}$ as it does not require system specific binary interaction parameters from experimental data and is applicable to low pressure VLE.

4.3.2. Model Selection

In this work, the Non-Random Two-Liquid Renon and Prausnitz, (1968) and UNIQUAC Abrams and Prausnitz, (1975) Gibbs free energy (activity coefficient) models were used to account for the non-idealities of the liquid-phase, while the vapour-phase non-ideality was accounted for using the virial equation of state with the Hayden and O'Connell, (1975) correlation.

The selection of the excess Gibbs free energy models, and the virial equation of state used in this work was based on the superior performance of these model combinations when compared to other models that were considered. Furthermore, the models are widely accepted to describe the phase behaviour of non-ideal systems in the low pressure (sub-atmospheric pressure) region, especially where strong intermolecular interactions such as association may occur Raal and Mühlbauer, (1998), Walas, (2013).

4.4. Experimental

4.4.1. Materials

Distilled, deionized water produced in-house, was used along with butanediol components sourced from Sigma-Aldrich to conduct the experimental measurements. Supplier mass purities were stated to be >0.99 mass fraction. The components were treated with a molecular sieve for 36 hours before they were used. The compositions of the pure components were validated by performing gas chromatography (GC) sampling, Karl-Fischer titration and refractive index measurements.

A Shimadzu GC 2014 was used to determine the compositions of the liquid- and vapour-phase samples using a POROPAK-Q column (2 m x 2.2 mm). The carrier gas selected for the GC was helium and a thermal conductivity detector was used. Suitable operating conditions for the GC were selected for optimal and accurate sampling; a temperature of 513.15 K for the injector, column and sample detector with a carrier gas flow of 30 ml/min. GC results of the pure component species revealed relative GC peak areas of >99.99%. To determine the water content of the butanediols, a Karl-Fischer (MKS 500) apparatus was used. The results were found to be less than 0.005 mass fraction. An ATAGO RX-7000 α refractometer (sodium D-line = 589 nm) with a supplier uncertainty of 0.00010 was used to determine the refractive indices. The results of the analyses of the pure component species are presented in Table 4.1.

4.4.2. Equipment and Uncertainties

To conduct the VLE measurements of the water and butanediol binary systems, the dynamic apparatus commissioned and procedure outlined by Joseph *et al.*, (2001) was used. This has also been described in

more detail in previous work by the Thermodynamics Research Unit at UKZN Benecke *et al.*, (2019), Mavalal *et al.*, (2019). Figure 4.1 shows a schematic of the dynamic still that was used to conduct the measurements. The operating pressures of the still were maintained by the action of an automatic pressure controller (ABB F080) utilizing vacuum and atmospheric air to maintain the desired pressure in the still.

The temperature was manipulated by using a voltage variac connected to a heater cartridge within the boiling chamber of the still. To mitigate temperature loss, the boiling chamber is insulated. Temperatures were measured using a type-A Pt-100 probe. Calibration of the temperature probe was performed using a WIKA CTB 9100 temperature standard. The standard combined temperature uncertainty was found to be 0.10 K. The pressure of the system was measured utilizing a WIKA P-10 transducer. The pressure transducer was calibrated using a WIKA CPH 6000 standard. The uncertainty of the device from the supplier was stated as 0.050 kPa. The standard combined uncertainty for pressure was found to be 0.12 kPa.

The proposed area ratio method outlined by Raal and Mühlbauer, (1998) was used to calibrate the gas chromatograph thermal conductivity detector. Standard gravimetrically prepared samples using a Mettler-Toledo mass balance (model AB204-S) with an uncertainty of 0.00010 g, were used. The combined standard uncertainty for the composition was calculated to be ± 0.0040 mole fraction and includes uncertainty due to chemical impurities. Uncertainties of the temperature, pressure and composition were determined by the propagation of errors of type A and B and included supplier uncertainty, uncertainty from calibration and uncertainty from repeatability. The uncertainty calculations followed the NIST JCGM ISO, (2008) guide. The equilibrium condition was established by observing a steady condensation drop rate, (60-90 drops per min), a continuous steady flow through the Cottrell tube, and a constant composition upon sampling (conducted in triplicate).

4.5. Results and Discussion

The vapour pressures of the pure components of water and butane-2,3-diol were measured using the dynamic method, the results of which are presented in Table 4.2 with comparisons to vapour pressures using parameters from the literature for the Antoine and Wagner equations, reported by Poling *et al.*, (2001) and NIST ThermoData Engine via Aspen Plus® V10 NIST, (2019). A good correlation was found between the measured data and the data from the literature correlations, within the experimental uncertainty in temperature and pressure. The minor deviations can also be ascribed to the uncertainties introduced by the purities of the pure components used. It must be noted that due to the limitations of the equipment and procedure used regarding the achievable vacuum and pressure uncertainty, the vapour pressure of pure

butane-1,4-diol was not measured, as the values are very low, approaching the pressure uncertainty. Nevertheless, the comparison of the vapour pressures of water and butane-2,3-diol to the literature data validates the accuracy of the temperature and pressure measurements by the dynamic apparatus.

The water (1) + butane-1,4-diol (2) system has been measured previously in the literature Jelinek *et al.*, (1976), Huang and Zhang, (1987) at some overlapping conditions presented here. P-x data is available for this system at 353 and 363 K. T-x-y data is also available at approximately 373.3 K. This data is compared to the data presented in this work in Figure 4.2. A close correlation exists at most conditions, however there is a difference of approximately 1 kPa between the two data sets at 363 K in the range of $x_1 = 0.6$ to 0.85. This difference was attributed to the relative uncertainties of the various relevant parameters between the two studies, and the method used for the measurements.

The results of the vapour-liquid equilibrium data measurements for the water (1) + butane-1,4-diol (2) and water (1) + butane-2,3-diol (2) system are presented in Tables 4.3-4.4 and Figures 4.3-4.6. Since pure component vapour pressure data for butane-1,4-diol were not measured in this work, the data were predicted using the Extended Antoine equation available on the Aspen Plus® software in order to calculate the activity coefficients for the relevant mixtures. The experimental activity coefficients are greater than 1 suggesting a positive deviation from Raoult's Law. The systems do not exhibit azeotropes in the range measured in this work and the phase behaviour is mostly typical, however, a wide phase envelope exists between the liquid- and vapour-phase, with a steep P-y curve. The vapour composition for the water (1) + butane-1,4-diol (2) could not be measured in the very dilute butane-1,4-diol region, due to the steepness of the P-y curve in this region, as repeatable measurements could not be obtained using the manual phase sampling technique. A recommendation would be to use a static-analytic apparatus with an auto-sampling device such as a ROLSI™ to measure these points.

To confirm the thermodynamic consistency of the vapour-liquid equilibrium data, the area test of Redlich and Kister, (1948) and the point test of Christiansen and Fredenslund, (1975) was conducted using the Aspen Plus® V10 software package. A criterion of 10% tolerance was used for the area test and 0.01 for the point test. The results shown in Table 4.5 validate the thermodynamic consistency of the measured VLE data by these tests. The relevant plots are presented in Appendix D, Figures D1-D2.

The experimental data was modelled using the γ - Φ approach with the Non-Random Two-liquid (NRTL) and Universal Quasi-Chemical (UNIQUAC) activity coefficient models to account for the liquid-phase

non-ideality and the Hayden-O'Connell correlation (HOC) for the virial equation of state, used to account for the vapour-phase non-ideality. This was performed on the Aspen Plus® process simulation software. For the activity coefficient model regression, a single set of temperature dependent model parameters were determined for each system.

For the fitting procedure used in this work, the pressure residual was minimized:

$$\delta P = \sum_{k=1}^N (P^{exp} - P^{calc})^2 \quad (4.3)$$

Where N is the total number of measured data points and P^{exp} and P^{calc} are the respective measured and model-calculated pressures.

The root mean square deviation (RMSD) with respect to pressure and the absolute average deviation (δy_i) in vapour composition was calculated according to the procedure outlined by Van Ness and Abbott., (1982):

$$RMSD = \sqrt{\frac{\delta P}{N}} \quad (4.4)$$

$$\delta y_1 = \frac{abs(y_1^{exp} - y_1^{calc})}{N} \quad (4.5)$$

The model parameters from the regression of the experimental VLE data and fitting deviations are presented in Table 4.6. The NRTL-HOC and UNIQUAC-HOC models perform quite well, and most residuals are within the relevant experimental uncertainty with UNIQUAC providing a lower RMSD in pressure for both systems.

The experimental and modelled activity coefficient behaviours for each system is presented in Figures 4.7 and 4.8. The experimental activity coefficients are generally well represented by at least one model. The infinite dilution activity coefficients (γ_i^∞) predicted by each model is presented in Table 4.7. It is evident that these predicted values are highly model dependent, although the predicted relative temperature rank of each γ_i^∞ , is the same in the majority of cases. The model independent extrapolation method of Maher and Smith Maher and Smith, (1979) was also applied, (Appendix E, Table E1) and compared reasonably well with the model-extrapolated values.

The experimental and model calculated relative volatilities ($\alpha_{1,2}$) were determined by:

$$\alpha_{1,2} = \frac{y_1}{x_1} / \frac{y_2}{x_2} \quad (4.6)$$

These relative volatilities are present in Figures 4.9-4.10. The relative volatilities show a general trend of decreasing with increasing temperature for both systems. Minor differences between experimental and model are attributed to the sensitive nature of $\alpha_{1,2}$ to small differences between the experimental and calculated composition values Gmehling *et al.*, (2012). The non-linear shapes of the relative volatility curves further highlight the non-ideality of the studied systems.

Figures 4.11-4.12 show the plots of Gibbs excess energy as a function of composition. A positive $\frac{G^E}{RT}$ was observed for both systems, that decreased with increasing temperature. The $\frac{G^E}{RT}$ vs. x_1 curves for the water (1) + butane-1,4-diol (2) system are quite symmetrical with maxima at approximately $x_1 = 0.5$. However, the behaviour of $\frac{G^E}{RT}$ vs. x_1 for the water (1) + butane-2,3-diol (2) is slightly asymmetrical with maxima approaching $x_1 = 0.65$. A strong correlation between the experimental and model calculated excess Gibbs energies was observed, with NRTL-HOC providing a clearly superior representation of the experimental data in both systems. This is an interesting result, considering the UNIQUAC-HOC model fits provide a lower RMSD for both systems.

The regressed NRTL-HOC model parameters, which provided the best fit to the VLE data presented, were used to predict the excess enthalpy (H^E) behaviour of the binary systems via the Gibbs-Helmholtz relation, and compared to available literature data. The model parameters presented in Table 4.6 provided a poor prediction of H^E data from literature, which is likely due to the different temperature ranges. The VLE data in this work was then regressed simultaneously with H^E data from the literature, to assess if a more reasonable representation of H^E could be obtained. This was at the expense of the quality of the fit for the pressure and vapour composition, as well as the representation of the experimental activity coefficients. It was also found that in the case of the water (1) + butane-2,3-diol (2) system, the representation by the regressed model with H^E data, did not comply with the infinite dilution test when simultaneously regressed with the H^E data of Checoni and Francesconi, (2009). However, a reasonable result was observed when the VLE data for the water (1) + butane-1,4-diol (2) system was simultaneously regressed with the excess enthalpy data of Nagamachi and Francesconi, (2006) and Amaya and Fujishiro, (1956). The results of these

excess enthalpy predictions are presented in Figure 4.13, while the VLE- H^E simultaneously regressed model parameters are provided in Table 4.8. Note that the data of Nagamachi and Francesconi, (2006) and Amaya and Fujishiro, (1956) do not correlate with each other at 298 K. The models from this work can provide a qualitative representation of the literature data, and the trends with temperature are replicated.

4.6. Conclusion

The vapour-liquid equilibrium phase behaviour of the water + butane-1,4-diol and water + butane-2,3-diol was successfully measured using a low-pressure dynamic apparatus. Thermodynamic consistency and stability tests were conducted and passed thereby confirming the consistency of the data obtained. The VLE phase behaviour was found to be non-ideal. The NRTL-HOC and UNIQUAC-HOC models correlated the VLE experimental data well. The RMSD calculation for pressure and the Absolute Average Deviation (AAD) values in the vapour-phase mole fraction was found to be within the experimental uncertainty. The lowest RMSD value was obtained from the UNIQUAC-HOC model for both the water + butane-1,4-diol system at 0.046 kPa and the water + butane-2,3-diol at 0.036 kPa. The NRTL-HOC model provided a better representation of the $\frac{G^E}{RT}$ vs. x_1 behaviour.

Table 4.1. Chemical purities and suppliers.^a

Component	CAS RN.	Supplier	Refractive Index (RI) at 0.101 MPa. ^a		Minimum Stated Mass Fraction Purity	GC Peak Relative Area (Mass Fraction Purity)
			Experimental	Literature ^b		
Water	7732-18-5	-	1.3332 (293.15K)	1.333 (293.15K)	-	0.9999
Butane-2,3-diol ^c	513-85-9	Sigma Aldrich	1.4311 (298.15K)	1.4310 (298.15K)	≥0.990	0.9999
Butane-1,4-diol ^c	110-63-4	Sigma Aldrich	1.4462 (293.15K)	1.4460 (293.15K)	≥0.990	0.9999

^aStandard uncertainties u are $u(RI) = 0.0010$, $u(T) = 0.010$ K, $u(P) = 0.0020$ MPa, ^b Haynes, (2014), ^cPurified by molecular sieving.

Table 4.2. Experimental vapour pressures and comparison to literature correlation.^a

Component	T/K	P/kPa		
		Experimental	Literature	
			Antoine correlation Poling <i>et al.</i> , (2001)	Wagner equation NIST, (2019)
Water	353.1	47.2	47.2	47.3
	353.2	47.6	47.4	47.4
	363.2	70.0	70.1	70.2
	373.2	101.2	101.2	101.5
Butane-2,3-diol	353.1	1.2	1.2	1.0
	363.2	2.1	2.2	1.9
	373.2	3.6	3.7	3.4

^aStandard uncertainties u_c are $u_c(T) = 0.010$ K, $u_c(P) = 0.12$ kPa

Table 4.3. Vapour-liquid equilibrium data for the water (1) + butane-1,4-diol.^a

<i>T</i> / K = 353.2					<i>T</i> / K = 363.2					<i>T</i> / K = 373.2				
<i>P</i> / kPa	<i>x</i> ₁	<i>y</i> ₁	γ ₁	γ ₂	<i>P</i> / kPa	<i>x</i> ₁	<i>y</i> ₁	γ ₁	γ ₂	<i>P</i> / kPa	<i>x</i> ₁	<i>y</i> ₁	γ ₁	γ ₂
1.6	0.018	0.939	1.772	1.007	2.4	0.016	0.921	1.984	1.002	2.9	0.012	0.873	2.123	1.003
2.4	0.029	0.961	1.734	1.010	2.8	0.019	0.933	1.960	1.002	5.0	0.023	0.928	2.025	1.008
3.7	0.046	0.975	1.668	1.008	5.0	0.038	0.963	1.836	1.004	6.8	0.033	0.947	1.936	1.006
5.3	0.069	0.983	1.600	1.010	7.5	0.062	0.976	1.713	1.007	10.7	0.058	0.967	1.768	1.008
6.1	0.081	0.985	1.561	1.008	8.4	0.071	0.979	1.671	1.009	12.0	0.068	0.971	1.713	1.008
6.7	0.091	0.987	1.550	1.017	9.9	0.087	0.982	1.612	1.012	14.1	0.084	0.976	1.642	1.011
12.4	0.193	0.994	1.363	1.030	18.1	0.189	0.991	1.368	1.037	27.1	0.198	0.989	1.350	1.042
17.3	0.288	0.996	1.273	1.061	24.7	0.281	0.994	1.260	1.063	35.2	0.278	0.992	1.255	1.065
20.0	0.345	0.997	1.230	1.075	28.2	0.331	0.995	1.222	1.078	40.2	0.328	0.993	1.215	1.080
23.9	0.431	0.998	1.176	1.096	35.3	0.434	0.997	1.164	1.110	49.4	0.422	0.995	1.160	1.109
26.1	0.479	0.998	1.153	1.113	38.6	0.484	0.997	1.143	1.127	53.7	0.467	0.996	1.140	1.125
31.1	0.592	0.999	1.112	1.163	45.5	0.589	0.998	1.105	1.170	64.1	0.578	0.997	1.099	1.171
36.4	0.724	0.999	1.063	1.247	53.9	0.724	0.999	1.064	1.260	75.2	0.702	0.998	1.061	1.248
40.1	0.792	-	-	-	56.3	0.783	-	-	-	79.7	0.781	-	-	-
41.4	0.844	-	-	-	58.9	0.831	-	-	-	84.0	0.830	-	-	-
42.2	0.896	-	-	-	61.9	0.886	-	-	-	88.9	0.884	-	-	-
44.0	0.950	-	-	-	64.4	0.931	-	-	-	93.0	0.928	-	-	-
44.8	0.971	-	-	-	67.1	0.970	-	-	-	97.5	0.966	-	-	-
47.6	1.000	1.000	1.000	-	70.0	1.000	1.000	1.000	-	101.3	1.000	1.000	1.000	-

^aStandard uncertainties u_c , $u_c(T) = 0.10$ K, $u_c(P) = 0.12$ kPa, $u_c(x_1) = u_c(y_1) = 0.0040$

Table 4.4. Vapour-liquid equilibrium data for the water (1) + butane-2,3-diol.^a

$T / \text{K} = 353.1$					$T / \text{K} = 363.2$					$T / \text{K} = 373.2$				
P / kPa	x_1	y_1	γ_1	γ_2	P / kPa	x_1	y_1	γ_1	γ_2	P / kPa	x_1	y_1	γ_1	γ_2
1.2	0.000	0.000	-	1.000	2.1	0.000	0.000	-	1.000	3.6	0.000	0.000	-	1.000
2.0	0.009	0.415	2.052	1.000	4.8	0.020	0.559	1.918	1.004	5.9	0.014	0.393	1.727	1.006
3.0	0.019	0.603	2.034	1.000	5.2	0.024	0.599	1.891	1.006	6.8	0.019	0.472	1.730	1.011
3.9	0.029	0.700	2.004	1.000	5.3	0.025	0.610	1.886	1.003	7.5	0.023	0.523	1.740	1.008
7.4	0.069	0.849	1.953	1.002	10.1	0.064	0.801	1.838	1.010	13.7	0.061	0.749	1.701	1.010
8.4	0.081	0.869	1.924	1.003	12.1	0.080	0.835	1.832	1.016	16.4	0.077	0.794	1.698	1.006
9.2	0.091	0.881	1.923	1.004	14.5	0.100	0.866	1.821	1.011	19.6	0.097	0.832	1.690	1.006
17.0	0.191	0.942	1.791	1.024	23.4	0.181	0.924	1.725	1.014	32.6	0.178	0.907	1.660	1.015
22.2	0.272	0.959	1.674	1.035	31.4	0.261	0.949	1.639	1.019	44.1	0.259	0.938	1.590	1.017
25.3	0.322	0.966	1.618	1.053	35.9	0.312	0.958	1.583	1.033	51.0	0.310	0.950	1.554	1.022
29.9	0.412	0.974	1.505	1.083	43.1	0.403	0.969	1.487	1.063	61.9	0.401	0.963	1.477	1.050
32.8	0.473	0.978	1.445	1.121	47.2	0.464	0.974	1.420	1.088	68.5	0.462	0.969	1.428	1.070
37.5	0.593	0.984	1.323	1.235	54.8	0.585	0.980	1.314	1.208	79.4	0.583	0.978	1.320	1.167
41.1	0.708	0.988	1.217	1.461	60.0	0.696	0.985	1.215	1.414	86.1	0.694	0.983	1.207	1.340
43.4	0.794	0.990	1.149	1.821	63.8	0.786	0.988	1.145	1.749	91.0	0.785	0.986	1.131	1.651
44.4	0.844	0.991	1.106	2.205	65.9	0.838	0.989	1.110	2.082	93.0	0.836	0.987	1.086	1.965
45.1	0.885	0.992	1.073	2.721	66.6	0.879	0.990	1.071	2.482	94.6	0.878	0.989	1.053	2.386
46.1	0.947	0.994	1.026	4.344	68.1	0.943	0.993	1.024	3.683	97.7	0.942	0.992	1.017	3.670
47.2	1.000	1.000	1.000	-	70.0	1.000	1.000	1.000	-	101.2	1.000	1.000	1.000	-

^aStandard uncertainties u_c , $u_c(T) = 0.10 \text{ K}$, $u_c(P) = 0.12 \text{ kPa}$, $u_c(x_1) = u_c(y_1) = 0.0040$

Table 4.5. Results of thermodynamic consistency tests using the NRTL-HOC model.

System	Calculated Criterion		Consistency Test Result
	Area Test (%)	Point Test	
water (1) + butane-1,4-diol (2)			
$T / K = 353.2$	0.339	0.008	Passed both tests
$T / K = 363.2$	1.839	0.009	Passed both tests
$T / K = 373.2$	4.007	0.010	Passed both tests
water (1) + butane-2,3-diol (2)			
$T / K = 353.1$	1.326	0.006	Passed both tests
$T / K = 363.2$	2.032	0.002	Passed both tests
$T / K = 373.2$	1.471	0.003	Passed both tests

Table 4.6. Regressed Model Parameters.

Parameter	System			
	water (1) + butane-1,4-diol (2)		water (1) + butane-2,3-diol (2)	
	NRTL ^a	UNIQUAC ^b	NRTL ^a	UNIQUAC ^b
a_{12}	-1.916	-1.629	-0.366	0.277
a_{21}	4.077	0.475	-2.651	-0.610
b_{12}/K	904.450	-64.582	809.741	-1.422
b_{21}/K	-1274.367	153.903	1027.661	-2.491
$\alpha_{12,NRTL}^*$	0.300	-	0.736	-
RMSD/kPa	0.070	0.046	0.329	0.036
δy_1	0.001	0.001	0.001	0.004

*Treated as an adjustable parameter

Table 4.7. Infinite dilution activity coefficients from each model.

System	NRTL-HOC		UNIQUAC-HOC	
	γ_1^∞	γ_2^∞	γ_1^∞	γ_2^∞
water (1) + butane-1,4-diol (2)				
$T/K = 353.2$	1.869	2.253	1.951	2.736
$T/K = 363.2$	2.089	2.079	2.023	2.845
$T/K = 373.2$	2.282	1.971	2.093	2.953
water (1) + butane-2,3-diol (2)				
$T/K = 353.1$	2.068	8.515	1.899	6.732
$T/K = 363.2$	1.923	7.615	1.898	6.727
$T/K = 373.2$	1.789	6.734	1.897	6.723

Table 4.8. Regressed Model Parameters for H^E calculation

Parameter	System	
	water (1) + butane-1,4-diol (2)	
	NRTL ^a	UNIQUAC ^b
a_{12}	1.822	-0.735
a_{21}	1.468	0.411
b_{12}/K	-488.052	-359.551
b_{21}/K	-335.139	167.859
$\alpha_{12,NRTL}$	2.157	-
RMSD/kPa	0.090	0.048
δy_1	0.002	0.002

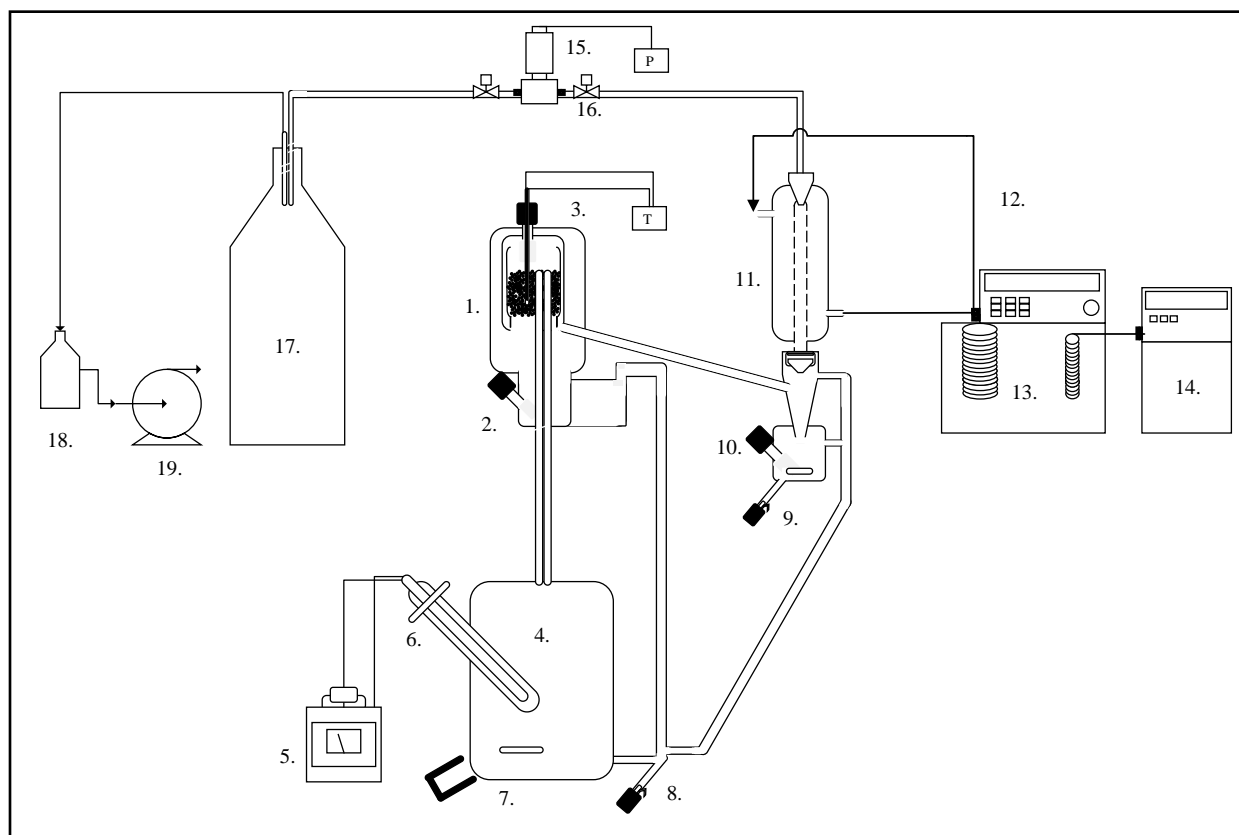


Figure 4.1. Layout of the apparatus of Joseph *et al.*, (2001) used in this work (as shown in Mavalal *et al.*, (2019)).

1-Equilibrium chamber. 2-Liquid sampling port. 3-Temperature measurement. 4-Boiling chamber. 5-Variable heat supply to boiler. 6- Heater cartridge and sleeve. 7- Magnetic stirrer and bead. 8- Boiler drain valve. 9- Condensate drain valve. 10- Vapour condensate sampling point. 11- Condenser. 12- Coolant line to condenser. 13. Coolant bath and controller. 14- Chiller. 15- Pressure measurement. 16. Isolation valves. 17- Ballast tank. 18. Cold trap. 19. Vacuum pump.

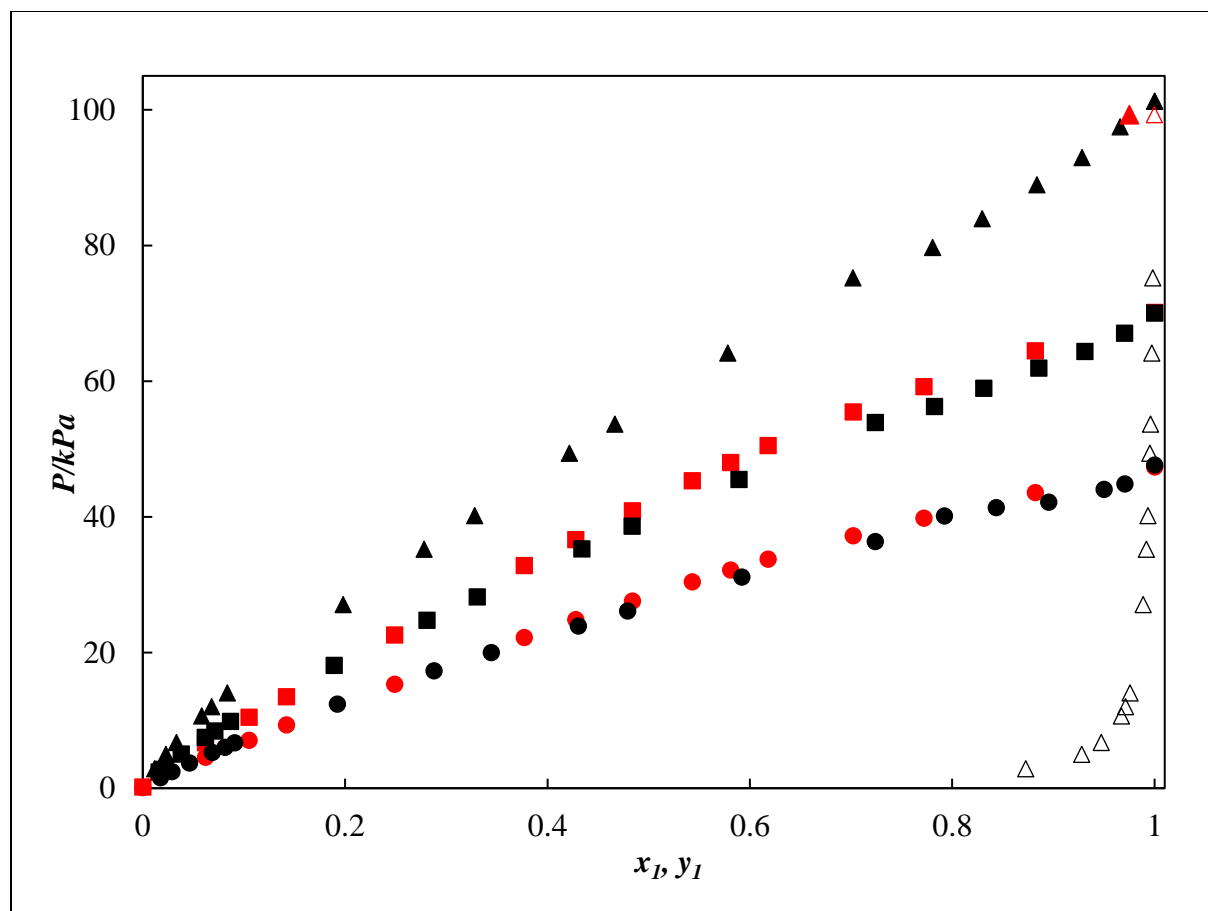


Figure 4.2. Vapour-liquid equilibrium data for the water (1) + butane-1,4-diol system, with comparison to available literature data. P-x at 353.2 K, ●-This work, ●- Huang and Zhang, (1987), P-x at 363.2 K, ■-This work, ■- Huang and Zhang, (1987), P-x at 373.2 K, ▲-This work, P-y at 373.2 K, △-This work, P-x at 373.32 K, ▲- Jelinek *et al.*, (1976), P-y at 373.32 K, △- Jelinek *et al.*, (1976).

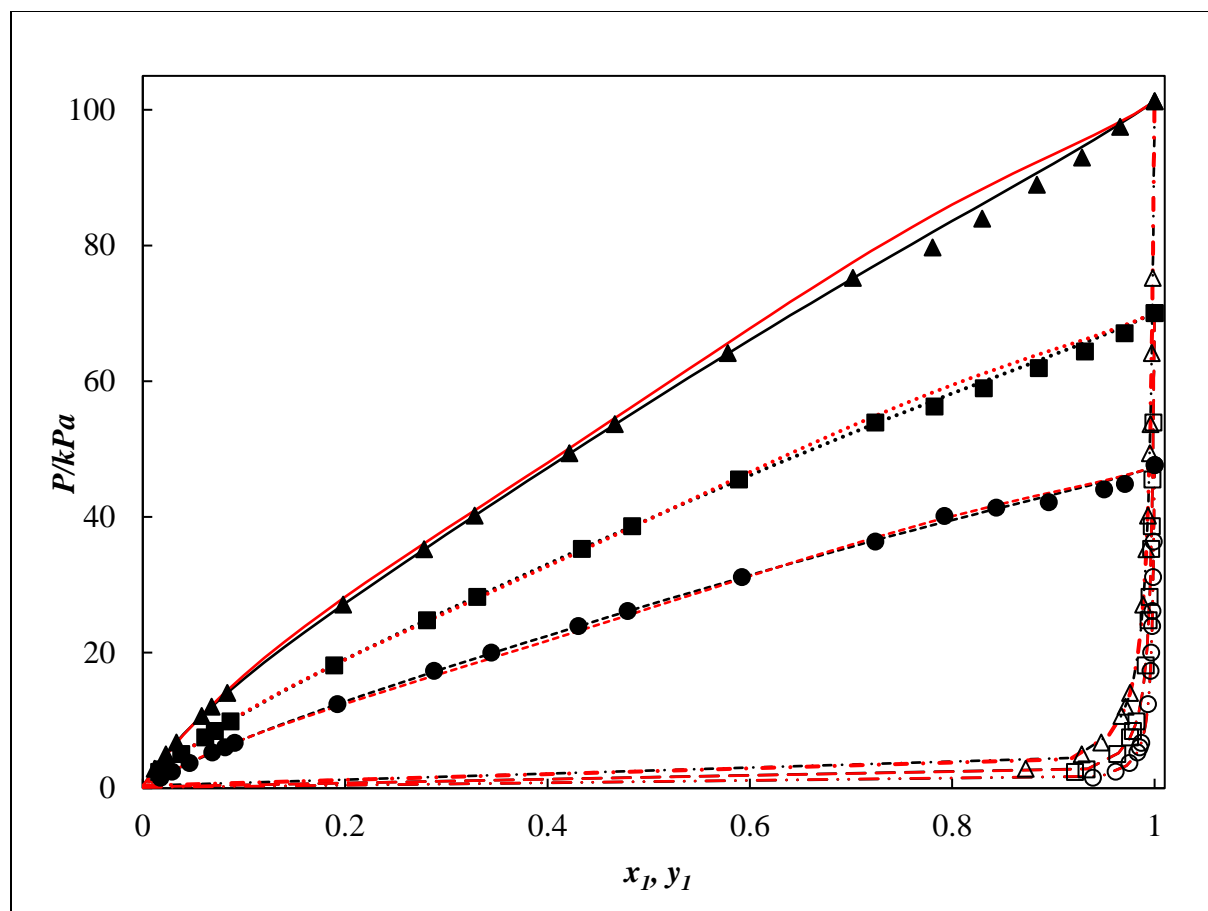


Figure 4.3. P-x-y data for the water (1) + butane-1,4-diol system. Experimental (P-x, P-y): at 353.2 K, (\bullet , \circ), 363.2 K, (\blacksquare , \square), 373.2 K, (\blacktriangle , \triangle). Model (P-x, P-y): at 353.2 K, (- - -, - - -), 363.2 K, (\cdots , - - -), 373.2 K, (-, - -). Black lines represent the NRTL-HOC model, red lines represent the UNIQUAC-HOC model.

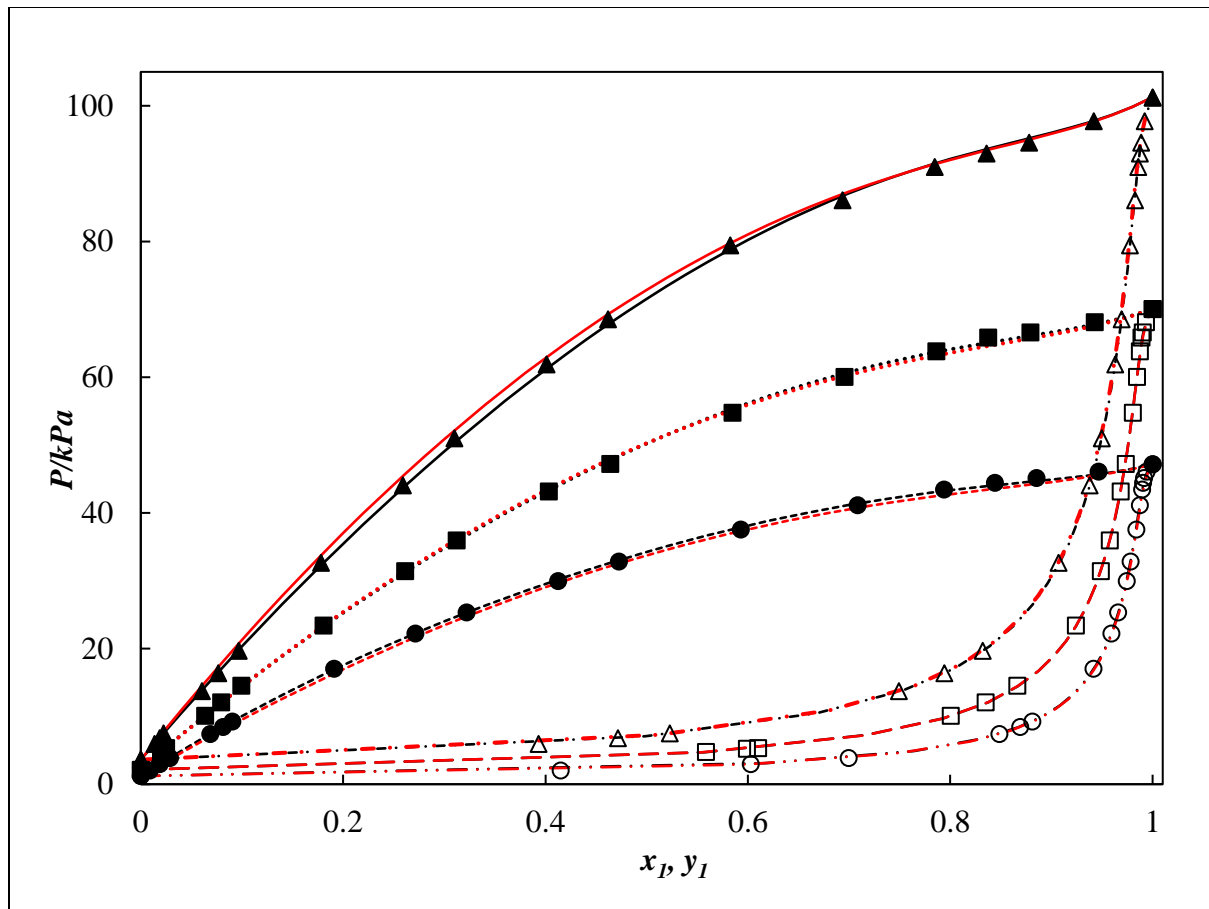


Figure 4.4. P-x-y data for the water (1) + butane-2,3-diol system. Experimental (P-x, P-y): at 353.1 K, (\bullet , \circ), 363.2 K, (\blacksquare , \square), 373.2 K, (\blacktriangle , \triangle). Model (P-x, P-y): at 353.2 K, (- - -, - · - ·), 363.2 K, (\cdots , - - -), 373.2 K, (-, - · -). Black lines represent the NRTL-HOC model, red lines represent the UNIQUAC-HOC model.

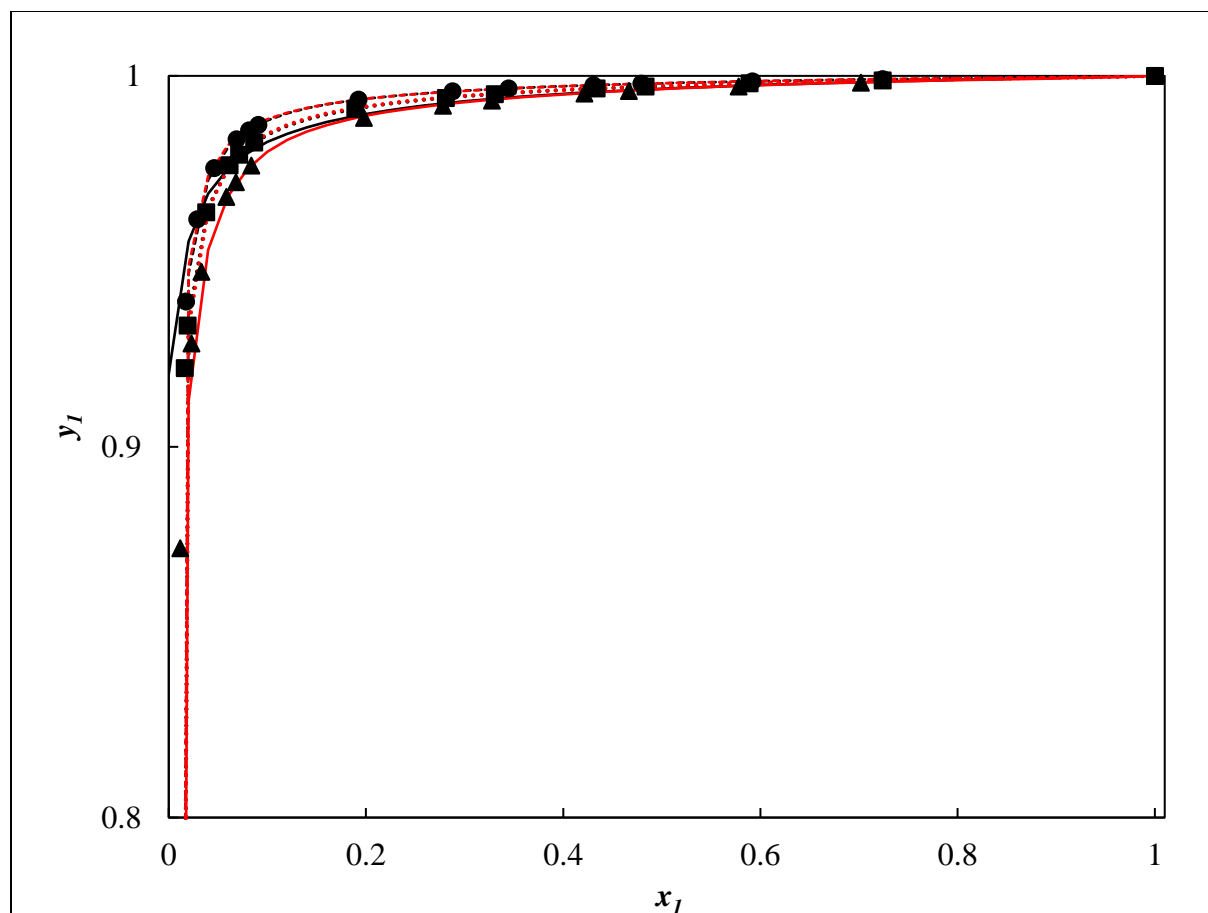


Figure 4.5. y_1 vs. x_1 for the water (1) + butane-1,4-diol system. Experimental: ●-353.2 K, ■-363.2 K, ▲-373.2 K. Model: (- -)-353.2 K, (···)- 363.2 K, (—)-373.2 K. Black lines represent the NRTL-HOC model, red lines represent the UNIQUAC-HOC model.

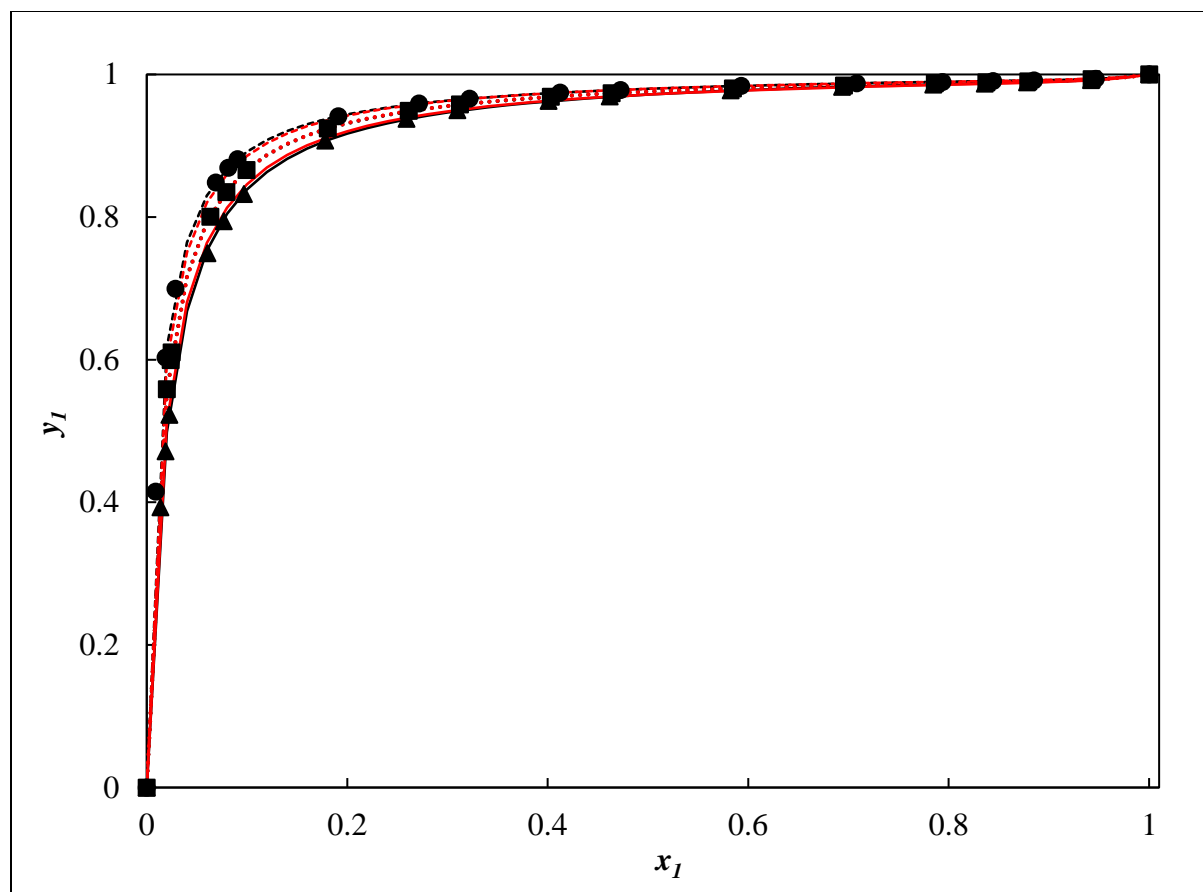


Figure 4.6. y_1 vs. x_1 for the water (1) + butane-2,3-diol system. Experimental: ●-353.2 K, ■-363.2 K, ▲-373.2 K. Model: (- -)-353.2 K, (···)- 363.2 K, (—)-373.2 K. Black lines represent the NRTL-HOC model, red lines represent the UNIQUAC-HOC model.

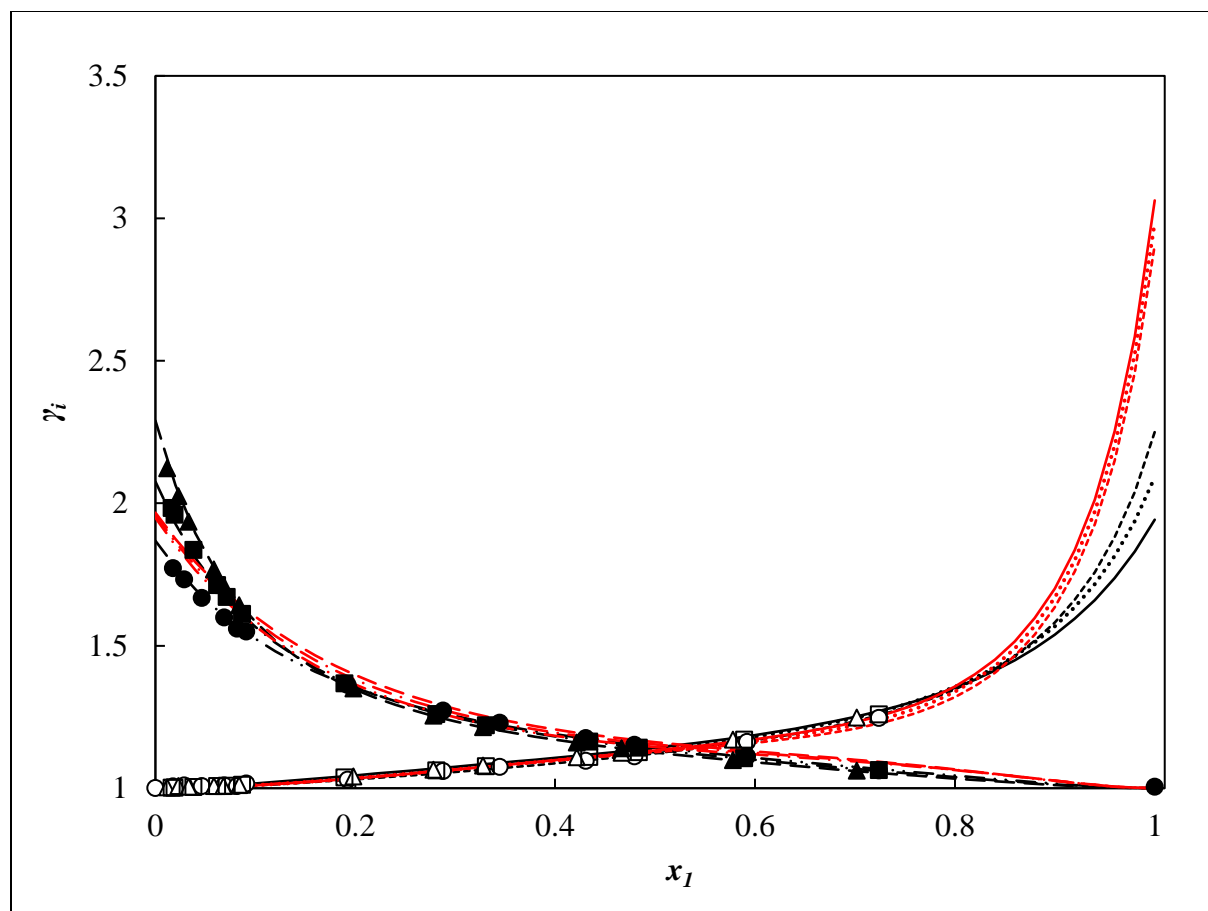


Figure 4.7. γ_i - x_i data for the water (1) + butane-1,4-diol system. Experimental (γ_1, γ_2): at 353.2 K, (\bullet , \circ), 363.2 K, (\blacksquare , \square), 373.2 K, (\blacktriangle , \triangle). Model (γ_1, γ_2): at 353.2 K, ($- \cdot -$, $- - -$), 363.2 K, ($- - -$, \cdots), 373.2 K, ($- - -$, $-$). Black lines represent the NRTL-HOC model, red lines represent the UNIQUAC-HOC model.

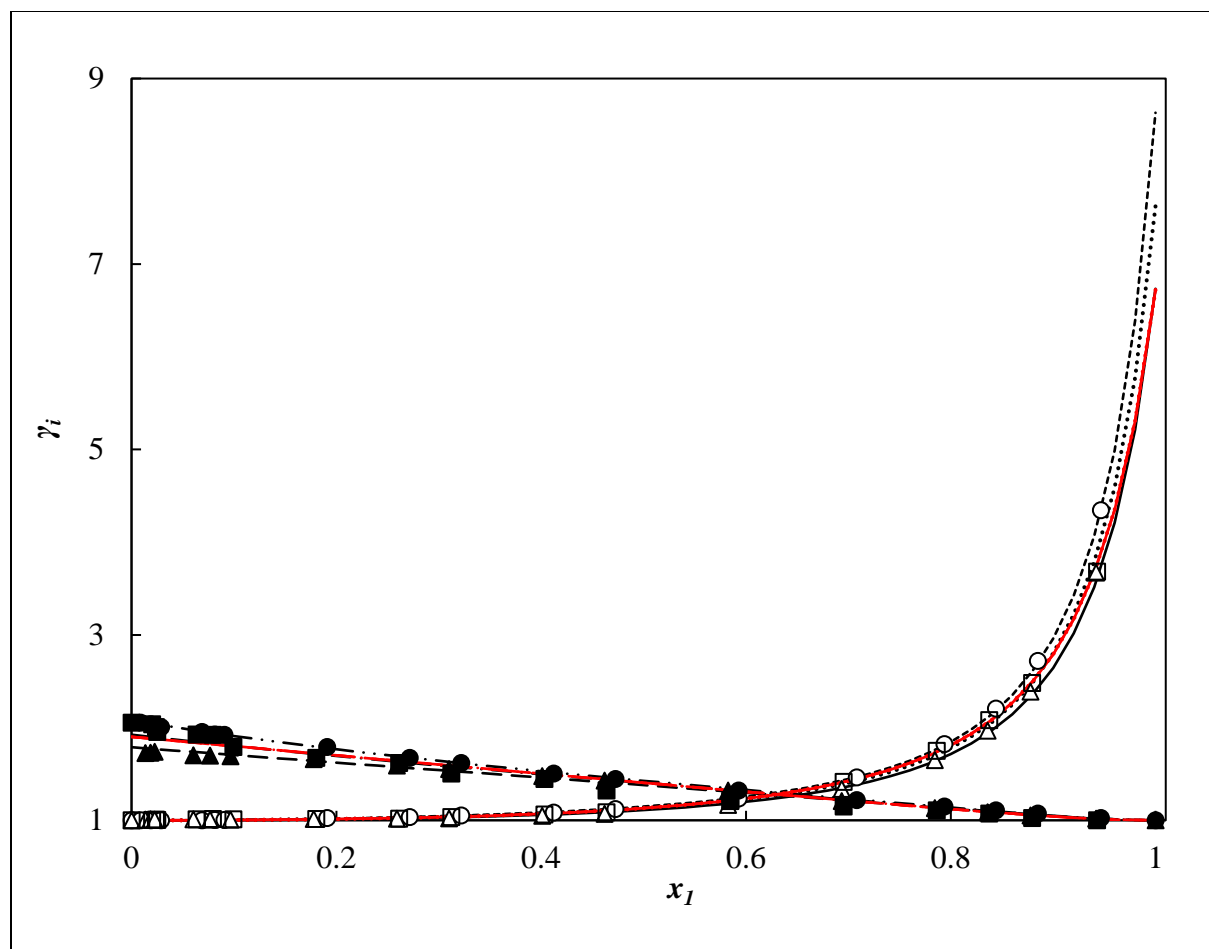


Figure 4.8. γ_i - x_i data for the water (1) + butane-2,3-diol system. Experimental (γ_1, γ_2): at 353.1 K, (\bullet , \circ), 363.2 K, (\blacksquare , \square), 373.2 K, (\blacktriangle , \triangle). Model (γ_1, γ_2): at 353.2 K, ($-\cdots-$, $- - -$), 363.2 K, ($- - -$, \cdots), 373.2 K, ($-\cdots-$, $-$). Black lines represent the NRTL-HOC model, red lines represent the UNIQUAC-HOC model.

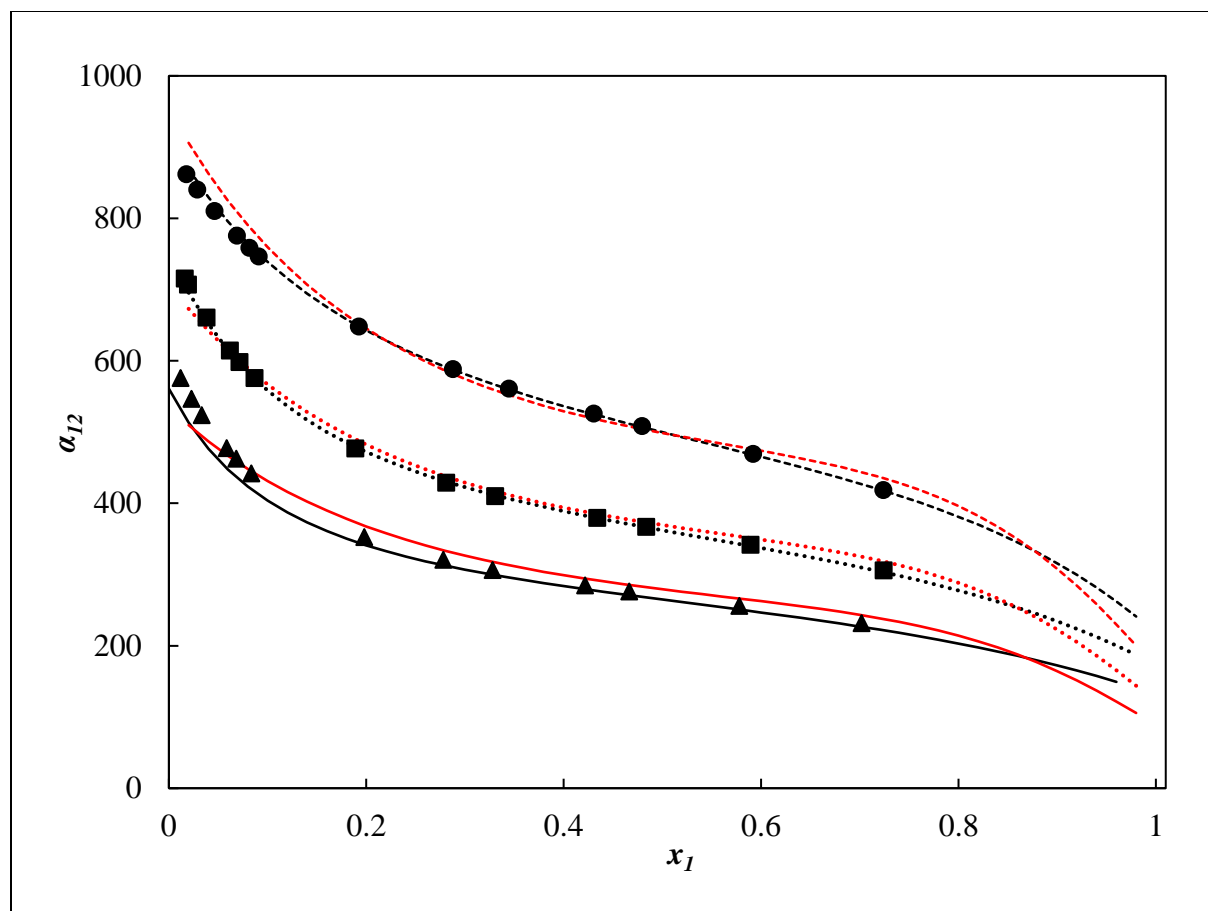


Figure 4.9. α_{12} vs. x_1 for the water (1) + butane-1,4-diol system. Experimental: ●-353.2 K, ■-363.2 K, ▲-373.2 K. Model: (- -)-353.2 K, (···)- 363.2 K, (—)-373.2 K. Black lines represent the NRTL-HOC model, red lines represent the UNIQUAC-HOC model.

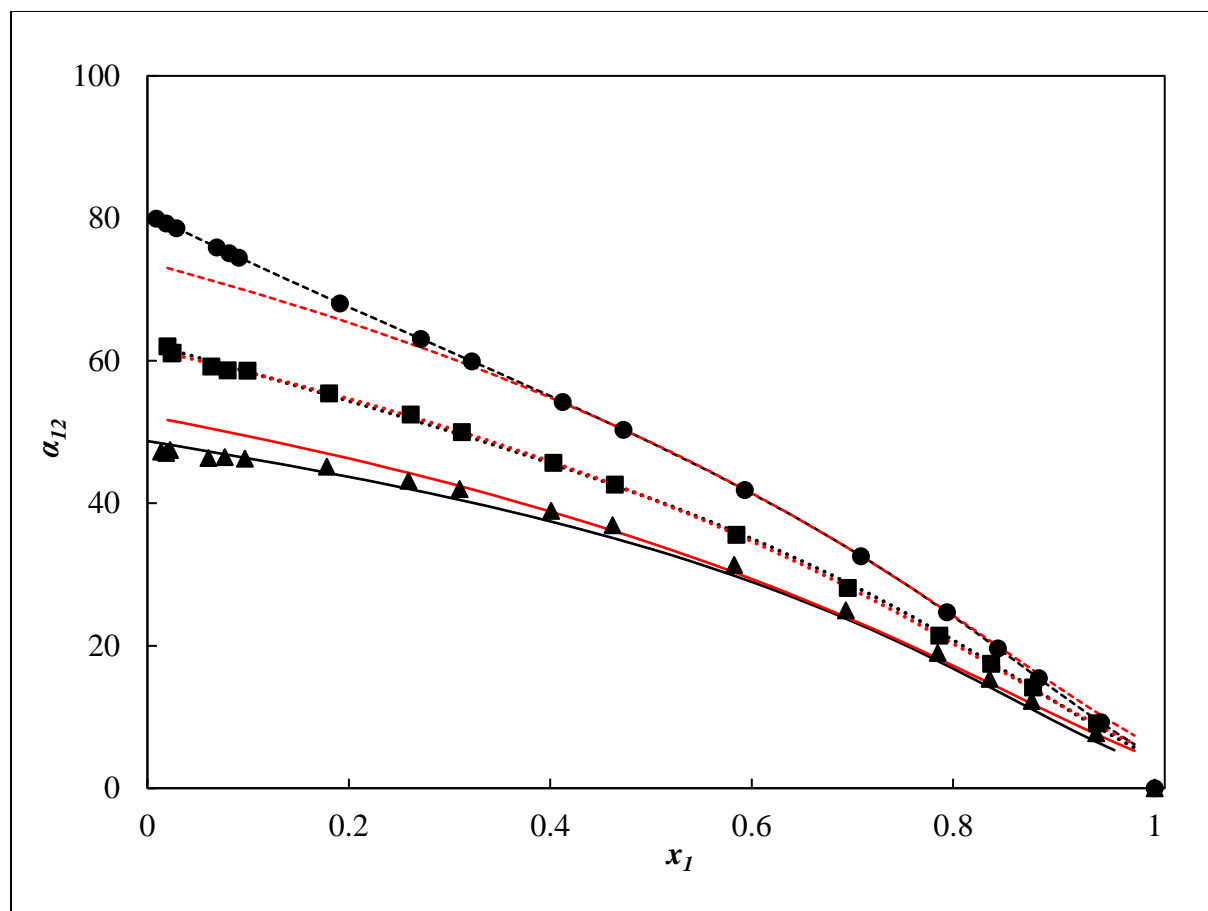


Figure 4.10. α_{12} vs. x_1 for the water (1) + butane-2,3-diol system. Experimental: ●-353.2 K, ■-363.2 K, ▲-373.2 K. Model: (---)-353.2 K, (···)- 363.2 K, (—)-373.2 K. Black lines represent the NRTL-HOC model, red lines represent the UNIQUAC-HOC model.

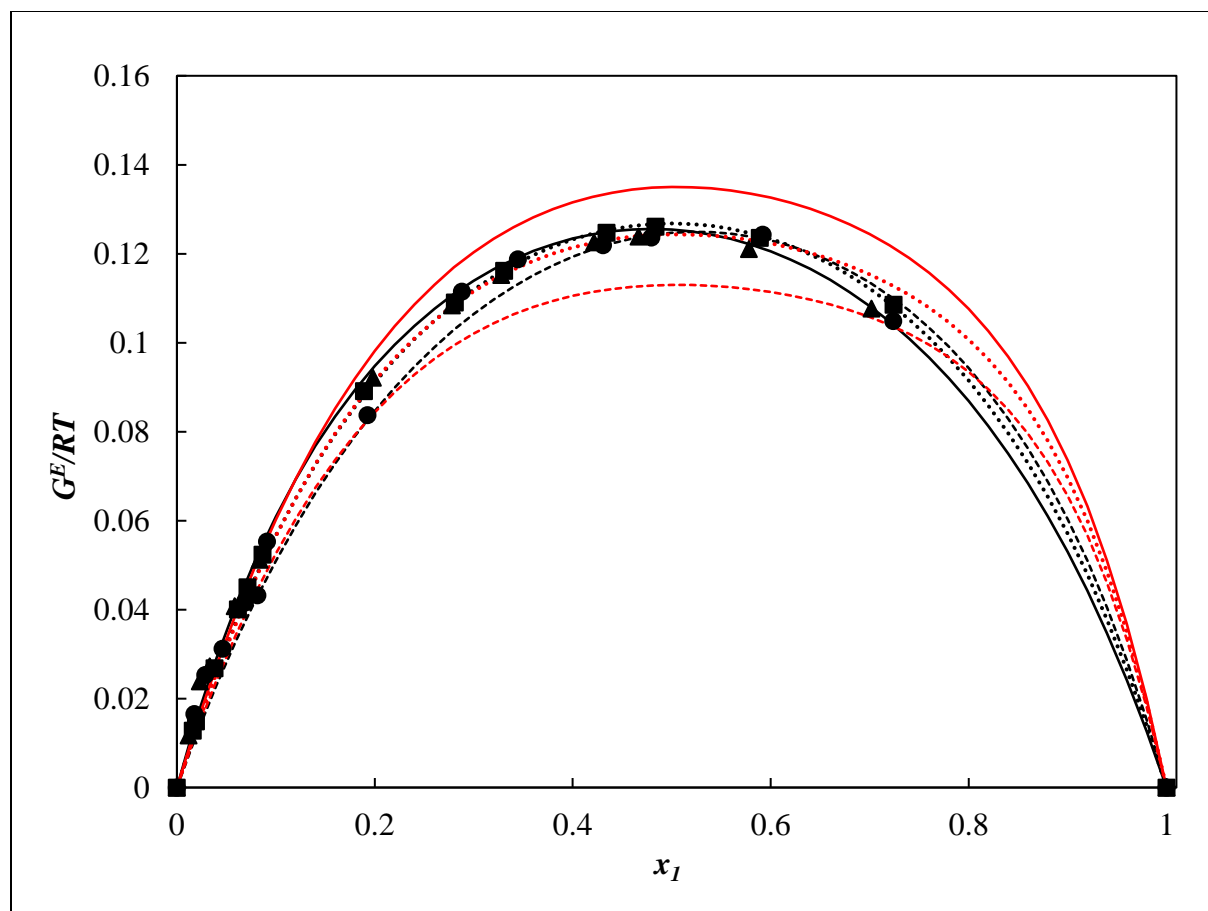


Figure 4.11. G^E/RT vs. x_1 for the water (1) + butane-1,4-diol system. Experimental: ●-353.2 K, ■-363.2 K, ▲-373.2 K. Model: (- - -)-353.2 K, (···)- 363.2 K, (—)-373.2 K. Black lines represent the NRTL-HOC model, red lines represent the UNIQAC-HOC model.

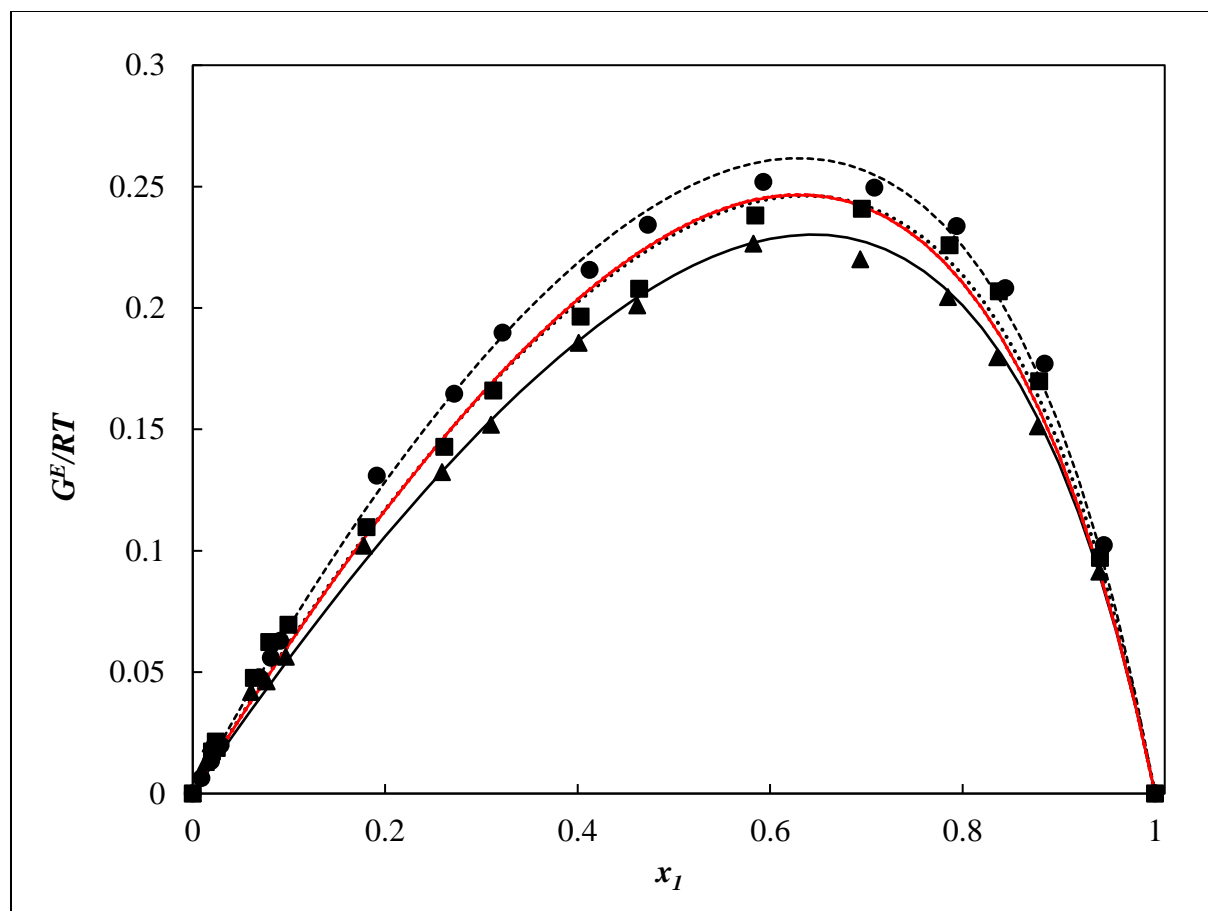


Figure 4.12. G^E/RT vs. x_1 for the water (1) + butane-2,3-diol system. Experimental: ●-353.2 K, ■-363.2 K, ▲-373.2 K. Model: (- - -)-353.2 K, (···)- 363.2 K, (—)-373.2 K. Black lines represent the NRTL-HOC model, red lines represent the UNIQUAC-HOC model.

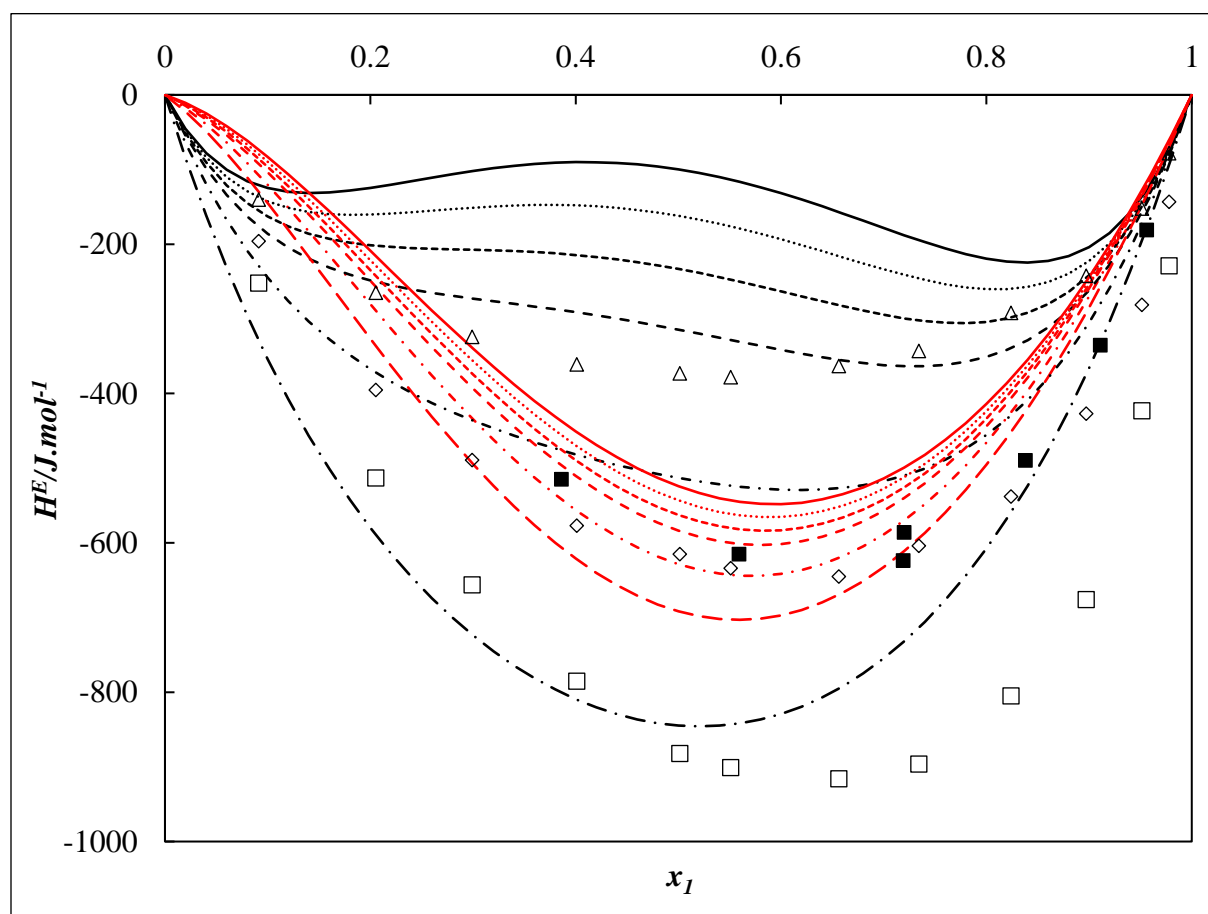


Figure 4.13. H^E vs. x_1 for the water (1) + butane-1,4-diol system. Literature: ■-298.136 K Amaya and Fujishiro, (1956), □-298.15 K, ◇-323.15, △-343.15 K Nagamachi and Francesconi, (2006) . Model: (—) -298.15 K, (---) - 323.15 K, (— — —) -343.15 K, (- - -) -353.15 K, (····) -363.15 K, (— · —) -373.15 K. Black lines represent the NRTL-HOC model prediction, red lines represent the UNIQUAC-HOC model prediction.

CHAPTER FIVE

Isothermal Vapour-Liquid Equilibrium Measurements for the butan-1-ol + butane-1,4-diol/butane-2,3-diol system within 353.2 – 388.2 K

5.1. Abstract

In this study, the isothermal binary vapour-liquid equilibrium (VLE) data for the butan-1-ol + butane-1,4-diol/butane-2,3-diol system was measured and modelled, for use in the design and rating of separation processes. P - T - x - y equilibrium measurements were performed at four temperatures from approximately 353 – 388 K. A dynamic-analytical apparatus was utilized to perform the measurements at sub-atmospheric conditions. The measured data was modelled by employing the γ - Φ approach. The liquid-phase correction was accounted for using the Non-Random Two-Liquid and Universal Quasi-Chemical activity coefficient models while the Hayden and O'Connell correlation for the virial equation of state was used to account for the vapour-phase correction. Thermodynamic consistency tests were performed using the point and area tests for the measured experimental data and the data sets passed both tests.

5.2. Introduction

The study of renewable biofuels and their development from sucrose crop sources has recently become a key area of research focus. Such biofuels can be used in their pure state without further processing with a few engine modifications or alternatively, can be blended with other fuels and used as “drop-in” fuels Waldron, (2010), Harvey *et al.*, (2016), Zhang *et al.*, (2017), Haider *et al.*, (2018), van Dyk *et al.*, (2019). Biofuels such as butane-1,4-diol and butane-2,3-diol have been identified as viable due to their high octane-numbers Harvey *et al.*, (2016), Satam *et al.*, (2019). Butane-1,4-diol has a global market volume approaching 2 million tons per year and is also used in the manufacture of automotive plastics, electronics and textiles Burgard *et al.*, (2016). Butane-2,3-diol is used as an intermediate in the production of butan-2-one and has a projected global market volume of approximately 32 million tons per year Haider *et al.*, (2018).

A bioconversion process utilizing microorganisms such as *Escherichia coli*, can produce butane-1,4-diol in a single conversion step Waldron, (2010), Burgard *et al.*, (2016), Satam *et al.*, (2019) while butane-2,3-diol can be produced by the fermentation of biomass using microorganisms such *Bacillus licheniformis* Penner *et al.*, (2017), Harvianto *et al.*, (2018). These processes produce butane-1,4-diol and butane-2,3-diol in an aqueous solution with smaller concentrations of the desired components. Before the butanediols can be

used for blending purposes or as feedstock in other processes, excess water must be removed from the diol products. The dehydration step is regarded as an energy intensive step Haider *et al.*, (2018).

While conventional distillation is a suitable separation technique to perform the dehydration step, the process demands a high energy input in the form of high-pressure steam due to the boiling points of the butanediol constituents exceeding 450 K Shao and Kumar, (2009b), Penner *et al.*, (2017). Separation processes such as pervaporation (Shao and Kumar, (2009a), (2009b)), reactive distillation Li *et al.*, (2012), liquid-liquid extraction Wu *et al.*, (2012) and salting-out extraction Wu *et al.*, (2014) have been identified as alternate techniques for the concentration of the required butanediol products.

The literature suggests that the separation process with the greatest techno-economical merit involves the removal of water using a solvent extraction and recovery step by distillation and then concentrating the butanediol products by the removal of trace amounts of water Haas *et al.*, (2005), Penner *et al.*, (2017), Haider *et al.*, (2018), Harvianto *et al.*, (2018), Satam *et al.*, (2019). Due to its techno-economic feasibility and relatively low environmental impact, butan-1-ol has been identified as an optimum solvent to achieve the required separation of the butanediol components Othmer *et al.*, (1941), Frank *et al.*, (2008), Wu *et al.*, (2008), Birajdar *et al.*, (2014), Gai *et al.*, (2018), Haider *et al.*, (2018)

The recovery of the aqueous-extraction solvent for re-use still remains an energy intensive section in the separation process and several processes for this recovery have been proposed in the literature Haas *et al.*, (2005), Penner *et al.*, (2017), Haider *et al.*, (2018), Harvianto *et al.*, (2018), Satam *et al.*, (2019). However, those process designs that are proposed in the literature were performed with incomplete isothermal vapour-liquid phase equilibrium data for the butan-1-ol and butanediol systems, as the vapour-liquid equilibrium data describing these systems at the optimum process conditions have not been previously measured. In the design of high purity separation processes, experimental isothermal vapour-liquid equilibrium is preferred to perform energy balances across trays by the heat of mixing of the components involved in the separation process.

It is necessary to develop thermodynamic models to accurately perform the design of separation processes. To ensure that correct binary interaction parameters are utilized in thermodynamic models, such as the Non-Random Two-Liquid (NRTL) and Universal Quasi-Chemical (UNIQUAC) activity coefficient models, novel isothermal P - x - y phase equilibria data have been measured for the butan-1-ol + butane-1,4-diol and butan-1-ol + butane-2,3-diol systems at 353.2, 363.2, 373.2 and 388.2 K using a dynamic vapour-liquid

equilibrium apparatus for vacuum measurements designed by Raal and Mühlbauer, (1998). The experimental VLE data was modelled by employing the combined γ - Φ approach. Thermodynamic consistency tests, such as the area and point tests were performed on the measured experimental VLE data.

5.3. Theory

5.3.1. Modelling Approach

The γ - Φ approach is a commonly used method for the modelling of experimental VLE data at moderate- and low-pressure. The γ - Φ approach has been reviewed extensively by Raal and Mühlbauer, (1998). At low pressures, it can be assumed that an ideal solution reference state is applicable to the liquid-phase hence, an activity coefficient model is used to account for the non-ideality present in the liquid-phase. The non-ideality of the vapour-phase is accounted for by the fugacity coefficient in solution using an equation of state. This relationship can be described by the modified Raoult's law with vapour correction factor. The relationship has been derived by several authors (e.g. Raal and Mühlbauer, (1998), Walas, (2013)) and is given by:

$$y_i \Phi_i P = x_i \gamma_i P_i^{sat} \quad (5.1)$$

Where i represents the component of interest, x_i and y_i is the liquid- and vapour-phase compositions respectively, P is the total pressure of the system, P_i^{sat} is the saturated pressure and, γ_i and Φ_i are the correction factors of the liquid-phase (the activity coefficient for species i) and vapour-phase (vapour-phase correction factor) respectively. The vapour-phase correction factor is defined by:

$$\Phi_i = \frac{\hat{\phi}_i}{\phi_i^{sat}} \exp \left[\frac{-V_i^L (P - P_i^{sat})}{RT} \right] \quad (5.2)$$

Where $\hat{\phi}_i$ and ϕ_i^{sat} are the fugacity coefficients in solution and fugacity coefficient at saturation of component i , the molar volume of the liquid is V_i^L , T is the temperature and R is the universal gas constant. To determine $\hat{\phi}_i$ and ϕ_i^{sat} , usually the virial equation of state is used for low pressure systems as it does not require regressed binary interaction parameters for its application, and can usually adequately describe the vapour phase at these conditions (Walas, (2013)).

5.3.2. Model Selection

In this work, the Universal Quasi-Chemical (UNIQUAC) (Abrams and Prausnitz, (1975)) and the Non-Random Two-Liquid (Renon and Prausnitz, (1968)) excess Gibbs energy (activity coefficient) models were used to account for the liquid-phase non-ideality. The virial equation of state with the Hayden O'Connell (HOC) Hayden and O'Connell, (1975) correlation was employed to account for the vapour-phase non-ideality. The UNIQUAC and NRTL activity coefficient models were selected in conjunction with the virial equation of state due to their characteristic superior performance in representing the experimental low-pressure VLE data for oxygenated systems Walas, (2013).

5.4. Experimental

5.4.1. Materials

In this work, butan-1-ol, butane-1,4-diol and butane-2,3-diol were used to conduct the VLE experimental data measurements and were sourced from Sigma-Aldrich with the supplier mass purities stated as >0.99 mass fraction. To dehydrate the chemicals of trace amounts of water, the components were initially treated with a molecular sieve (3\AA KnNa12-n[(AlO₂)₁₂(SiO₂)₁₂]) for 36 hours before use. To validate the purity of the pure component species and the water content, measurements were performed using gas chromatography (GC) sampling, Karl-Fischer titration, and refractive index methods. A Shimadzu GC 2014 was used to determine the liquid- and vapour-phase compositions with a POROPAK-Q column (2 m x 2.2 mm) installed. To ensure optimal and accurate sampling, suitable operating conditions for the GC were selected. An injector, column and detector temperature of 513.15 K was used with helium carrier gas (30 ml/min). Pure component analyses using the GC revealed relative GC peak areas of >0.99. The water content of the butan-1-ol and the butanediols was determined using a Karl-Fischer (MKS 500) apparatus revealing a water concentration, for all components considered, of <0.0005 mass fraction. To determine the refractive indices of the considered components, a refractometer, ATAGO RX-7000 α (sodium D-line = 589 nm) with a supplier uncertainty of 0.00010 was used. The results of the analyses of the pure component species are presented in Table 5.1.

5.4.2. Equipment and Uncertainties

The dynamic vapour-liquid equilibrium apparatus and procedure outlined in the work of Joseph *et al.* Joseph *et al.*, (2001) was used to conduct the low-pressure VLE measurements of the butan-1-ol and butanediol binary systems. Figure 5.1 represents a schematic of the dynamic apparatus setup employed to perform the measurements of the binary systems in this work. Pressure of the still was maintained by using an automatic

pressure controller (ABB F080). The pressure setpoint of the still was achieved and maintained using vacuum and atmospheric air. The temperature was maintained using a voltage supply to heater cartridges within the boiling chamber of the dynamic still. To ensure that heat loss of the boiling chamber is minimized, sufficient insulation is utilized. Temperatures were measured using a class-A Pt- probe. The calibration of the temperature probe was performed using a WIKA CTB 9100 temperature standard with an uncertainty of 0.02 K. The standard combined uncertainty for the temperature measurements was found to be 0.1 K. Pressure measurements were conducted using a WIKA P-10 transducer and was calibrated using a WIKA CPH 6000 standard. The supplier uncertainty was stated as 0.05 kPa while the standard combined uncertainty in pressure was found to be 0.12 kPa.

The thermal conductivity detector of the gas chromatograph was calibrated by the area ratio method outline in the work of Raal and Mühlbauer, (1998). Standard mixtures were prepared gravimetrically using a Mettler-Toledo mass balance (model AB204-S) with a supplier uncertainty of 0.0001 g. The standard combined uncertainty in composition was calculated and found to be ± 0.004 mole fraction. The procedures outlined in the work of NIST JCGM ISO, (2008) were used in the calculations for all uncertainties. The uncertainties were calculated by the propagation of errors of type A and B and included in the calculation was the uncertainty stipulated by the supplier, and the uncertainties from the calibration, repeatability during sampling and the component purities. The equilibrium condition was established by observing a steady condensation drop rate, (60-90 drops per min), a continuous steady flow through the Cottrell tube, and a constant composition upon sampling (conducted in triplicate)

5.5. Results and Discussion

The vapour pressures of the pure butan-1-ol and butane-2,3-diol were determined by the dynamic method. Due to the limitations of the apparatus used, the vapour pressures for pure butane-1,4-diol could not be measured in this work. The measured vapour pressures were compared against vapour pressures determined using parameters found in the literature. Antoine and Wagner parameters are reported in the work of Poling *et al.*, (2001) and NIST ThermoData Engine via Aspen Plus® V10 NIST, (2019) respectively, and these results are presented in Table 5.2. A close correlation is observed within 0.1 kPa between the measured and literature data thereby validating the accuracy of the experimental temperature and pressure measurements. The differences can be attributed to the uncertainties that are present in the experimental temperature and pressure measurements. Note that the vapour pressures for butane-2,3-diol were measured at two common temperatures in a previous work Mavalal and Moodley, (2020), but were repeated here with precise

correlation. Aspen Plus® V10 was used to predict the pure component vapour pressures of butane-1,4-diol for modelling purposes.

The results of the vapour-liquid equilibrium data measurements, for the system of butan-1-ol (1) + butane-1,4-diol (2) and butan-1-ol (1) + butane-2,3-diol (2), are presented in Tables 5.3 and 5.4, and are expressed graphically in Figures 5.2 to 5.5. The experimental data was modelled employing the γ - Φ approach with the liquid-phase non-ideality being accounted for using the Universal Quasi-Chemical (UNIQUAC) Abrams and Prausnitz, (1975) and the Non-Random Two-Liquid (NRTL) Renon and Prausnitz, (1968) activity coefficient models and the Hayden O'Connell (HOC) correlation in the virial equation of state Hayden and O'Connell, (1975) to account for the non-ideality in the vapour-phase. Figures 5.6 and 5.7 show that the activity coefficients of the experimental data are greater than 1, suggesting a positive deviation from Raoult's Law. The phase behaviours of the butan-1-ol and butanediol systems shows a wide phase envelope between the liquid- and vapour-phase. Both systems exhibited a steep P-y curve (more pronounced in the butane-1,4-diol systems) and no azeotrope was observed for the range of temperatures and pressures in which the data was measured. This more pronounced steepness in the butane-1,4-diol system is attributed to the differences in pure component vapour pressures between butan-1-ol and the butanediols. The ratio of the pure component vapour pressures is larger in the case of the butan-1-ol + butane-1,4-diol mixtures, than in the butan-1-ol + butane-2,3-diol mixtures. The non-ideality is also more pronounced in the butan-1-ol + butane-1,4-diol mixtures, indicated by the larger activity coefficients in the concentrated regions. This may be attributed to the location of the OH groups on the terminal positions of the butane-1,4-diol molecule which possibly promotes intermolecular interaction with the butan-1-ol molecules and intramolecular interactions with other butane-1,4-diol molecules, increasing non-ideal mixture characteristics, in comparison to the OH group locations on the interior carbon atoms in the butane-2,3-diol molecule. This attribute was also discussed by Zorębski *et al.*, (2014) for the non-ideality of volumetric properties for the same systems considered here.

To confirm the accuracy of the experimental measurements, thermodynamic consistency tests (the Area test of Redlich and Kister, (1948) and the point test of Christiansen and Fredenslund, (1975)) were conducted using the Aspen Plus® V10 software package. Consistency criteria of 10% tolerance was used in the area test and 0.01 for the point test. Table 5.5 shows the results of the thermodynamic consistency tests, with the relevant plots presented in Appendix D, Figures D3-D4. Because the butan-1-ol + butanediol systems pass both tests at the temperatures considered in this work, the data is suggested to be thermodynamically consistent.

The data were fit to the model combinations of UNIQUAC-HOC and NRTL-HOC. For the activity coefficient model, a single set of temperature dependent model parameters were regressed for each of the systems considered. For the fitting procedure used in this work, the pressure residual was minimized:

$$\delta P = \sum_{k=1}^N (P^{exp} - P^{calc})^2 \quad (5.3)$$

Where N is the number of measured experimental data points in each system, P^{exp} and P^{calc} is the experimental and calculated pressure, respectively.

The root mean square deviation (RMSD) in pressure and absolute average deviation (δy_1) in vapour composition was calculated by the method outlined in the work of Gibbs and Van Ness, (1972):

$$RMSD = \sqrt{\frac{\delta P}{N}} \quad (5.4)$$

$$\delta y_1 = \frac{abs(y_1^{exp} - y_1^{calc})}{N} \quad (5.5)$$

The model parameters from the regression of the experimental VLE data and the fitting deviations are presented in Table 5.6. Both the UNIQUAC-HOC and NRTL-HOC are similar in their performance of effectively modelling the butan-1-ol + butane-1,4-diol and butan-1-ol + butane-2,3-diol systems, as the RMSDs and AADs are within the experimental uncertainties in pressure and composition. The binary interaction parameters were regressed with temperature dependence so that VLE predictions can be made for these systems at intermediate temperatures within the range considered here. These parameters are useful for tray-to-tray energy balance calculations in distillation. The alpha parameter in the NRTL-HOC model was regressed according to the recommendations of Walas, (2013) as it provided a superior fit to the experimental data in both systems.

The experimental and modelled behaviour of the activity coefficients for each system is presented in Figures 5.6 and 5.7. It can be seen that the experimental activity coefficients are suitably correlated by both models and that the experimental temperature dependencies of the activity coefficients are replicated by the models. The activity coefficients at infinite dilution (γ_i^∞) that are predicted by the models are presented in Table 5.7. This data is essential for the design of high-purity separation processes including stripping, extraction of dilute materials, can be used to calculate Henry's constants, partition coefficients and solvent

selectivities, and has application in environmental safety considerations. Results of the activity coefficients at infinite dilution suggest that they are dependent on the activity coefficient model used. A trend of decreasing γ_i^∞ with increasing temperature was observed. The model independent extrapolation method of Maher and Smith, (1979) was also applied, (Appendix E, Table E1) and compared reasonably well with the model-extrapolated values.

The relative volatilities ($\alpha_{i,j}$) are calculated by:

$$\alpha_{i,j} = \frac{y_i}{x_i} \bigg/ \frac{y_j}{x_j} \quad (5.6)$$

The relative volatilities in this work are presented in Figures 5.8 to 5.11. A trend of decreasing $\alpha_{1,2}$ with increasing temperature is observed for both systems. The $\alpha_{i,j}$ is used in the design of distillation applications. It is also a useful parameter to consider when reporting VLE data as it highlights the quality of the equilibrium composition measurements (Mathias, (2017)). The minor differences observed when comparing experimental and model $\alpha_{i,j}$, especially in the dilute regions, is attributed to its sensitivity to minor changes in liquid- and vapour-phase compositions Gmehling *et al.*, (2019).

The plots of excess Gibbs energy as a function of liquid-phase composition are presented in Figures 5.12 and 5.13 and indicates the degree of departure from ideality at phase equilibrium of the mixtures. For both systems, a positive $\frac{G^E}{RT}$ was observed with decreasing behaviour as temperature is increased. For the system of butan-1-ol (1) + butane-1,4-diol (2), the plot of $\frac{G^E}{RT}$ against x_l displays a symmetrical nature with a maximum occurring at $x_l = 0.50$. The system of butan-1-ol (1) + butane-2,3-diol (2) displays a slight asymmetrical behaviour with a maximum occurring at $x_l = 0.55$. This is attributed to differences in the respective intermolecular interactions with the different isomers. The maxima of the $\frac{G^E}{RT}$ curve for the butan-1-ol (1) + butane-1,4-diol (2) systems is larger, confirming that the systems have a greater departure from ideality than the butan-1-ol (1) + butane-2,3-diol (2) systems. A strong correlation between the experimental and model calculated excess Gibbs energies were observed. It can be observed that the NRTL-HOC model provides a superior representation of the experimental Gibbs energies in both systems.

5.6. Conclusion

The vapour-liquid equilibrium phase behaviours of the butan-1-ol + butane-1,4-diol and butan-1-ol + butane-2,3-diol systems were successfully measured using a low-pressure dynamic apparatus. To confirm the accuracy and validity of the experimental VLE data, thermodynamic consistency tests were conducted which showed the data to be consistent. The VLE behaviour of the systems in this work was found to be non-ideal which is attributed to the differences in molecule sizes as well as the intermolecular forces exhibited by the oxygenated hydrocarbons considered. Both systems exhibited a steep P-y curve typical of systems of large differences in pure component vapour pressures. The activity coefficient models namely UNIQUAC (Abrams and Prausnitz, (1975)) and NRTL (Renon and Prausnitz, (1968)), and the HOC (Hayden and O'Connell, (1975)) correlation for the virial equation of state correlated the experimental VLE data well with a positive deviation from Raoult's Law which was more pronounced in the butane-1,4-diol systems. This may be attributed to location of the OH groups on the terminal positions of the molecules which possibly promotes superior intermolecular and intramolecular interaction in comparison to the butane-2,3-diol molecules. The RMSD calculation for pressure and the AAD values in the composition of the vapour-phase was within the experimental uncertainty. The lowest RMSD value was obtained from the NRTL-HOC model at 0.032 kPa for the butan-1-ol + butane-1,4-diol system, while both the NRTL-HOC and UNIQUAC-HOC models yielded an RMSD of 0.008 kPa for the butan-1-ol + butane-2,3-diol system. The γ_i^∞ values were found to decrease with increasing temperature. The systems both exhibited a positive $\frac{G^E}{RT}$ vs. x_1 behaviour, with butan-1-ol (1) + butane-1,4-diol (2) exhibiting a maximum at $x_1 = 0.50$ and butan-1-ol (1) + butane-2,3-diol (2) exhibiting a maximum at $x_1 = 0.55$. NRTL-HOC model provided a superior representation of the $\frac{G^E}{RT}$ vs. x_1 behaviour for both systems.

Table 5.1. Chemical purities and suppliers.^a

Component	CAS RN.	Supplier	Refractive Index (RI) at 0.101 MPa. ^a		Minimum Stated Mass Fraction Purity	GC Peak Relative Area (Mass Fraction Purity)
			Experimental	Literature ^b		
butan-1-ol ^c	71-36-3	Sigma	1.3990	1.3988	≥0.990	0.9999
		Aldrich	(293.15K)	(293.15K)		
butane-2,3-diol ^c	513-85-9	Sigma	1.4310	1.4310	≥0.990	0.9999
		Aldrich	(298.15K)	(298.15K)		
butane-1,4-diol ^c	110-63-4	Sigma	1.4461	1.4460	≥0.990	0.9999
		Aldrich	(293.15K)	(293.15K)		

^aStandard combined uncertainty u_c is $u_c(RI) = 0.0010$ and standard uncertainties are $u(T) = 0.01$ K, $u(P) = 0.002$ MPa, ^b Haynes, (2014), ^cPurified by molecular sieving.

Table 5.2. Experimental vapour pressures and comparison to literature correlation.^a

Component	T / K	P / kPa		
		Experimental	Literature	
			Antoine correlation Poling <i>et al.</i> , (2001)	Wagner equation NIST, (2019)
<hr/>				
butan-1-ol				
	353.2	21.9	21.8	21.9
	363.2	34.3	34.2	34.3
	373.2	51.9	51.9	52.0
	388.2	91.9	91.9	92.0
butane-2,3-diol				
	353.2	1.2	1.3	1.2
	363.2	2.1	2.2	2.1
	373.2	3.6	3.7	3.6
	388.2	7.6	7.5	7.6

^aStandard combined uncertainties u_c are $u_c(T) = 0.01 \text{ K}$, $u_c(P) = 0.12 \text{ kPa}$

Table 5.3. Vapour-liquid equilibrium data for the butan-1-ol (1) + butane-1,4-diol^a

$T / \text{K} = 353.2$					$T / \text{K} = 363.2$				
P / kPa	x_1	y_1	γ_1	γ_2	P / kPa	x_1	y_1	γ_1	γ_2
1.4	0.040	0.936	1.565	1.006	1.4	0.023	0.830	1.555	1.001
2.1	0.060	0.957	1.560	1.008	2.3	0.041	0.895	1.528	1.006
2.7	0.081	0.967	1.511	1.013	3.2	0.059	0.928	1.502	1.004
3.3	0.100	0.974	1.486	1.011	4.2	0.080	0.944	1.479	1.006
5.0	0.159	0.983	1.420	1.024	5.0	0.099	0.956	1.455	1.007
7.0	0.240	0.989	1.328	1.023	7.6	0.159	0.972	1.387	1.011
8.3	0.299	0.992	1.270	1.046	10.9	0.241	0.982	1.316	1.028
10.9	0.419	0.995	1.195	1.071	12.9	0.299	0.986	1.262	1.040
12.2	0.479	0.996	1.166	1.091	16.9	0.420	0.990	1.178	1.087
14.3	0.591	0.997	1.107	1.160	18.7	0.480	0.993	1.143	1.114
15.9	0.679	0.998	1.069	1.229	21.2	0.561	0.994	1.105	1.155
17.3	0.759	0.998	1.043	1.312	24.5	0.680	0.996	1.054	1.249
19.9	0.900	-	-	-	26.9	0.759	0.997	1.037	1.326
20.6	0.940	-	-	-	31.1	0.899	0.999	1.009	1.478
21.0	0.961	-	-	-	32.3	0.939	-	-	-
21.4	0.981	-	-	-	33.0	0.961	-	-	-
21.9	1.000	1.000	1.000	-	33.6	0.999	-	-	-
					34.3	1.000	1.000	1.000	-
$T / \text{K} = 373.2$					$T / \text{K} = 388.2$				
P / kPa	x_1	y_1	γ_1	γ_2	P / kPa	x_1	y_1	γ_1	γ_2
2.1	0.022	0.830	1.550	1.001	3.5	0.020	0.751	1.478	1.002
3.4	0.040	0.895	1.485	1.001	8.4	0.059	0.898	1.427	1.007
4.8	0.059	0.928	1.442	1.003	11.0	0.081	0.924	1.408	1.008
6.1	0.080	0.944	1.423	1.006	13.1	0.100	0.938	1.380	1.008
7.5	0.101	0.956	1.404	1.004	19.9	0.160	0.961	1.336	1.011
11.4	0.161	0.972	1.353	1.028	28.2	0.241	0.975	1.277	1.018
16.0	0.239	0.982	1.291	1.036	34.0	0.299	0.981	1.242	1.033
19.4	0.300	0.986	1.248	1.048	44.8	0.419	0.987	1.169	1.061
24.5	0.400	0.990	1.182	1.073	49.9	0.481	0.990	1.136	1.083
28.6	0.490	0.993	1.129	1.123	56.4	0.560	0.992	1.103	1.127
32.1	0.559	0.994	1.111	1.128	65.7	0.679	0.995	1.058	1.207
37.5	0.680	0.996	1.067	1.195	71.9	0.760	0.996	1.035	1.282
41.1	0.761	0.997	1.043	1.269	83.2	0.901	0.998	1.007	1.464
47.1	0.899	0.999	1.010	1.499	86.5	0.941	-	-	-
48.9	0.939	0.999	1.004	1.547	88.3	0.960	-	-	-
50.0	0.959	-	-	-	91.0	0.990	-	-	-
51.5	0.995	-	-	-	91.9	1.000	1.000	1.000	-
51.9	1.000	1.000	1.000	-					

^aStandard combined uncertainties u_c , $u_c(T) = 0.10 \text{ K}$, $u_c(P) = 0.12 \text{ kPa}$, $u_c(x_1) = u_c(y_1) = 0.0040$

Table 5.4. Vapour-liquid equilibrium data for the butan-1-ol (1) + butane-2,3-diol.^a

$T / \text{K} = 353.2$					$T / \text{K} = 363.2$				
P / kPa	x_1	y_1	γ_1	γ_2	P / kPa	x_1	y_1	γ_1	γ_2
1.2	0.000	0.000	-	1.000	2.1	0.000	0.000	-	1.000
1.8	0.021	0.328	1.305	1.004	2.9	0.020	0.257	1.286	1.000
2.3	0.040	0.487	1.293	1.004	3.8	0.041	0.424	1.275	1.000
2.8	0.061	0.595	1.283	1.005	4.5	0.060	0.528	1.265	1.001
3.3	0.080	0.663	1.270	1.003	5.4	0.081	0.605	1.255	1.002
3.8	0.100	0.714	1.262	1.005	6.1	0.100	0.656	1.246	1.002
5.3	0.160	0.806	1.230	1.008	8.4	0.159	0.762	1.219	1.004
7.2	0.240	0.870	1.194	1.016	11.2	0.240	0.838	1.184	1.012
8.5	0.300	0.898	1.168	1.023	13.3	0.301	0.872	1.160	1.021
11.0	0.419	0.933	1.123	1.044	17.2	0.420	0.917	1.116	1.045
12.2	0.480	0.945	1.101	1.064	19.0	0.479	0.932	1.097	1.061
13.7	0.559	0.957	1.075	1.089	21.4	0.559	0.947	1.074	1.081
15.9	0.680	0.972	1.044	1.140	25.0	0.680	0.965	1.044	1.135
17.4	0.760	0.980	1.029	1.187	27.3	0.760	0.975	1.029	1.176
20.1	0.900	0.992	1.012	1.304	31.2	0.901	0.990	1.005	1.310
20.8	0.939	0.995	1.008	1.318	32.4	0.939	0.994	1.003	1.346
21.2	0.959	0.997	1.007	1.375	33.1	0.960	0.996	1.002	1.388
21.6	0.979	0.998	1.007	1.482	33.7	0.980	0.999	1.001	1.413
21.9	1.000	1.000	1.000	-	34.3	1.000	1.000	1.000	-
$T / \text{K} = 373.2$					$T / \text{K} = 388.2$				
P / kPa	x_1	y_1	γ_1	γ_2	P / kPa	x_1	y_1	γ_1	γ_2
3.6	0.000	0.000	-	1.000	7.6	0.000	0.000	-	1.000
4.8	0.019	0.257	1.270	1.000	9.6	0.019	0.222	1.252	1.000
6.0	0.040	0.424	1.260	1.000	11.7	0.040	0.380	1.249	1.000
7.2	0.060	0.528	1.251	1.000	13.7	0.060	0.480	1.235	1.000
8.4	0.081	0.605	1.242	1.001	15.8	0.081	0.558	1.225	1.001
9.5	0.100	0.656	1.232	1.002	17.6	0.100	0.611	1.210	1.003
12.9	0.159	0.762	1.207	1.005	23.5	0.159	0.726	1.199	1.006
17.2	0.240	0.838	1.176	1.011	30.9	0.240	0.811	1.164	1.009
20.3	0.300	0.872	1.154	1.019	36.1	0.300	0.849	1.137	1.019
26.2	0.421	0.917	1.113	1.039	46.3	0.421	0.901	1.098	1.038
29.0	0.481	0.932	1.095	1.052	51.2	0.481	0.919	1.081	1.052
32.6	0.560	0.947	1.073	1.077	57.7	0.560	0.938	1.067	1.068
37.9	0.680	0.965	1.043	1.129	67.1	0.680	0.959	1.039	1.113
41.4	0.759	0.975	1.028	1.174	73.2	0.759	0.971	1.026	1.156
47.6	0.900	0.990	1.011	1.299	84.2	0.900	0.988	1.009	1.270
49.5	0.942	0.994	1.006	1.371	87.2	0.940	0.993	1.005	1.310
50.4	0.961	0.996	1.006	1.418	88.8	0.959	0.995	1.004	1.342
51.4	0.986	0.999	1.002	1.452	90.4	0.980	0.998	1.002	1.415
51.9	1.000	1.000	1.000	-	91.9	1.000	1.000	1.000	-

^aStandard combined uncertainties u_c , $u_c(T) = 0.10 \text{ K}$, $u_c(P) = 0.12 \text{ kPa}$, $u_c(x_1) = u_c(y_1) = 0.0040$

Table 5.5. Results of thermodynamic consistency tests using the NRTL-HOC model.

System	Calculated Criterion		Consistency Test Result
	Area Test (%)	Point Test	
butan-1-ol (1) + butane-1,4-diol (2)			
$T / K = 353.2$	0.398	0.002	Passed both tests
$T / K = 363.2$	0.181	0.010	Passed both tests
$T / K = 373.2$	0.001	0.001	Passed both tests
$T / K = 388.2$	0.372	0.006	Passed both tests
butan-1-ol (1) + butane-2,3-diol (2)			
$T / K = 353.2$	2.003	0.001	Passed both tests
$T / K = 363.2$	1.146	0.001	Passed both tests
$T / K = 373.2$	0.502	0.001	Passed both tests
$T / K = 388.2$	1.471	0.001	Passed both tests

Table 5.6. Regressed model parameters

Parameter	System			
	butan-1-ol (1) + butane-1,4-diol (2)		butan-1-ol (1) + butane-2,3-diol (2)	
	NRTL	UNIQUAC	NRTL	UNIQUAC
a_{12}	-0.102	-0.614	0.656	-1.320
a_{21}	-0.716	0.695	-0.636	1.087
b_{12}/K	184.127	175.882	-114.565	369.764
b_{21}/K	354.445	-262.148	238.843	-330.889
$\alpha_{12,NRTL}^*$	1.696	-	1.100	-
RMSD/kPa	0.032	0.035	0.008	0.008
δy_1	0.001	0.001	0.001	0.004

*Treated as an adjustable parameter

Table 5.7. Infinite dilution activity coefficients from each model

System	NRTL-HOC		UNIQUAC-HOC	
	γ_1^∞	γ_2^∞	γ_1^∞	γ_2^∞
butan-1-ol (1) + butane-1,4-diol (2)				
$T/K = 353.2$	1.639	1.813	1.607	1.709
$T/K = 363.2$	1.595	1.772	1.567	1.675
$T/K = 373.2$	1.548	1.732	1.529	1.642
$T/K = 388.2$	1.483	1.672	1.476	1.593
butan-1-ol (1) + butane-2,3-diol (2)				
$T/K = 353.2$	1.310	1.448	1.308	1.443
$T/K = 363.2$	1.291	1.436	1.292	1.436
$T/K = 373.2$	1.273	1.423	1.274	1.426
$T/K = 388.2$	1.248	1.405	1.246	1.405

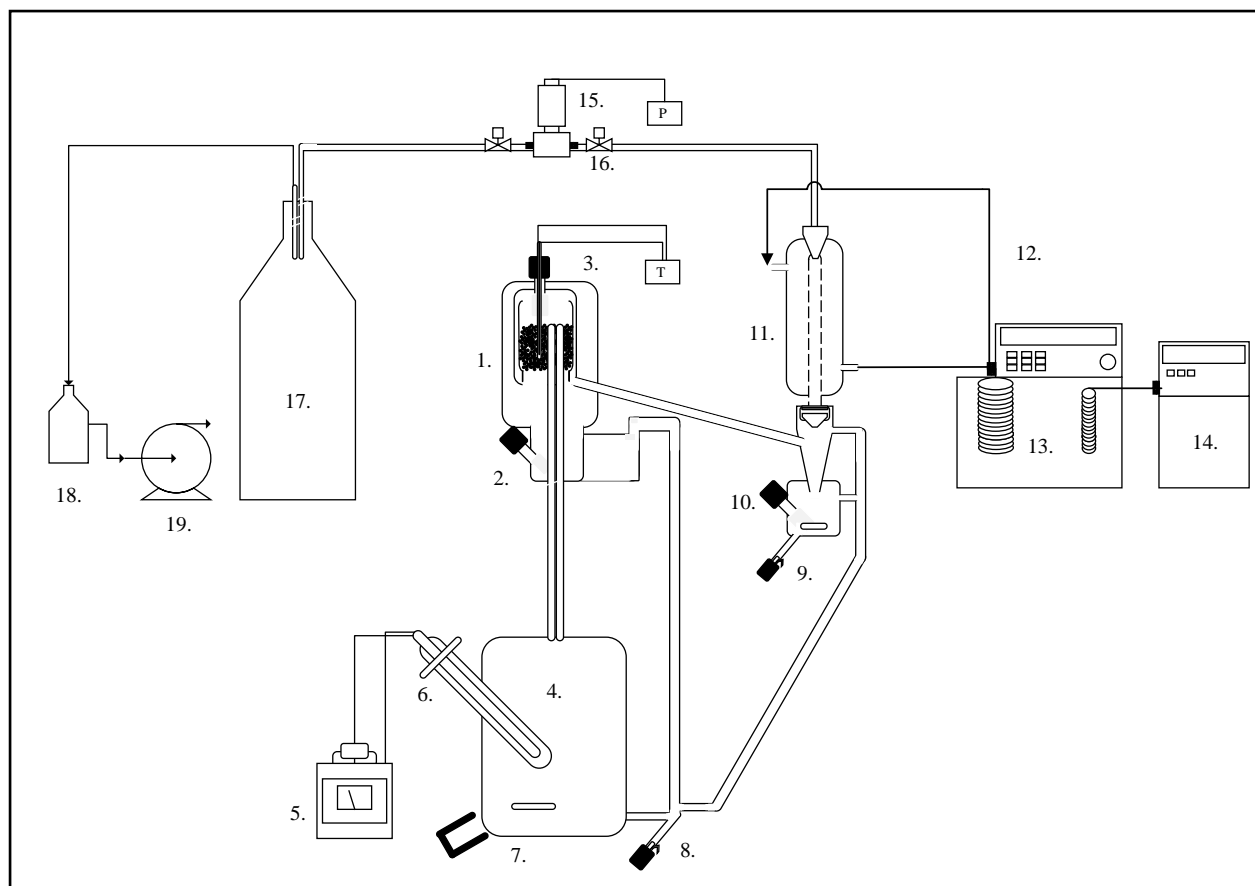


Figure 5.1. Layout of the apparatus of Joseph *et al.*, (2001) used in this work (as shown in Mavalal *et al.*, (2019)).

1-Equilibrium chamber. 2-Liquid sampling port. 3-Temperature measurement. 4-Boiling chamber. 5-Variable heat supply to boiler. 6- Heater cartridge and sleeve. 7- Magnetic stirrer and bead. 8- Boiler drain valve. 9- Condensate drain valve. 10- Vapour condensate sampling point. 11- Condenser. 12- Coolant line to condenser. 13. Coolant bath and controller. 14- Chiller. 15- Pressure measurement. 16. Isolation valves. 17- Ballast tank. 18. Cold trap. 19. Vacuum pump.

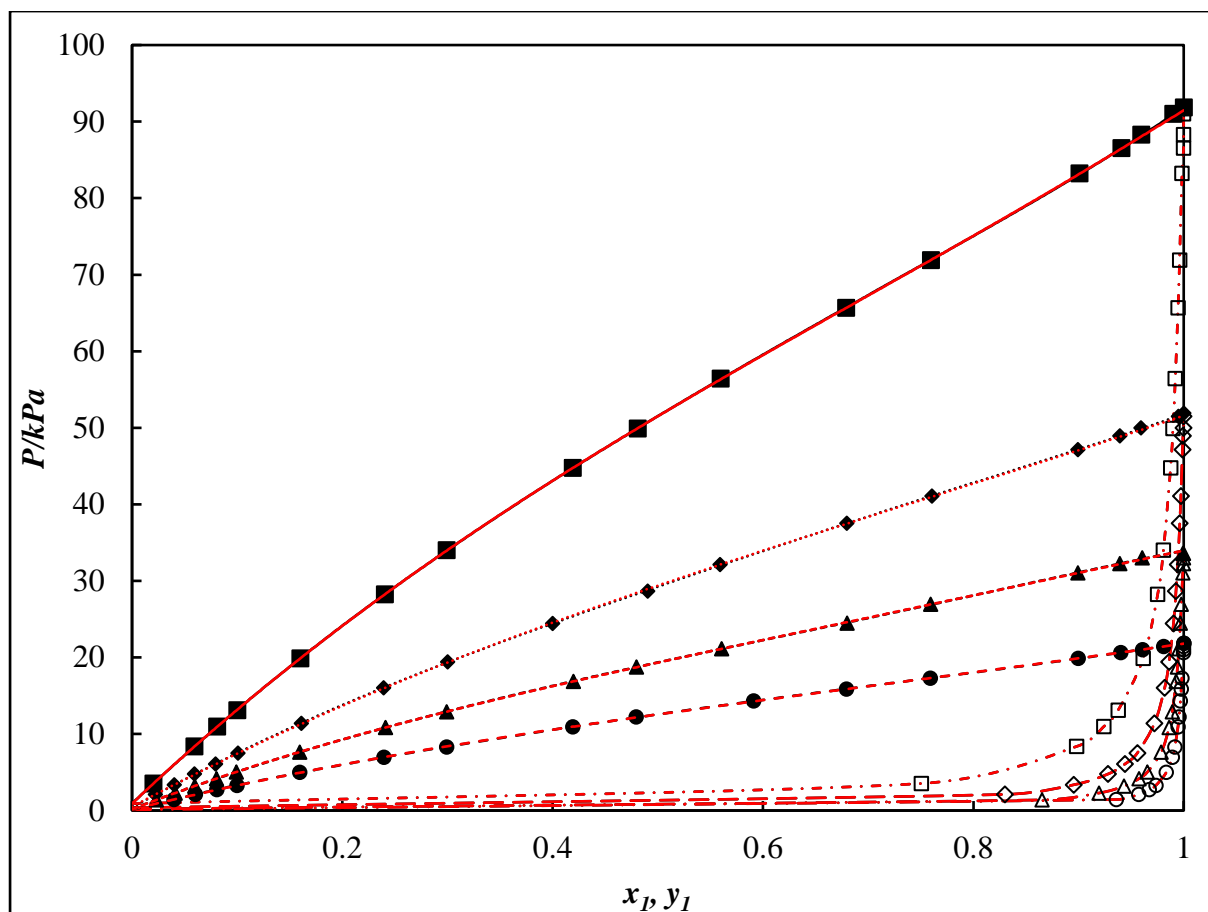


Figure 5.2. P - x - y data for the butan-1-ol (1) + butane-1,4-diol system. Experimental (P - x , P - y): at 353.2 K, (\bullet , \circ), 363.2 K, (\blacktriangle , \triangle), 373.2 K, (\blacklozenge , \lozenge), 388.2 K, (\blacksquare , \square). Model (P - x , P - y): at 353.2 K, ($---$, $---$), 363.2 K, ($---$, $---$), 373.2 K, ($---$, $---$), 388.2 K, ($---$, $---$). Black lines represent the NRTL-HOC model, red lines represent the UNIQUAC-HOC model.

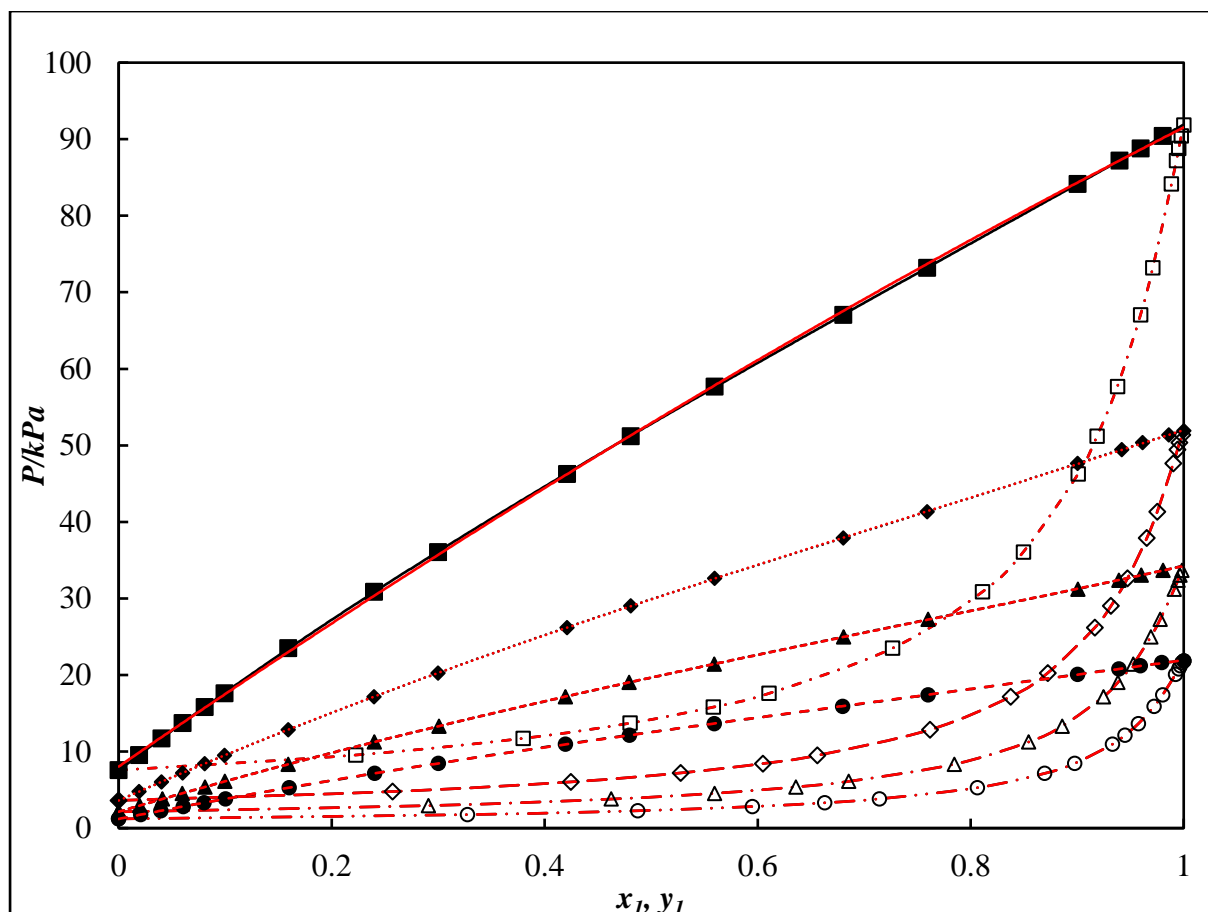


Figure 5.3. P - x - y data for the butan-1-ol (1) + butane-2,3-diol system. Experimental (P - x , P - y): at 353.2 K, (\bullet , \circ), 363.2 K, (\blacktriangle , \triangle), 373.2 K, (\blacklozenge , \lozenge), 388.2 K, (\blacksquare , \square). Model (P - x , P - y): at 353.2 K, ($---$, $---$), 363.2 K, ($---$, $---$), 373.2 K, ($---$, $---$), 388.2 K, ($-$, $-$). Black lines represent the NRTL-HOC model, red lines represent the UNIQUAC-HOC model.

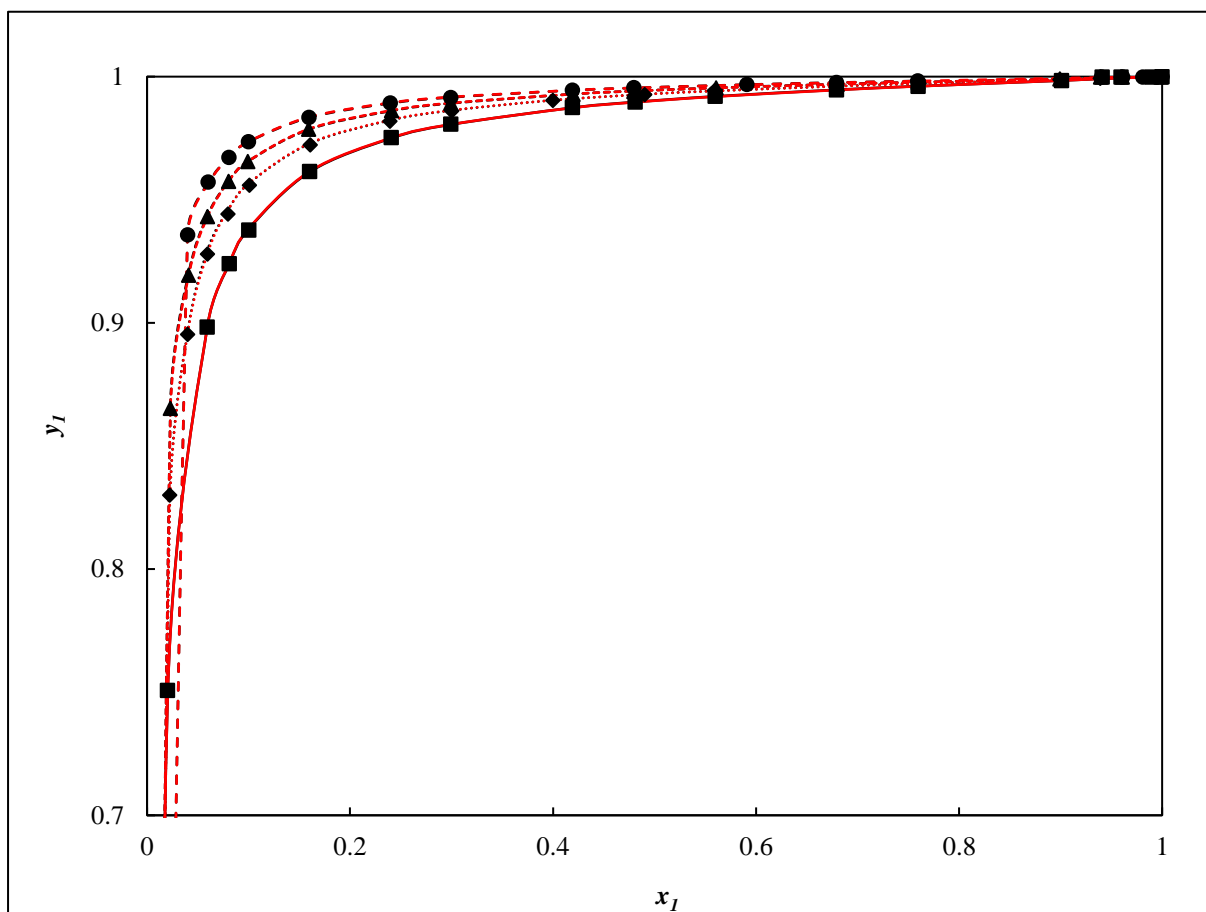


Figure 5.4. y_1 vs. x_1 for the butan-1-ol (1) + butane-1,4-diol system. Experimental: ●-353.2 K, ▲-363.2 K, ◆-373.2 K, ■-388.2 K. Model: (---)-353.2 K, (- - -)- 363.2 K, (⋯)-373.2 K, (—)-388.2 K. Black lines represent the NRTL-HOC model, red lines represent the UNIQUAC-HOC model.

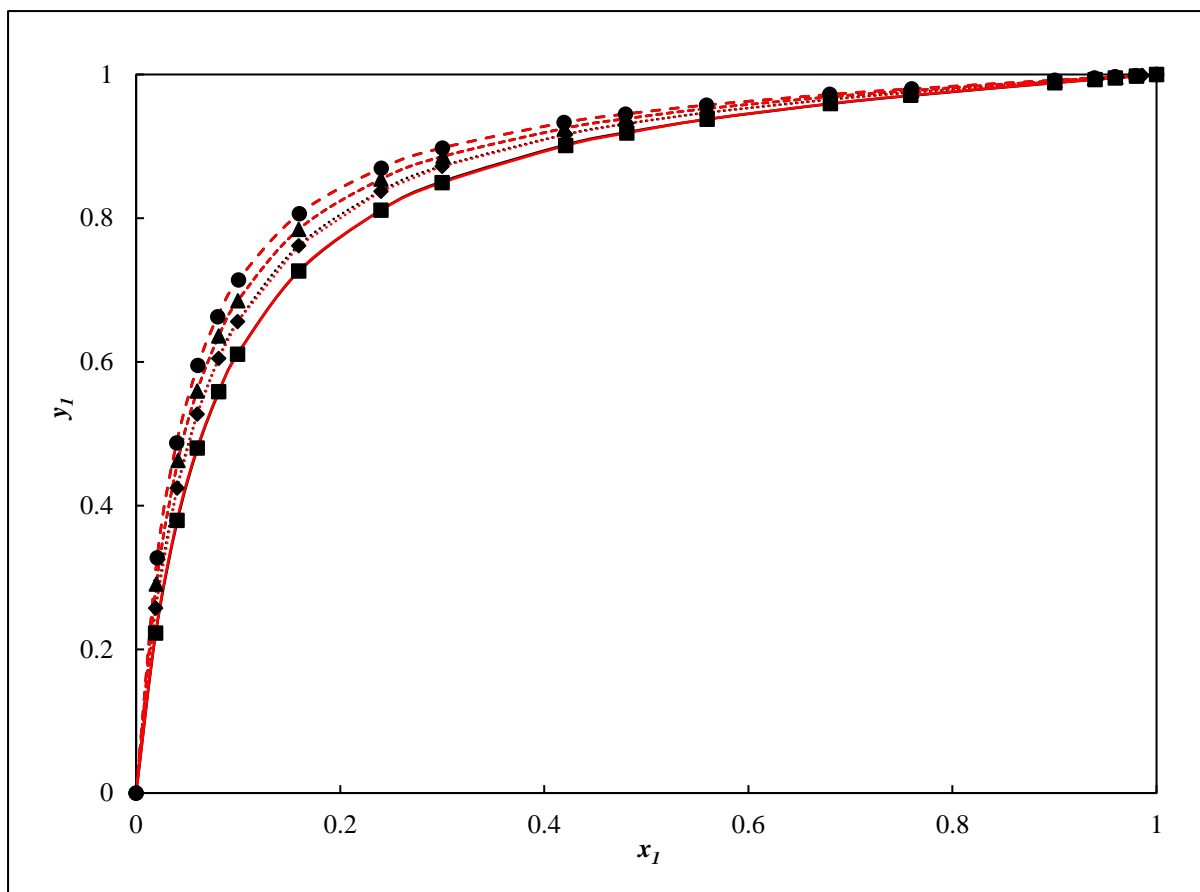


Figure 5.5. y_I vs. x_I for the butan-1-ol (1) + butane-2,3-diol system. Experimental: ●-353.2 K, ▲-363.2 K, ◆-373.2 K, ■-388.2 K. Model: (---)-353.2 K, (-.-)-363.2 K, (···)-373.2 K, (—)-388.2 K. Black lines represent the NRTL-HOC model, red lines represent the UNIQUAC-HOC model.

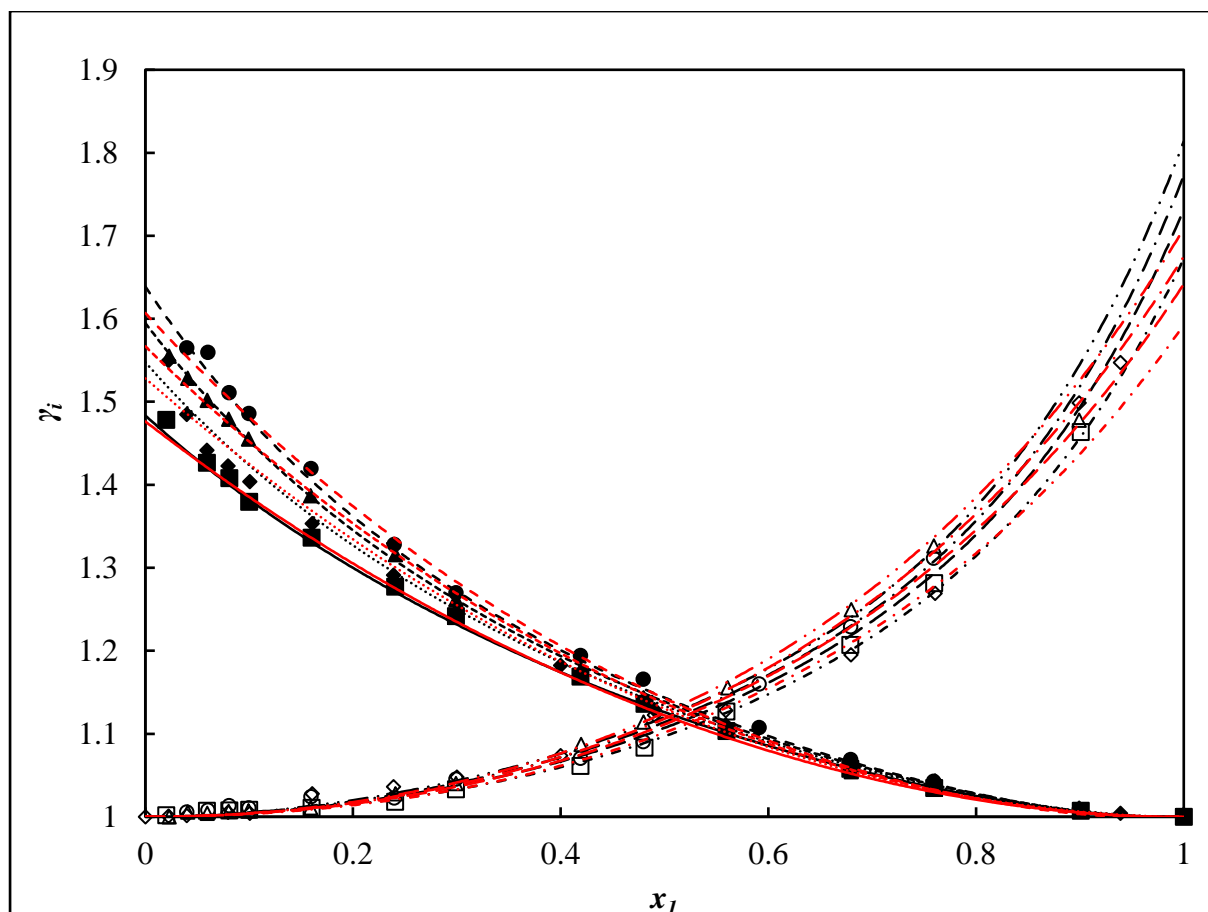


Figure 5.6. γ_i - x_1 data for the butan-1-ol (1) + butane-1,4-diol system. Experimental (γ_1, γ_2): at 353.2 K, (\bullet, \circ), 363.2 K, ($\blacktriangle, \triangle$), 373.2 K, (\blacklozenge, \lozenge), 388.2 K, (\blacksquare, \square). Model (γ_1, γ_2): at 353.2 K, (---, ---), 363.2 K, (- - -, - · -), 373.2 K, (···, ---), 388.2 K, (-, - · -). Black lines represent the NRTL-HOC model, red lines represent the UNIQUAC-HOC model.

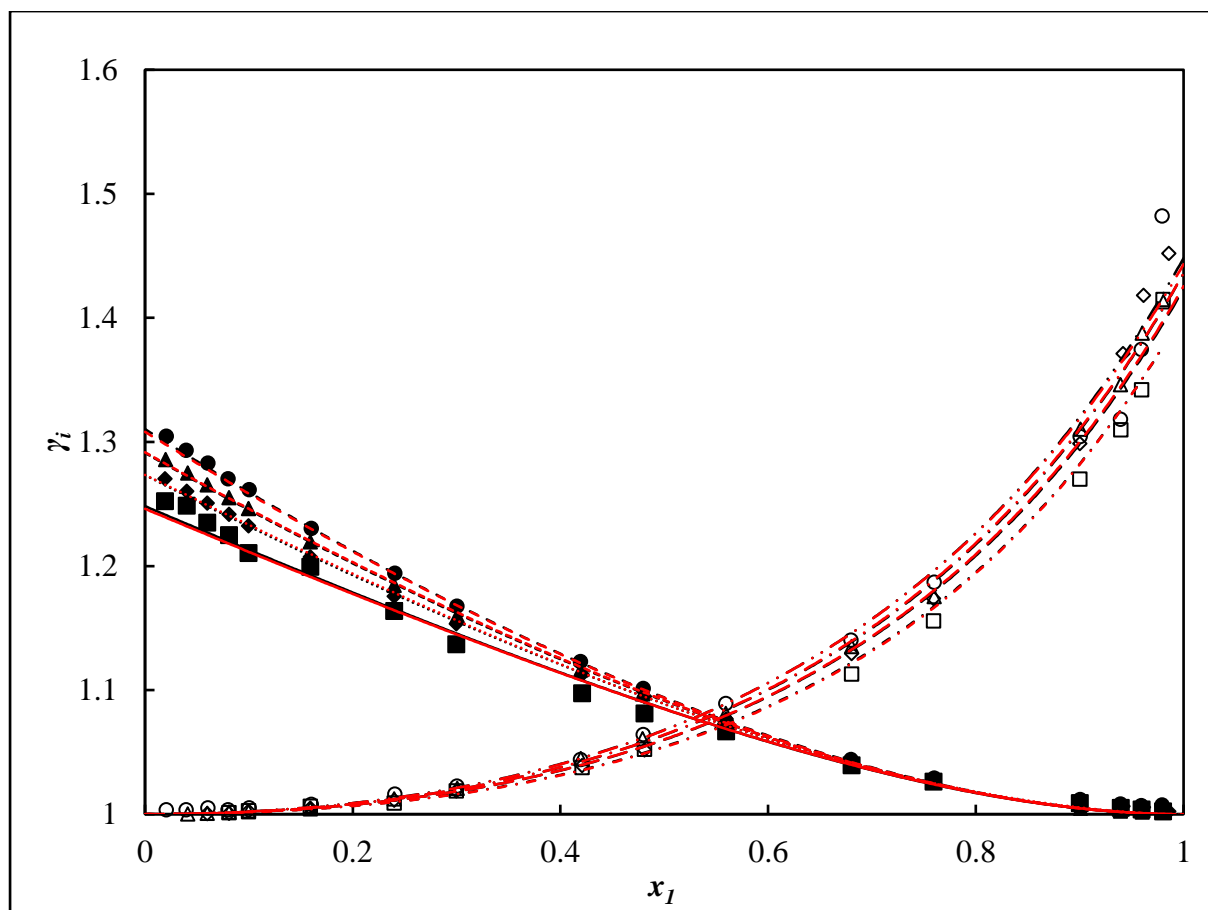


Figure 5.7. γ_i - x_1 data for the butan-1-ol (1) + butane-2,3-diol system. Experimental (γ_1, γ_2): at 353.2 K, (\bullet, \circ), 363.2 K, ($\blacktriangle, \triangle$), 373.2 K, (\blacklozenge, \lozenge), 388.2 K, (\blacksquare, \square). Model (γ_1, γ_2): at 353.2 K, (---, -·-), 363.2 K, (- - -, -·-), 373.2 K, (···, - - -), 388.2 K, (-, -·-). Black lines represent the NRTL-HOC model, red lines represent the UNIQUAC-HOC model.

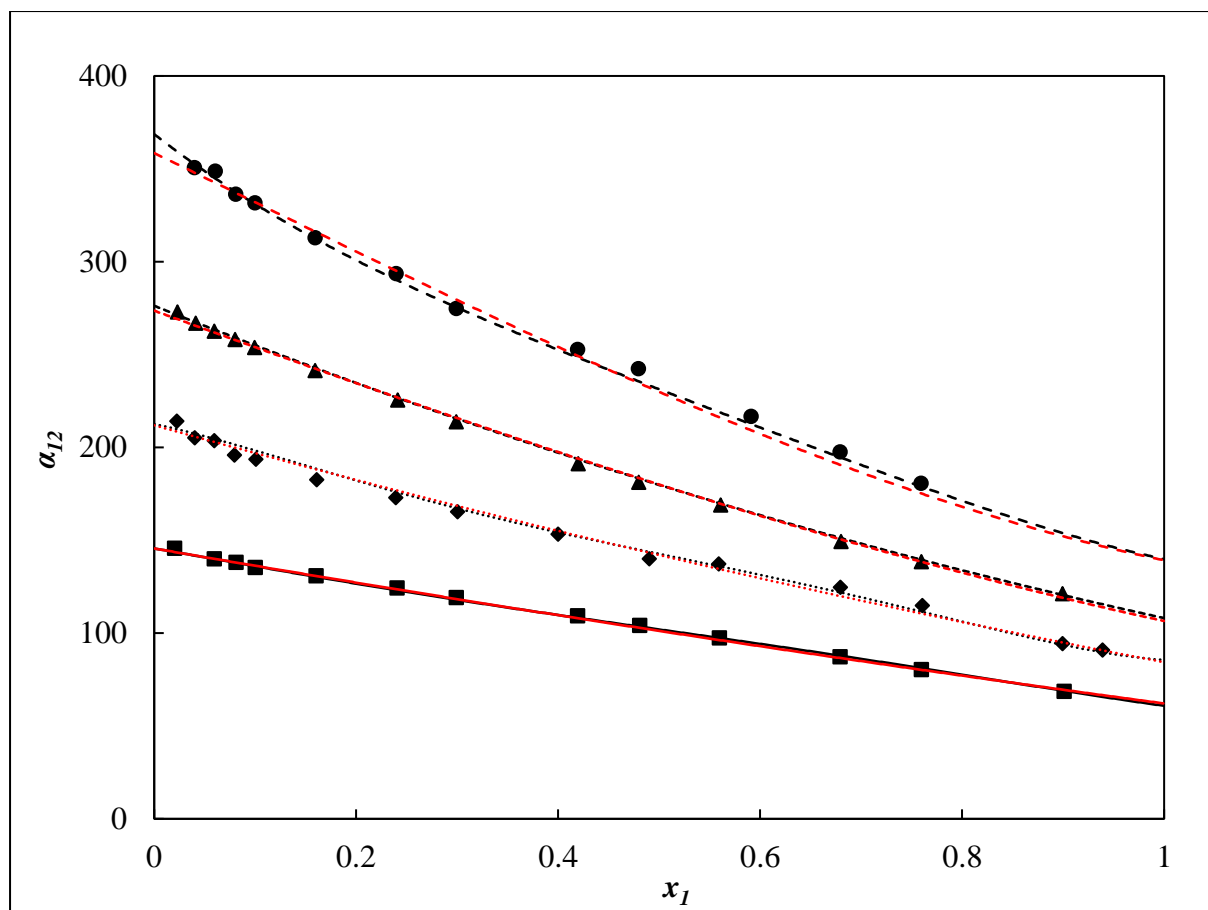


Figure 5.8. α_{12} vs. x_1 for the butan-1-ol (1) + butane-1,4-diol system. Experimental: ●-353.2 K, ▲-363.2 K, ◆-373.2 K, ■-388.2 K. Model: (---)-353.2 K, (- - -)- 363.2 K, (···)-373.2 K, (—)-388.2 K. Black lines represent the NRTL-HOC model, red lines represent the UNIQUAC-HOC model.

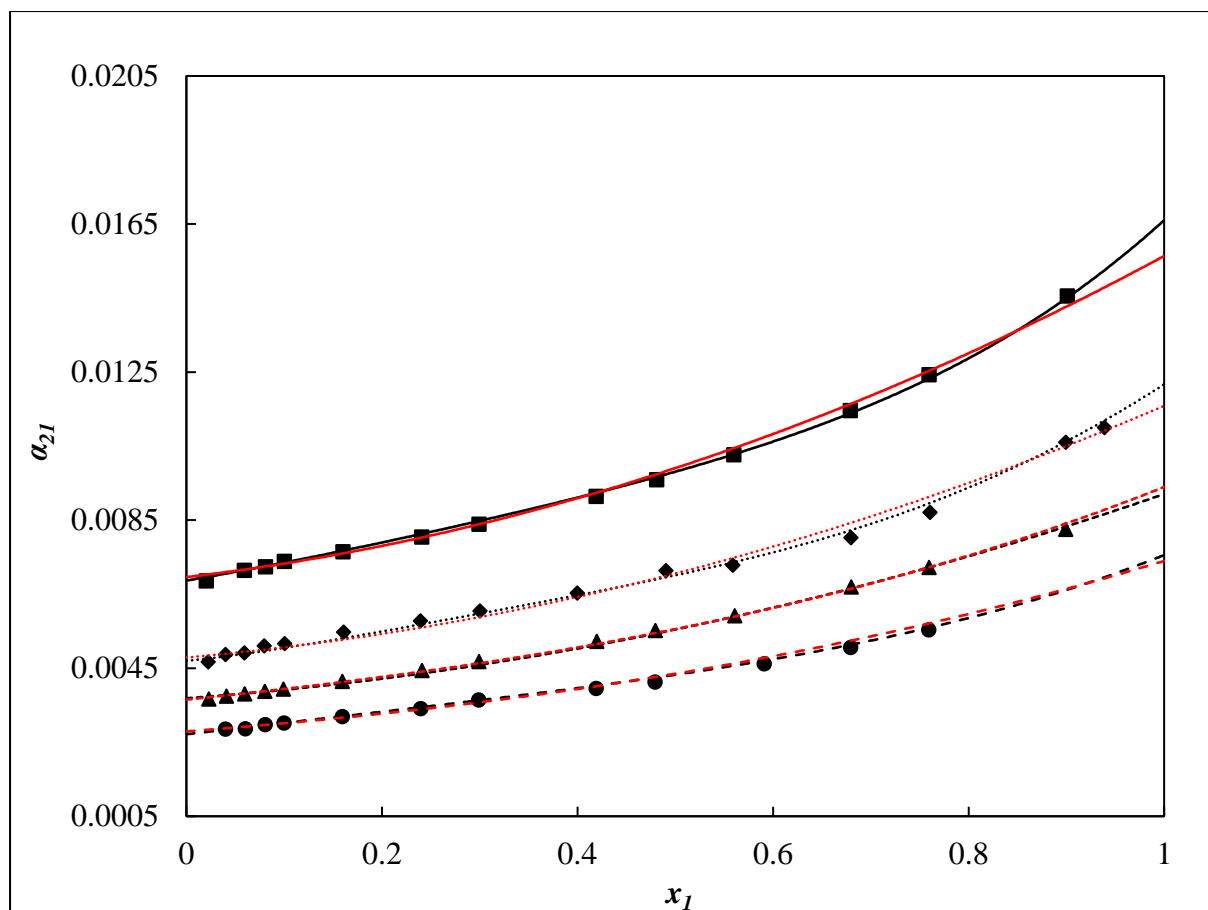


Figure 5.9. α_{21} vs. x_1 for the butan-1-ol (1) + butane-1,4-diol system. Experimental: \bullet -353.2 K, \blacktriangle -363.2 K, \blacklozenge -373.2 K, \blacksquare -388.2 K. Model: (---)-353.2 K, (-.-)- 363.2 K, (···)-373.2 K, (—)-388.2 K. Black lines represent the NRTL-HOC model, red lines represent the UNIQUAC-HOC model.

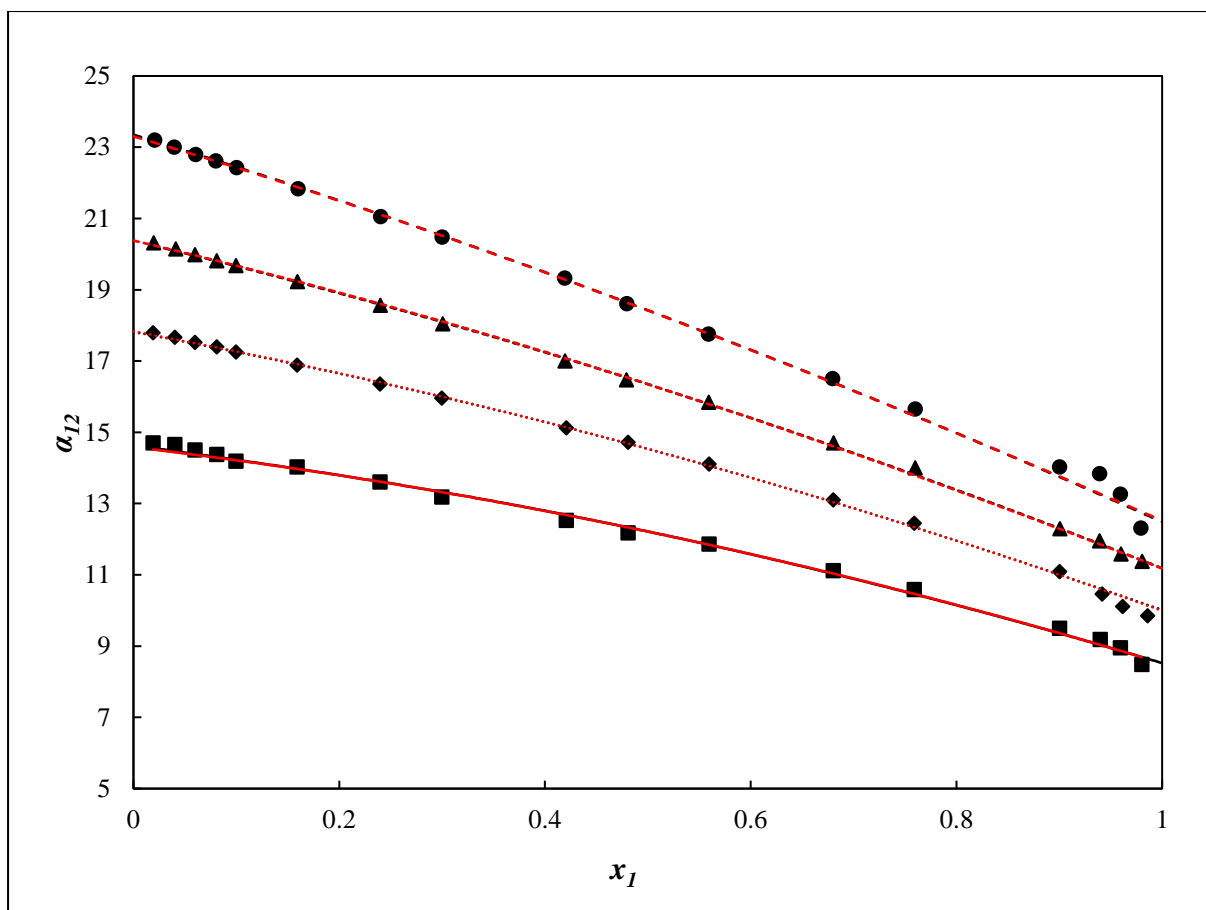


Figure 5.10. α_{12} vs. x_1 for the butan-1-ol (1) + butane-2,3-diol system. Experimental: ●-353.2 K, ▲-363.2 K, ◆-373.2 K, ■-388.2 K. Model: (---)-353.2 K, (- - -)- 363.2 K, (···)-373.2 K, (—)-388.2 K. Black lines represent the NRTL-HOC model, red lines represent the UNIQUAC-HOC model.

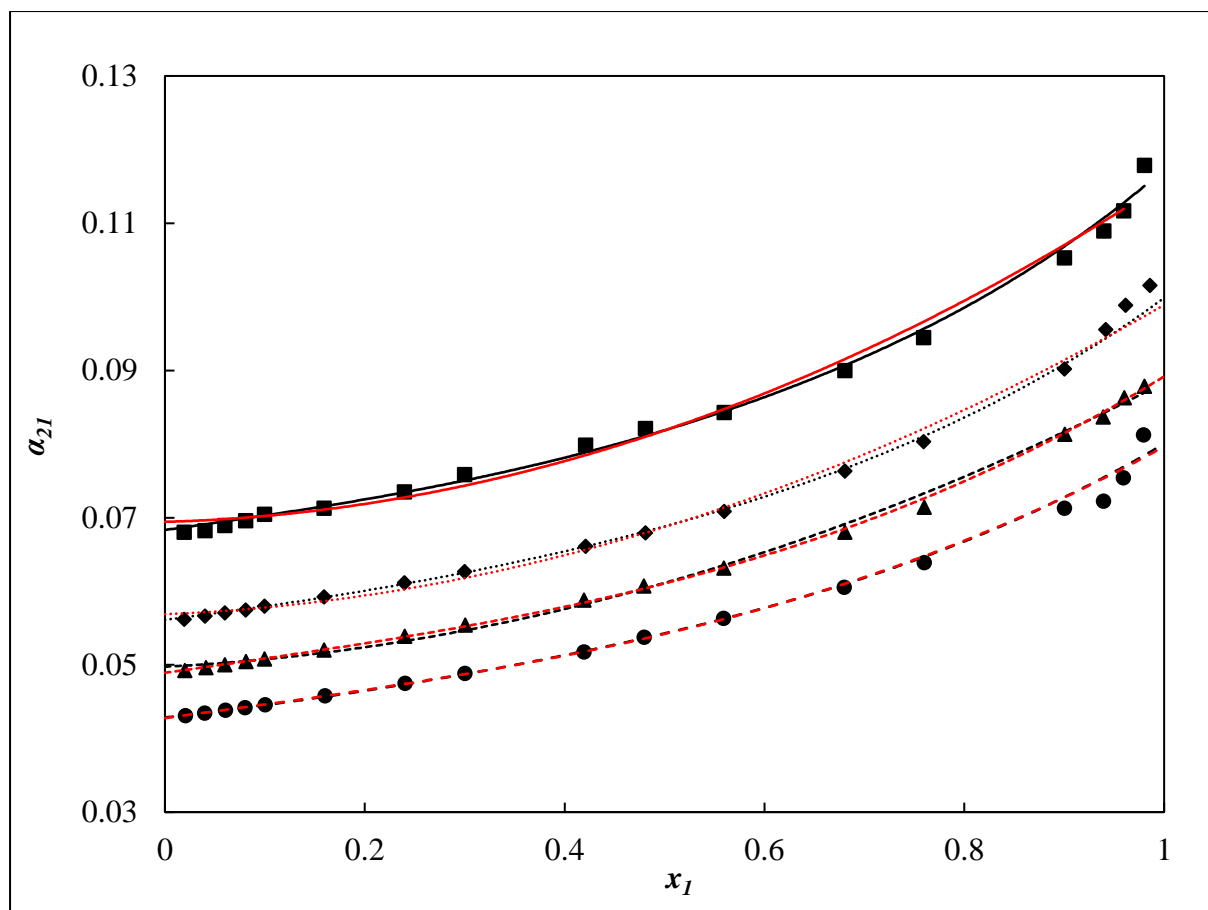


Figure 5.11. α_{21} vs. x_1 for the butan-1-ol (1) + butane-2,3-diol system. Experimental: ●-353.2 K, ▲-363.2 K, ◆-373.2 K, ■-388.2 K. Model: (---)-353.2 K, (- - -)- 363.2 K, (···)-373.2 K, (—)-388.2 K. Black lines represent the NRTL-HOC model, red lines represent the UNIQUAC-HOC model.

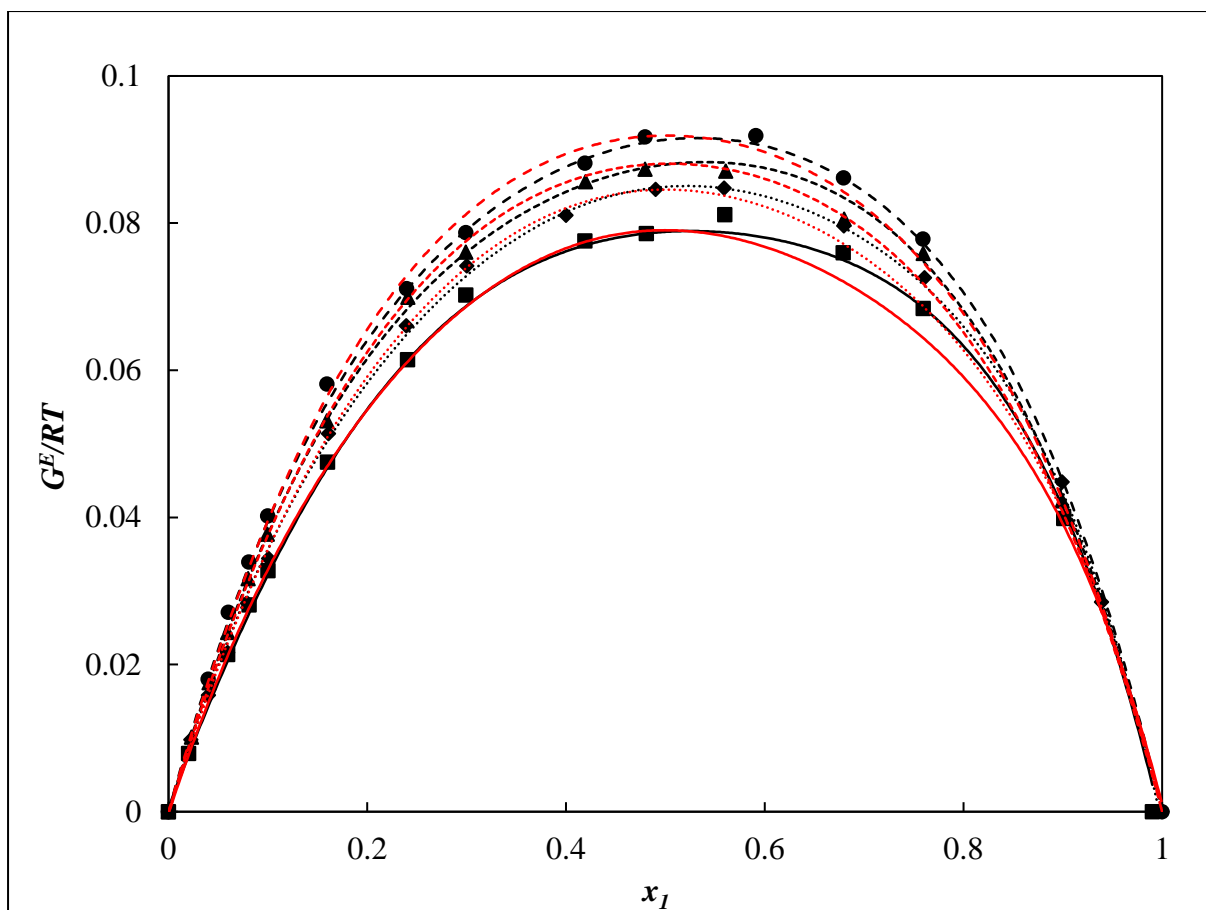


Figure 5.12. G^E/RT vs. x_1 for the butan-1-ol (1) + butane-1,4-diol system. Experimental: ●-353.2 K, ▲-363.2 K, ◆-373.2 K, ■-388.2 K. Model: (---)-353.2 K, (-.-)-363.2 K, (···)-373.2 K, (—)-388.2 K. Black lines represent the NRTL-HOC model, red lines represent the UNIQUAC-HOC model.

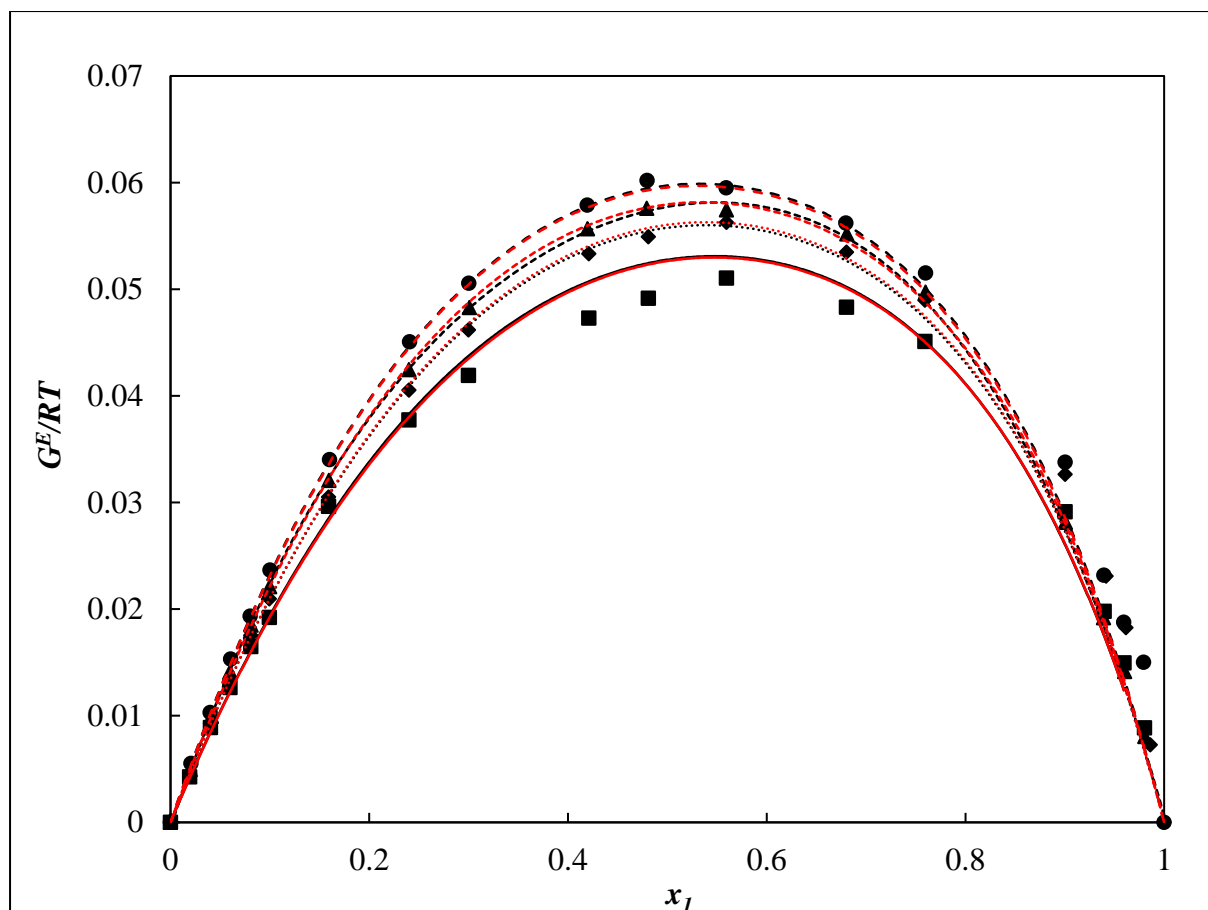


Figure 5.13. G^E/RT vs. x_1 for the butan-1-ol (1) + butane-2,3-diol system. Experimental: ●-353.2 K, ▲-363.2 K, ◆-373.2 K, ■-388.2 K. Model: (---)-353.2 K, (-.-)-363.2 K, (···)-373.2 K, (—)-388.2 K. Black lines represent the NRTL-HOC model, red lines represent the UNIQUAC-HOC model.

CHAPTER SIX

Techno-economic analysis of alternate process pathways for butane-1,4-diol and butane-2,3-diol purification from aqueous mixtures for use as a biofuel

Abstract

In this work, rigorous simulation and preliminary economic evaluation was conducted to explore alternate process pathways for the isolation of butane-1,4-diol and butane-2,3-diol from aqueous mixtures, derived from biological reaction pathways. The purpose of this purification (to 0.99 wt. fraction) is to valorise the butanediols for potential use as a biofuel, or alternatively as a marketable chemical for other industrial applications. The process pathways are designed on Aspen Plus® simulation software and include conventional distillation, extraction-assisted distillation and extraction-assisted distillation with heat integration. The processes were optimized to reduce duties and costs using conventional procedures. Conventional distillation was found to be the most economically feasible process alternative for the butane-1,4-diol purification, with an estimated total annual cost in the range of \$4,532,846.67 and \$4,635,070.52 for a payback period of 3 years, while extraction assisted distillation with heat integration was found to be the economically viable option for butane-2,3-diol purification with total annual costs in the range of \$2,997,204.58 and \$3,988,868.70 for a payback period of 3 years.

6.1. Introduction

An emerging research area is the development of biofuels, solvents and polymers from renewable sources. Biofuels for transportation are fuels that can be used interchangeably with petroleum derived fuels (“drop-in” fuels) in the pure state or as a blending component. Butane-1,4-diol and butane-2,3-diol have been identified as suitable drop-in fuels in certain transport applications due to their high calorific values, octane-numbers and heating values (Parate *et al.*, (2018), van Dyk *et al.*, (2019)). Butanediols are also commodity chemicals used as commercial solvents or in the manufacturing of polymers such as spandex, polyesters and pharmaceuticals. These butanediols can be produced industrially by chlorohydration of butene with a subsequent hydrolysis step or hydrogenation and hydrolysis. This is a highly energy intensive process. Alternatively, a biochemical process can also be used which involves the fermentation of biomass by certain classes of microbes (Menon and Rao, (2012), Tahri *et al.*, (2013), Karnaouri *et al.*, (2016), Patel *et al.*, (2017), Haider *et al.*, (2018), Satam *et al.*, (2019)). These biochemical processes can be renewable and can have a lower energy consumption (Haider *et al.*, (2018), Satam *et al.*, (2019)). However, a low concentration aqueous mixture (approximately 8-10% by mass) of butanediol is produced, that must be dehydrated before use (Haider

et al., (2018), Satam *et al.*, (2019)). Conventional distillation is a technically sound process for this dehydration and subsequent purification but is highly energy intensive as high-pressure steam must often be used as the heating medium, due to low concentrations of the butanediols and their high boiling points relative to water (Burgard *et al.*, (2016), Haider *et al.*, (2018)). Alternate dehydration processes include pervaporation, reactive extraction, liquid-liquid extraction and salting-out extraction. Each separation technology possesses its own benefits, drawbacks and limitations with respect to its applicability in industrial operation and commercial-scale production, with the most promising options presented in the literature being hybrid techniques involving solvent extraction and recovery by distillation to first remove excess water and subsequently concentrate the butanediol product composition (Haider *et al.*, (2018)). Butan-1-ol has been shown to be an efficient solvent for the extraction of butane-2,3-diol from aqueous mixtures (Harvianto *et al.*, (2018)). However, those processes were designed based on model parameters derived from limited phase equilibrium data as the vapour-liquid equilibrium (VLE) phase behaviour of the butan-1-ol/water + butane-2,3-diol was previously inadequate in the literature, yielding broadly qualitative proposed designs. Furthermore, only conventional distillation-based processes have been evaluated rigorously for the dehydration of butane-1,4-diol from a biochemical process path. In recent studies, Mavalal and Moodley (Mavalal and Moodley, (2020), (2021)) have expanded the literature for the VLE behaviour of butan-1-ol/water + butane-1,4-diol/butane-2,3-diol and have provided temperature dependent model parameters to improve separation design estimates. In this work, these improved parameters are used to perform techno-economic analyses for two separate separation processes to purify butane-1,4-diol or butane-2,3-diol aqueous mixtures, with feeds derived from biochemical process paths proposed in the literature.

The Butane-1,4-diol Production Process.

The work of Satam *et al.*, (2019) provides a possible process route for the production of butane-1,4-diol (1,4-BDO) biofuel, see Figure 6.1. The conversion of biomass to the 1,4-BDO biofuel is achieved by charging diluted dextrose with compressed air into a bioconversion reactor. This reactor is operated in batch mode. The dextrose syrup is converted to 1,4-BDO by the microbial action of the *Escherichia coli* or *E. Coli* bacterium. When the desired conversion is achieved, the broth produced in the bioconversion reactor is heated to 333 K for 5 minutes to kill the *E. Coli* cells. The spent cells in the reactor broth are removed by action of microfiltration. The microfiltered retentate then undergoes ultrafiltration where process water is used to wash the reactor broth to ensure that components such as proteins and other macroparticles are removed. To remove sugars and multi-valent cations, the ultrafiltration retentate undergoes nanofiltration. Cations (NH_4^+ , Na^+ , K^+) and anions (Cl^- , acetate, glutamate) are removed from the filtered reactor broth by undergoing a cation and anion exchange. The broth is then transferred to an evaporator (operated under vacuum) so that some water and low-boiling organics are removed. The evaporator unit includes an internal scrubber where water is used to entrain

any 1,4-BDO present in the vapour. The scrubbed vapour is compressed in a mechanical vapour re-compressor before being condensed. The heat duty from the scrubbed vapour is first exchanged with the incoming broth from the filtration steps (heat integration) to allow for this condensation. The condensed scrubbed vapour is a mixture of water and ethanol and can be regarded as wastewater Satam *et al.*, (2019).

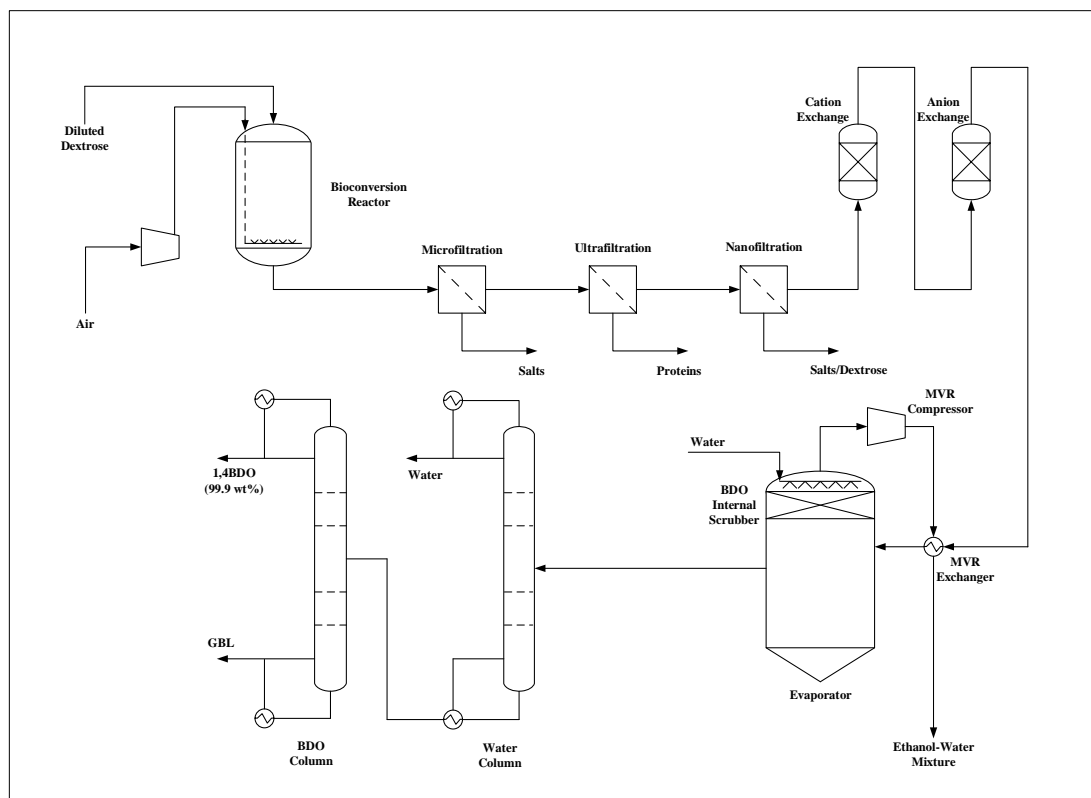


Figure 6.1. Flow diagram of the butane-1,4-diol production process redrawn from Satam *et al.*, (2019).

The proposed design for this production route of 1,4-BDO includes a two-column downstream purification step where the aqueous-mixture of water and 1,4-BDO is to be separated and concentrated to acquire a 1,4-BDO product purity of 99.0% (w/w) and a minimum recovery of at least 90.0% (wt.). The composition of the aqueous 1,4-BDO mixture that is transferred to the separation section is presented in Table 6.1.

Table 6.1 Feed compositions for the 1,4-BDO separation design Satam *et al.*, (2019).

Components	Mass (%)
Butane-1,4-diol	6.521
Water	93.277
Glucose	0.002
Ethanol	0.196
Oxolan-2-one	0.004
Pyrrolidin-2-one (<i>ppm</i>)	2.807

The Butane-2,3-diol Production Process.

The flow diagram of the proposed biochemical reaction and separation process for butane-2,3-diol (2,3-BDO) production is shown in Figure 6.2 (Haider *et al.*, (2018)). The biomass feed (mixture of hexose and pentose sources) is cleaned and broken down in a crushing unit. Extracted sugars from biomass are hydrolysed into fermentable forms in a pre-treatment step, and subsequently fermented by enzymatic activity of *Bacillus licheniformis* to produce butane-2,3-diol in a stirred reactor. The 2,3-BDO reaction broth is then transferred to a train of filtration units where glucose and the microbes are recovered and recycled to the bioconversion reactor. The aqueous mixture of water and 2,3-BDO is separated in a two-column downstream purification step. In this separation process, water is removed through the distillate of the first column while the 2,3-BDO is concentrated to 99.0% (w/w) with a minimum recovery of at least 90% (wt.) in the distillate of the second column. The composition of the aqueous feed mixture to the separation section is presented in Table 6.2.

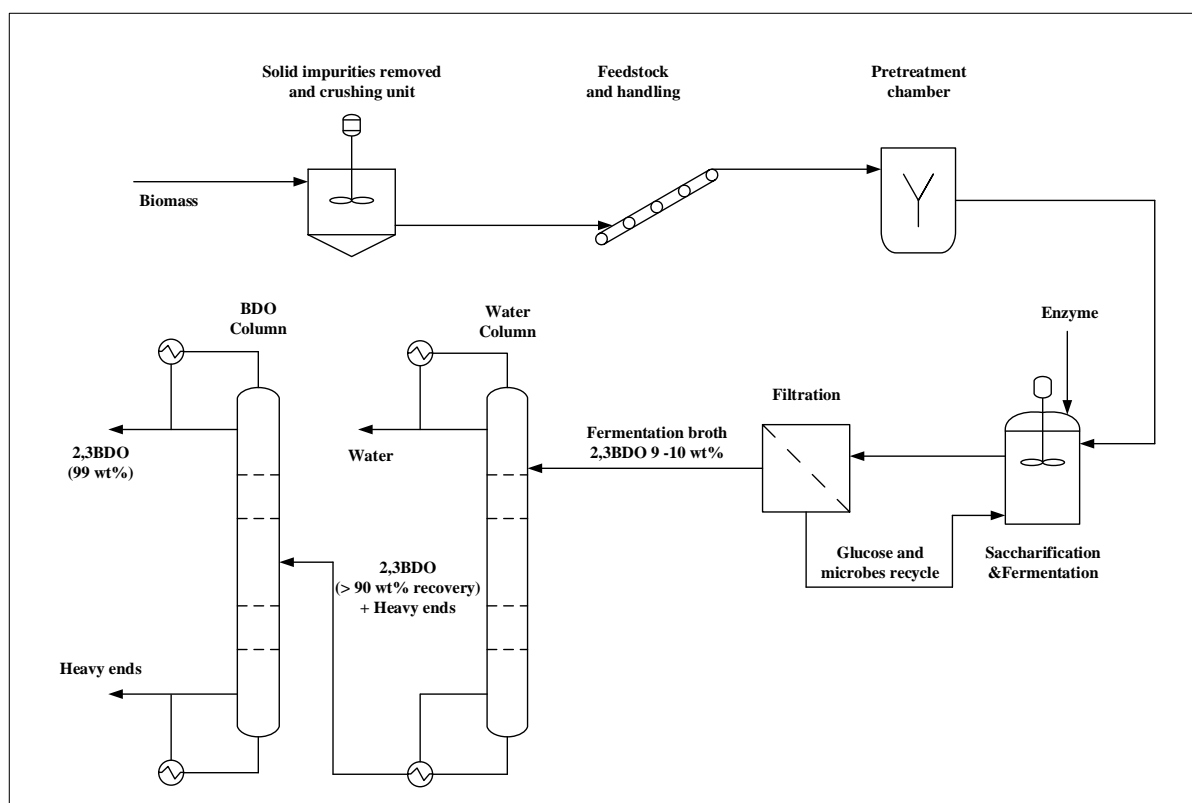


Figure 6.2. Flow diagram of the butane-2,3-diol production process redrawn from Haider *et al.*, (2018).

Table 6.2 Feed compositions for the 2,3-BDO separation design Haider *et al.*, (2018).

Components	Mass (%)
Water	87.500
Butane-2,3-diol	9.300
Formic acid	0.027
Acetic acid	0.890
Lactic acid	0.071
Succinic acid	0.203
Ethanol	1.050
3-Hydroxybutan-2-one	0.934

Rationale for Hybrid Separation Scheme

As mentioned, conventional distillation (as originally proposed in these designs) is an energy intensive but technically feasible process, where water can be distilled off, while the butanediol is refined further in a second column. The process is energy intensive because both 1,4-BDO and 2,3-BDO are of a hydrophilic nature and their respective boiling points are far greater than that of water (Penner *et al.*, (2017)). The merits of separation alternatives such as pervaporation (Shao and Kumar, (2009b),

(2009a)), reactive extraction (Li *et al.*, (2012)), liquid-liquid extraction (Wu *et al.*, (2012)), and salting-out extraction (Wu *et al.*, (2014)) have been discussed in previous work (Haider *et al.*, (2018)). Liquid-liquid extraction using butan-1-ol with subsequent purification of the extract and raffinate by distillation was shown to be technically and economically feasible. However, those proposed processes in the literature were designed based on model parameters derived from insufficient vapour-liquid equilibrium (VLE) data for the relevant systems, yielding broadly qualitative designs. With improved model parameters derived from the novel experimental data measured in this work, the designs are improved in terms of accuracy and rigour.

6.2. Methods and Procedure

6.2.1. Design Approach

The proposed design for purifying the butandiols from the reaction processes presented by Satam *et al.*, (2019) for 1,4-BDO and Haider *et al.*, (2018) for 2,3-BDO biofuel requires a two-column separation step, utilizing the conventional distillation technique. Due to the chemical nature of the components involved in this separation step, an energy intensive operation results. High-boiling mixtures that are to be significantly concentrated require the use of higher quality steam and larger process equipment. While the two-column separation step to achieve the biofuel cut is viable, consideration must be given to the practicality and effect on the operational cost of the process.

The work presented by Haider *et al.* (2018) provides insight into two alternative separation processes for the concentration of the aqueous mixtures containing 2,3-BDO and 1,4-BDO. The first separation route, shown in Figure 6.3, is a single column (VL-101 - BDO Purification Column) using the conventional distillation separation technique. In this separation step, a multicomponent feed mixture is separated into the desirable product component/s, with an overhead distillate and a bottoms stream. The feed in this separation process is generally a liquid or vapour-liquid mixture. Conventional distillation requires that a vapour-phase is formed in the column. The liquid- and vapour-phase are allowed to make contact by means of moving counter-currently across trays or packing. The components that require separation in the feed must have different volatilities to allow for the required separation cuts and fractionation into the desired components. Conventional distillation differs from other separation techniques (absorption, adsorption, stripping etc.) due to the second phase, in this case a vapour-phase, initiating from a thermal source in contrast to other separation techniques where a required second phase is intentionally introduced to a column which could contain a component/s which are generally not present in the feed mixture (Seader *et al.*, (1998)). Due to the high boiling nature of 1,4-BDO and 2,3-BDO, it is likely that these biofuel products will be present in the bottoms stream or

a side stream from the stripping section (section beneath the feed point of the column) while the water from the aqueous mixture with other light components will be present in the overhead distillate.

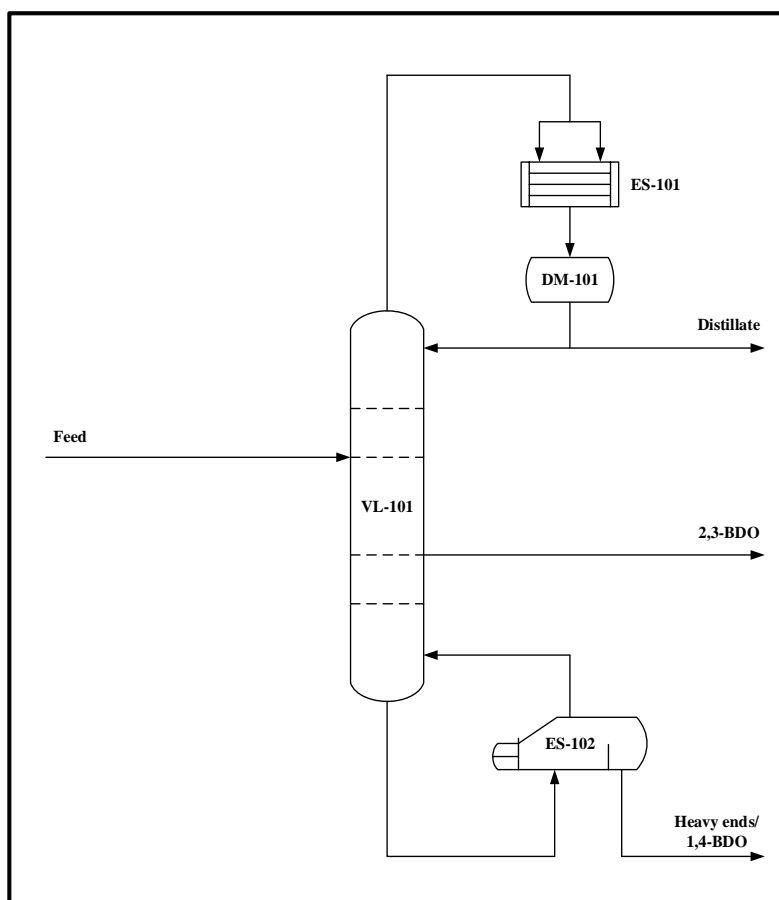


Figure 6.3. Conventional distillation separation route.

The second separation route is a hybrid system separation process employing the liquid-liquid extraction and conventional distillation separation techniques. The separation process of liquid-liquid extraction involves contacting a multicomponent liquid-phase feed with a second liquid-phase which is referred to as a solvent. The solvent is either completely or partially immiscible with at least one of the components in the feed mixture. The nature of the solvent will allow for the partial dissolving of one or more of component species in the feed resulting in a partial separation of that species from the feed. The solvent that is used for liquid-liquid extraction may either be a pure component or a blend of components. There are two scenarios to consider with respect to the nature of the feed: if the feed is organic, water is commonly used as the solvent to remove hydrophilic organics, however, if the feed is an aqueous mixture, such as in the case of the 1,4-BDO and 2,3-BDO feed stream, an organic solvent is used which is partially miscible with water (Seader *et al.*, (1998)). To ensure an efficient separation is achieved in liquid-liquid extraction, a minimum solvent-to-feed ratio is determined. The solvent-to-

feed ratio is used as a process optimization lever and is varied based on the process dynamics of the system.

Figure 6.4 shows the proposed hybrid extraction-assisted distillation design. The aqueous mixture of water and 2,3-BDO or 1,4-BDO is transferred to the top of VL-101 (BDO Extraction Column) which is a trayed liquid-liquid extraction column. The organic extraction solvent is fed to the bottom of VL-101. The solvent is then contacted with the aqueous feed and extracts the BDO biofuel and some water. The now combined solvent with BDO biofuel is referred to as the extract phase while the majority of the water, lighter components and remaining solvent forms a raffinate phase. The extract phase is then fed to VL-102 (BDO purification column), a conventional distillation column, where the BDO is concentrated and recovered according to product specification. For the purposes of this design, a product purity of 99.9% (wt) and mass recovery of 90% was targeted, taken from the stipulation of the original design in literature, yielding a valorised product. Due to the boiling nature of the BDO species, the extraction solvent will mostly be recovered in the overhead distillate. The raffinate phase is fed to VL-103 (Solvent Recovery Column). The extraction solvent will be recovered in the overhead distillate of VL-103 while most of the water present in the raffinate will distribute to the bottoms of VL-103. The overhead distillate of VL-102 and VL-103 are fed to DM-103, Solvent Receiver Drum, which is a decanter. The solvent and water mixture form two liquid phases at the heterogenous azeotrope concentration between water and the extraction solvent, which the decanter separates due to the occurrence of liquid-liquid equilibrium. The decanter contents will distribute in levels according to the density of the two liquid phases that form within the vessel. DM-103 will produce an aqueous phase (water-rich phase) and an organic phase (solvent-rich phase) and in doing so, break the azeotrope formed between water and the solvent. The aqueous phase is recycled to VL-102 to recover some of the extraction solvent while the organic phase is recycled to VL-101 to select the required BDO biofuel. Some of the extraction solvent may be lost in the bottoms of VL-102 and hence, a make-up stream of the extraction solvent may be required to ensure that the solvent-to-feed ratio is maintained.

6.2.2. Simulation Methodology

The use of computer simulation software to perform the design and rating of chemical processes is an established practice in the chemical engineering industry. Simulation software in the chemical industry is preferred as they avoid the need to perform tedious and time-demanding calculations and the development of experimentation to perform the design of separation processes (Al-Malah, (2016)). Aspen Plus® is the leading chemical process simulation package that can be used to perform the design, optimization, rating and monitoring of chemical processes. Aspen Plus® allows the user to develop simple to complex process models and the simulations are solved using the complex built-in numerical methods. Aspen Plus® boasts a wide range of pure component databases which are constantly updated to ensure accuracy and validity when executing process modelling (Luyben, (2013)). A user is able to develop and simulate an entire chemical process from raw material feed stock to final product. The Aspen Plus® Model library boasts a varied number of unit models (blocks) to describe a physical plant unit operation including but not limited to multicomponent separation systems, heat exchangers, chemical reactors and recycle streams. The Aspen software is able to perform balances on a mass, molar and energy basis, solving and predicting thermodynamic relationships (phase and chemical equilibria), perform correlations for heat, mass and momentum transfer and use reaction kinetic data to perform reaction calculations (Al-Malah, (2016)).

In this work, Aspen Plus® was used to perform the design of the conventional distillation and extraction-assisted distillation separation routes. The work presented by Luyben, (2013) contains information regarding the procedure of developing steady-state design for a separation process using Aspen Plus®. Kister, (1992) and Lieberman and Lieberman, (2014) discuss the practical aspects of separation design such as tray types, tray efficiencies, selection of reboiler type and utility requirements. The information presented in these design guides was used in the development of the steady state separation routes.

6.2.3. Aspen Plus® Model Library

When developing a chemical process using Aspen Plus®, a user must exercise some degree of consideration as to which model, or block, from the Aspen Plus® Model Library is to be used. Some models that are made available assist with quick or “shortcut” calculations for a particular unit operation. For the purposes of this design, the blocks which perform a more rigorous simulation is preferred and selected. These blocks are discussed below.

6.2.3.1. Separation Blocks

DSTWU Block

The DSTWU block is used to perform quick design calculation estimates for a conventional distillation column with a single feed stream and two product streams (light key component in the overhead distillate and heavy key component in the bottoms). This block requires that the condenser is either a partial or total condenser. The DSTWU block executes shortcut design calculations based on the minimum number of input parameters that are to be specified and the Winn-Underwood-Gilliland method. The user is required to identify the light and heavy key components that participate in the separation and specify their respective recoveries in the overhead distillate. The user may enter either the minimum reflux ratio or the minimum number of theoretical trays. Based on the specifications input, the DSTWU block determines the optimal feed stage location, the duties of the reboiler and condenser and either the actual reflux ratio (if number of theoretical stages was specified) or the required number of theoretical stages (if the minimum reflux ratio was specified). The results from the DSTWU block can then be used as input specifications for a more rigorous separation block in Aspen Plus®. The DSTWU block was used to determine initial estimates for the design parameters to be used in the design of VL-101 in the conventional distillation route and VL-102 and VL-103 in the extraction-assisted distillation route. In both separation routes, the light and heavy key components as well as their recoveries in the distillate were inputted. The R/R_{min} ratio was specified, along with a total condenser and the column operating pressure.

RadFrac Block

The RadFrac block is a rigorous model that is used for the simulation of vapour- and liquid-phase separations by incorporating the rigorous solution of MESH (material, efficiencies, summation and heat balance) equations. The RadFrac block is one of the more robust and superior blocks available in the Aspen Plus® Model Library as it can be used to model separation techniques such as conventional distillation, absorption, stripping, extractive distillation and azeotropic distillation. Further, RadFrac is best suited for separation systems with components exhibiting two- or three-phase behaviour, components with varied boiling ranges and systems exhibiting significant strong liquid-phase nonideality. The block can be specified as either equilibrium-based (used in this work) or rate-based. Condenser type, reboiler type and the number of stages are to be specified. The mass balance of the column is specified by inputting either the distillate rate, bottom rate, distillate-to-feed ratio or the bottoms to feed ratio. The energy balance is specified by inputting the reflux rate, reflux ratio, boil-up rate, boil-up ratio, or one of the condenser duties. The feed stream as well as the location of product or pseudo streams is to be specified. The column pressure is also required. Aspen Plus® allows the user to perform the design and rating of columns and their internals by using the *Column Internals* feature.

The single column (VL-101) (Figure 6.3) in the conventional distillation route, and VL-102 and VL-103 (Figure 6.4 and Figure 6.5) was modelled using the Radfrac block. While the results from the DSTWU block assists in providing RadFrac input specifications, these serve only as estimates. Flowsheeting options such as *Design Specs*, *Calculator* and *Transfer* in conjunction with *Sensitivity* from *Model Analysis Tools* were used to optimize the RadFrac block to ensure that the required product cut and recovery is achieved. The *Column Internals* feature determines a suitable column diameter based on the input specifications to the RadFrac block.

The RadFrac block assumes that each stage in the model is an equilibrium stage. While this is a fair assumption, a true representation of the design would be to consider the overall efficiency of the trays in the column. The work of Duss and Taylor, (2018) outlines a method of determining the overall efficiency of a section in a column. The outlined method was followed to determine the efficiency of the rectifying section (section of the column above feed location) and stripping section (section of the column beneath the feed location) to determine the actual number of trays required to achieve the desired separation and subsequently determine the actual height of the column.

Extract Block

The Extract block is a model used for the rigorous simulation of the liquid-liquid extraction separation technique. The Extract model can have multiple feeds, side products and pseudo streams. Unlike the RadFrac block, the Extract block can only perform rating calculations. As such, parameters such as tray type, tray spacing, and tray geometry cannot be specified. Input parameters such as the number of stages and the column operating pressure is required.

While the RadFrac block is able to determine the height and diameter of the column, the Extract block cannot. Seader *et al.*, (1998) proposed a method for determining the diameter of a column employing the liquid-liquid extraction technique. This method was used to determine the diameter of the column. An additional characteristic of the Extract block assumes an equilibrium for the stipulated stages. To account for tray efficiency, the method of determining the overall efficiency in the service of liquid-liquid extraction was presented by Fair and Humphrey, (1984). This method was used to determine the overall tray efficiency and, hence, the actual number of stages of the extraction columns in the extraction-assisted distillation route.

Flash2 Block

The Flash2 block is used to model unit operations such as flash vessels, knock-out drums and separations requiring a single stage. The Flash2 block performs vapour-liquid or vapour-liquid-liquid calculations. For the design considered in this work, the Flash2 block is used to simulate the reflux

drums of the respective conventional distillation columns. This block can also be used to aid the HeatX block if the HeatX block serves as a reboiler-type heat exchanger (explained below). For this design, the pressure drop and heat duty of the block was specified.

Decanter

The Decanter block is used to simulate unit operations such as decanters and single stage separations without the presence of a vapour-phase. The Decanter block can perform calculations pertaining to liquid-liquid equilibrium. DM-103 (Figure 6.4 and Figure 6.5) is modelled using the decanter block.

6.2.3.2. Heat Exchanger Blocks

HeatX Block

The HeatX block is used to simulate heat exchangers of the shell and tube configuration. The block can model exchangers designed to operate in counter-current or co-current flow patterns. A feature of the HeatX block is its ability to model exchangers of the various TEMA types. The block is able to model single- and two-phase streams, perform a complete zone analysis and calculate the overall heat transfer coefficient. The HeatX block is able to run in various modes such as shortcut, design and rating. The block is also able to determine the fouling factors associated with a simulated exchanger. The HeatX block allows for the connection of only four streams (one hot and cold fluid feed and one hot and cold fluid outlet). All heat exchangers in the conventional distillation and extraction-assisted distillation proposed designs were modelled using the HeatX block.

As an input specification, the RadFrac block requires a selection of the condenser and reboiler type. The results of the RadFrac block provides an estimate of the reboiler duty only. Heat exchanger parameters such as overall heat transfer coefficient, surface area, fouling factors etc., are not determined by the RadFrac block. As such, pseudo streams from the RadFrac block were used as an input to perform the rigorous design of the heat exchangers using the HeatX block. The Aspen Plus® convention for the RadFrac block treats the first and last stage as the condenser and reboiler respectively. To model the condenser, a pseudo stream (vapour-only) from the second stage of the RadFrac block was used as a feed to the HeatX block, while a reboiler-pseudo stream from the last stage of the RadFrac block was used as a feed to the HeatX block. All condensers and reboilers in this simulation were modelled in this fashion.

If one is to model a kettle-type reboiler, individual liquid- and vapour-phase outlet streams cannot be modelled using the HeatX block. The heating medium stream would be considered the hot fluid side while the mixture requiring vaporization is the cold fluid side. Because the HeatX block allows only for

a single cold and hot outlet stream, the vaporized stream exiting the HeatX block is a vapour-liquid mixture. If one requires fluid properties for either the vapour-phase or liquid-phase only, the combined vapour-liquid stream can be transferred to a Flash2 block. By specifying a pressure drop of 0 kPa and heat duty of 0 kW as input specifications for the Flash2 block, the combined vapour-liquid mixture can be separated into vapour and liquid streams, in the model.

6.2.4. Convergence

6.2.4.1. Block Convergence

Extract Block

The convergence method used for the outside loop was the Broyden method for solving while the inside loop uses a combined Broyden and Wegstein solver. The maximum number of iterations for the outside loop was set to 200 to allow for the Extract block to successfully converge. These convergence specifications were used for all design scenarios with the Extract block in this work.

RadFrac Block

For the basic convergence of the RadFrac block, the algorithm that was selected was *Nonideal* and the maximum number of iterations was set to 200. A *Chemical* initialization method was also selected. These convergence specifications were used for all design scenarios with the RadFrac block in this work.

6.2.5. Recycle Streams

Two streams were identified as recycle streams for the extraction-assisted distillation separation route. The water-rich phase from DM-103 is recycled to the VL-103 column, while the solvent-rich stream from DM-103 is recycled to the extraction column (Figure 6.4 and Figure 6.5). To aid the solver and to ensure that the simulation converged and arrived at a solution, tear streams were first identified. Flowsheets with recycle loops are solved iteratively by Aspen Plus®. When a tear stream is identified and specified, Aspen Plus® will determine a convergence method, and determine a sequence to execute the solving of the flowsheet. Because the two recycle streams were explicitly identified as tear streams, Aspen Plus® will create convergence blocks to solve them, using the Wegstein convergence method. In addition, Aspen Plus® will also determine the best suited convergence sequence when solving the flowsheet automatically. Convergence inputs such as solver methods and sequencing can be changed but for the work performed in this design, the default selections of Aspen Plus® were used.

6.2.6. Solvent Selection

Several factors were considered for the solvent selection including capacity and distribution, selectivity, cost, availability, longevity and ease of recovery. Harvianto *et al.*, (2018) have presented LLE data for the water + butane-2,3-diol system in several solvents including heavy alcohols, 2-methypropan-1-ol and butan-1-ol. Butan-1-ol was shown to have a competitive selectivity and favourable distribution coefficient. Gai *et al.*, (2018) have shown that butan-1-ol is selective to butane-1,4-diol over water. Since butan-1-ol is a common industrial solvent, is of relatively low cost with a reasonable longevity, and can be recovered from water by heterogenous distillation, it was chosen as the extractive solvent in this study for the purification of the butanediols from the aqueous mixtures.

6.2.7. Thermodynamic Models

Since hybrid separation networks are proposed in this work, model selection and model parameters must be carefully considered. A thermodynamic study for the major components involved in the separation routes for the acquisition of the BDO biofuels was performed. It is imperative to accurately model the phase behaviour and interactions of the components in the system in order to account for the liquid- and vapour-phase nonideality. The National Institute of Standards and Technology (NIST) ThermoLit databank was consulted to find experimental binary vapour-liquid equilibrium (VLE) data for the components that were considered. For this separation, the major components that were considered include butan-1-ol, water, butane-1,4-diol and butane-2,3-diol.

The binary system of water (1) + butan-1-ol (2) is well studied in the literature and experimental results are available for both vapour-liquid and liquid-liquid equilibrium. There is no available experimental data for the binary system of butan-1-ol (1) + butane-1,4-diol/butane-2,3-diol (2) and water (1) + butane-2,3-diol (2), while a limited set of VLE experimental data is available for the binary system of water (1) + butane-1,4-diol (2). To accurately design the separation routes required for the acquisition of the BDO biofuels, novel isothermal VLE experimental data was measured for these binary systems as part of this work (Mavalal and Moodley, (2020), (2021)). Isothermal measurements for the binary system of water (1) + butane-1,4-diol/butane-2,3-diol (2) was measured in the temperature range of 353.1 – 373.2K (see Chapter Four) and for the binary system of butan-1-ol (1) + butane-1,4-diol/butane-2,3-diol (2) in the temperature range of 353.2 – 388.2 K (see Chapter 5).

The regressed binary parameters for the NRTL-HOC and UNIQUAC-HOC thermodynamic models were specified in Aspen Plus® and used for the design of the separation routes to acquire the BDO biofuels. The Aspen Plus® LLE Databank was used to provide binary parameters for the water (1) + butan-1-ol (2) binary system. Residue curve maps for the systems of water (1) + butan-1-ol (2) + butane-

1,4-diol/butane-2,3-diol (3) are presented in Figure 6.6a and 6.6b respectively showing the partial immiscibility of water and butan-1-ol. Missing binary parameters for minor components involved in the separation were estimated using the UNIFAC group contribution activity coefficient model Fredenslund *et al.*, (1975), across the range of temperature of each design scenario.

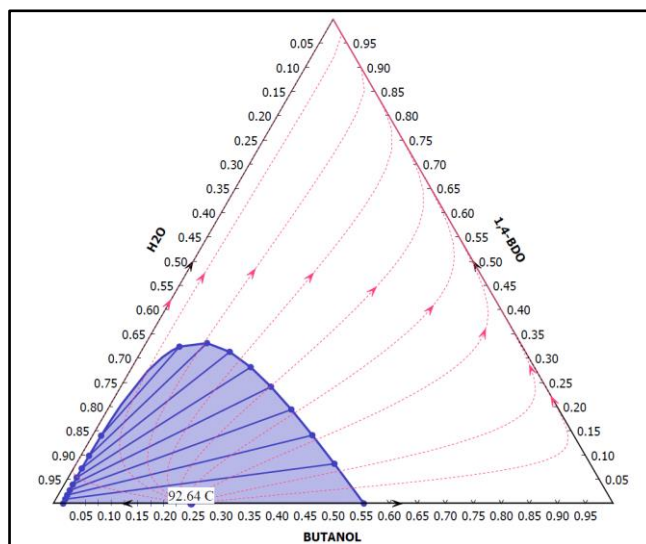


Figure 6.6a. Residue curve map for the ternary system of water (1) + butan-1-ol (2) + butane-1,4-diol (3).

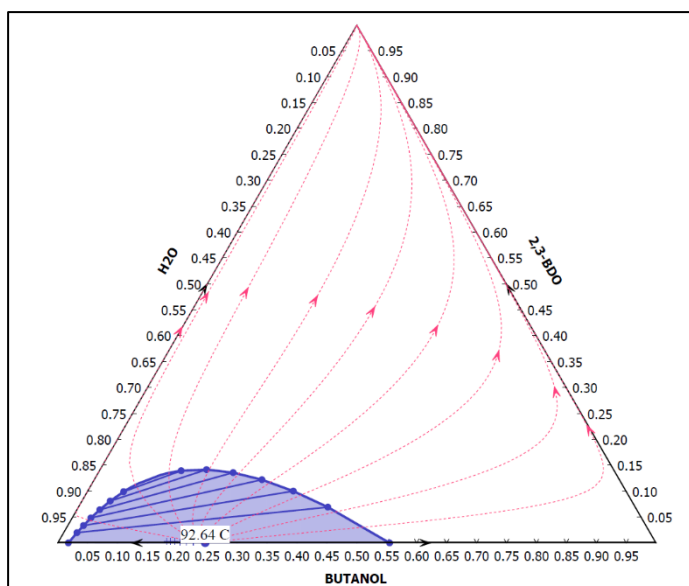


Figure 6.6b. Residue curve map for the ternary system of water (1) + butan-1-ol (2) + butane-2,3-diol (3).

For the design of the conventional distillation and extraction-assisted distillation separation routes, the thermodynamic models that were used for the blocks varied. For the conventional distillation separation route, VL-101 was modelled using the NRTL (Renon and Prausnitz, (1968)) thermodynamic model for the liquid phase. For the extraction-assisted distillation route, the extraction column (VL-101) and the decanter (DM-103) was modelled using the NRTL thermodynamic model for the liquid phase while the conventional distillation columns (VL-102 and VL-103) were modelled using the UNIQUAC (Abrams and Prausnitz, (1975)) thermodynamic model. This was done so that unique binary interaction model parameters could be used for the vapour-liquid and liquid-liquid operations, which are significantly different. Since the performances of the activity coefficient models to represent the key phase behaviours were shown to be quite similar in the preceding chapters, this decision did not affect the design significantly.

6.3. Cost Analysis

The purpose of this design is to determine which of the separation routes is considered more economically feasible due to the high energy demand of each separation route. This is achieved by a cost analysis. The conventional distillation route employs a single column to achieve the desired fractionation of the BDO biofuel product. The extraction-assisted distillation route employs three specific columns to achieve the desired separation in acquiring the BDO product. Additionally, this separation route makes use of a solvent. The total annual cost (TAC) of each design is calculated to determine which of these design scenarios is the most economically viable. The TAC takes into account the total capital cost (equipment costs) and the operating costs (utilities and solvent). The TAC is determined by assuming a 3-year payback period and is calculated as follows:

$$TAC = \left(\frac{\text{Capital Cost}}{\text{Payback Period}} \right) + \text{Operating Cost} \quad (6.1.)$$

In this work, two methods of costing were performed as a means to validate the cost estimation for each design scenario. The first method, or the manual method, involves calculating the capital cost and operating cost based on the size of equipment and the magnitude of the heat duties of each of the heat exchangers. These equations and utility estimates were taken from the work of Douglas, (1988) and Turton *et al.*, (2008). The equations for determining the cost of equipment based on their sizing is presented in Table 6.3 and the utility estimation is found in Table 6.4.

Table 6.3 Design equations to determine the capital cost of columns and heat exchangers
Hussain *et al.*, (2018).

Equipment	Design Equations for Economics
Column capital cost	$17,640(D)^{1.066}(L)^{0.802}$ D is the column diameter in meters L is the column height in meters
Heat exchanger capital cost (Condenser and reboiler)	$7,296(A)^{0.65}$ A is the area of the exchanger in square meters

Table 6.4 Cost of the considered utilities Douglas, (1988), Turton *et al.*, (2008).

Utility	Utility Cost and Conditions
Low pressure steam	\$7.78/GJ (6 bar, 160°C)
Medium pressure steam	\$8.22/GJ (11 bar, 184°C)
High pressure steam	\$9.88/GJ (42 bar, 260°C)
Cooling water	\$0.354/GJ

The second method of determining the capital and operational cost of the considered design scenarios is by using the Aspen Process Economic Analyser. Before using the Economic Analyser software, the steady-state design built in Aspen Plus® must converge with no errors or warnings. When the simulation has run and converged, the Aspen Plus® Economic Analyser can be activated. Economic Analyser is a separate software that uses inputs from Aspen Plus® and automatically estimates the process cost from the flowsheet. The process of mapping allows for the unit blocks specified in the flowsheet to be correlated with actual equipment available on Economic Analyser so that preliminary equipment sizing can be performed, and the required cost estimates are obtained. Heat exchangers in the steady-state design flowsheet are matched TEMA standards. Table 6.5 shows the cost estimation of utilities as per Aspen Plus® Economic Analyser.

Table 6.5 Cost of the considered utilities as per Aspen Process Economic Analyser.

Utility	Utility Cost and Conditions
Electricity (kW)	\$4.63/h
Cooling water	\$30.11/h
High pressure steam (400 psi)	\$717.20/h

The cost of the solvent was acquired from Qureshi *et al.*, (2020) as this is the most recent cost estimate for butan-1-ol on the market. The cost of the solvent is estimated to be \$0.79/kg.

6.4. Results and discussion

6.4.1. Butane-1,4-diol production

6.4.1.1. Conventional Distillation – Simulation Methodology

The results of the 1,4-BDO simulation via the conventional distillation process route is shown in Figure 6.7 and Table 6.6. The results include the design flowrates, compositions, temperatures and exchanger duties. Optimization was carried out using a sequential quadratic programming algorithm (Schefflan, (2011), Al-Malah, (2016)) to reduce reboiler duties and minimize total annual cost. The tray numbers, feed point, and product streams were then adjusted with reflux ratio to again reduce duties.

VL-101 – 1,4-BDO Purification Column

The conventional distillation separation route utilizes a single column to purify the 1,4-BDO biofuel. The feed composition that was used for this design scenario is shown in Table 6.1. First, a DSTWU block was used to acquire preliminary design estimates for the RadFrac block. From the work of Luyben, (2013) an initial estimate for the R/R_{min} ratio has a range of 1.2 – 1.5. A R/R_{min} ratio of 1.2 and a column pressure of 101.3 kPa was specified for the DSTWU block. Water was identified as the light key component and oxolan-2-one (an impurity) was identified as the heavy component. The results of the DSTWU block estimated a minimum reflux ratio of 0.002, with 19 stages being the minimum requirement to achieve this separation. The feed stage location was estimated to be the 5th stage, with a distillate-to-feed ratio of 0.986.

The DSTWU results were then used as initial estimates for the RadFrac block. A design specification was used to vary the reflux ratio of the column to achieve a mass purity of 0.99 for 1,4-BDO. A reflux ratio of 0.046 ensures that the product specification for 1,4-BDO was achieved. The distillate-to-feed ratio was varied to achieve the required mass recovery for 1,4-BDO. A distillate-to-feed ratio of 0.935 ensures that a 90% mass recovery of 1,4-BDO is achieved in the column bottoms stream. A sensitivity analysis was performed to determine the most suitable feed location as well as the number of stages to achieve this separation. The optimal feed stage location occurs where the reboiler duty of the column is a minimum (Luyben, (2013)). The most suitable feed stage location occurs at stage 7 while 23 stages is required to achieve a mass product purity of 0.99.

The sensitivity analysis revealed 23 stages is required for the separation to occur at the desired product specifications. This suggests that 21 theoretical trays are required for this separation as Aspen Plus® convention counts the reboiler and condenser as stages. Following the method outlined by Duss and Taylor, (2018), an efficiency of 56% was calculated for the rectifying section and an efficiency of 34% was calculated for the stripping section. The actual number of trays required for this separation is 56 with the feed tray being the 12th tray.

The column internals and sizing tool was used to determine the diameter of the column. A sieve tray was selected for the tray type for this column due to its low cost when compared to other tray types such as valve trays (Kister, (1992)). A tray spacing of 0.6096 m was selected for this column with a calculated diameter of 2.28 m. Accounting for the space required for the section above the first tray and the space required for liquid in the column sump, a column height of 38.40 m was calculated. At the specified conditions, unwanted column operation such as flooding and weeping do not occur according to the rigorous simulation. The design methodology that was used to design the VL-101 – 1,4-BDO Purification Column was also performed for all subsequent columns employing the conventional distillation separation technique.

ES-101 – Purification Column Condenser

A total condenser was selected for the design of the column's overhead condenser. The column was designed with a top pressure of 101.3 kPa. As such, typical cooling water was selected as the utility for ES-101 (Lieberman and Lieberman, (2014)). ES-101 was designed to operate counter-currently with a minimum temperature approach of 10 K. This cooling fluid, approach and arrangement was used for all condenser designs. The design heat duty of this exchanger is 12,262.4 kW and requires a surface area of 232.89 m². The design methodology that was used to design the ES-101 – Purification Column Condenser was also used for all subsequent column condensers.

ES-102 – Purification Column Reboiler

A kettle-type reboiler was selected for the service of this column. Although a significant cost is associated with implementing a kettle reboiler, this reboiler is able to provide a high degree of vaporization as is required for this process. Further, a kettle-type reboiler is easy to maintain when compared to other reboiler types such as thermosiphons and forced-circulation reboilers. High pressure steam is the utility that is required for the service of this exchanger. ES-102 was designed to operate with a minimum temperature approach of 10 K. This heating fluid, approach and arrangement was used for all reboiler designs. The heat duty generated by ES-101 is 14,009 kW and requires a surface area of 194.74 m². The design methodology that was used to design the ES-102 – Purification Column Reboiler was also used for all subsequent column reboilers.

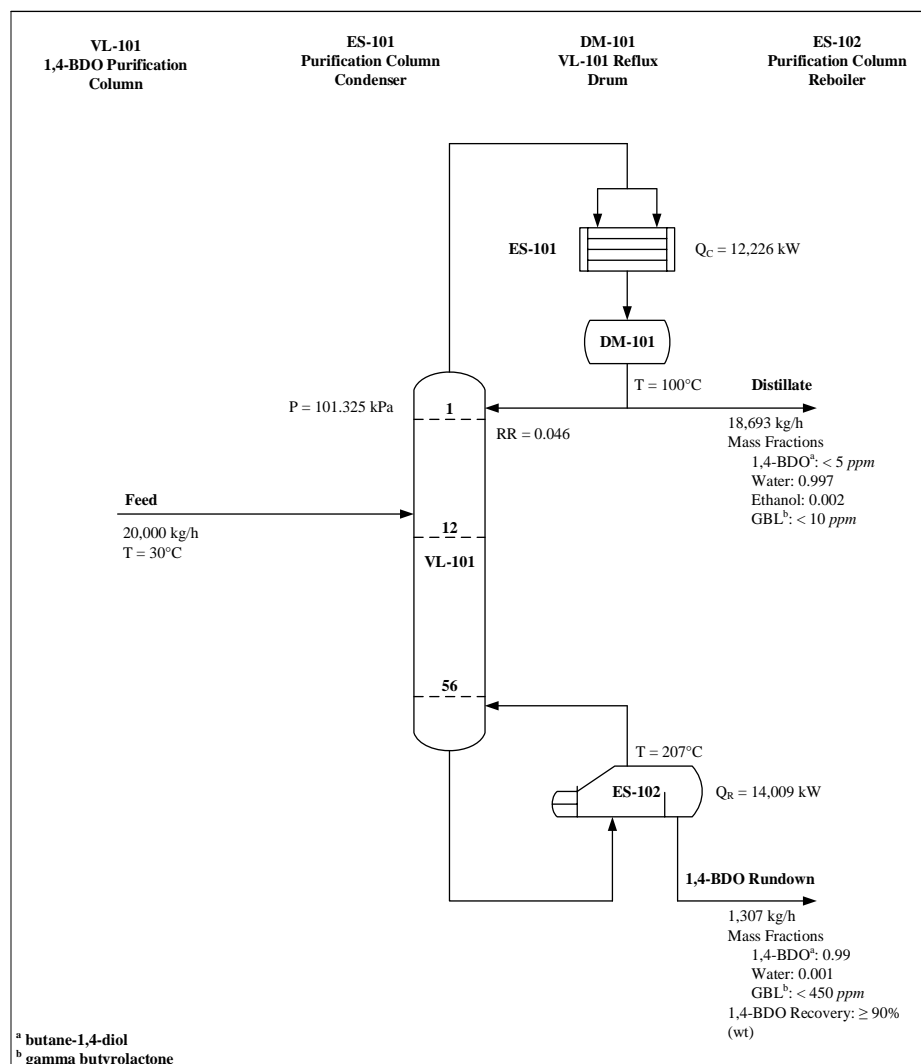


Figure 6.7. Results of the conventional distillation separation route for butane-1,4-diol.

Table 6.6 Results of the conventional distillation separation route for butane-1,4-diol.

Design Parameter	
Total trays	56
Feed tray	12
Side draw tray	-
Reflux ratio	0.046
Condenser duty (kW)	12,226
Reboiler duty (kW)	14,009
Column diameter (m)	2.28
Column length (m)	38.40
Efficiency: Rectifying section	56%
Efficiency: Stripping section	34%

6.4.1.2. Extraction-Assisted Distillation – Simulation Methodology

The results of the simulation for the extraction assisted distillation route for 1,4 BDO purification is shown in Figure 6.8 and Table 6.7. The results include the design flowrates, compositions, temperatures and exchanger duties.

VL-101 – 1,4-BDO Extraction Column

The DSTWU block served as means to determine preliminary column parameters without performing rigorous calculations for a column employing the conventional distillation technique. A block to perform shortcut calculations for liquid-liquid extraction does not exist. To determine preliminary design parameters for this extraction column, a sensitivity analysis was performed varying the number of stages and the solvent-to-feed ratio while noting the mass recovery of the 1,4-BDO biofuel in the extract phase. In this initial estimate simulation, a pure butan-1-ol stream was considered. Given the thermodynamic nature of the components involved in this separation, a significant flowrate of solvent is required to attain a suitable mass recovery of 1,4-BDO. A minimum solvent-to-feed ratio of 1.87 was calculated to achieve a mass recovery of 95% of 1,4-BDO in the extract-phase with 28 theoretical stages. The operating conditions of the extraction column was specified at 298.15 K and 101.325 kPa. The solvent feed to the extraction column was then changed to match an estimation of the composition of the possible solvent recycle. The sensitivity analysis was performed again and a solvent-to-feed ratio of 2.14 and 32 theoretical stages was required to achieve a mass recovery of 95% of 1,4-BDO in the extract-phase. The Extraction block assumes each stage in the block is an equilibrium stage. As such the method outlined by Fair and Humphrey, (1984) was used to determine the overall efficiency of the extraction column. An efficiency of 69% was calculated and as a result, the actual number of trays that is required to facilitate this process is 47 trays. The feed stream of an extraction column conventionally enters at the topmost tray of the column while the solvent enters at the bottom of the section of trays. The design methodology that was used to design the VL-101 – 1,4-BDO Extraction Column was also performed for all subsequent columns employing the conventional distillation separation technique.

VL-102 – 1,4-BDO Purification Column

VL-102 – 1,4-BDO Purification Column employs the conventional distillation separation technique. Initially, a R/R_{min} of 1.2, with butan-1-ol as the light key and 1,4-BDO as the heavy key was specified in a DSTWU block. The results of the DSTWU block estimated a minimum reflux ratio of 0.012, a distillate-to-feed ratio of 0.98, 12 theoretical stages and a feed stage of 8 would result in a product specification of 0.99 mass purity of 1,4-BDO and a mass recovery of 90% in the bottoms of VL-102. These estimates were then used in the RadFrac block. Design specifications and sensitivity analyses revealed that a reflux ratio of 0.054, a distillate-to-feed ratio 0.97, a feed location on the 8th stage and a total of 16 stages would result in the product specification being met. An efficiency calculation revealed

that the rectifying section is 52% efficient while the stripping section is 36% efficient. As such, the total number of actual trays that is required is 34 with the feed tray being the 15th tray. A sieve-type tray was selected for this column. The diameter of this column was calculated to be 3.22 m with a height of 25.00 m.

VL-103 – Solvent Recovery Column

VL-103 – Solvent Recovery Column employs the conventional distillation separation technique. Initially, a *R/R_{min}* of 1.2, with butan-1-ol as the light key and water as the heavy key was specified in a DSTWU block. The results of the DSTWU block estimated a minimum reflux ratio as 5.515, a distillate-to-feed ratio of 0.08, 12 theoretical stages and a feed stage of 3 would result in a product specification of 0.96 mass purity for water in the bottoms of VL-103 and the maximum recovery of butan-1-ol in the distillate stream.

These estimates were then used in the RadFrac block. Design specifications and sensitivity analyses revealed that a reflux ratio of 5.544, a distillate-to-feed ratio 0.14, a feed location on the 2nd stage and a total of 12 stages would result in the product specification for water and the maximum recovery of butan-1-ol being met. An efficiency calculation revealed that the rectifying section is 65% efficient while the stripping section is 72% efficient. As such, the total number of actual trays that is required is 15 trays with the feed trays being the 3rd tray. A sieve-type tray was selected for this column. The diameter of this column was calculated to be 2.09 m with a height of 13.41 m.

Recycle Loops

The overhead distillate streams were transferred to DM-103 – Decanter. The liquid phase from the water - butan-1-ol heterogenous azeotrope enters DM-103. However, the nature of the water-butan-1-ol mixture allows for the formation of two liquid-phases; the first-liquid phase rich in water and the second-liquid phase rich in butan-1-ol. The water-rich stream with a mass purity of 0.910 water is recycled to the VL-102 – Solvent Recovery Column and the solvent-rich stream with a mass purity of 0.770 butan-1-ol is recycled to the VL-101 – 1,4-BDO Extraction Column. The recycle streams were connected and converged. Each of the recycle streams were selected as tear streams. There is some degree of solvent loss with the water stream of VL-103. As such, a make-up stream of 6 kg/h of pure butan-1-ol is fed to the extraction column.

ES-101 – Purification Column Condenser, ES-102 – Purification Column Reboiler, ES-103 – Recovery Column Condenser, ES-104 – Recovery Column Reboiler

The design duty of ES-101 is 11,169 kW with a total surface area of 207.65 m², while the heat duty of ES-102 is 14,657 kW with a total surface area of 377.24 m². The duty of ES-103 is 7,676 kW with a

total surface area of 147.90 m², and the heat duty of ES-104 is 9,594 kW with a total surface area of 72.35 m².

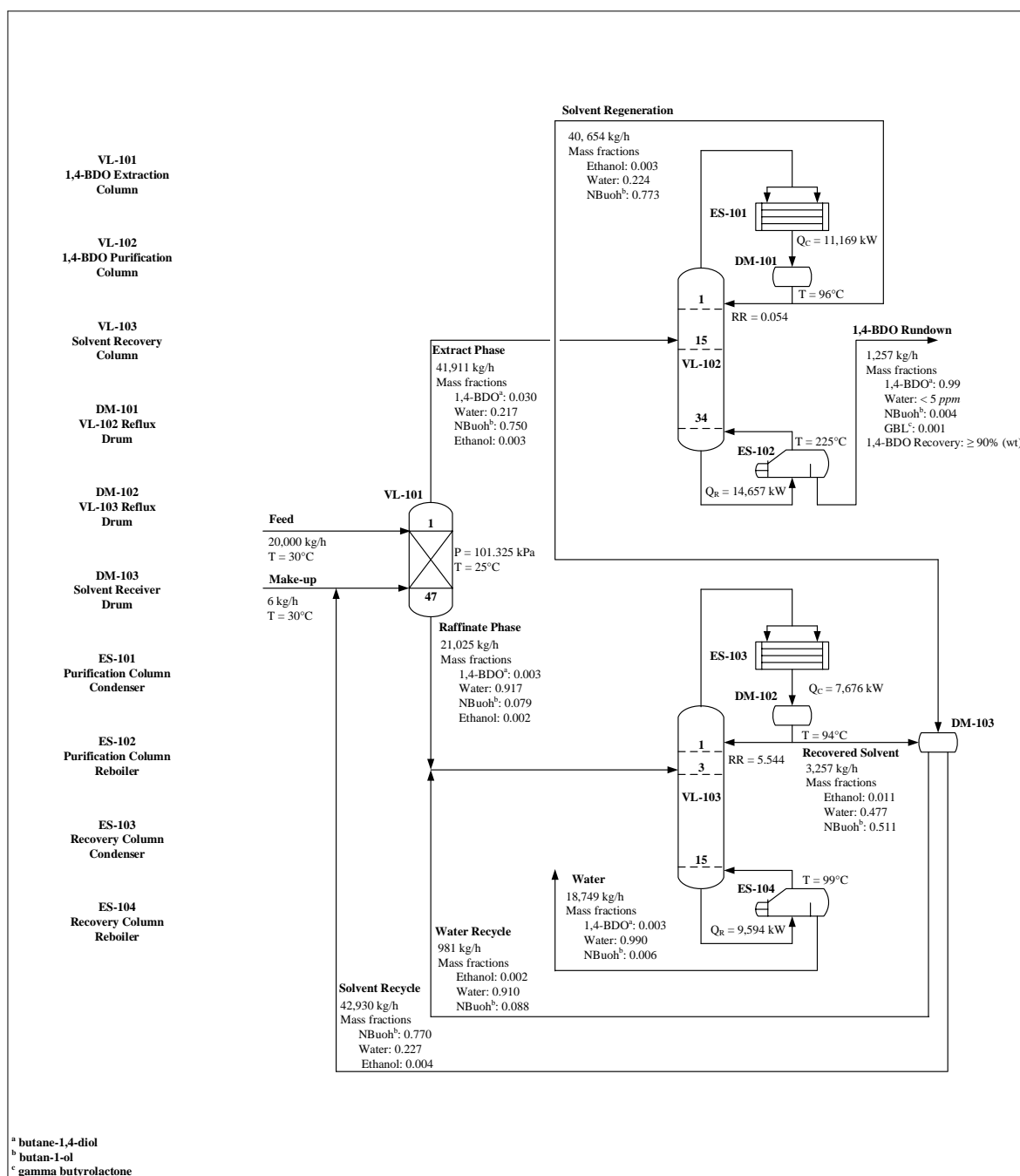


Figure 6.8. Results of the extraction-assisted distillation separation route for butane-1,4-diol.

Table 6.7 Results of the extraction-assisted distillation separation route for butane-1,4-diol.

Design Parameter	VL-101	VL-102	VL-103
Total trays	47	34	15
Feed tray	-	15	3
Side draw tray	-	-	-
Reflux ratio	-	0.054	5.544
Condenser duty (kW)	-	11,169	7,676
Reboiler duty (kW)	-	14,657	9,594
Column diameter (m)	1.49	3.22	2.09
Column length (m)	32.92	24.99	13.41
Efficiency: Overall column	69%	-	-
Efficiency: Rectifying section	-	52%	65%
Efficiency: Stripping section	-	36%	70%

6.4.1.3. Heat Integration – Simulation Methodology

Two streams have been identified as possessing sufficient heat duty to pre-heat the feed to VL-102 – 1,4-BDO Purification Column and the feed to VL-103 – Solvent Recovery Column. A shell and tube heat exchanger ES-105 – Solvent Pre-Cooler is used as a feed pre-heater for VL-102 – 1,4-BDO Purification Column and ES-106 – Raffinate Pre-Heater as a feed pre-heater for VL-103 – Solvent Recovery Column. The results of this simulation route are shown in Figure 6.9 and Table 6.8. The results include the design flowrates, compositions, temperatures and exchanger duties.

ES-105 – Solvent Pre-Cooler

The overhead distillate of VL-102 provides 2,782 kW of heat duty to ES-105 with a surface area of 220.22 m². The temperature of the feed to VL-102 is raised from approximately 303 K to 349 K. As a result, the duty of the VL-102 reboiler decreased from 14,657 kW and a total surface area of 377.24 m² to 11,875 kW with a total surface area 305.97 m².

ES-106 – Raffinate Pre-Heater

The bottoms stream of VL-103 provides 1,358 kW of heat duty to ES-106 with a surface area of 103.75 m². The temperature of the feed to VL-103 is raised from 303 K to 350 K. As a result, the duty of the VL-102 reboiler decreased from 9,594 kW with a total surface area of 72.35 m² to 8,184 kW with a total surface area 61.82 m².

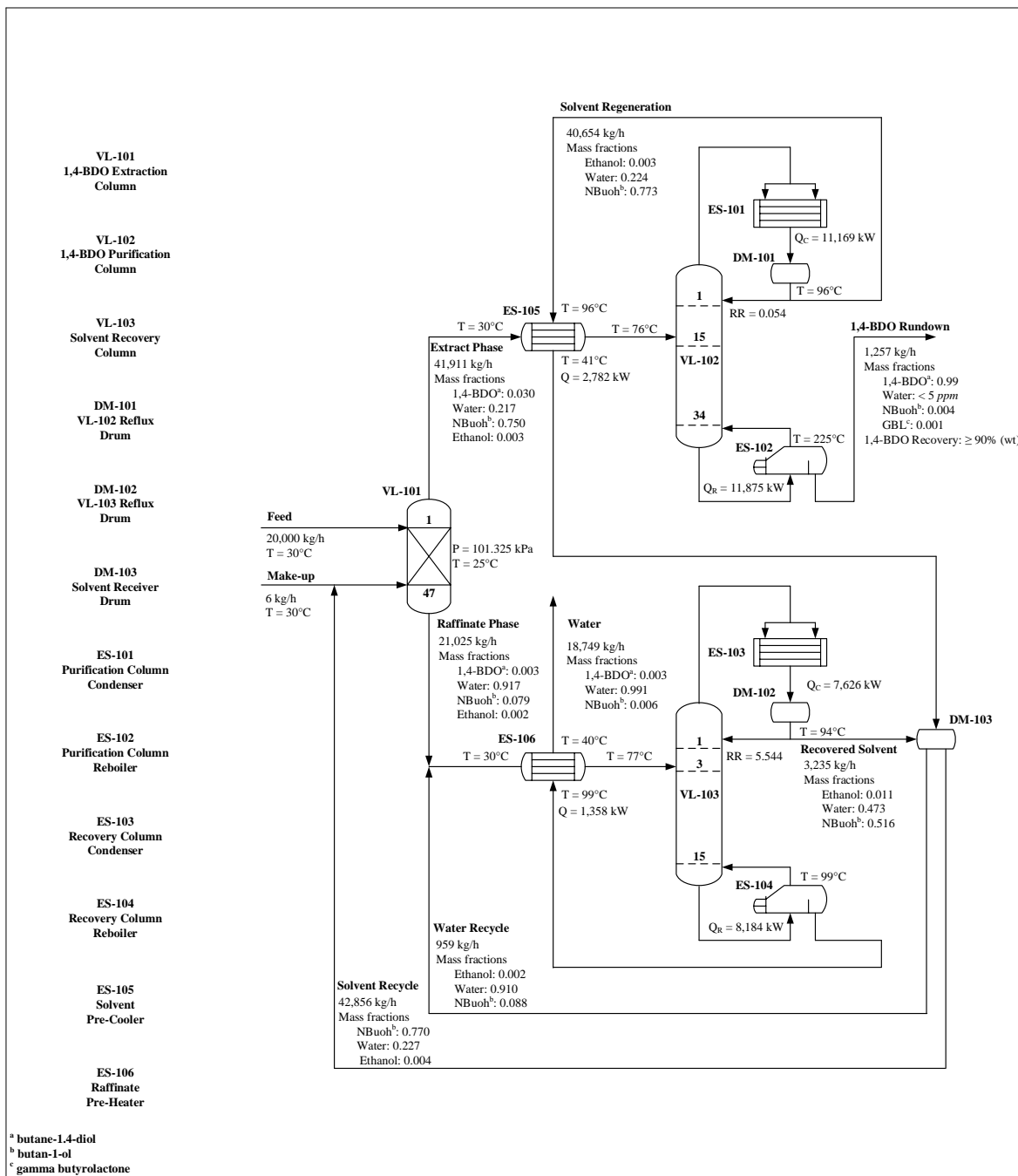


Figure 6.9. Results of the extraction-assisted distillation separation route with heat integration for butane-1,4-diol.

Table 6.8 Results of the extraction-assisted distillation separation route with heat integration for butane-1,4-diol.

Design Parameter	VL-101	VL-102	VL-103
Total trays	47	34	15
Feed tray	-	15	3
Side draw tray	-	-	-
Reflux ratio	-	0.054	5.544
Condenser duty (kW)	-	11,169	7,626
Reboiler duty (kW)	-	11,875	8,184
Column diameter (m)	1.49	3.22	2.09
Column length (m)	32.92	24.99	13.41
Efficiency: Overall column	69%	-	-
Efficiency: Rectifying section	-	52%	65%
Efficiency: Stripping section	-	36%	70%

6.4.1.4. Cost Analysis

A cost analysis was performed for the separation routes that were considered for the acquisition and concentration of 1,4-BDO; conventional distillation, extraction-assisted distillation and heat integration of the extraction-assisted distillation. Two methods were used to determine the associated capital and operating cost and the total annual cost of each of the design scenarios that were considered. The first method of determining the cost is a manual method where unit dimensions (diameter, length, tray spacing etc.) and exchanger duty and total surface areas are used in determining cost equations. This method is outlined in the work of Douglas, (1988) and Turton *et al.*, (2008). The second method of determining the associated cost of the process is using Aspen Process Economic Analyser. Both cost methods are compared below. The total annual cost was calculated for 344 operational days for each year. To account for shutdowns (planned and unplanned), 21 days of the year are set aside.

Conventional Distillation

Manual Method

Table 6.9 and Figure 6.10 show the results of the manual costing method. In this simulation route, the cost of VL-101 – 1,4-BDO Purification Column, ES-101 – Purification Column Condenser, ES-102 – Purification Column Reboiler and DM-101 – VL-101 Reflux Drum contribute to the capital cost. A capital cost of \$1,176,615.25 was calculated. Utility costs (cooling water and high-pressure steam) are considered as operational cost. An operational cost of \$4,242,865.44 was calculated. Assuming a payback period of 3 years, a total annual cost of \$4,635,070.52 was determined.

Aspen Process Economic Analyser

Table 6.9 and Figure 6.11 show the results of the Aspen Process. A capital cost of \$1,445,600.00 and an operational cost of \$4,050,980.00 was estimated. Assuming a payback period of 3 years, a total annual cost of \$4,532,846.67 was calculated.

A comparison between the two costing methods reveals that the estimates are in reasonable agreement, which increases confidence in these estimates. It is clear from both costing methods that the utility usage is the greatest contributor to the total annual cost.

Table 6.9 Cost analysis of the conventional distillation separation route for butane-1,4-diol.

	Manual Method	Aspen Process Economic Analyser
Capital Cost	-	-
<i>Separators</i>	-	-
VL-101 - Purification Column (\$ 10 ⁶)	0.794	0.796
<i>Heat Exchangers</i>	-	-
ES-101 - Purification Column Condenser (\$ 10 ⁶)	0.252	0.208
ES-102 - Purification Column Reboiler (\$ 10 ⁶)	0.102	0.239
<i>Auxiliary Equipment</i>	-	-
DM-101 - VL-101 Reflux Drum (\$ 10 ⁶)	0.006	0.158
PC-101 - VL-101 Reflux Pump (\$ 10 ⁶)	0.023	0.045
Total Capital Cost (\$ 10⁶)	1.177	1.446
Total Operating Cost (\$ 10⁶)	4.243	4.051
Total Annual Cost (\$ 10⁶)	4.635	4.533

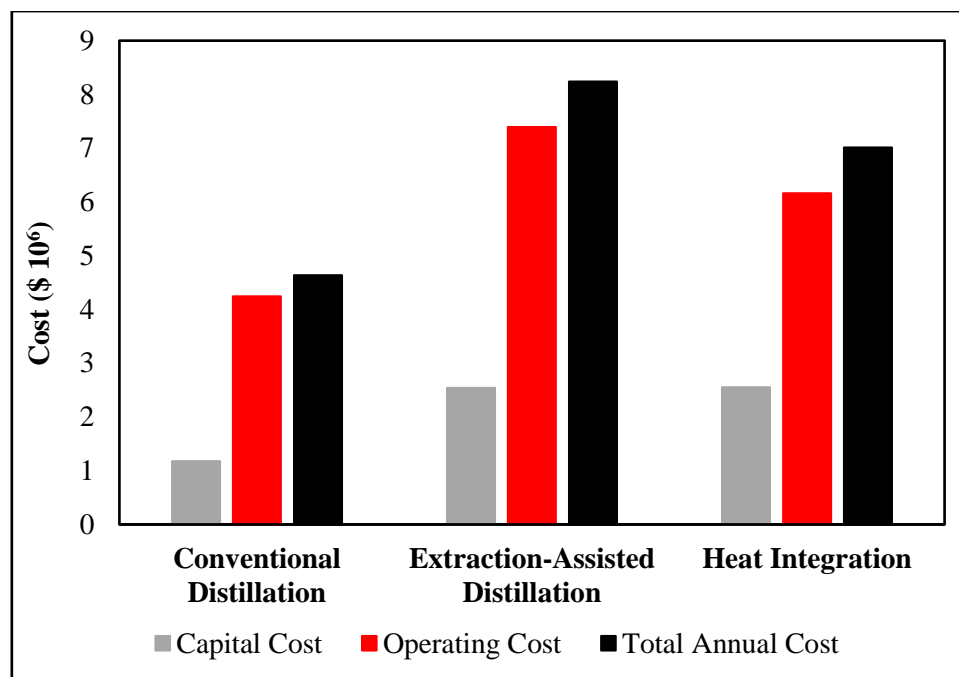


Figure 6.10. Cost analysis of the separation routes for 1,4-BDO calculated by the manual method.

Extraction-Assisted Distillation without Heat Integration

Manual Method

Figure 6.10 and Table 6.10 show the results of the manual costing method. In this simulation route, the cost of VL-101 – 1,4-BDO Extraction Column, VL-102 – 1,4-BDO Purification Column, VL-103 – Solvent Recovery Column and their respective condensers, reboilers and reflux drums contribute to the capital cost. A capital cost of \$2,539,126.71 was calculated. Utility costs such as cooling water, high pressure steam and solvent requirement are considered as operational costs. An operational cost of \$7,392,686.08 was calculated. Assuming a payback period of 3 years, a total annual cost of \$8,239,061.65 was determined.

Table 6.10 Cost analysis of the extracted-assisted distillation separation route for butane-1,4-diol without heat integration.

	Manual Method	Aspen Process Economic Analyser
Capital Cost	-	-
<i>Separators</i>	-	-
VL-101 - BDO Extraction Column (\$ 10 ⁶)	0.446	0.446
VL-102 - BDO Purification Column (\$ 10 ⁶)	0.812	2.382
VL-103 - Solvent Recovery Column (\$ 10 ⁶)	0.311	0.857
<i>Heat Exchangers</i>	-	-
ES-101 - Purification Column Condenser (\$ 10 ⁶)	0.234	0.199
ES-102 - Purification Column Reboiler (\$ 10 ⁶)	0.345	0.379
ES-103 - Recovery Column Condenser (\$ 10 ⁶)	0.188	0.153
ES-104 - Recovery Column Reboiler (\$ 10 ⁶)	0.118	0.146
<i>Auxiliary Equipment</i>	-	-
DM-101 - VL-101 Reflux Drum (\$ 10 ⁶)	0.026	0.200
DM-102 - VL-101 Reflux Drum (\$ 10 ⁶)	0.023	0.158
DM-103 - Solvent Receiver Drum (\$ 10 ⁶)	0.025	0.195
PC-101 - VL-102 Reflux Pump (\$ 10 ⁶)	0.006	0.045
PC-102 - VL-103 Reflux Pump (\$ 10 ⁶)	0.005	0.038
Total Capital Cost (\$ 10⁶)	2.539	5.199
Total Operating Cost (\$ 10⁶)	7.393	7.759
Total Annual Cost (\$ 10⁶)	8.239	9.492

Aspen Process Economic Analyser

Table 6.10 and Figure 6.10 show the results of the Aspen Process Economic Analyser costing method. A capital cost of \$5,198,760.45 and an operational cost of \$7,759,133.33 was estimated. Assuming a payback period of 3 years, a total annual cost of \$9,492,053.48 was calculated.

A comparison between the two costing methods reveals that while there are differences between the estimated costs, they are in agreement with respect to the order of magnitude for the operating cost and total annual cost. There is a discrepancy between the manual and Aspen estimated cost for the capital cost. Despite this discrepancy, the increase in capital cost in the extraction-assisted distillation route compared against the conventional distillation route is justified as the extraction-assisted distillation design incorporates more unit operations and equipment. The operational cost increase when compared to the conventional distillation route is justified due to the high boiling point of the 1,4-BDO component, high internal recycle rates and the low feed purity. The operating cost involved in the extraction-assisted

distillation route greatly impacts the total annual cost which is significantly more than the total annual cost of the conventional distillation route.

Extraction-Assisted Distillation with Heat Integration

Manual Method

Table 6.11 and Figure 6.10 show the results of the manual costing method. The capital cost component of the total annual cost for the heat integrated process route includes two additional heat exchangers: ES-105 – Solvent Pre-Cooler and ES-106 – Raffinate Pre-Heater. A capital cost of \$2,552,482.52 was calculated. Utility costs such as cooling water, high pressure steam and solvent requirement are considered as operational costs. An operational cost of \$6,161,302.61 was calculated. Assuming a payback period of 3 years, a total annual cost of \$7,012,130.12 was determined.

Aspen Process Economic Analyser

Table 6.11 and Figure 6.11 show the results of the economic analyser costing method. A capital cost of \$3,534,460.45 and an operational cost of \$6,570,160.00 was estimated. Assuming a payback period of 3 years, a total annual cost of \$7,748,313.48 was calculated.

A comparison between the two costing methods reveals that there is an approximately 40% difference between the estimated capital costs, however they are in agreement with respect to the order of magnitude. It is clear from both costing methods that the utility usage is the greatest contributor to the total annual cost. Due to the additional two heat exchangers (ES-105 and ES-106) the capital cost estimated for the heat integration process is higher than that of the conventional distillation and extraction-assisted distillation separation routes. While the operating cost for the heat integration separation route is significantly higher than that of the conventional distillation route, it is less than the operational cost of the extraction-assisted separation. The increased temperature of the feeds entering VL-102 and VL-103 directly impacts the heat duties of the VL-102 and VL-103 reboilers by decreasing the required duty. A decrease in the required reboiler duty suggests a significantly lower demand for high pressure steam. While the total annual cost of the heat integration route is less than that of the extraction-assisted route, it is still greater than the total annual cost of the conventional distillation route. This result confirms the advantages of implementing heat-integration into the design of chemical processes. While heat-integration will result in an increase in capital cost, it does cause a decrease in a processes operational cost in this case. From the total annual cost for each of the separation routes, the conventional distillation separation route is the most economically viable option for 1,4 BDO purification.

Table 6.11 Cost analysis of the extracted-assisted distillation with heat integration separation route for butane-1,4-diol.

	Manual Method	Aspen Process Economic Analyser
Capital Cost	-	-
<i>Separators</i>	-	-
VL-101 - BDO Extraction Column (\$ 10 ⁶)	0.446	0.446
VL-102 - BDO Purification Column (\$ 10 ⁶)	0.812	0.776
VL-103 - Solvent Recovery Column (\$ 10 ⁶)	0.311	0.471
<i>Heat Exchangers</i>	-	-
ES-101 - Purification Column Condenser (\$ 10 ⁶)	0.234	0.199
ES-102 - Purification Column Reboiler (\$ 10 ⁶)	0.128	0.347
ES-103 - Recovery Column Condenser (\$ 10 ⁶)	0.087	0.152
ES-104 - Recovery Column Reboiler (\$ 10 ⁶)	0.057	0.135
ES-105 - Solvent Pre-Cooler (\$ 10 ⁶)	0.243	0.208
ES-106 - Raffinate Pre-Heater (\$ 10 ⁶)	0.149	0.145
<i>Auxiliary Equipment</i>	-	-
DM-101 - VL-101 Reflux Drum (\$ 10 ⁶)	0.026	0.200
DM-102 - VL-101 Reflux Drum (\$ 10 ⁶)	0.023	0.157
DM-103 - Solvent Receiver Drum (\$ 10 ⁶)	0.025	0.195
PC-101 - VL-102 Reflux Pump (\$ 10 ⁶)	0.006	0.057
PC-102 - VL-103 Reflux Pump (\$ 10 ⁶)	0.005	0.047
Total Capital Cost (\$ 10⁶)	2.552	3.534
Total Operating Cost (\$ 10⁶)	6.161	6.570
Total Annual Cost (\$ 10⁶)	7.012	7.748

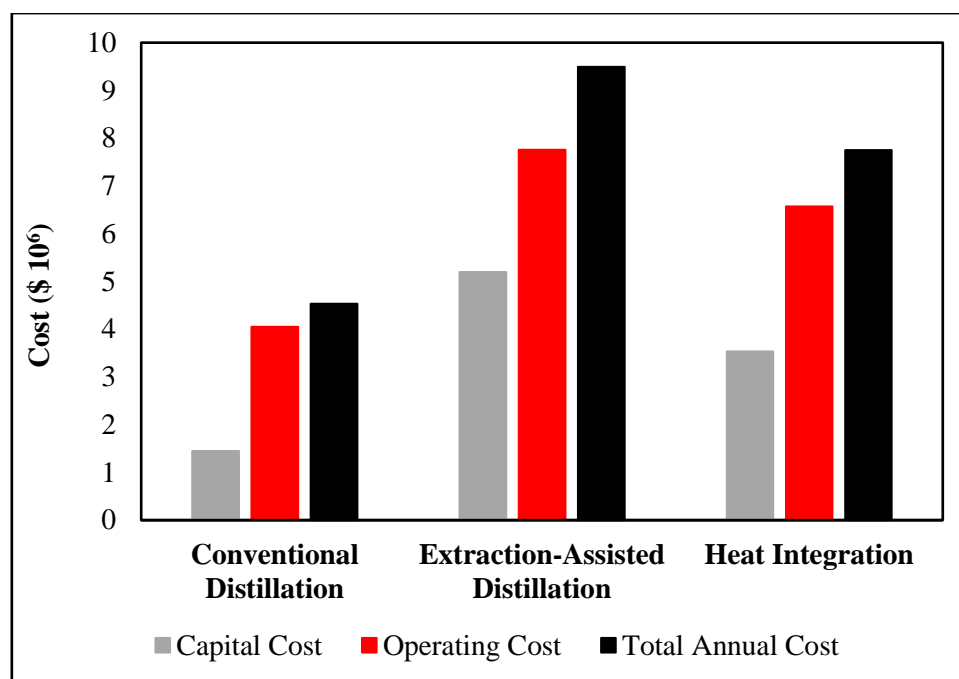


Figure 6.11. Cost analysis of the separation routes for 1,4-BDO calculated by Aspen Process Economic Analysis.

6.4.2. Butane-2,3-diol production

6.4.2.1. Conventional Distillation – Simulation Methodology

The results of the simulation of the 2,3-BDO purification via the conventional distillation route are shown in Figure 6.12 and Table 6.12. The results include the design flowrates, compositions, temperatures and exchanger duties.

VL-101 – 2,3-BDO Purification Column

VL-101 – 2,3-BDO Purification Column employs the conventional distillation separation technique. Initially, a R/R_{min} of 1.2 was selected, with 3-hydroxybutan-2-one (an impurity) selected as the light key and 2,3-BDO as the heavy key in a DSTWU block. The results of the DSTWU block estimated that a minimum reflux ratio of 0.156, a distillate-to-feed ratio of 0.93, 17 theoretical stages and a feed stage of 9 would result in a product specification of 0.99 mass purity of 2,3-BDO and a mass recovery of 90% in the bottoms of VL-101.

These estimates were then used in the RadFrac block. Design specifications and sensitivity analyses revealed that a reflux ratio of 0.321, a distillate-to-feed ratio 0.91, a feed location on the 11th stage and a total of 20 stages would result in the product specification being met. Unlike the 1,4-BDO Purification Column, the chemical profile possesses a unique behaviour. The 2,3-BDO component, although a heavy

boiling component, cannot be recovered in the bottoms stream due to the presence of significant heavy-boiler minor components in the feed stream. As such a sensitivity analysis was performed to determine the optimal stage to remove a side-draw product. The 15th stage is the optimal stage for a side-draw, ensuring a recovery of 0.99 mass purity. An efficiency calculation revealed that the rectifying section is 68% efficient while the stripping section is 65% efficient. As such, the total number of actual trays that is required is 28 trays with the feed tray being the 16th tray and the side draw from the 22nd tray. A sieve-type tray was selected for this column. The diameter of this column was calculated to be 3.14 m with a height of 21.34 m. The design methodology that was used to design VL-101 – 2,3-BDO Purification Column was also performed for all subsequent columns employing the conventional distillation separation technique to concentrate 2,3-BDO.

ES-101 – Purification Column Condenser and ES-102 – Purification Column Reboiler

The design duty of ES-101 is 14,687 kW with a total surface area of 292.55 m². ES-102 is a kettle-type reboiler. The design heat duty of ES-102 is 16,301 kW with a total surface area of 289.14 m².

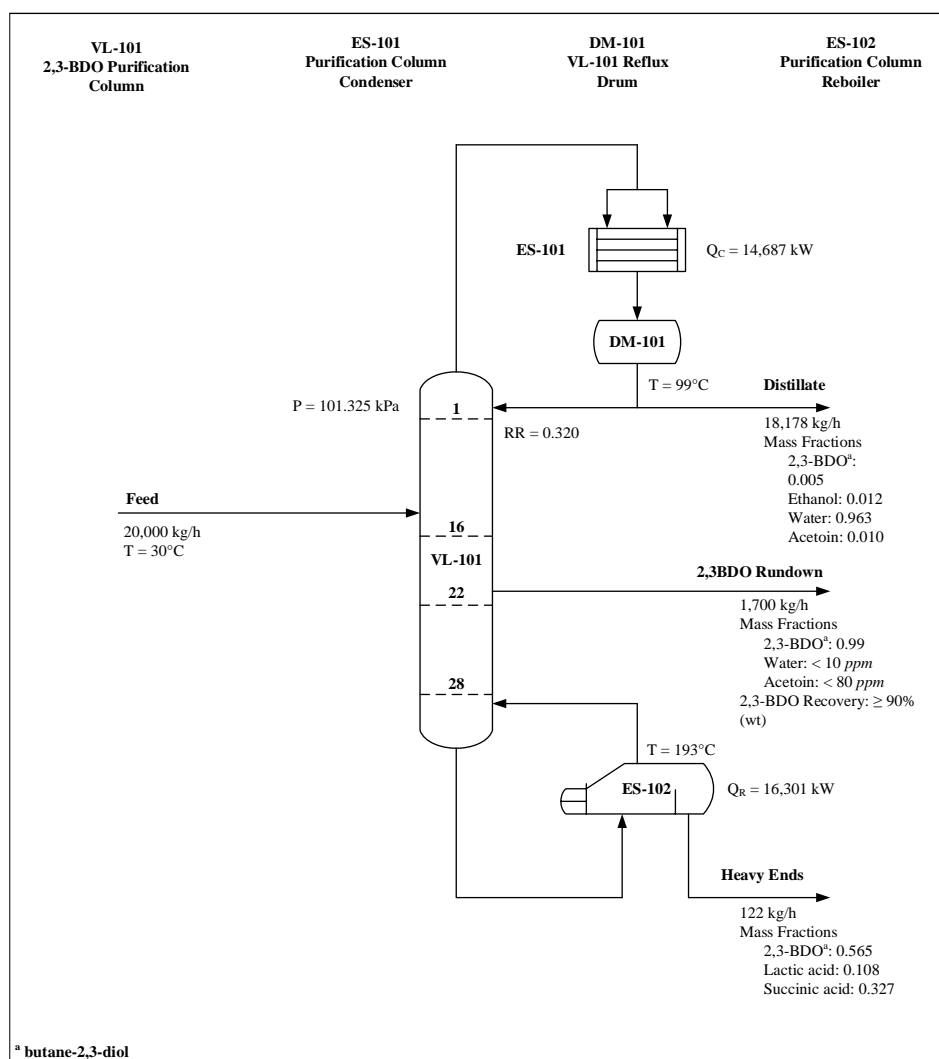


Figure 6.12. Results of the conventional distillation separation route for butane-2,3-diol.

Table 6.12 Results of the conventional distillation separation route for the butane-2,3-diol.

Design Parameter	
Total trays	28
Feed tray	16
Side draw tray	22
Reflux ratio	0.320
Condenser duty (kW)	14,687
Reboiler duty (kW)	16,301
Column diameter (m)	3.15
Column length (m)	21.34
Efficiency: Rectifying section	68%
Efficiency: Stripping section	65%

6.4.2.2. Extraction-Assisted Distillation – Simulation Methodology

The results of the simulation for extraction assisted distillation route for 2,3-BDO production is shown in Figure 6.13 and Table 6.13. The results include the design flowrates, compositions, temperatures and exchanger duties.

VL-101 – 2,3-BDO Extraction Column

To determine preliminary design parameters for this extraction column, a sensitivity analysis was performed varying the number of stages and the solvent-to-feed ratio while noting the mass recovery of the 2,3-BDO biofuel in the extract phase. A minimum solvent-to-feed ratio, using a pure butan-1-ol solvent feed of 0.48 was calculated to achieve a mass recovery of 95% of 2,3-BDO in the extract-phase with 7 theoretical stages. The operating conditions of the extraction column was specified at 298 K and 101.3 kPa. The solvent feed to the extraction column was then changed to match an estimation of the composition of the possible solvent recycle. The sensitivity analysis was performed again and a solvent-to-feed ratio of 0.63 and 9 theoretical stages is required to achieve a mass recovery of 95% of 2,3-BDO in the extract-phase. An efficiency of 55% was calculated and as a result, the actual number of trays that is required to facilitate this process is 58 trays. The feed stream enters at the top most tray of the column while the solvent enters at the bottom of the section of trays.

VL-102 – 2,3-BDO Purification Column

VL-102 – 2,3-BDO Purification Column employs the conventional distillation separation technique. Initially, of R/R_{min} of 1.2, with butan-1-ol as the light key and 2,3-BDO as the heavy key was specified in a DSTWU block. The results of the DSTWU block estimated that a minimum reflux ratio is 0.174, a distillate-to-feed ratio of 0.87, 9 theoretical stages and a feed stage of 6 would result in a product specification of 0.99 mass purity of 2,3-BDO and a mass recovery of 90% in the bottoms of VL-102. These estimates were then used in the RadFrac block. Design specifications and sensitivity analyses revealed that a reflux ratio of 0.423, a distillate-to-feed ratio 0.855, a feed location on the 5th stage and with 11 stages would result in the product specification being met. A side draw from the 9th stage ensures the mass purity and recovery of the 2,3-BDO biofuel is achieved. An efficiency calculation revealed that the rectifying section is 59% efficient while the stripping section is 62% efficient. As such, the total number of actual trays that is required is 16 trays with the feed trays being the 8th tray and a sidedraw is taken from the 14th tray. A sieve-type tray was selected for this column. The diameter of this column was calculated to be 1.77 m with a height of 14.02 m.

VL-103 – Solvent Recovery Column

VL-103 – Solvent Recovery Column employs the conventional distillation separation technique. Initially, of R/R_{min} of 1.2, with butan-1-ol as the light key and water as the heavy key was specified in

a DSTWU block. The results of the DSTWU block estimated a minimum reflux ratio is 5.515, a distillate-to-feed ratio of 0.08, 12 theoretical stages and a feed stage of 3 would result in a product specification of 0.96 mass purity for water in the bottoms of VL-103 and the maximum recovery of butan-1-ol in the distillate stream.

These estimates were then used in the RadFrac block. Design specifications and sensitivity analyses revealed that a reflux ratio of 0.210, a distillate-to-feed ratio 0.16, a feed location on the 2nd stage and a total of 10 stages would result in the product specification for water and the maximum recovery of butan-1-ol being met. An efficiency calculation revealed that the rectifying section is 65% efficient while the stripping section is 68% efficient. As such, the total number of actual trays that is required is 13 trays with the feed tray being the 3rd tray. A sieve-type tray was selected for this column. The diameter of this column was calculated to be 1.30 m with a height of 12.19 m.

Recycle Loops

The water-rich stream with a mass purity of 0.868 water is recycled to VL-102 – Solvent Recovery Column and the solvent-rich stream with a mass purity of 0.703 butan-1-ol is recycled to the VL-101 – 2,3-BDO Extraction Column. The recycle streams were connected and converged. Each of the recycle streams were selected as tear streams. Due to the solvent loss with the water stream of VL-103, a make-up stream with a 4 kg/h flowrate of pure butan-1-ol is fed to the extraction column.

ES-101 – Purification Column Condenser, ES-102 – Purification Column Reboiler, ES-103 – Recovery Column Condenser, ES-104 – Recovery Column Reboiler

The design duty of ES-101 is 4,459 kW with a total surface area of 75.30 m² and the design heat duty of ES-102 is 5,473 kW with a total surface area of 92.40 m². The design duty of ES-103 is 2,561 kW with a total surface area of 45.27 m² while the design heat duty of ES-104 is 4,510 kW with a total surface area of 34.62 m².

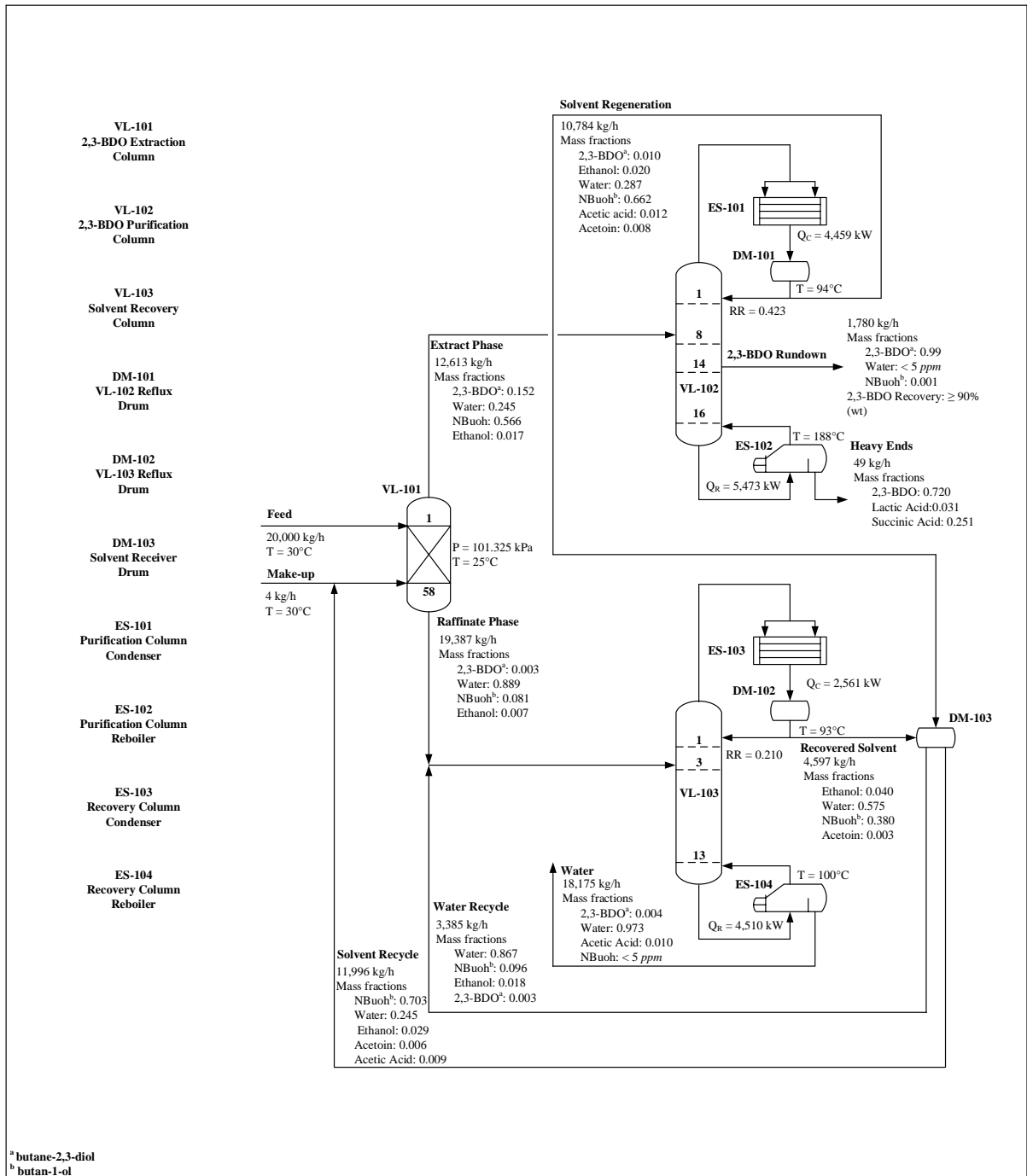


Figure 6.13. Results of the extraction-assisted distillation separation route for butane-2,3-diol.

Table 6.13 Results of the extraction-assisted distillation separation route for butane-2,3-diol.

Design Parameter	VL-101	VL-102	VL-103
Total trays	58	16	13
Feed tray	-	8	3
Side draw tray	-	14	-
Reflux ratio	-	0.423	0.210
Condenser duty (kW)	-	4,459	2,561
Reboiler duty (kW)	-	5,473	4,510
Column diameter (m)	1.36	1.77	1.30
Column length (m)	39.62	14.02	12.19
Efficiency: Overall column	55%	-	-
Efficiency: Rectifying section	-	59%	65%
Efficiency: Stripping section	-	62%	68%

6.4.2.3. Heat Integration – Simulation Methodology

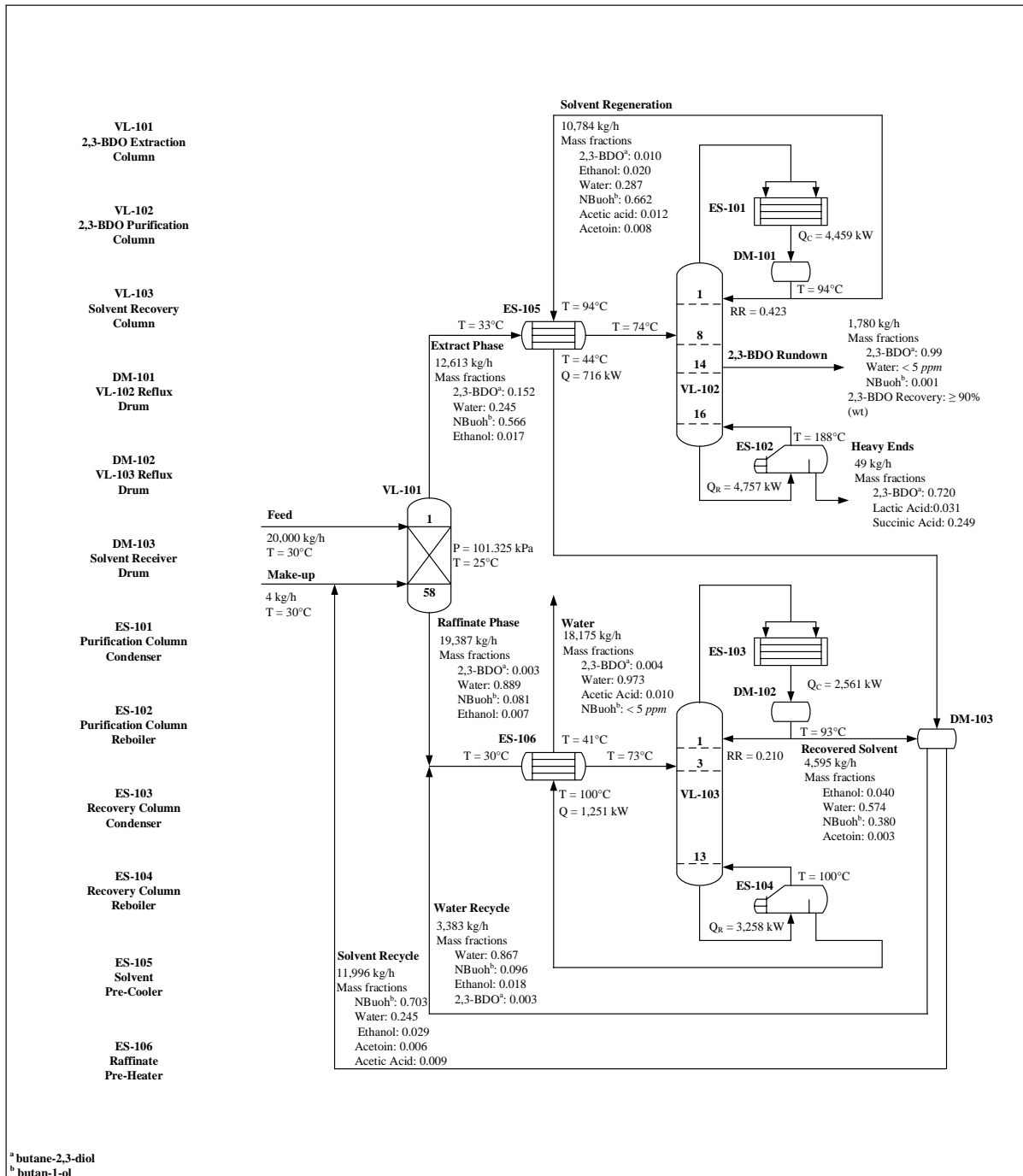
Two streams have been identified as possessing sufficient heat duty to pre-heat the feed to VL-102 – 2,3-BDO Purification Column and the feed to VL-103 – Solvent Recovery Column. A shell and tube heat exchanger ES-105 – Solvent Pre-Cooler is used as a feed pre-heater for VL-102 – 2,3-BDO Purification Column and ES-106 – Raffinate Pre-Heater as a feed pre-heater for VL-103 – Solvent Recovery Column. The results of this simulation route are shown in Figure 6.14 and Table 6.14. The results include the design flowrates, compositions, temperatures and exchanger duties.

ES-105 – Solvent Pre-Cooler

The overhead distillate of VL-102 provides 716 kW of heat duty to ES-105 with a surface area of 55.15 m². The temperature of the feed to VL-102 is raised from 306 K to 347 K. As a result, the duty of the VL-102 reboiler decreased from 5,473 kW with a total surface area of 92.40 m² to 4757 kW with a total surface area 80.28 m².

ES-106 – Raffinate Pre-Heater

The bottoms stream of VL-103 provides 1,251 kW of heat duty to ES-106 with a surface area of 83.83 m². The temperature of the feed to VL-103 is raised from 303 K to 346 K. As a result, the duty of the VL-102 reboiler decreased from 4,510 kW with a total surface area of 34.62 m² to 3,258 kW with a total surface area 25.01 m².



^a butane-2,3-diol
^b butan-1-ol

Figure 6.14. Results of the extraction-assisted distillation separation route with heat integration for butane-2,3-diol.

Table 6.14 Results of the extraction-assisted distillation separation route with heat integration for butane-2,3-diol.

Design Parameter	VL-101	VL-102	VL-103
Total trays	58	16	13
Feed tray	-	8	3
Side draw tray	-	14	-
Reflux ratio	-	0.423	0.210
Condenser duty (kW)	-	4,459	2,561
Reboiler duty (kW)	-	4,757	3,258
Column diameter (m)	1.36	1.77	1.3
Column length (m)	39.62	14.02	12.19
Efficiency: Overall column	55%	-	-
Efficiency: Rectifying section	-	59%	65%
Efficiency: Stripping section	-	62%	68%

6.4.2.4. Cost Analysis

The two methods of cost analysis discussed above were again used to determine the associated capital and operating cost and the total annual cost of each of the design scenarios that were considered.

Conventional Distillation

Manual Method

Table 6.15 and Figure 6.15 show the results of the manual costing method. In this simulation route, the cost of VL-101 – 2,3-BDO Purification Column, ES-101 – Purification Column Condenser, ES-102 – Purification Column Reboiler and DM-101 – VL-101 Reflux Drum contribute to the capital cost. A capital cost of \$1,142,508.85 was calculated. Utility costs (cooling water and high-pressure steam) are considered as operational cost. An operational cost of \$4,941,242.63 was calculated. Assuming a payback period of 3 years, a total annual cost of \$5,322,078.91 was determined.

Table 6.15 Cost analysis of the conventional distillation separation route for butane-2,3-diol.

	Manual Method	Aspen Process Economic Analyser
Capital Cost	-	-
<i>Separators</i>	-	-
VL-101 - Purification Column (\$ 10 ⁶)	0.697	0.958
<i>Heat Exchangers</i>	-	-
ES-101 - Purification Column Condenser (\$ 10 ⁶)	0.292	0.236
ES-102 - Purification Column Reboiler (\$ 10 ⁶)	0.124	0.335
<i>Auxiliary Equipment</i>	-	-
DM-101 - VL-101 Reflux Drum (\$ 10 ⁶)	0.006	0.158
PC-101 - VL-101 Reflux Pump (\$ 10 ⁶)	0.023	0.047
Total Capital Cost (\$ 10⁶)	1.143	1.734
Total Operating Cost (\$ 10⁶)	4.941	4.645
Total Annual Cost (\$ 10⁶)	5.322	5.223

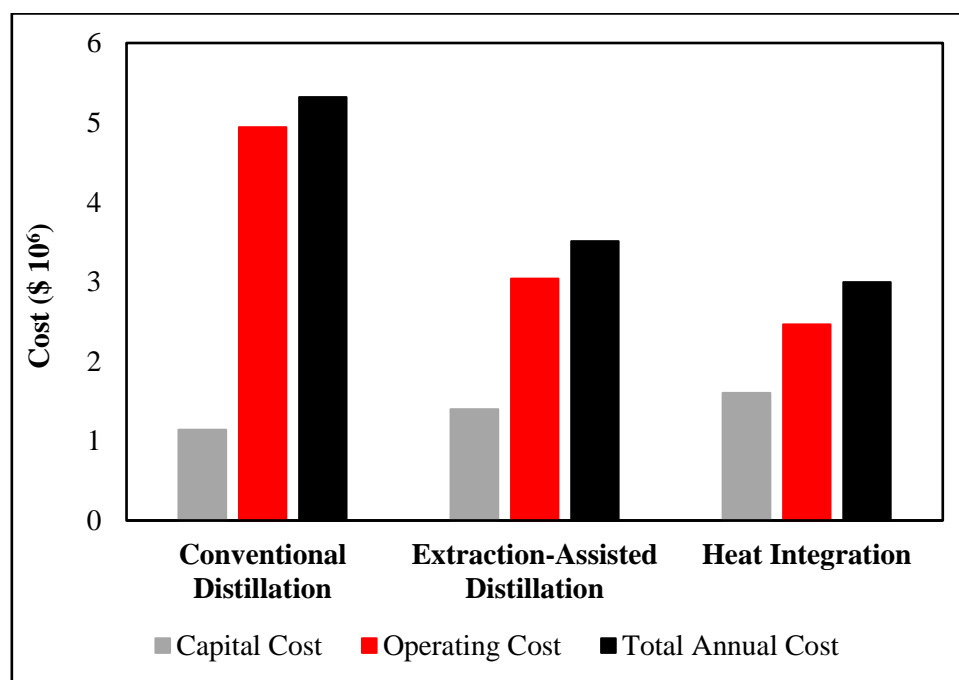


Figure 6.15. Cost analysis of the separation routes for 2,3-BDO calculated by the manual method.

Aspen Process Economic Analyser

Table 6.15 and Figure 6.16 show the results of the economic analyser costing method. A capital cost of \$1,734,000.00 and an operational cost of \$4,644,835.00 was estimated. Assuming a payback period of 3 years, a total annual cost of \$5,222,835.00 was calculated.

A comparison between the two costing methods reveals that while there are differences between the estimated capital costs (exceeding 50%), they are in agreement with respect to the order of magnitude. It is clear from both costing methods that the utility usage is the greatest contributor to the total annual cost.

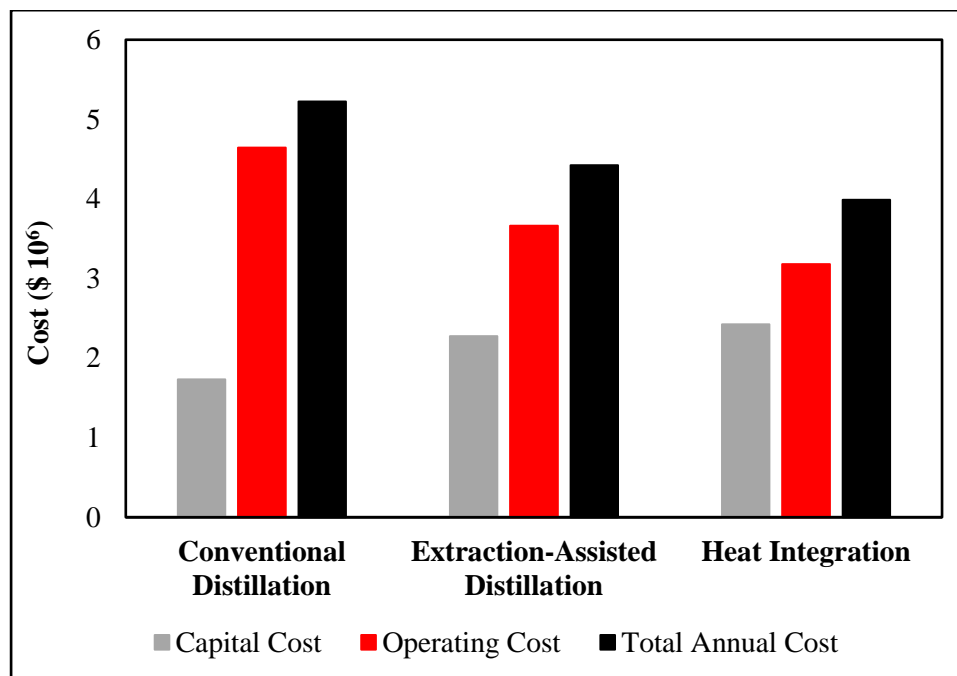


Figure 6.16. Cost analysis of the separation routes for 2,3-BDO calculated by Aspen Process Economic Analyser.

Extraction-Assisted Distillation without Heat Integration

Manual Method

Figure 6.15 and Table 6.16 show the results of the manual costing method. In this simulation route, the cost of VL-101 – 2,3-BDO Extraction Column, VL-102 – 2,3-BDO Purification Column, VL-103 – Solvent Recovery Column and their respective condensers, reboilers and reflux drums contribute to the capital cost. A capital cost of \$1,400,298.19 was calculated. Utility costs such as cooling water, high pressure steam and solvent requirement are considered as operational costs. An operational cost of \$3,040,845.76 was calculated. Assuming a payback period of 3 years, a total annual cost of \$3,507,611.83 was determined.

Aspen Process Economic Analyser

Table 6.16 and Figure 6.16 show the results of the economic analyser costing method. A capital cost of \$2,277,366.11 and an operational cost of \$3,662,680.00 was estimated. Assuming a payback period of 3 years, a total annual cost of \$4,421,802.04 was calculated.

A comparison between the two costing methods reveals that while there are significant differences between the estimated costs, they are in agreement with respect to the order of magnitude for the operating cost and total annual cost.

However, comparing corresponding methods, the increase in capital cost in the extraction-assisted distillation route compared against the conventional distillation route is justified as the extraction-assisted distillation design incorporates more unit operations and equipment. The operational cost for the extraction-assisted distillation showed a significant decrease when compared to the conventional distillation route. This is likely due to the lower boiling point of butan-2,3-diol in comparison to butane-1,4-diol considered in the analogous case presented in the previous section. The operating cost involved in the extraction-assisted distillation route greatly impacts the total annual cost which is significantly less than the total annual cost of the conventional distillation route. From this estimation alone, it is evident that the extraction-assisted distillation separation route is more economically viable than the conventional distillation separation route for this case.

Table 6.16 Cost analysis of the extracted-assisted distillation separation route for butane-2,3-diol without heat integration.

	Manual Method	Aspen Process Economic Analyser
Capital Cost	-	-
Separators	-	-
VL-101 - BDO Extraction Column (\$ 10 ⁶)	0.469	0.469
VL-102 - BDO Purification Column (\$ 10 ⁶)	0.269	0.435
VL-103 - Solvent Recovery Column (\$ 10 ⁶)	0.174	0.348
Heat Exchangers	-	-
ES-101 - Purification Column Condenser (\$ 10 ⁶)	0.121	0.115
ES-102 - Purification Column Reboiler (\$ 10 ⁶)	0.138	0.185
ES-103 - Recovery Column Condenser (\$ 10 ⁶)	0.087	0.104
ES-104 - Recovery Column Reboiler (\$ 10 ⁶)	0.073	0.105
Auxiliary Equipment	-	-
DM-101 - VL-101 Reflux Drum (\$ 10 ⁶)	0.020	0.149
DM-102 - VL-101 Reflux Drum (\$ 10 ⁶)	0.018	0.137
DM-103 - Solvent Receiver Drum (\$ 10 ⁶)	0.019	0.148
PC-101 - VL-102 Reflux Pump (\$ 10 ⁶)	0.006	0.045
PC-102 - VL-103 Reflux Pump (\$ 10 ⁶)	0.005	0.038
Total Capital Cost (\$ 10⁶)	1.400	2.277
Total Operating Cost (\$ 10⁶)	3.041	3.663
Total Annual Cost (\$ 10⁶)	3.508	4.422

Extraction-Assisted Distillation with Heat Integration

Manual Method

Figure 6.15 and Table 6.17 show the results of the manual costing method. The capital cost component of the total annual cost for the heat integration process route now includes additional heat exchangers; ES-105 – Solvent Pre-Cooler and ES-106 – Raffinate Pre-Heater. A capital cost of \$1,602,972.78 was calculated. Utility costs such as cooling water, high pressure steam and solvent requirement are considered as operational costs. An operational cost of \$2,462,880.32 was calculated. Assuming a payback period of 3 years, a total annual cost of \$2,997,204.58 was determined.

Aspen Process Economic Analyser

Figure 6.16 and Table 6.17 show the results of the economic analyser costing method. A capital cost of \$2,422,166.11 and an operational cost of \$3,181,480.00 was estimated. Assuming a payback period of 3 years, a total annual cost of \$3,988,868.70 was calculated.

A comparison between the two costing methods reveals that while there are significant differences between the estimated costs, they are in agreement with respect to the order of magnitude. It is clear from both costing methods that the utility usage is the greatest contributor to the total annual cost. Due to the additional two heat exchangers (ES-105 and ES-106) the capital cost estimated for the heat integration process is higher than that of the conventional distillation and extraction-assisted distillation separation routes. The operating cost for the heat integration separation route is significantly lower than that of the conventional distillation route and the extraction-assisted distillation separation route. The increased temperature of the feeds entering VL-102 and VL-103 directly impacts the heat duties of the VL-102 and VL-103 reboilers by decreasing the required duty. A decrease in the required reboiler duty suggests a significantly lower demand for high pressure steam. The total annual cost of the heat integration route is less than that of the conventional distillation and extraction-assisted separation route. This result suggests the advantages of implementing hybrid separation with heat-integration into the design of chemical processes. While heat-integration results in an increase in capital cost, it does cause a decrease in processes operational cost. From the total annual cost for each of the separation routes, the heat integrated extraction-assisted distillation separation route is the most economically viable for 2,3-BDO production.

Table 6.17 Cost analysis of the extracted-assisted distillation with heat integration separation route for butane-2,3-diol.

	Manual Method	Aspen Process Economic Analyser
Capital Cost	-	-
<i>Separators</i>	-	-
VL-101 - BDO Extraction Column (\$ 10 ⁶)	0.469	0.469
VL-102 - BDO Purification Column (\$ 10 ⁶)	0.269	0.408
VL-103 - Solvent Recovery Column (\$ 10 ⁶)	0.174	0.317
<i>Heat Exchangers</i>	-	-
ES-101 - Purification Column Condenser (\$ 10 ⁶)	0.121	0.115
ES-102 - Purification Column Reboiler (\$ 10 ⁶)	0.126	0.152
ES-103 - Recovery Column Condenser (\$ 10 ⁶)	0.087	0.104
ES-104 - Recovery Column Reboiler (\$ 10 ⁶)	0.059	0.103
ES-105 - Solvent Pre-Cooler (\$ 10 ⁶)	0.099	0.112
ES-106 - Raffinate Pre-Heater (\$ 10 ⁶)	0.130	0.125
<i>Auxiliary Equipment</i>	-	-
DM-101 - VL-101 Reflux Drum (\$ 10 ⁶)	0.020	0.149
DM-102 - VL-101 Reflux Drum (\$ 10 ⁶)	0.018	0.137
DM-103 - Solvent Receiver Drum (\$ 10 ⁶)	0.019	0.148
PC-101 - VL-102 Reflux Pump (\$ 10 ⁶)	0.006	0.045
PC-102 - VL-103 Reflux Pump (\$ 10 ⁶)	0.005	0.038
Total Capital Cost (\$ 10⁶)	1.603	2.422
Total Operating Cost (\$ 10⁶)	2.463	3.181
Total Annual Cost (\$ 10⁶)	2.997	3.989

6.5. Conclusions

Conventional and extraction assisted distillation were successfully simulated for the purification of 1,4-BDO and 2,3-BDO from aqueous mixtures. The effectiveness of butan-1-ol as an extraction solvent for the extraction assisted distillation process was proven by simulation. Technical analyses showed that feasible purification schemes for 1,4-BDO and 2,3-BDO can be designed using either separation alternative, with butanediol purities and recoveries exceeding 0.99 and 0.9 wt. fraction respectively. The economic analysis showed that conventional distillation is the most economically viable option for the purification of 1,4-BDO, with an estimated total annual cost in the range of \$4,532,846.67 and \$4,635,070.52 for a payback period of 3 years. For the extraction assisted distillation process path, the total annual cost reduced from the range of \$8,239,061.65 and \$9,492,053.48 to the range of \$6,570,160.00 and \$7,012,130.12 after heat integration. It was found that the total operating cost after heat integration was in excess of that from the conventional distillation process, hence the economic feasibility of this process alternative is limited, and conventional distillation is recommended for this case. This can be attributed to the high boiling point of 1,4-BDO, and large internal recycle rates necessitating large reboiler duties in the additional columns of the hybrid separation scheme.

For the 2,3-BDO purification, the conventional distillation total annual cost was estimated in the range of \$5,222,835.00 to \$5,322,078.91. This value was in excess of the total annual cost of the extraction assisted distillation without heat integration process path, which was in the range of \$3,507,611.83 to \$4,421,802.04. This total annual cost reduced to the range of \$2,997,204.58 and \$3,988,868.70 after heat integration. Hence, for the 2,3-BDO purification, extraction assisted distillation with heat integration is the economically viable option for this case, reducing costs by over 42% in comparison to conventional distillation, and by approximately 15% in comparison to the non-heat integrated extraction assisted distillation process alternative.

CHAPTER SEVEN

Culminating Discussion

The binary vapour-liquid equilibrium data measured in the experimental studies were regressed using Aspen Plus® software to determine binary interaction model parameters. The parameters were then used to design the relevant separation schemes for the butanediol systems. In this chapter, a brief summary of the experimental work is presented, along with a summary of the separation design.

7.1. Chemicals and uncertainties

The chemicals used in this study were procured from Sigma-Aldrich with a supplier stated purity exceeding 99%. The diols and butan-1-ol were dried by a molecular sieve prior to use, and their water content was confirmed to be below 0.0005 mass fraction by Karl Fischer titration using an MKS 500 device. The purities of the components used were confirmed by gas chromatograph (Shimadzu GC 2014) and refractive index analysis (ATAGO RX-7000 α refractometer (sodium D-line = 589 nm) with a supplier uncertainty of 0.0001). GC peak areas of >0.99 fraction were determined. These results are presented in Chapters 4 and 5.

The area ratio method described by Raal and Mühlbauer, (1998) was used for the GC thermal conductivity detector calibration. Standard mixtures were prepared gravimetrically using a Mettler-Toledo AB204-S mass balance, with an uncertainty of 0.0001 g. The standard combined uncertainty for the VLE compositions did not exceed 0.0040 mole fraction.

The VLE measurements were controlled using an ABB F080 pressure controller, using vacuum and atmospheric air for regulation. The equilibrium pressure was determined using a WIKA P-10 transducer, calibrated with a WIKA CPC 3000 pressure controller as a standard. The standard combined uncertainty in pressure was found to be 0.12 kPa. The temperature measurements at equilibrium were determined using a type-A Pt-100 temperature probe, calibrated with a WIKA CTB 9100 temperature standard. The standard combined uncertainty in temperature was found to be 0.10 K.

Calibration plots for composition, temperature and pressure are presented in Appendix A (Figures A1-A12), while the uncertainty breakdown for these parameters is presented in Appendix B, Table B1.

7.2. VLE measurements and modelling.

7.2.1. Confirmation of equipment and procedure

In order to confirm the equipment and procedure used, vapour pressure measurements for the chemical used in the novel study, and a binary test system measurement were conducted using the VLE apparatus. The results of the vapour pressure measurements are compared to model predictions in Chapter 3, Figure 3.3. The system measured was the water (1) + propan-1-ol (2) mixture at 313.2 K, which compared well with literature data, as shown graphically in Figure 3.4 in Chapter 3. Deviations between the test measurement and literature data did not exceed 0.5 kPa.

7.2.2. Novel binary VLE data

Subsequent to the confirmation of procedure, novel binary VLE measurements were conducted for the key component separations relevant to the purification of butane-1,4-diol and butane-2,3-diol from aqueous mixtures. These measurements included isothermal P-x-y data for the water + butane-1,4-diol system at 353.2, 363.2 and 373.2 K, the water + butane-2,3-diol system at 353.1, 363.2 and 373.2 K, and the butan-1-ol + butane-1,4-diol and butan-1-ol + butane-2,3-diol systems at 353.2, 363.2, 373.2 and 388.2 K. The behaviour of these systems was non-ideal, including significant non-ideality in the vapour-phase.

Consistency tests were applied to the data measured. This included the area test of Redlich & Kister (1948) and point test of Christiansen & Fredenslund (1975). These tests confirmed that the data measured were thermodynamically consistent.

The data was modelled by the γ - Φ approach, using the NRTL-HOC and UNIQUAC-HOC model combinations. Both models fit the data reasonably well. The lowest RMSD value for pressure in the water systems was obtained from the UNIQUAC-HOC model for both the water + butane-1,4-diol system yielding 0.046 kPa and the water + butane-2,3-diol at 0.036 kPa. The NRTL-HOC model provided a better representation of the G^E/RT vs. x_1 behaviour. For the butan-1-ol systems, the lowest RMSD value for pressure was obtained from the NRTL-HOC model at 0.032 kPa for the butan-1-ol + butane-1,4-diol system, while both the NRTL-HOC and UNIQUAC-HOC models yielded an RMSD of 0.008 kPa for the butan-1-ol + butane-2,3-diol system.

7.2. Separation scheme design

The binary interaction parameters regressed from the experimental work were used to design several process alternatives for the purification of butane-1,4-diol and butane-2,3-diol from aqueous mixtures

resulting from biological reaction processes. The details of this design procedure are presented in Chapter 6. Three separation process pathways were considered which included conventional distillation, extraction assisted distillation and extraction assisted distillation with heat integration.

The systematic approach followed to execute the proposed hybrid simulation is summarized below Haider *et al.*, (2018):

1. Solvent screening considering technical merit, economic factors and environmental impact
2. Thermodynamic model selection and validation of parameters
3. Technically sound conventional distillation design as a base case for comparison
4. Hybrid extraction-distillation-heterogenous distillation simulation
5. Sensitivity and optimization of the design
6. Economical analysis based on Total Annual Cost (TAC)

Optimization was carried out using a sequential quadratic programming algorithm (Schefflan, (2011), Al-Malah, (2016)) as shown in Figure 7.1, to reduce reboiler duties and minimize total annual cost. Tray numbers, feed, and product streams were then adjusted with reflux ratio to again reduce duties.

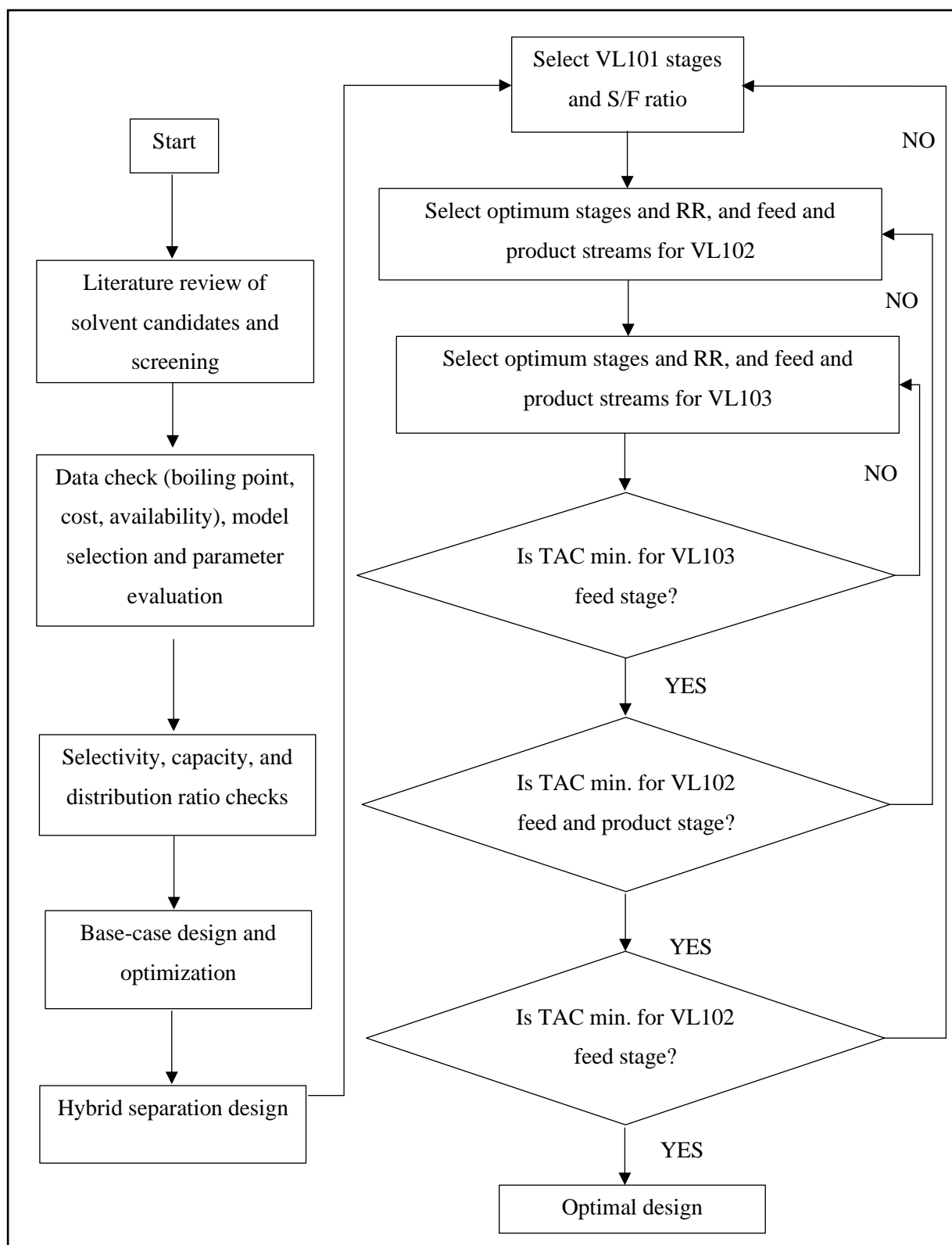


Figure 7.1. Flow diagram used for the sequential optimization approach for solvent selection and simulation design. Adapted from Haider *et al.*, (2018).

After technical analysis was finalized and the proposed designs were optimized, economic evaluation was conducted to establish the economic feasibility of the proposed designs.

Consider Figure 7.2 and Figure 7.3. Figure 7.2 shows a comparison of the manual and Aspen estimated costs for the 1,4-BDO separation routes and Figure 7.3 shows a comparison of the manual and Aspen estimated costs for the 2,3-BDO separation routes. If one considers the conventional distillation separation route, the 1,4-BDO route is the most economically viable by just under 42%. Due to the high-boiling point of 1,4-BDO and recycle rates, it stands to reason that a larger quantity of heating utility is required to produce the 1,4-BDO biofuel, while meeting both the mass purity and mass recovery specification. Considering the extraction-assisted distillation separation route, a solvent-to-feed ratio of 2.14 is required to achieve the required product specification of 1,4-BDO. The extraction column (VL-101) for the 1,4-BDO separation is charged with a total (feed and solvent) flowrate of 62,936 kg/h. From this total flowrate, 67% is recovered as the flowrate of the extract-phase (41,911 kg/h) of which, only 3.00% is the 1,4-BDO component which requires concentrating. The 1,4-BDO Purification Column (VL-102) is required to recover (on a mass basis), at least 90% of the 1,4-BDO of the feed, in the bottoms. As such, a significant heat duty is required in the reboiler of VL-102 to perform the required concentration. The reboiler heat duty for the conventional distillation route is 14,009 kW while the reboiler heat duty of VL-102 for the extraction-assisted distillation separation route alone is 14,657 kW. This is a significant difference in the reboiler duties, thus supporting the economic feasibility of the conventional distillation separation route.

While heat integration decreases the operating cost of the 1,4-BDO and 2,3-BDO separation process, only the 2,3-BDO showed a significant decrease (15%) with respect to the total annual cost between the extraction-assisted distillation and heat integration separation routes that was competitive with the conventional distillation process route. A significant decrease in operating cost and hence total annual cost is observed (12%) for the 2,3-BDO extraction-assisted distillation when compared to the 1,4-BDO conventional distillation separation route for similar production rates. As such, across all separation routes for both 1,4-BDO and 2,3-BDO, while conventional distillation for 1,4-BDO is more economically viable than extraction-assisted distillation, 2,3-BDO can be purified by heat integrated extraction-assisted distillation at a lower cost.

This is a significant finding as the heat of combustion of 1,4-BDO is only about 1.4% higher than that of 2,3-BDO, and the combustion products are virtually the same. Hence, if comparing the two fluids as biofuels, 2,3-BDO can likely be produced at a lower cost than 1,4-BDO, with a similar calorific value. The 1,4-BDO purification process still has merit if a biologically derived process alternative is required for 1,4-BDO production for use in applications excluding biofuel.

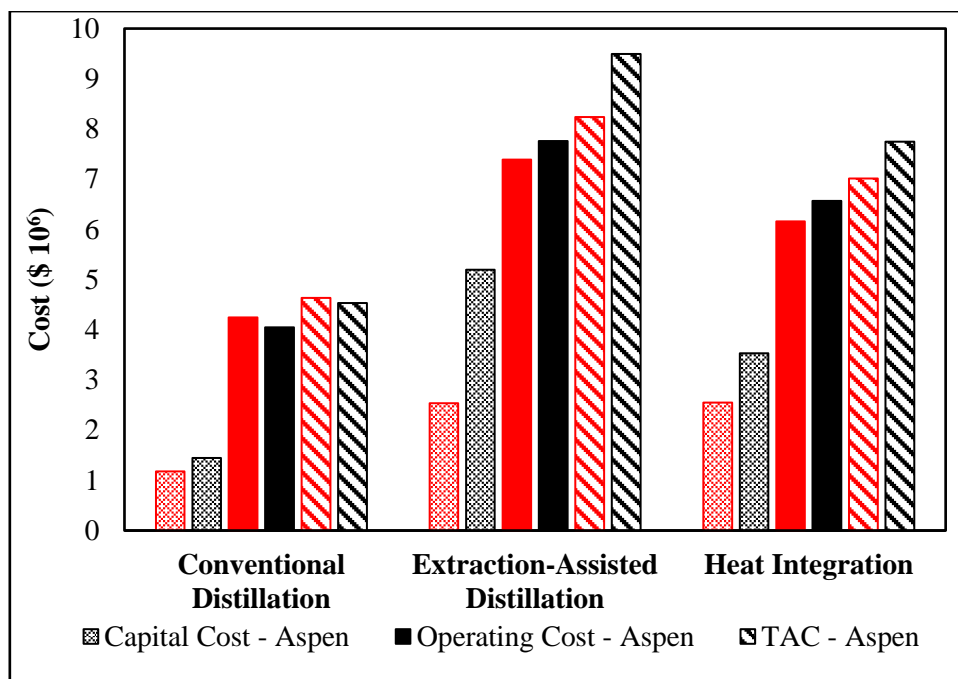


Figure 7.2. Comparison of the manual method and Aspen Process Economic Analysis for the 1,4-BDO separation routes. Red bars are the manual method, black bars Aspen Process Economic Analysis.

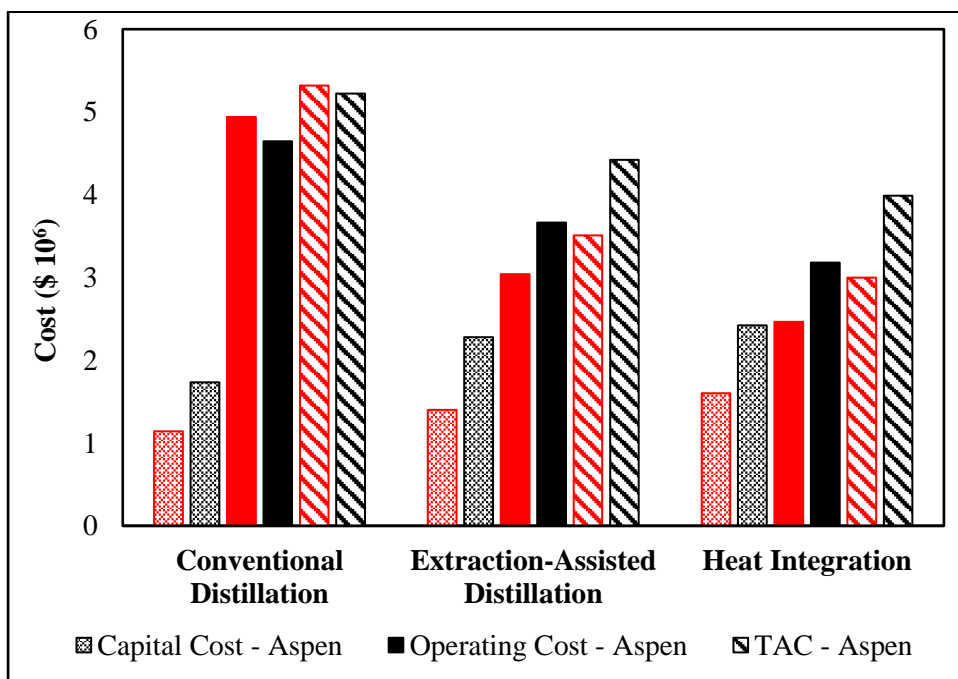


Figure 7.3. Comparison of the manual method and Aspen Process Economic Analysis for the 2,3-BDO separation routes. Red bars are the manual method, black bars Aspen Process Economic Analysis.

CHAPTER EIGHT

Conclusions

- The vapour-liquid equilibrium phase behaviour of the water + butane-1,4-diol, water + butane-2,3-diol, butan-1-ol + butane-1,4-diol and butan-1-ol + butane-2,3-diol was successfully characterized using a low-pressure dynamic VLE apparatus. The measured data passed the area consistency test (within 4%) and the point consistency test (within 1 %).
- The VLE behaviour of the systems in this work was found to be non-ideal which is attributed to the differences in molecule sizes as well as the intermolecular forces exhibited by the oxygenated hydrocarbons considered. All systems exhibited steep P-y curves typical of systems of large differences in pure component vapour pressures with a positive deviation from Raoult's Law which was more pronounced in the butane-1,4-diol systems. This may be attributed to location of the OH groups on the terminal positions of the molecules which possibly promotes superior intermolecular and intramolecular interaction in comparison to the butane-2,3-diol molecules.
- The RMSD calculation for pressure and the Absolute Average Deviation (AAD) values in the vapour-phase mole fraction was found to be within the experimental uncertainty. The lowest RMSD value was obtained from the UNIQUAC-HOC model for both the water + butane-1,4-diol system at 0.046 kPa and the water + butane-2,3-diol at 0.036 kPa. There was no significant difference in performance of the NRTL-HOC and UNIQUAC-HOC models for the butan-1-ol + butane-1,4-diol and butan-1-ol + butane-2,3-diol systems with RMSDs in pressure of 0.032-0.035 and 0.008, respectively. In all cases the NRTL-HOC model provided a better representation of the $\frac{G^E}{RT}$ vs. x_1 behaviour.
- The technical feasibility of butan-1-ol as an extraction solvent for the purification of butane-1,4-diol and butane-2,3-diol aqueous mixtures was proven by simulation with butanediol purities and recoveries exceeding 0.99 and 0.9 wt fraction, respectively. Conventional distillation was also shown to be technically feasible.
- The economic analysis showed that conventional distillation is the most economically viable option for the purification of butane-1,4-diol, with an estimated total annual cost in the range of \$4,532,846.67 and \$4,635,070.52 for a payback period of 3 years. Extraction assisted distillation with and without heat integration was shown to not be economically feasible for the

purification of butane-1,4-diol from a biological reaction process. This was attributed to the high boiling point of 1,4-BDO, and large internal recycle rates necessitating large reboiler duties in the additional columns of the hybrid separation scheme

- For the butane-2,3-diol purification, extraction assisted distillation with heat integration was found to be the economically viable option, reducing costs by over 42% in comparison to conventional distillation, and by approximately 15% in comparison to the non-heat integrated extraction assisted distillation process alternative. Total annual costs were estimated in the range of \$2,997,204.58 and \$3,988,868.70 after heat integration.

CHAPTER NINE

Recommendations

- Because of the very steep P-y curves in the butane-1,4-diol VLE systems, it was not possible to measure the vapour phase compositions in the butane-1,4-diol dilute regions using the dynamic method for VLE. It is recommended that the data in this region be measured by a static-analytic method with online GC-analysis. This method will allow for these dilute region measurements to be determined with high accuracy.
- Alternate biological process conditions and microbes should be explored which have a higher butanediol conversion with higher product concentrations. This will improve the economics of the separation schemes as smaller quantities of water would need to be removed for equivalent butanediol recoveries.
- Extraction solvents with higher selectivity to the butanediols should be explored via liquid-liquid equilibrium measurements and solvent screening. By employing a solvent with a higher selectivity to the butanediols, the process economics can be further improved.

References

- Abrams, D.S. and Prausnitz, J.M., (1975). Statistical thermodynamics of liquid mixtures: A new expression for the excess Gibbs energy of partly or completely miscible systems. *AIChE Journal*, 21 (1), 116–128.
- Al-Malah, K.I.M., (2016). *Aspen plus*. Wiley Online Library.
- Amaya, K. and Fujishiro, R., (1956). Heats of Dilution of Polyvinylalcohol Solutions. II. *Bulletin of the Chemical Society of Japan*, 29 (7), 830–833.
- Barker, J., (1953). Determination of Activity Coefficients from total pressure measurements. *Australian Journal of Chemistry*, 6 (3), 207.
- Benecke, T.P., Narasigadu, C., Iwarere, S.A., Nelson, W.M., and Ramjugernath, D., (2019). Vapor–Liquid Equilibrium Measurements of Ether Alcohol Blends for Investigation on Reformulated Gas. *Journal of Chemical & Engineering Data*, 64 (1), 115–123.
- Birajdar, S.D., Padmanabhan, S., and Rajagopalan, S., (2014). Rapid Solvent Screening Using Thermodynamic Models for Recovery of 2,3-Butanediol from Fermentation by Liquid–Liquid Extraction. *Journal of Chemical & Engineering Data*, 59 (8), 2456–2463.
- Bondi, A., (1964). van der Waals Volumes and Radii. *The Journal of Physical Chemistry*, 68 (3), 441–451.
- Burgard, A., Burk, M.J., Osterhout, R., Van Dien, S., and Yim, H., (2016). Development of a commercial scale process for production of 1,4-butanediol from sugar. *Current Opinion in Biotechnology*, 42, 118–125.
- Checoni, R.F. and Francesconi, A.Z., (2009). Experimental Study of the Excess Molar Enthalpy of Ternary Mixtures Containing Water + (1,2-Propanediol, or 1,3-Propanediol, or 1,2-Butanediol, or 1,3-Butanediol, or 1,4-Butanediol, or 2,3-Butanediol)+Electrolytes at 298.15 K and Atmospheric Pressure. *Journal of Solution Chemistry*, 38 (8), 1055–1070.
- Christiansen, L.J. and Fredenslund, A., (1975). Thermodynamic consistency using orthogonal collocation or computation of equilibrium vapor compositions at high pressures. *AIChE Journal*, 21 (1), 49–57.

- Cottrell, F.G., (1919). On The Determination Of Boiling Points Of Solutions. *Journal of the American Chemical Society*, 41 (5), 721–729.
- Coulson, E.A., Hales, J.L., and Herington, E.F.G., (1948). Fractional distillation. II. The use of dilute solutions of thiophene in benzene as test mixtures and a comparison with mixtures of benzene and ethylene dichloride. *Transactions of the Faraday Society*, 44, 636.
- Douglas, M.J., (1988). *Conceptual design of chemical processes*. McGrawHill.
- Duss, M. and Taylor, R., (2018). Predict distillation tray efficiency. *Chem. Eng. Prog.*, 114 (7), 24–30.
- van Dyk, S., Su, J., Mcmillan, J.D., and Saddler, J. (John), (2019). Potential synergies of drop-in biofuel production with further co-processing at oil refineries. *Biofuels, Bioproducts and Biorefining*, 13 (3), 760–775.
- Fair, J.R. and Humphrey, J.L., (1984). Liquid-Liquid Extraction: Possible Alternative To Distillation. *Solvent Extraction and Ion Exchange*, 2 (3), 323–352.
- Frank, T.C., Dahuron, L., Holden, B.S., Prince, W.D., Seibert, A.F., and Wilson, L.C., (2008). *Perry's Chemical Engineers' Handbook. Section 15*. McGraw-Hill Publishing.
- Fredenslund, A., Gmehling, J., and Rasmussen, P., (1977). *Vapour-Liquid Equilibria Using UNIFAC a Group-Contribution Method*. first ed. Elsevier.
- Fredenslund, A., Jones, R.L., and Prausnitz, J.M., (1975). Group-contribution estimation of activity coefficients in nonideal liquid mixtures. *AIChE Journal*, 21 (6), 1086–1099.
- Gai, H., Lin, K., Feng, Y., Xiao, M., Guo, K., and Song, H., (2018). Conceptual design of an extractive distillation process for the separation of azeotropic mixture of n-butanol-isobutanol-water. *Chinese Journal of Chemical Engineering*, 26 (10), 2040–2047.
- Gibbs, R.E. and Van Ness, H.C., (1972). Vapor—Liquid Equilibria from Total-Pressure Measurements. A New Apparatus. *Industrial and Engineering Chemistry Fundamentals*, 11 (3), 410–413.
- Gillespie, D.T.C., (1946). Vapor-Liquid Equilibrium Still for Miscible Liquids. *Industrial & Engineering Chemistry Analytical Edition*, 18 (9), 575–577.
- Gmehling, J., Kleiber, M., Kolbe, B., and Rarey, J., (2019). *Chemical thermodynamics for process simulation*. John Wiley & Sons.

- Gmehling, J., Kolbe, B., Kleiber, M., and Rarey, J., (2012). *Chemical Thermodynamics for Process Simulation*. Methods in Ecology and Evolution.
- Haas, T., Jaeger, B., Weber, R., Mitchell, S.F., and King, C.F., (2005). New diol processes: 1,3-propanediol and 1,4-butanediol. *Applied Catalysis A: General*, 280 (1), 83–88.
- Haider, J., Harvianto, G.R., Qyyum, M.A., and Lee, M., (2018). Cost- and Energy-Efficient Butanol-Based Extraction-Assisted Distillation Designs for Purification of 2,3-Butanediol for Use as a Drop-in Fuel. *ACS Sustainable Chemistry & Engineering*, 6 (11), 14901–14910.
- Harvey, B.G., Merriman, W.W., and Quintana, R.L., (2016). Renewable Gasoline, Solvents, and Fuel Additives from 2,3-Butanediol. *ChemSusChem*, 9 (14), 1814–1819.
- Harvianto, G.R., Haider, J., Hong, J., Van Duc Long, N., Shim, J.-J., Cho, M.H., Kim, W.K., and Lee, M., (2018). Purification of 2,3-butanediol from fermentation broth: process development and techno-economic analysis. *Biotechnology for Biofuels*, 11 (1), 18.
- Hayden, J.G. and O’Connell, J.P., (1975). A Generalized Method for Predicting Second Virial Coefficients. *Industrial & Engineering Chemistry Process Design and Development*, 14 (3), 209–216.
- Haynes, W.M., (2014). *CRC Handbook of Chemistry and Physics, 95th Edition*. 95th ed. N. Hoboken: CRC Press.
- Heertjies, P.M., (1960). Determination of Vapour-Liquid Equilibrium of Binary Mixtures. *Chemical and Process Engineering*, 41, 385–386.
- Hort, E. V. and Taylor, P., (2003). Acetylene-Derived Chemicals. *In: Kirk-Othmer Encyclopedia of Chemical Technology*. Hoboken, NJ, USA: John Wiley & Sons, Inc.
- Huang, R. and Zhang, D., (1987). Determination and Correlation of Isothermal Vapor-Liquid Equilibrium Data for the Binary System of Water-1, 4-Butanediol. *Petrol Chem. Technol.*, 16, 497–502.
- Hussain, A., Minh, L.Q., Qyyum, M.A., and Lee, M., (2018). Design of an Intensified Reactive Distillation Configuration for 2-Methoxy-2-methylheptane. *Industrial & Engineering Chemistry Research*, 57 (1), 316–328.

- ISO, (2008). JCGM 100:2008. *International Organization for Standardization Geneva ISBN*, 50 (September), 134.
- Jelinek, K., Leseck, F., and Sivokova, M., (1976). Vapour-liquid equilibrium in binary water + 1,2-propylene glycol, water + diethylene glycol and water + 1,4-butandiol systems. *Collect. Czech. Chem. Commun.*, 41, 2650–2656.
- Joseph, M., Raal, J., and Ramjugernath, D., (2001). Phase equilibrium properties of binary systems with diacetyl from a computer controlled vapour–liquid equilibrium still. *Fluid Phase Equilibria*, 182 (1–2), 157–176.
- Joseph, M., (2001). Computer-aided Measurement of Vapour-Liquid Equilibria in a Dynamic Still at Sub-Atmospheric Pressures. University of Natal.
- Karnaouri, A., Matsakas, L., Topakas, E., Rova, U., and Christakopoulos, P., (2016). Development of Thermophilic Tailor-Made Enzyme Mixtures for the Bioconversion of Agricultural and Forest Residues. *Frontiers in Microbiology*, 7.
- Kister, H.Z., (1992). *Distillation design*. McGraw-Hill New York.
- Kneisl, P., Zondlo, J.W., Whiting, W.B., and Bedell, M., (1989). The effect of fluid properties on ebulliometer operation. *Fluid Phase Equilibria*, 46 (1), 85–94.
- Köpke, M., Mihalcea, C., Liew, F., Tizard, J.H., Ali, M.S., Conolly, J.J., Al-Sinawi, B., and Simpson, S.D., (2011). 2,3-Butanediol Production by Acetogenic Bacteria, an Alternative Route to Chemical Synthesis, Using Industrial Waste Gas. *Applied and Environmental Microbiology*, 77 (15), 5467–5475.
- Li, Y., Wu, Y., Zhu, J., and Liu, J., (2012). Separation of 2,3-butanediol from fermentation broth by reactive-extraction using acetaldehyde-cyclohexane system. *Biotechnology and Bioprocess Engineering*, 17 (2), 337–345.
- Lieberman, N.P. and Lieberman, E.T., (2014). *Working Guide to Process Equipment*. McGraw-Hill Education.
- Luyben, W.L., (2013). *Distillation design and control using Aspen simulation*. John Wiley & Sons.
- Maher, P.J. and Smith, B.D., (1979). Infinite Dilution Activity Coefficient Values from Total Pressure

- VLE Data. Effect of Equation of State Used. *Industrial & Engineering Chemistry Fundamentals*, 18 (4), 354–357.
- Mathias, P.M., (2017). Guidelines for the Analysis of Vapor–Liquid Equilibrium Data. *Journal of Chemical & Engineering Data*, 62 (8), 2231–2233.
- Mavalal, S., Chetty, T., and Moodley, K., (2019). Isothermal Vapor–Liquid Equilibrium Measurements for the Pentan-2-one + Propan-1-ol/Butan-1-ol System within 342–363 K. *Journal of Chemical & Engineering Data*, acs.jced.9b00100.
- Mavalal, S. and Moodley, K., (2020). Isothermal vapour-liquid equilibrium measurements for the water + butane-1,4-diol/butane-2,3-diol system within 353.1–373.2 K. *Fluid Phase Equilibria*, 512, 112518.
- Mavalal, S. and Moodley, K., (2021). Isothermal Vapour-Liquid Equilibrium Measurements for the butan-1-ol + butane-1,4-diol/butane-2,3-diol system within 353.2–388.2 K. *Fluid Phase Equilibria*, 527, 112827.
- Menon, V. and Rao, M., (2012). Trends in bioconversion of lignocellulose: Biofuels, platform chemicals & biorefinery concept. *Progress in Energy and Combustion Science*, 38 (4), 522–550.
- Moodley, K. and Dorsamy, C.-L., (2018). Isothermal Vapor–Liquid Equilibrium Measurements of Butan-2-one + 2-Methyl-propan-1-ol/Pentan-1-ol. *Journal of Chemical & Engineering Data*, 63 (11), 4128–4135.
- Moodley, K., Dorsamy, C.L., Narasigadu, C., and Vemblanathan, Y., (2018). Excess Properties and Phase Equilibria for the Potential Biofuel System of Propan-2-ol and 2-Methyl-propan-1-ol at 333.15, 343.15, and 353.15 K. *Journal of Chemical and Engineering Data*, 63 (6), 2106–2113.
- Moodley, K., Naidoo, P., Raal, J.D., and Ramjugernath, D., (2013). Vapor-liquid equilibrium data for the morpholine-4-carbaldehyde + n-hexane or n-heptane binary systems using a static-synthetic apparatus. *Journal of Chemical and Engineering Data*, 58 (9), 2552–2566.
- Moodley, K., Naidoo, P., Raal, J.D., and Ramjugernath, D., (2019). Isothermal Vapor–Liquid Equilibrium Measurements for Alcohol + Water/ n -Hexane Azeotropic Systems Using Both

- Dynamic and Automated Static-Synthetic Methods. *Journal of Chemical & Engineering Data*, 64 (6), 2657–2670.
- Nagamachi, M.Y. and Francesconi, A.Z., (2006). Measurement and correlation of excess molar enthalpy for (1,2-propanediol, or 1,3-propanediol, or 1,4-butanediol+water) at the temperatures (298.15, 323.15, and 343.15) K. *The Journal of Chemical Thermodynamics*, 38 (4), 461–466.
- Narasigadu, C., (2011). Design of a Static Micro-Cell for Phase Equilibrium Measurements: Measurements and Modelling. PhD (Eng) Thesis, University of KwaZulu-Natal.
- Ndlovu, M., (2005). Development of a Dynamic Still for Measuring Low Pressure Vapour-liquid-liquid Equilibria: Systems of Partial Liquid Miscibility. MSc (Eng) Dissertation, University of KwaZulu-Natal.
- Van Ness, H.C., (1995). Thermodynamics in the treatment of vapor/liquid equilibrium (VLE) data. *Pure and Applied Chemistry*, 67 (6), 859–872.
- Van Ness, H.C. and Abbott., M.M., (1982). *Classical thermodynamics of nonelectrolyte solutions*. New York: McGraw-Hill.
- Van Ness, H.C., Byer, S.M., and Gibbs, R.E., (1973). Vapor-Liquid equilibrium: Part I. An appraisal of data reduction methods. *AIChE Journal*, 19 (2), 238–244.
- NIST, (2019). NIST Standard Reference Database 103a: ThermoData Engine.
- Othmer, D.F., (1928). Composition of Vapors from Boiling Binary Solutions 1. *Industrial & Engineering Chemistry*, 20 (7), 743–746.
- Othmer, D.F., White, R.E., and Trueger, E., (1941). Liquid-Liquid Extraction Data. *Industrial & Engineering Chemistry*, 33 (10), 1240–1248.
- Parate, R.D., Rode, C. V., and Dharme, M.S., (2018). 2,3-Butanediol Production from Biodiesel Derived Glycerol. *Current Environmental Engineering*, 5 (1), 4–12.
- Patel, A.K., Singhania, R.R., and Pandey, A., (2017). Production, Purification, and Application of Microbial Enzymes. *In: Biotechnology of Microbial Enzymes*. Elsevier, 13–41.
- Penner, D., Redepenning, C., Mitsos, A., and Viell, J., (2017). Conceptual Design of Methyl Ethyl Ketone Production via 2,3-Butanediol for Fuels and Chemicals. *Industrial & Engineering*

- Chemistry Research*, 56 (14), 3947–3957.
- Pitzer, K.S. and Curl, R.F., (1957). Empirical Equation for the Second Virial Coefficient. *Journal of the American Chemical Society*, 79, 2369–2370.
- Pividal, K.A., Birtigh, A., and Sandler, S.I., (1992). Infinite dilution activity coefficients for oxygenate systems determined using a differential static cell. *Journal of Chemical & Engineering Data*, 37 (4), 484–487.
- Poling, B.E., Prausnitz, J.M., and O’Connell, J.P., (2001). The properties of gases & liquids. *McGraw-Hill Education*, 1 (4), 409.
- Prausnitz, J.M., Lichtenthaler, R.N., and De Azevedo, E.G., (1998). *Molecular thermodynamics of fluid-phase equilibria*. Pearson Education.
- Qureshi, N., Lin, X., Liu, S., Saha, B.C., Mariano, A.P., Polaina, J., Ezeji, T.C., Friedl, A., Maddox, I.S., Klasson, K.T., Dien, B.S., and Singh, V., (2020). Global View of Biofuel Butanol and Economics of Its Production by Fermentation from Sweet Sorghum Bagasse, Food Waste, and Yellow Top Presscake: Application of Novel Technologies. *Fermentation*, 6 (2), 58.
- Raal, J.D. and Mühlbauer, A.L., (1998). *Phase Equilibria: Measurement and Computation*. Bristol, PA: Taylor and Francis.
- Raal, J.D. and Ramjugernath, D., (2005). 5 Vapour—liquid equilibrium at low pressure. In: R. Weir, ed. *Experimental Thermodynamics*. Elsevier, 71–87.
- Redlich, O. and Kister, A.T., (1948). Algebraic Representation of Thermodynamic Properties and the Classification of Solutions. *Industrial & Engineering Chemistry*, 40 (2), 345–348.
- Renon, H. and Prausnitz, J.M., (1968). Local compositions in thermodynamic excess functions for liquid mixtures. *AIChE Journal*, 14 (1), 135–144.
- Rose, A. and Williams, E.T., (1955). Vapor Liquid Equilibrium Self-Lagging Stills. *Industrial & Engineering Chemistry*, 47 (8), 1528–1533.
- Satam, C.C., Daub, M., and Realff, M.J., (2019). Techno-economic analysis of 1,4-butanediol production by a single-step bioconversion process. *Biofuels, Bioproducts and Biorefining*, 13 (5), 1261–1273.

- Schefflan, R., (2011). *Teach yourself the basics of Aspen Plus*. Wiley Online Library.
- Seader, J.D., Henley, E.J., and Roper, D.K., (1998). *Separation process principles*. Wiley New York.
- Shao and Kumar, A., (2009a). Separation of 1-butanol/2,3-butanediol using ZSM-5 zeolite-filled polydimethylsiloxane membranes. *Journal of Membrane Science*, 339 (1–2), 143–150.
- Shao and Kumar, A., (2009b). Recovery of 2,3-butanediol from water by a solvent extraction and pervaporation separation scheme. *Journal of Membrane Science*, 329 (1–2), 160–168.
- Smith, J.M., Van Ness, H.C., and Abbott, M., (2005). *Introduction to Chemical Engineering Thermodynamics*. McGraw-Hill Education.
- Tahri, N., Bahafid, W., Sayel, H., and El Ghachtouli, N., (2013). Biodegradation: Involved Microorganisms and Genetically Engineered Microorganisms. *In: Biodegradation - Life of Science*. InTech.
- Tsonopoulos, C., (1974). An empirical correlation of second virial coefficients. *AIChE Journal*, 20 (2), 263–272.
- Turton, R., Bailie, R.C., Whiting, W.B., and Shaeiwitz, J.A., (2008). *Analysis, synthesis and design of chemical processes*. Pearson Education.
- Walas, S.M., (2013). *Phase equilibria in chemical engineering*. Butterworth-Heinemann.
- Waldron, K.W., (2010). *Bioalcohol production: biochemical conversion of lignocellulosic biomass*. Elsevier.
- Wilson, G.M., (1964). Vapor-Liquid Equilibrium. XI. A New Expression for the Excess Free Energy of Mixing. *Journal of the American Chemical Society*, 86 (2), 127–130.
- Wisniak, J., Ortega, J., and Fernández, L., (2017). A fresh look at the thermodynamic consistency of vapour-liquid equilibria data. *The Journal of Chemical Thermodynamics*, 105, 385–395.
- Wu, Y.-Y., Chen, K., Zhu, J.-W., Wu, B., Ji, L., and Shen, Y.-L., (2014). Enhanced extraction of 2,3-butanediol by medley solvent of salt and n-butanol from aqueous solution. *The Canadian Journal of Chemical Engineering*, 92 (3), 511–514.
- Wu, Y.-Y., Pan, D.-T., Zhu, J.-W., Chen, K., Wu, B., and Ji, L.-J., (2012). Liquid-liquid equilibria of water+2,3-butanediol+isobutanol at several temperatures. *Fluid Phase Equilibria*, 325, 100–104.

- Wu, Y.-Y., Zhu, J.-W., Chen, K., Wu, B., Fang, J., and Shen, Y.-L., (2008). Liquid–liquid equilibria of water+2,3-butanediol+1-butanol at T=298.15K, T=308.15K and T=318.15K. *Fluid Phase Equilibria*, 265 (1–2), 1–6.
- Yerazunis, S., Plowright, J.D., and Smola, F.M., (1964). Vapor-liquid equilibrium determination by a new apparatus. *AIChE Journal*, 10 (5), 660–665.
- Zhang, Y., Liu, D., and Chen, Z., (2017). Production of C2–C4 diols from renewable bioresources: new metabolic pathways and metabolic engineering strategies. *Biotechnology for Biofuels*, 10 (1), 299.
- Zielkiewicz, J. and Konitz, A., (1991). (Vapour + liquid) equilibria of (N,N-dimethylformamide + water + propan-1-ol) at the temperature 313.15 K. *The Journal of Chemical Thermodynamics*, 23 (1), 59–65.
- Zorębski, E., Góralski, P., Godula, B., and Zorębski, M., (2014). Thermodynamic and acoustic properties of binary mixtures of 1-butanol with 1,2-butanediol. The comparison with the results for 1,3-, and 1,4-butanediol. *The Journal of Chemical Thermodynamics*, 68, 145–152.

Appendices

Appendix A: Calibrations

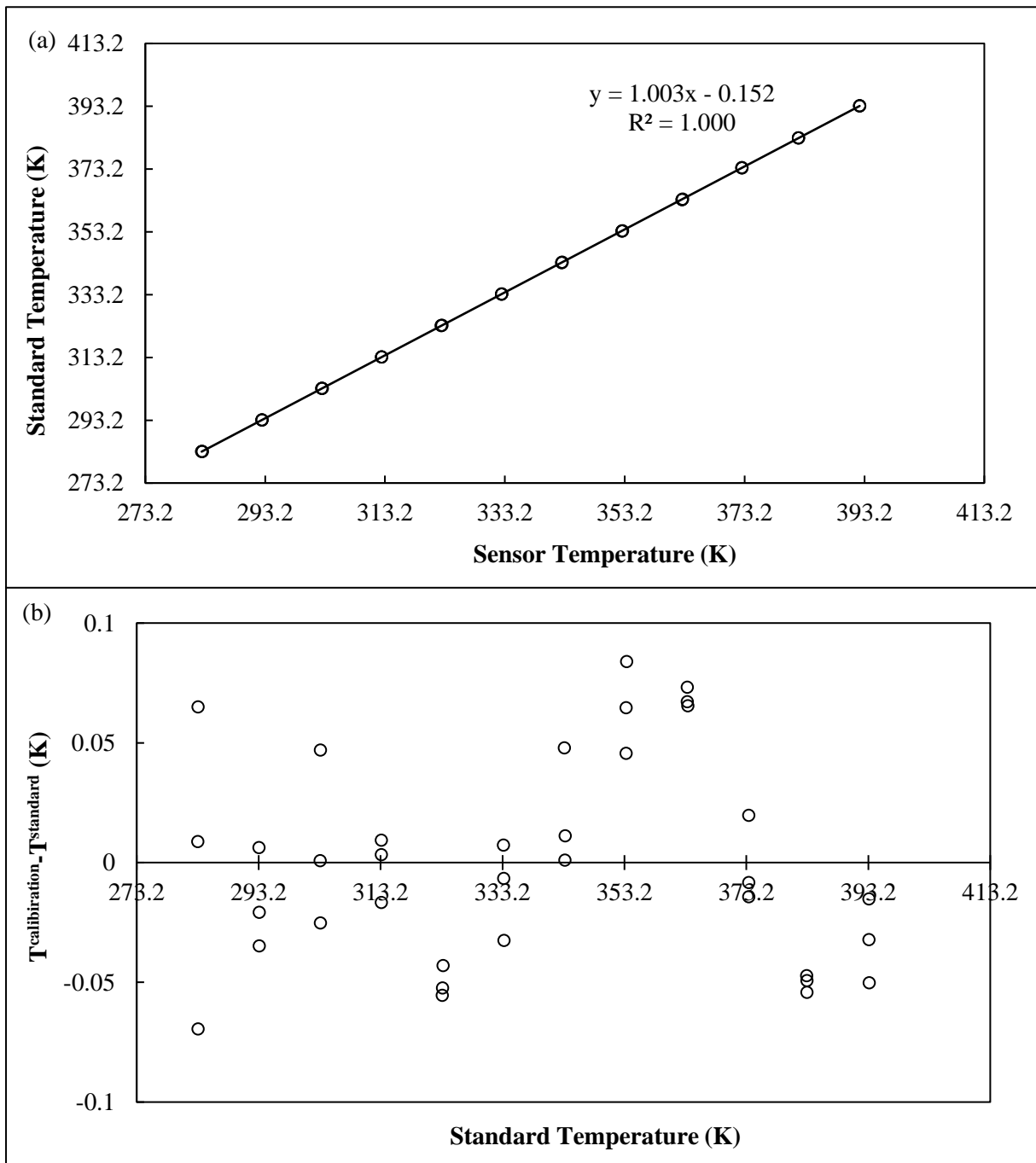


Figure A1. (a) Temperature calibration for Standard temperature vs. Pt-100 sensor with linear trendline. (b) Deviation plot for temperature.

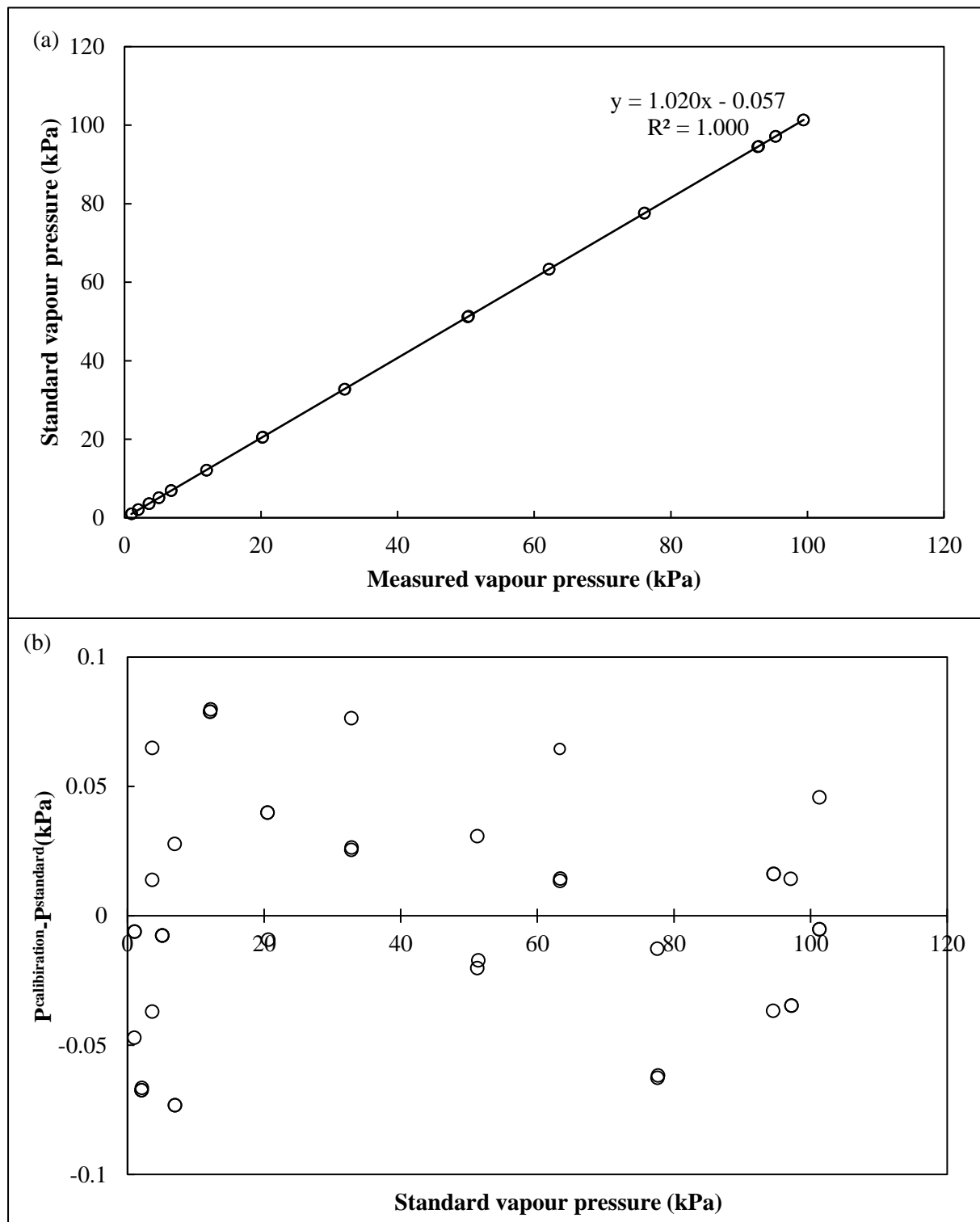


Figure A2. (a) Pressure calibration for Standard pressure vs. WIKA P-10 transducer with linear trendline. (b) Deviation plot for pressure.

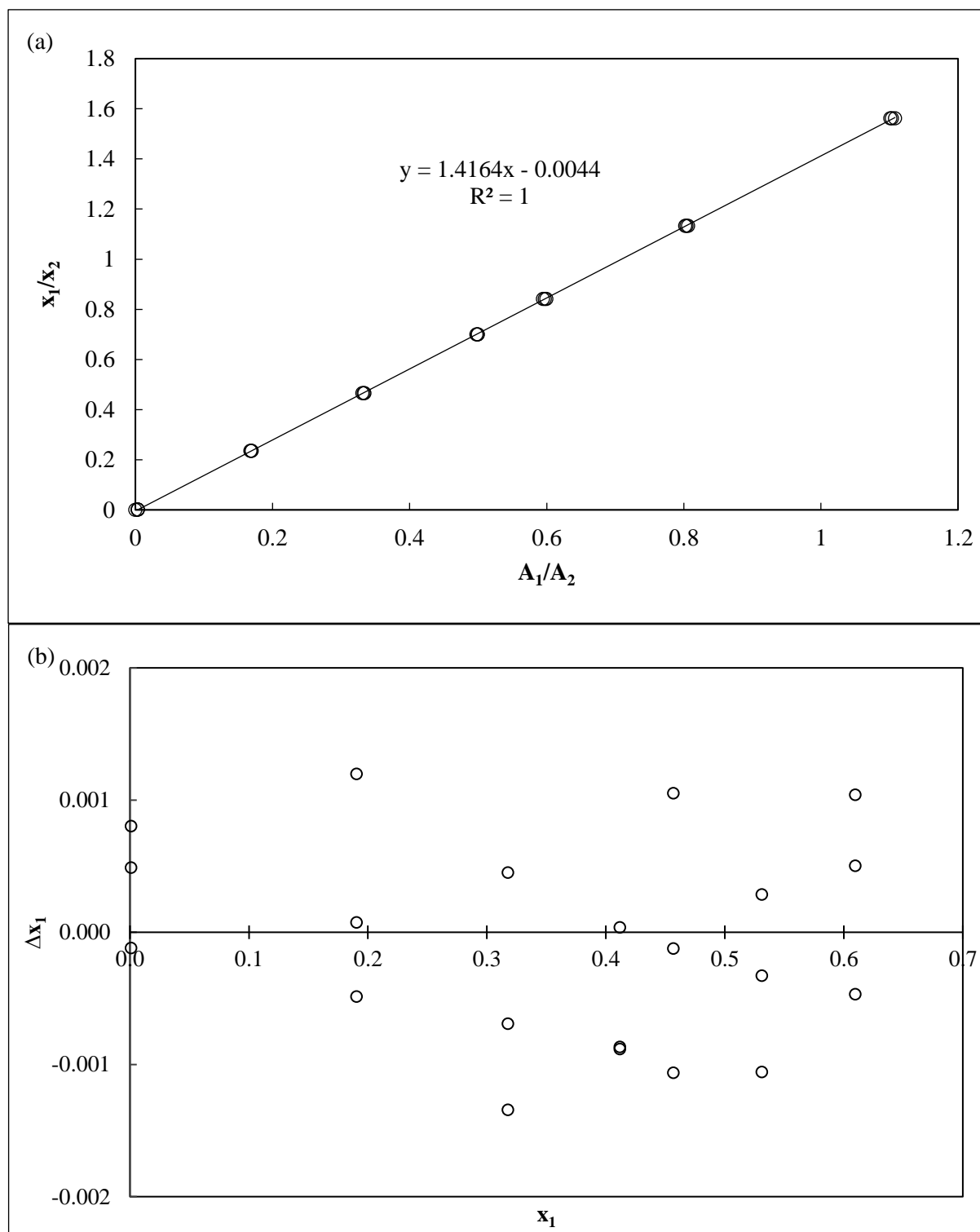


Figure A3. (a) GC area ratio calibration plot for water (1) + propan-1-ol (2) (water rich region) with best fit line. (b) Composition deviation plot for water (1) + propan-1-ol (2) (water rich region).

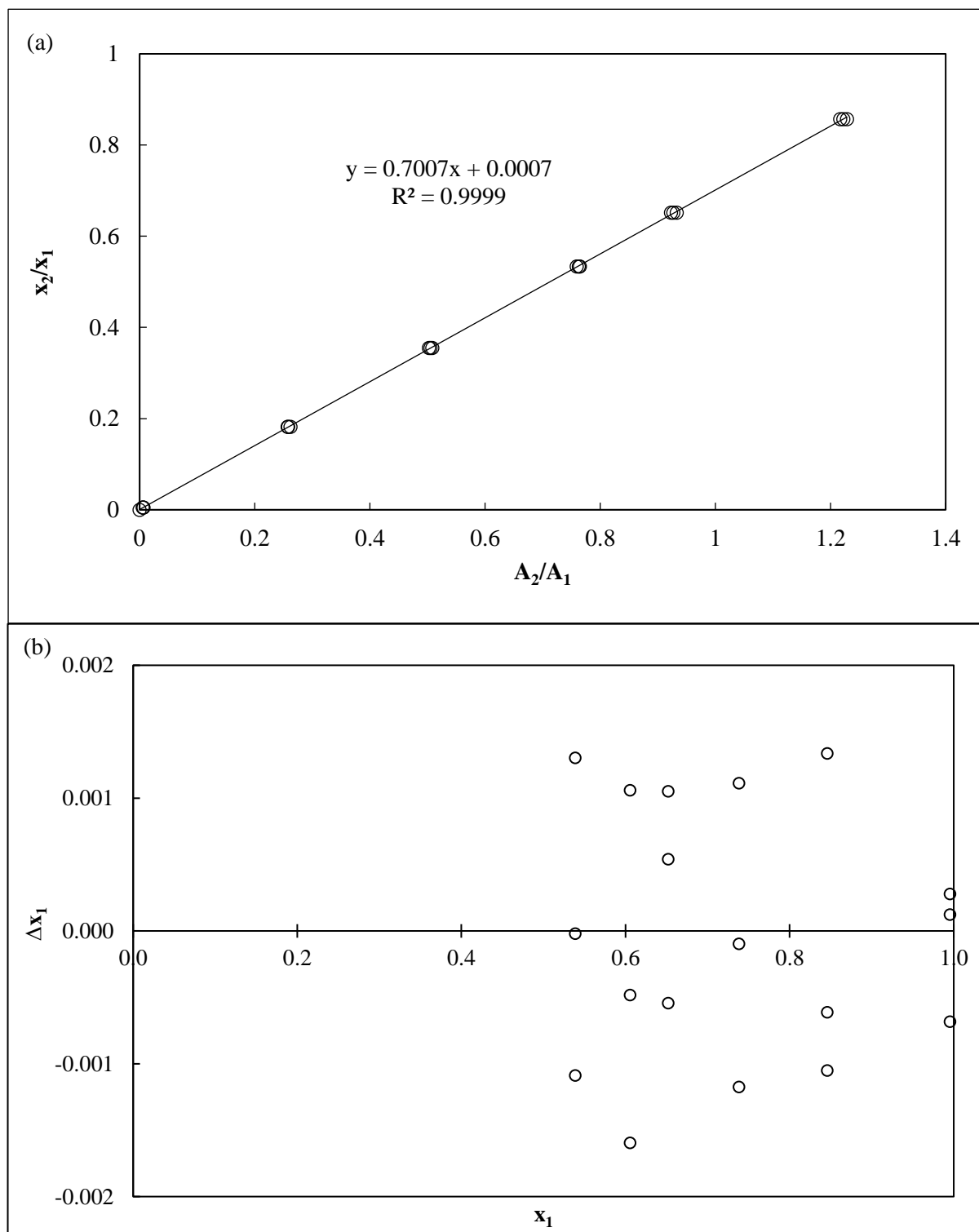


Figure A4. (a) GC area ratio calibration plot for water (1) + propan-1-ol (2) (propan-1-ol rich region) with best fit line. (b) Composition deviation plot for water (1) + propan-1-ol (2) (propan-1-ol rich region).

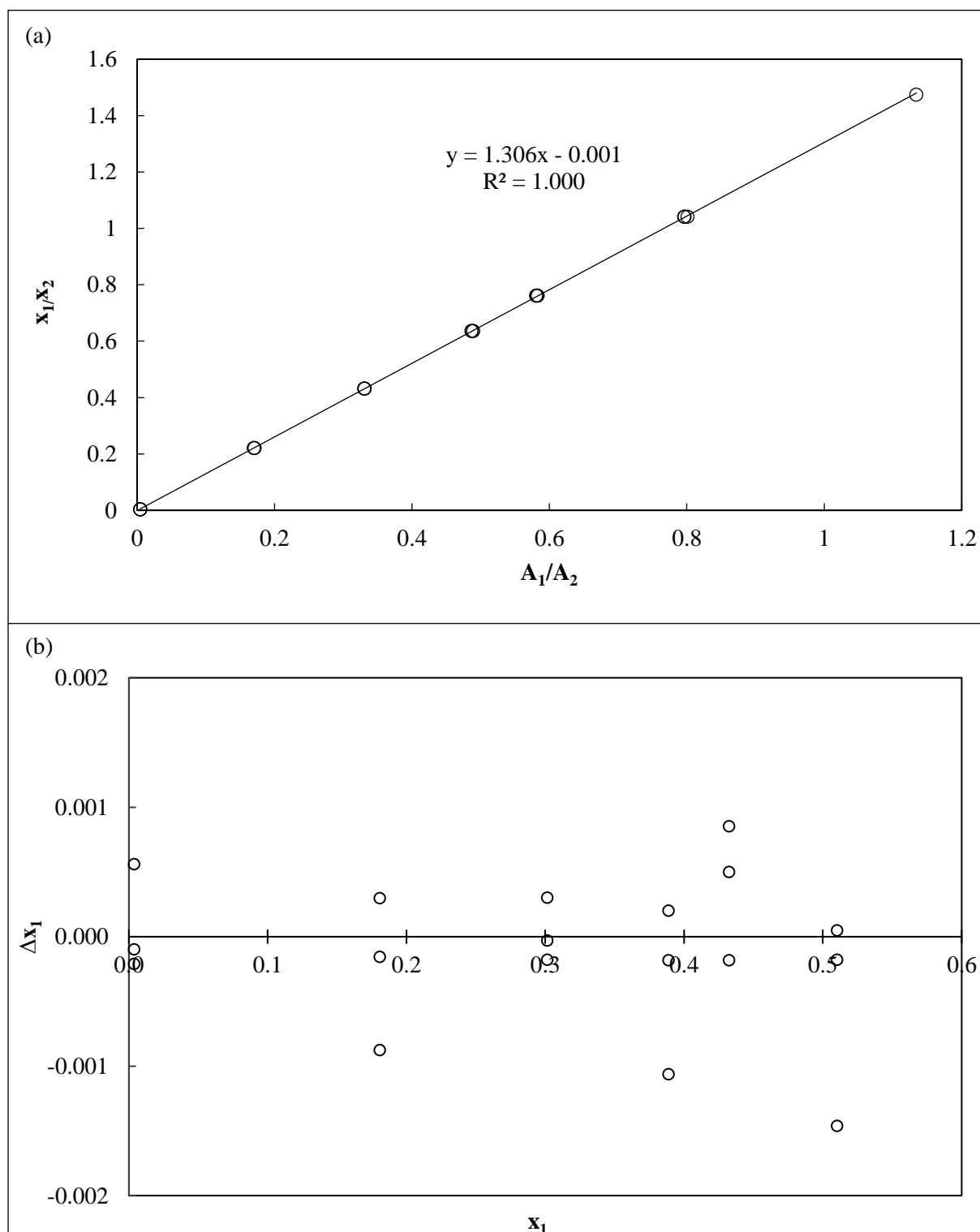


Figure A5. (a) GC area ratio calibration plot for water (1) + butane-1,4-diol (2) (water rich region) with best fit line. (b) Composition deviation plot for water (1) + butane-1,4-diol (2) (water rich region).

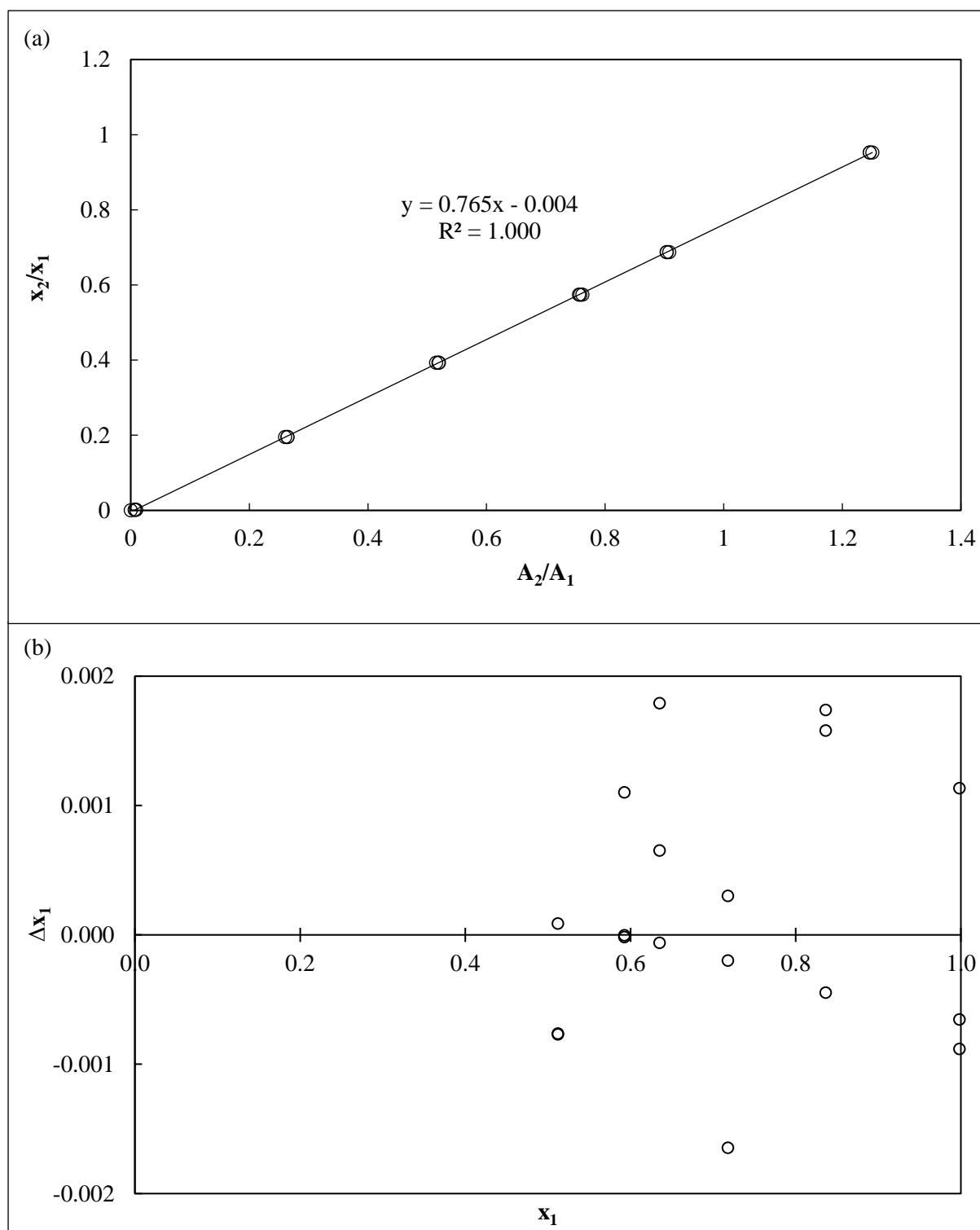


Figure A6. (a) GC area ratio calibration plot for water (1) + butane-1,4-diol (2) (butane-1,4-diol rich region) with best fit line. (b) Composition deviation plot for water (1) + butane-1,4-diol (2) (butane-1,4-diol rich region).

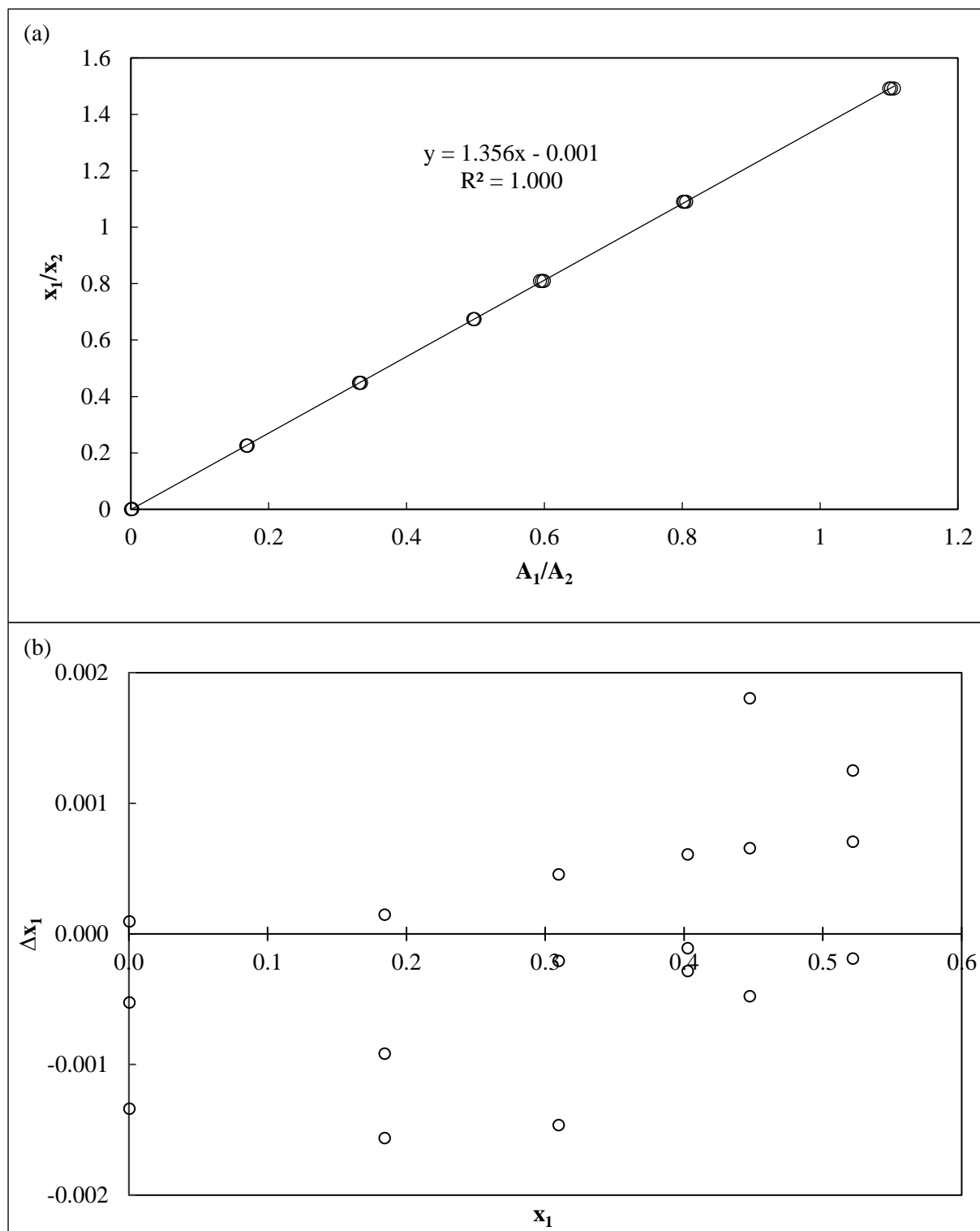


Figure A7. (a) GC area ratio calibration plot for water (1) + butane-2,3-diol (2) (water rich region) with best fit line. (b) Composition deviation plot for water (1) + butane-2,3-diol (2) (water rich region).

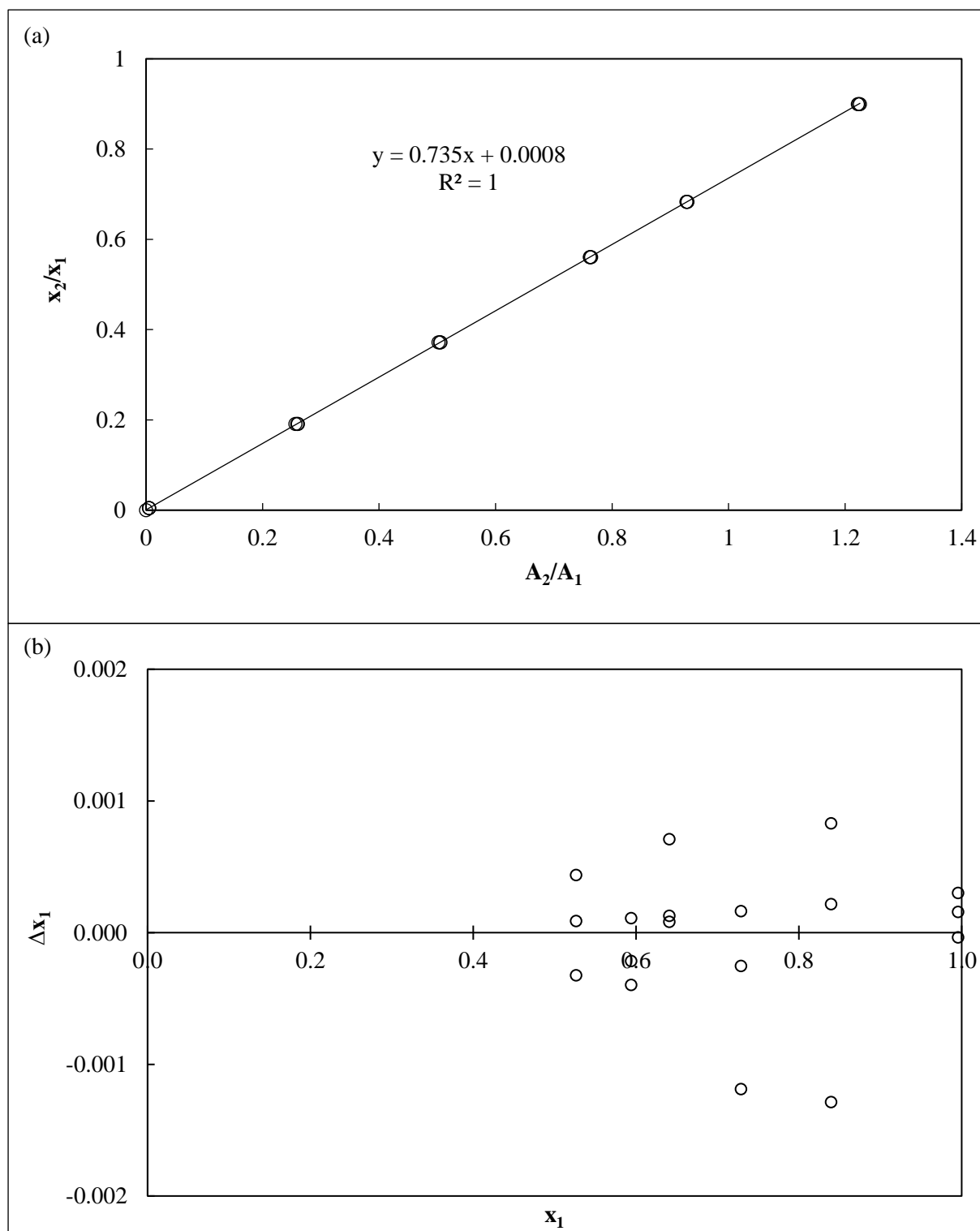


Figure A8. (a) GC area ratio calibration plot for water (1) + butane-2,3-diol (2) (butane-2,3-diol rich region) with best fit line. (b) Composition deviation plot for water (1) + butane-2,3-diol (2) (butane-2,3-diol rich region).

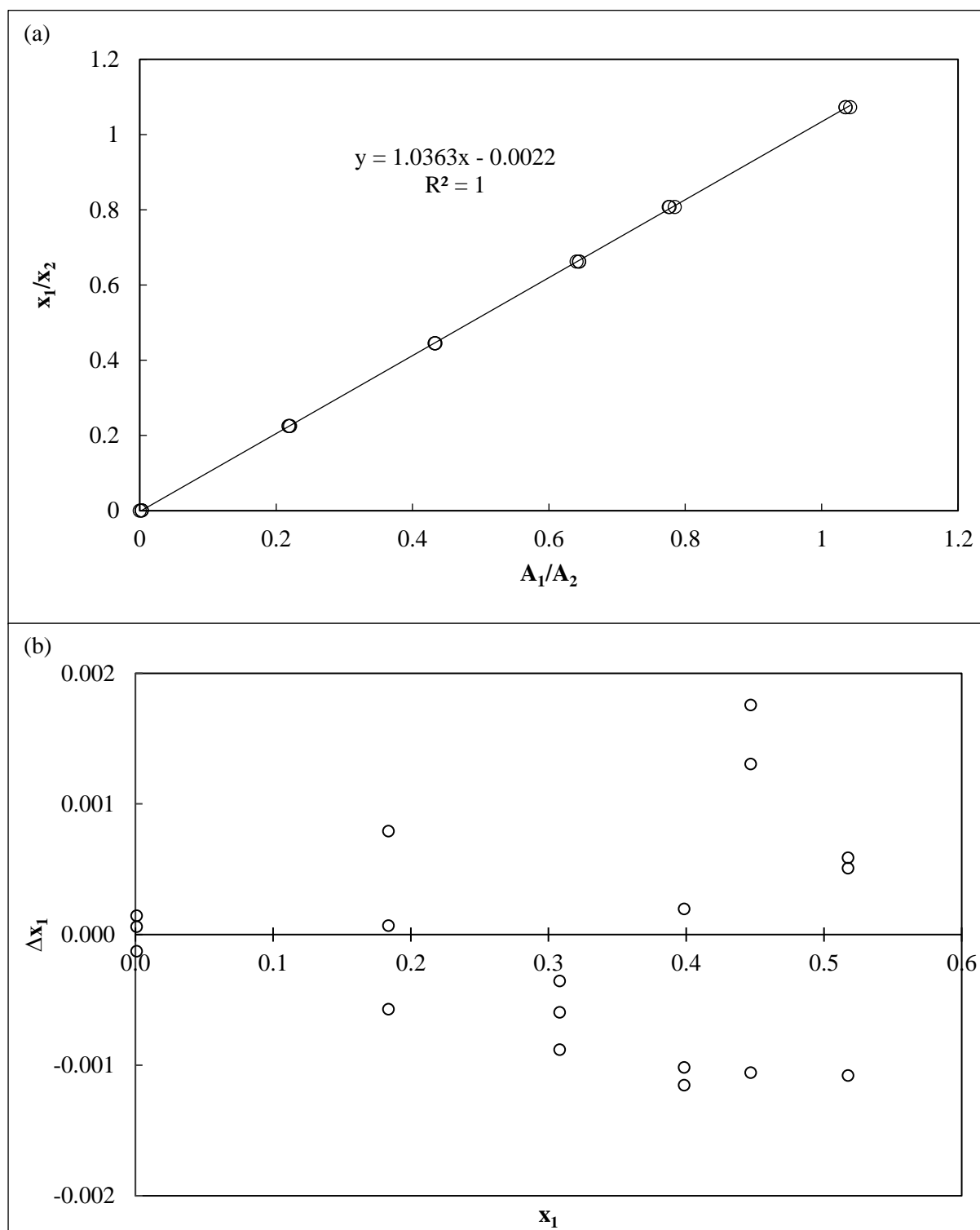


Figure A9. (a) GC area ratio calibration plot for butan-1-ol (1) + butane-1,4-diol (2) (butan-1-ol rich region) with best fit line. (b) Composition deviation plot for butan-1-ol (1) + butane-1,4-diol (2) (butan-1-ol rich region).

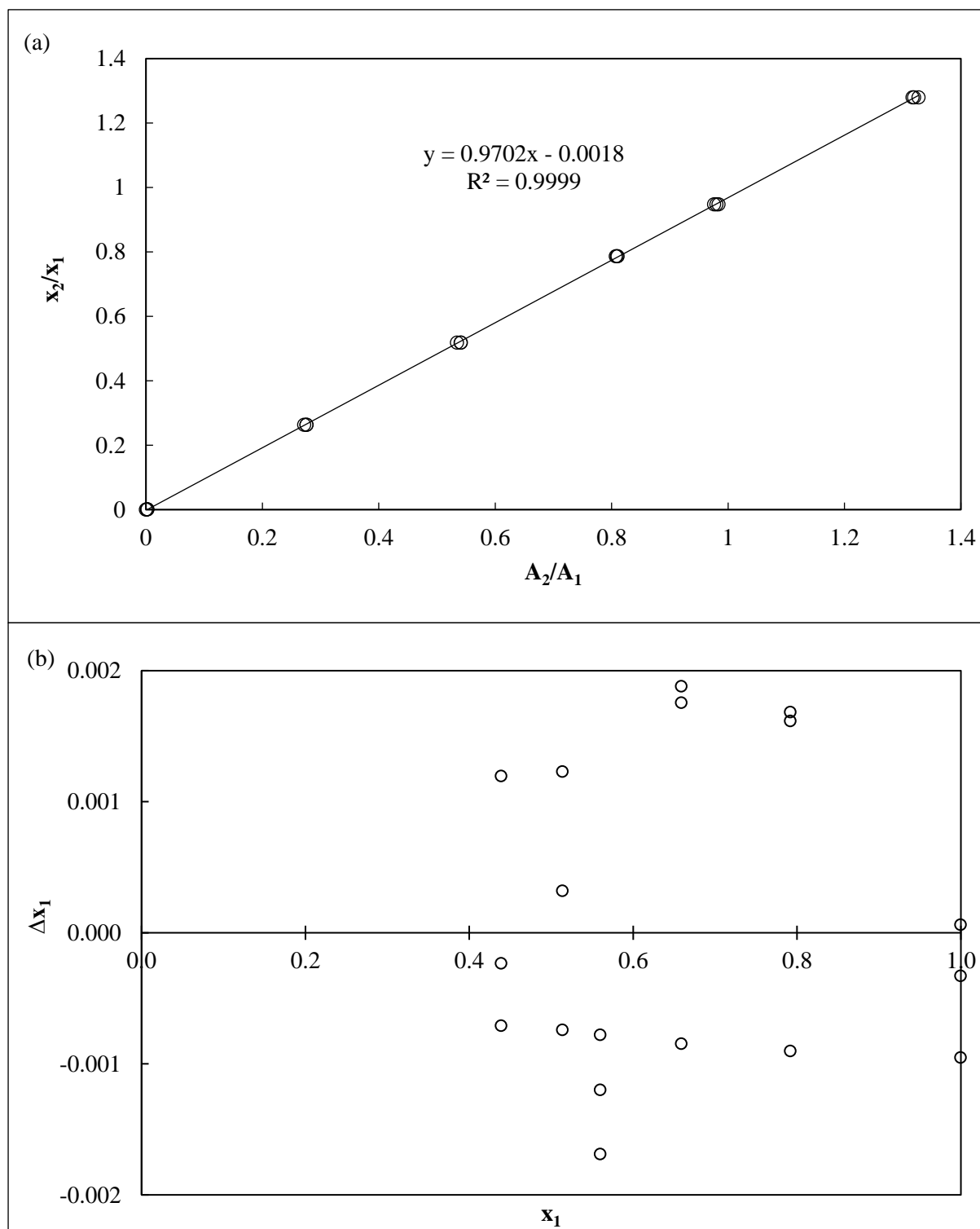


Figure A10. (a) GC area ratio calibration plot for butan-1-ol (1) + butane-1,4-diol (2) (butane-1,4-diol rich region) with best fit line. (b) Composition deviation plot for butan-1-ol (1) + butane-1,4-diol (2) (butane-1,4-diol rich region).

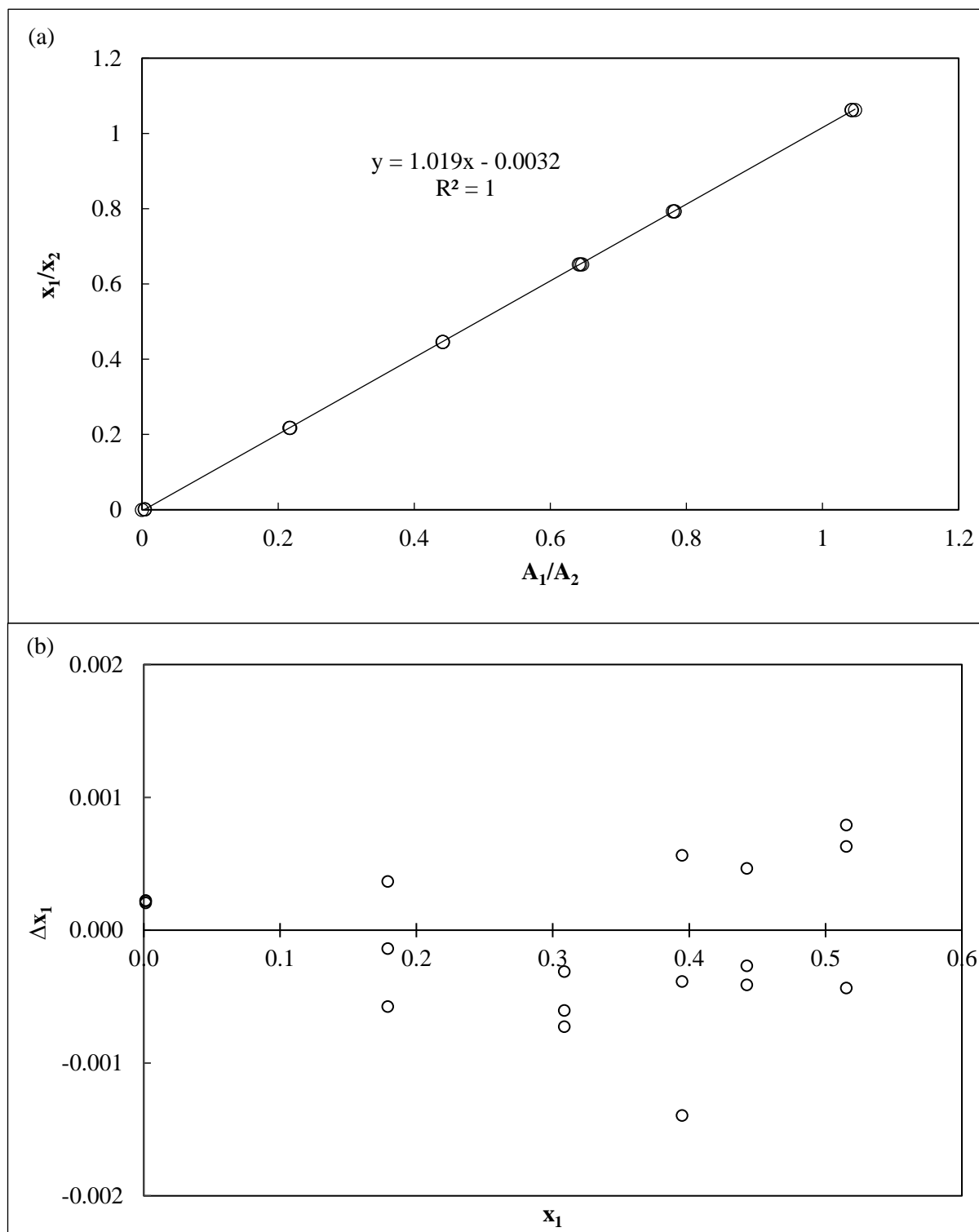


Figure A11. (a) GC area ratio calibration plot for butan-1-ol (1) + butane-2,3-diol (2) (butan-1-ol rich region) with best fit line. (b) Composition deviation plot for butan-1-ol (1) + butane-2,3,4-diol (2) (butan-1-ol rich region).

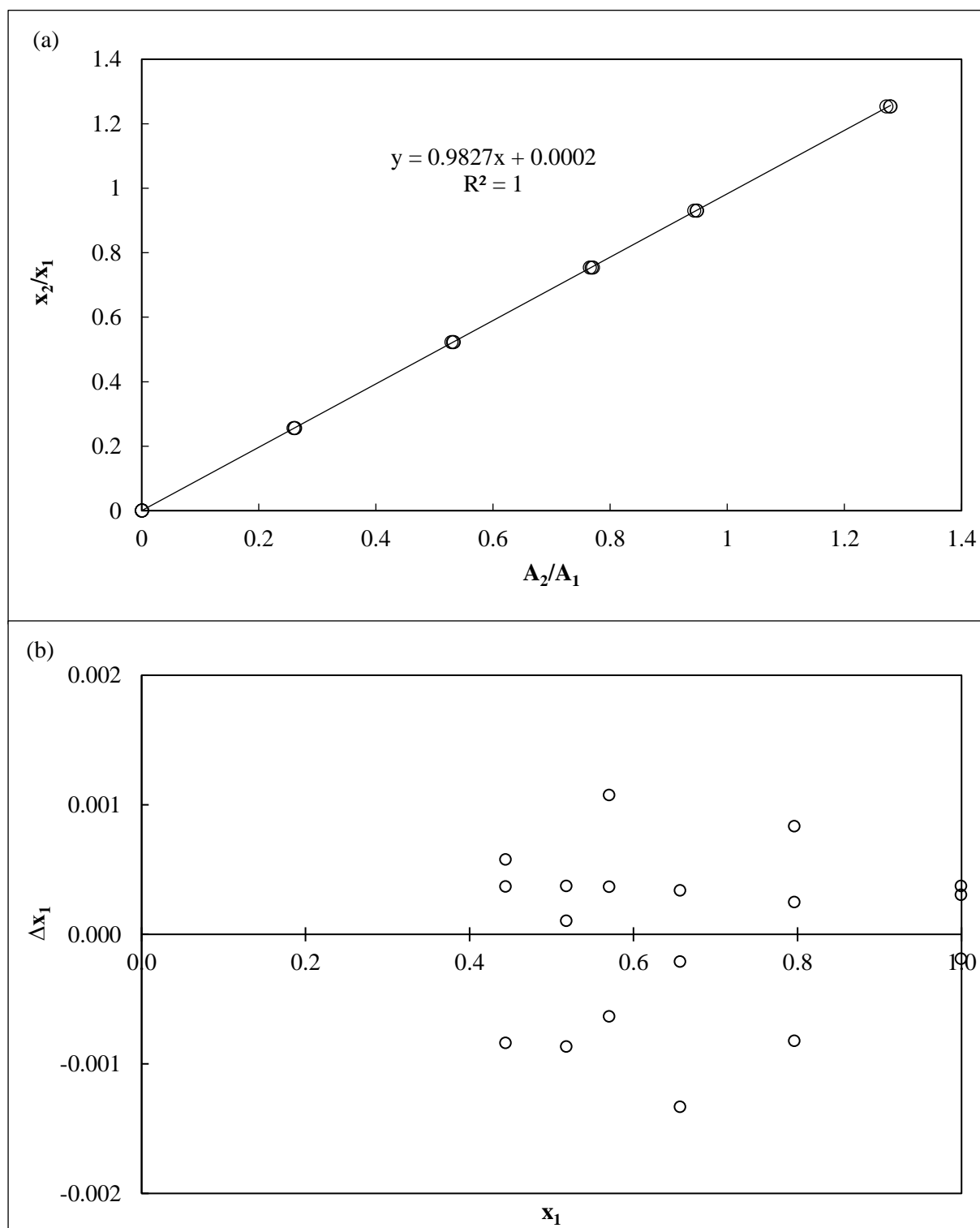


Figure A12. (a) GC area ratio calibration plot for butan-1-ol (1) + butane-2,3-diol (2) (butane-2,3-diol rich region) with best fit line. (b) Composition deviation plot for butan-1-ol (1) + butane-2,3-diol (2) (butane-2,3-diol rich region).

Appendix B: Uncertainty estimates

The standard equation given by the NIST for computing standard combined uncertainty ISO, (2008) is:

$$u_c(\theta) = \pm\sqrt{\sum_i u_i(\theta)^2} \quad (\text{B1})$$

Where θ refers to the parameter being evaluated for uncertainty. All sources of uncertainty, including calibration and measuring instruments are taken into account with equation (B1). The uncertainty factor breakdown is provided in Table B1.

Table B1. Uncertainty estimates for each contributing factor

Parameter	$u_i(\theta)$	Estimate
<u>Temperature/K</u>		
	$u_{calib}(T)$	0.05
	$u_{prec}(T)$	0.06
	$u_{stab}(T)$	0.06
	$u_c(T)$	0.10
<u>Pressure/kPa</u>		
	$u_{calib}(P)$	0.06
	$u_{prec}(P)$	0.03
	$u_{stab}(P)$	0.10
	$u_c(P)$	0.12
<u>Composition</u>		
	$u_{calib}(x_i)$	0.001
	$u_{bal}(x_i)$	0.001
	$u_{pur}(x_i)$	0.002
	$u_{rep}(x_i)$	0.003
	$u_c(x_i)$	0.004

Appendix C: Test system data

Table C1. P - x - y plot for the water (1) + propan-1-ol (2) system at 313.15 K.

$T / \text{K} = 313.2$		
P / kPa	x_1	y_1
7.0	0.000	0.000
7.1	0.005	0.022
7.6	0.022	0.088
8.3	0.064	0.210
9.2	0.139	0.344
10.0	0.206	0.419
10.3	0.240	0.448
10.8	0.324	0.503
11.0	0.353	0.518
11.2	0.436	0.554
11.3	0.483	0.570
11.4	0.637	0.607
11.4	0.692	0.615
11.3	0.803	0.624
10.9	0.933	0.657
9.8	0.971	0.741
9.4	0.980	0.786
8.4	0.993	0.897
7.4	1.000	1.000

*Standard combined uncertainties u_c , $u_c(T) = 0.10 \text{ K}$,
 $u_c(P) = 0.12 \text{ kPa}$, $u_c(x_1) = u_c(y_1) = 0.0040$

Table C2. Regressed model parameters for the water (1) + propan-1-ol (2) system at 313.15 K.

Parameter	Model	
	NRTL	UNIQUAC
a_{12}	-0.490	-2.345
a_{21}	0.130	1.742
$\alpha_{12,\text{NRTL}}^*$	0.486	-
RMSD/kPa	0.08	0.19
δy_1	0.001	0.010

*Treated as an adjustable parameter

Appendix D: Consistency tests

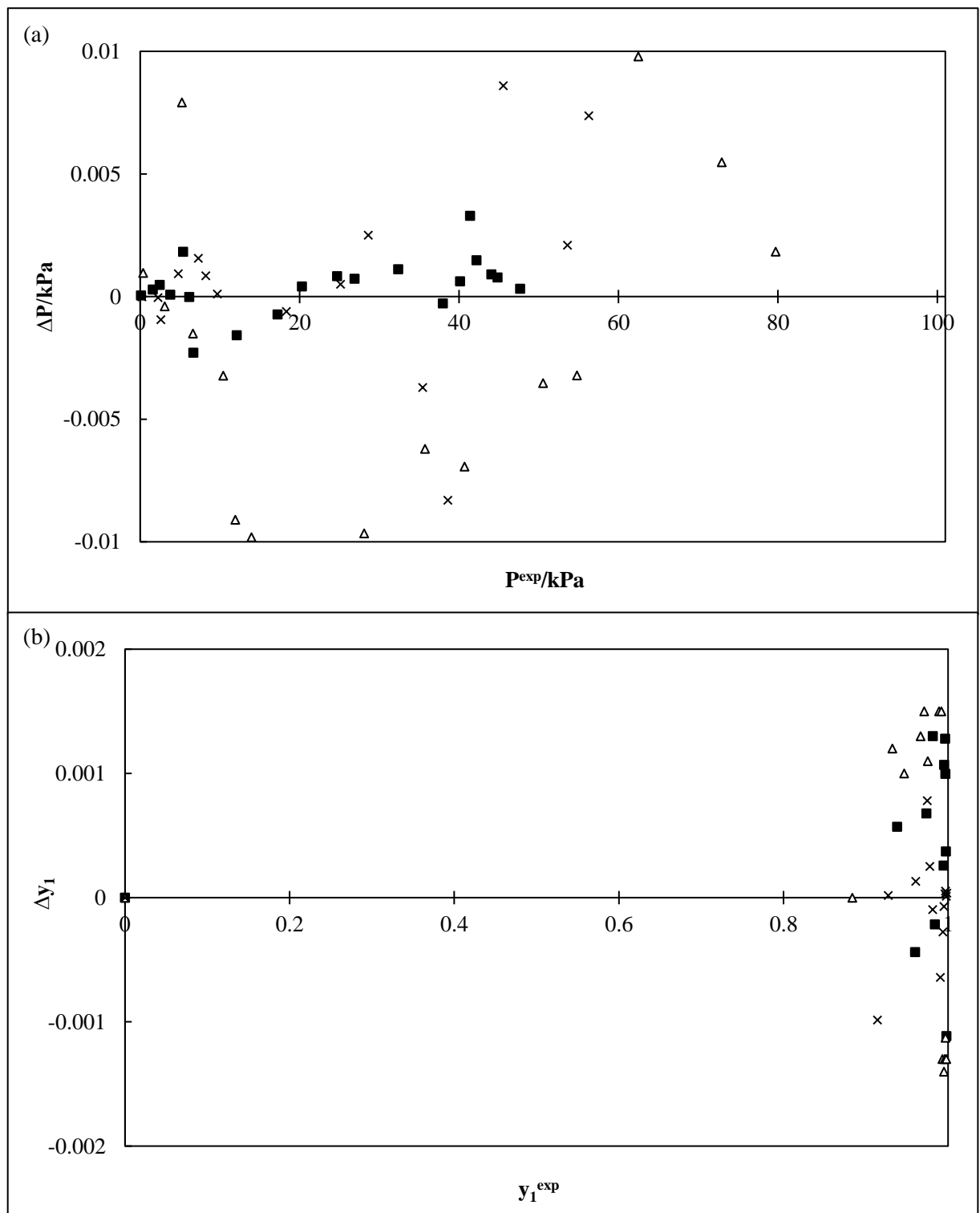


Figure D1. Plot for the point test for water (1) + butane-1,4-diol (2). (a) Pressure deviation plot.
(b) Vapour composition deviation plot.

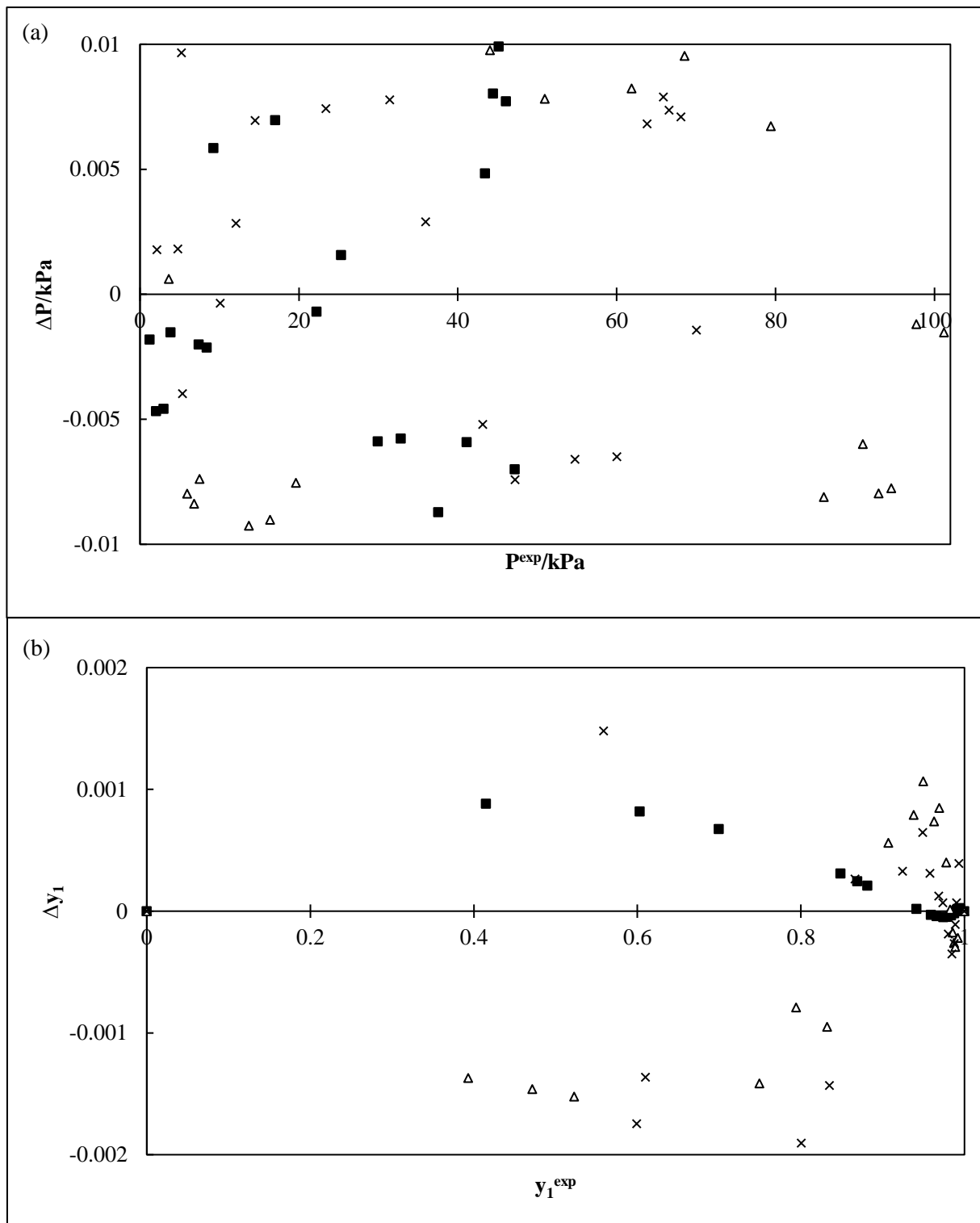


Figure D2. Plot for the point test for water (1) + butane-2,3-diol (2). (a) Pressure deviation plot.
(b) Vapour composition deviation plot.

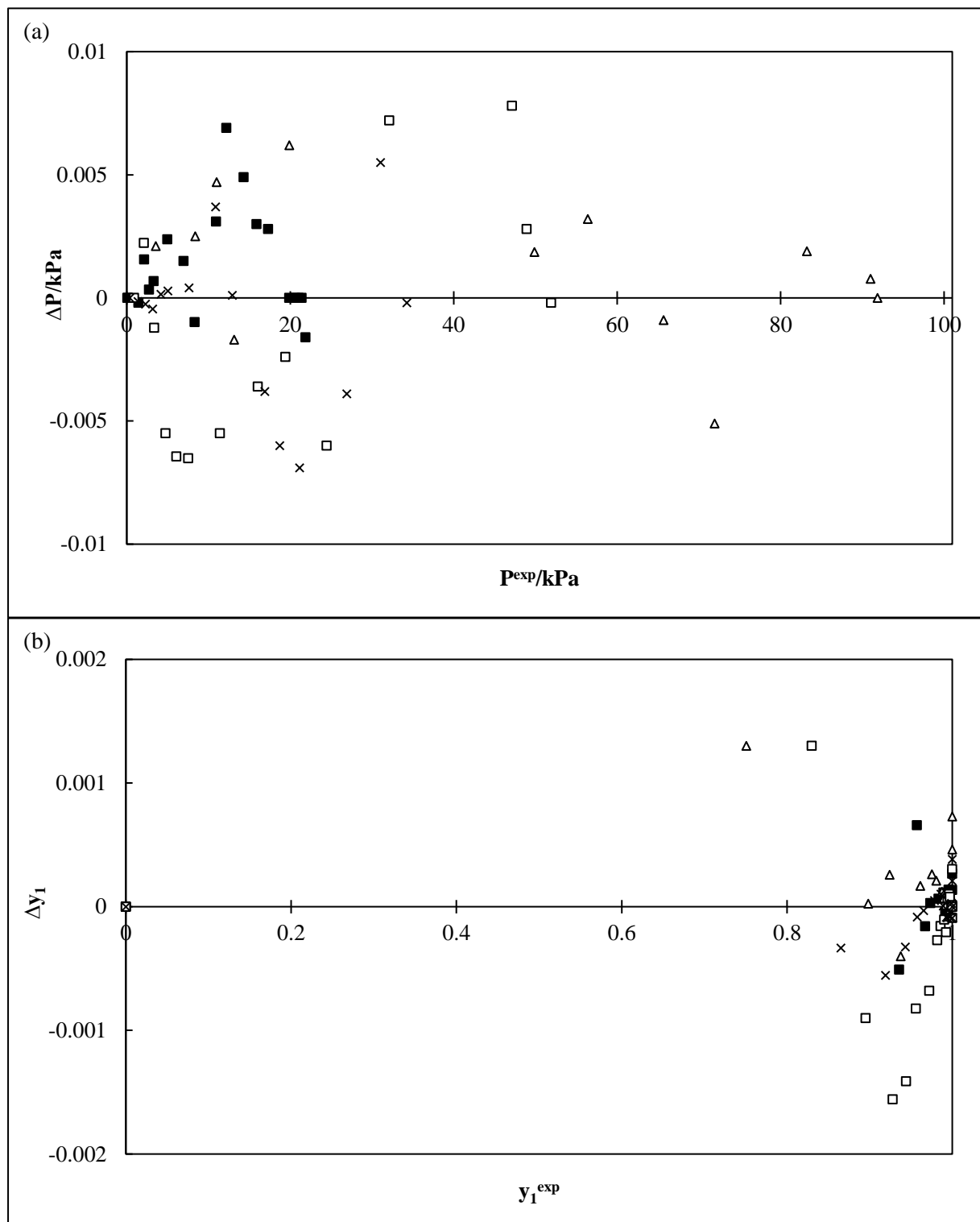


Figure D3. Plot for the point test for butan-1-ol (1) + butane-1,4-diol (2). (a) Pressure deviation plot. (b) Vapour composition deviation plot.

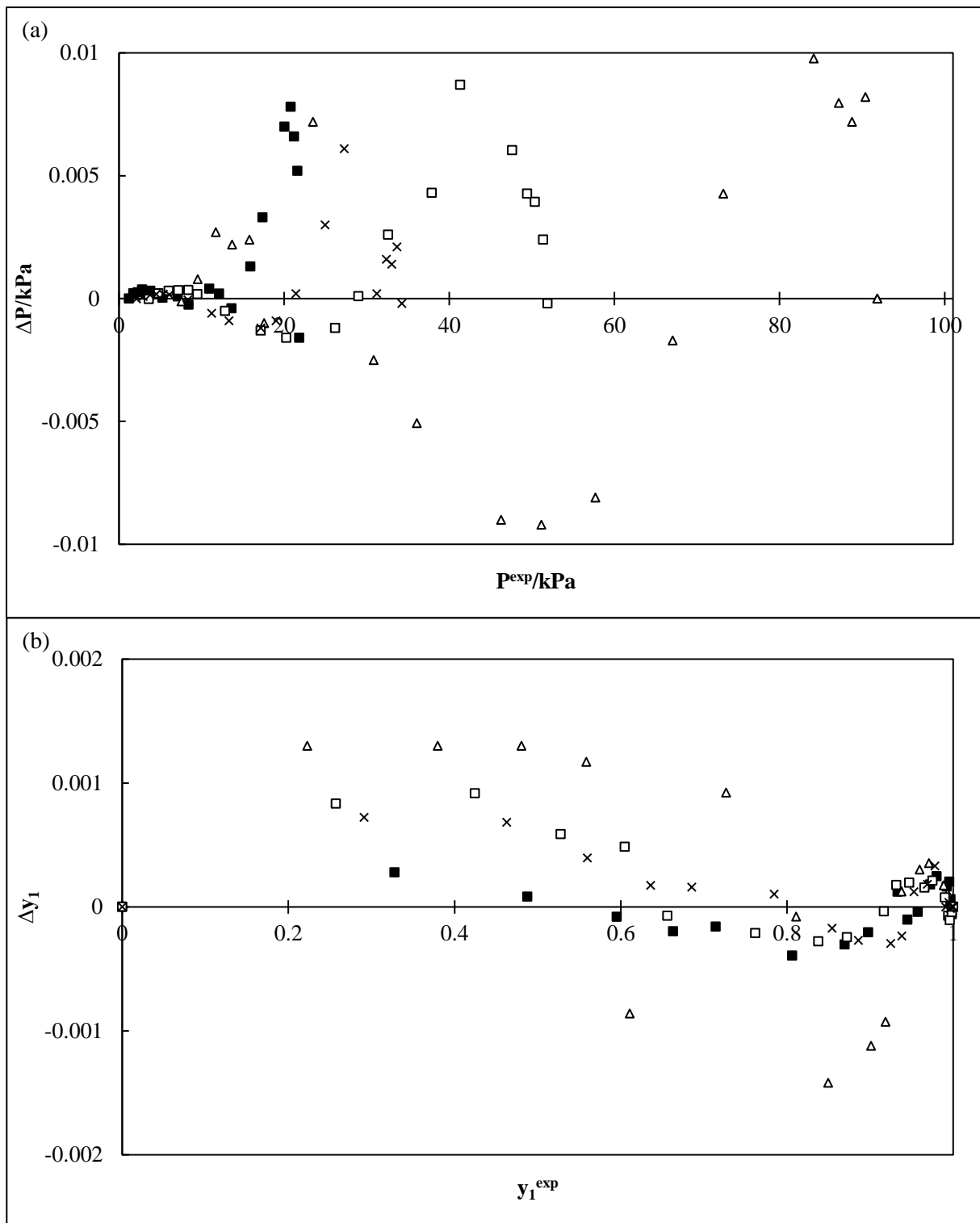


Figure D4. Plot for the point test for butan-1-ol (1) + butane-2,3-diol (2). (a) Pressure deviation plot. (b) Vapour composition deviation plot.

Appendix E: Extrapolated infinite dilution activity coefficients

Table E1. Extrapolated infinite dilution activity coefficients by the method of Maher and Smith, (1979).

System	Maher and Smith, (1979)	
	γ_1^∞	γ_2^∞
water (1) + butane-1,4-diol (2)		
$T / K = 353.2$	1.838	1.494
$T / K = 363.2$	2.089	1.505
$T / K = 373.2$	2.220	1.538
water (1) + butane-2,3-diol (2)		
$T / K = 353.1$	2.065	5.853
$T / K = 363.2$	1.930	4.849
$T / K = 373.2$	1.743	4.938
butan-1-ol (1) + butane-1,4-diol (2)		
$T / K = 353.2$	1.637	1.640
$T / K = 363.2$	1.587	1.630
$T / K = 373.2$	1.591	1.677
$T / K = 388.2$	1.505	1.610
butan-1-ol (1) + butane-2,3-diol (2)		
$T / K = 353.1$	1.317	1.492
$T / K = 363.2$	1.297	1.440
$T / K = 373.2$	1.280	1.487
$T / K = 388.2$	1.264	1.433